Department of Spatial Sciences

Multi-GNSS Integer Ambiguity Resolution Enabled Precise Positioning

Robert Odolinski

This thesis is presented for the Degree of
Doctor of Philosophy
of
Curtin University

January 2015

DECLARATION

To the best of my knowledge and belief this thesis contains no material previously published by any other person except where due acknowledgment has been made. This thesis contains no material which has been accepted for the award of any other degree or diploma in any university.

Robert Odolinski

24 January 2015

ABSTRACT

The next generations Global Navigation Satellite Systems (GNSSs) have the potential to enable a wide range of applications for positioning, navigation and timing. The positioning accuracy, reliability and satellite availability will be improved as compared to today's solutions, provided that a combination of the satellite systems is used. The GNSS receivers collect multi-GNSS code and carrier-phase observations with decimetre-level and millimetre-level precision respectively. However, only when the phase ambiguities can be solved to their true integer values is it possible to take full advantage of the precise phase measurements and solve very precise receiver positions. This technique is referred to as real-time kinematic (RTK). When the frequencies overlap between the systems one can further calibrate the so called between-receiver differential inter-system biases (ISBs) as to strengthen the model. A common 'pivot' satellite can then be used when parameterizing the double-differenced ambiguities. In this PhD thesis by publication multi-GNSS positioning results when combining the American Global Positioning System (GPS), Chinese BeiDou Navigation Satellite System (BDS), European Galileo and Japanese Quasi-Zenith Satellite System (QZSS) will be presented, based on real data. The combined systems will be evaluated in comparison to the single-systems, for short (atmosphere-fixed) to long (atmosphere-present) baselines. The analysis will consist of the receiver positioning precisions, integer ambiguity success rates, ambiguity/positioning convergence times, and measures of reliability. Reliability is the robustness of the underlying model. It will be shown that the combined systems can provide for improved reliability, ambiguity/positioning convergence times, integer ambiguity resolution and positioning performance over the single-systems. This holds particularly true when higher satellite elevation cut-off angles are used and the ISBs are calibrated, which can be of benefit in environments with restricted satellite visibility such as, e.g., urban canyons, open pit mines or when low-elevation multipath is present.

ACKNOWLEDGEMENTS

I would like to express my outmost gratitude to my supervisor Professor Peter Teunissen for his guidance and support during my candidacy. His knowledge within the geodesy and GNSS area has provided me with invaluable assets to continue my research for the many years to come. My acknowledgements go also to my co-supervisor Dr Dennis Odijk for his patience and feedback throughout these years.

I would further like to thank all my colleagues at the GNSS Research Centre for their support. Finally, but not least, I would like to thank my family and friends for understanding my busy life style during these past years. Thank you for believing in me and inspiring me to finalize this thesis.

LIST OF PUBLICATIONS

This PhD thesis by publication comprises of 6 first author peer-reviewed publications, 1 co-author peer-reviewed publication, supported by 1 first author non-peer reviewed publication. These articles have been published in the following journals and conference proceedings. Refer to Appendix A for copyright authorization, Appendix B for signed declarations for author contributions, and Appendix C for proof that two conference papers are peer-reviewed, and that one conference and one journal paper, respectively, have been accepted.

1. **Odolinski R**, Teunissen PJG, Odijk D (2014a) First combined COMPASS/BeiDou-2 and GPS positioning results in Australia. Part I: single-receiver and relative code-only positioning. Journal of Spatial Science, vol. 59, no. 1, p. 3-24. doi:10.1080/14498596.2013.840865
2. **Odolinski R**, Teunissen PJG, Odijk D (2014b) First combined COMPASS/BeiDou-2 and GPS positioning results in Australia. Part II: Single- and multiple-frequency single-baseline RTK positioning. Journal of Spatial Science, vol. 59, no. 1, p. 25-46. doi:10.1080/14498596.2013.866913
3. **Odolinski R**, Teunissen PJG, Odijk D (2013a) Quality analysis of a combined COMPASS/BeiDou-2 and GPS RTK positioning model. Proceedings of the International Global Navigation Satellite System Society (IGNSS) Symposium, Golden Coast, Australia, July 16-18, 2013
4. **Odolinski R**, Teunissen PJG, Odijk D (2013b) Combined GPS, BeiDou, Galileo, and QZSS single-epoch, single-frequency RTK performance analysis. In Proceedings of the International Association of Geodesy (IAG) symposium in Potsdam, Germany, September 1-6, 2013, accepted
5. **Odolinski R**, Teunissen PJG, Odijk D (2014c) Combined BDS, Galileo, QZSS and GPS single-frequency RTK. GPS Solutions. doi: 10.1007/s10291-014-0376-6
6. Teunissen PJG, **Odolinski R**, Odijk D (2014) Instantaneous BeiDou+GPS RTK positioning with high cut-off elevation angles. Journal of Geodesy, vol. 88, no. 4, p. 335-350. doi:10.1007/s00190-013-0686-4
7. **Odolinski R**, Teunissen PJG, Odijk D (2014d) Combined GPS+BDS+Galileo+QZSS for Long Baseline RTK Positioning. Proceedings of the Institute of Navigation (ION) GNSS, Tampa, Florida, USA, September 8-12
8. **Odolinski R**, Teunissen PJG, Odijk D (2014e) Combined GPS+BDS for short to long baseline RTK positioning. Measurement Science and Technology, accepted

TABLE OF CONTENTS

LIST OF FIGURES

LIST OF TABLES

1 INTRODUCTION

1. 1 Background

The Global Navigation Satellite Systems (GNSSs) can be used for many applications. Some of these applications require more precise positioning availability as compared to a code-only single point positioning (SPP) model. SPP is normally used for, e.g., car and maritime navigation on the open sea, by backpackers and hikers, and can obtain a few meter level positioning precisions. By making use of two receivers it is further possible to perform code-only relative point positioning (RPP), sometimes also referred to as differential GNSS (DGNSS), which can give positioning precisions at the decimetre to meter level. This provided that the receivers are separated by a short distance of a few kilometres to reduce relative atmosphere and satellite orbit errors. RPP can be used for precise aircraft applications, harbour entry by ships, GIS, and for many other disciplines (Misra and Enge, 2006).

One can also make use of more sophisticated receivers that collect both code and carrier-phase GNSS observations with decimetre-level and millimetre-level precision respectively. Once the so called phase ambiguities have been solved to their true integer values, one can then take full advantage of the very precise phase measurements to achieve mm-cm level real-time kinematic (RTK) positioning precisions. Provided that the baseline length is of at most a few kilometres, the relative slant ionospheric and tropospheric errors can be neglected. On the other hand, if the baseline length is of a few tens of kilometres (or more) these atmospheric errors need to be estimated as well. The troposphere is the lower part of the atmosphere with a height above the Earth's surface of 0-50 kilometres, whereas the ionosphere is the upper part with a height of 50-1000 kilometres (Teunissen and Kleusberg, 1998). The RPP/single-baseline RTK positioning techniques and an example of dual-frequency instantaneous RTK positioning scatter in local North, East and Up errors are depicted in Figure 1.1, as obtained by comparing the estimated positions to precise benchmark coordinates. Note in Figure 1.1 the about two-order of magnitude improvement in precision when going from ambiguity-float positioning (gray dots) to (correctly) ambiguity-fixed positioning (green dots). RTK can be used for, among many other industries, construction engineering, cadastral

surveying, tsunami, flooding and earthquake monitoring, precise farming, and the open pit mining industry.

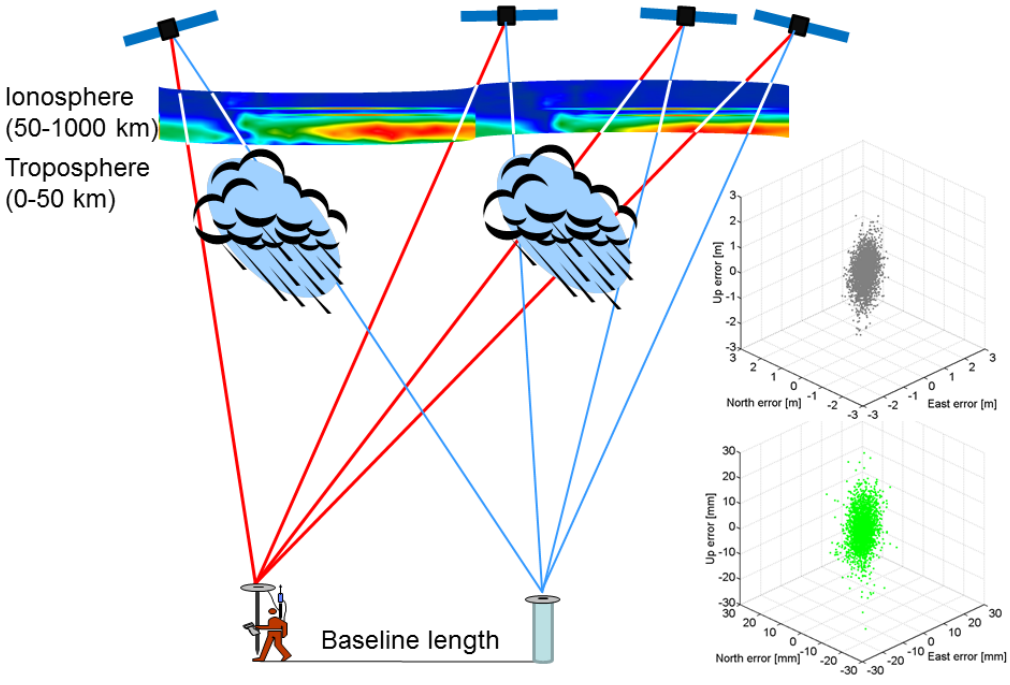

Figure 1.1 RPP and single-baseline RTK using two GNSS receivers (*left*), ambiguity-float (*top right*) and ambiguity-fixed (*bottom right*) dual-frequency instantaneous RTK receiver positioning errors in local North, East and Up

The American Global Positioning System (GPS) consists of 32 Medium Earth Orbit (MEO) satellites, and have been used for positioning for decades. The Chinese BeiDou Navigation Satellite System (BDS) attained Asia-Pacific regional operational status in the end of December 2011. BDS was formerly known as COMPASS. The current (2014) BDS constellation available for positioning consists of 5 Geostationary Earth Orbit (GEO), 5 Inclined Geo-Synchronous Orbit (IGSO) and 4 MEO satellites (see Figure 1.2). The full global BDS constellation is expected by 2020 and will consist of 5 GEO, 3 IGSO and 27 MEO satellites (CSNO, 2012). Since 2005 and 2008, respectively, two Galileo In-Orbit Validation Element (GIOVE) satellites are in orbit. These are currently (2014) not available for navigation, but since 2012 four Galileo In-Orbit Validation (IOV) MEO satellites are in orbit (ESA, 2013) for positioning (see Figure 1.2). By 2020 the full global Galileo

constellation will consist of 27 MEO and 3 spare satellites. The Quasi-Zenith Satellite System (QZSS) uses a traditional equatorial geostationary orbit but with a large orbital inclination, also referred to as a Highly inclined Elliptical Orbit (HEO) satellite (JAXA, 2013). The system is designed to enable users to receive QZSS signals from a high elevation angle in East Asia and Japan. Currently (2014) one HEO satellite is in orbit (see Figure 1.2) named MICHIBIKI, or QZS-1, which was launched in September 2010. By 2018 the full regional QZSS constellation is planned to consist of 3 GEO and 4 HEO satellites over Japan and the Asia-Pacific region (Boyd, 2014).

The ground tracks of all satellite systems considered in this thesis are depicted in Figure 1.2 (except GPS), as visible from the Curtin University station CUT0 for a satellite elevation cut-off angle of 10 degrees. The satellites' location is given as a dot at 29 April 2013, 10:05 a.m. local Perth time (UTC +8 hours), where BDS is represented by magenta, Galileo by green and QZSS by cyan colour. The GEO satellites are located along the equator, and the HEO/IGSO satellites are described by figure-of-eight loops. All the four systems' frequencies are further shown in Table 1.1.

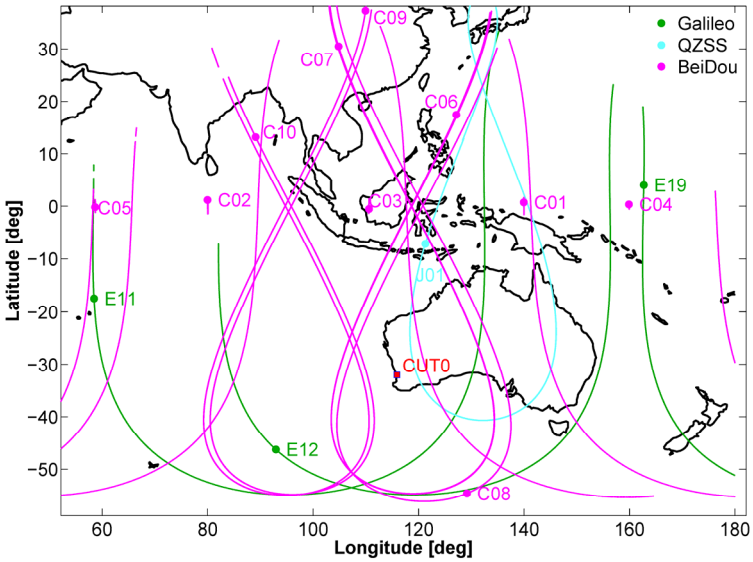

Figure 1.2 BDS (*magenta*), Galileo (*green*) and QZSS (*cyan*) ground tracks with satellites location (*dots*) given at 10:05 a.m. local Perth time, 29 April 2013 (Figure from Odolinski et al., 2014c)

Table 1.1 BDS, Galileo, QZSS and GPS signals (Odolinski et al., 2014c)

Satellite system	Band	Frequency (MHz)	Wavelength (cm)
BDS	B1	1561.098	19.20
BDS/Galileo	B2/E5b	1207.140	24.83
BDS	B3	1268.520	23.63
QZSS, GPS/Galileo	L1/E1	1575.420	19.03
QZSS, GPS	L2	1227.600	24.42
QZSS, GPS/Galileo	L5/E5a	1176.450	25.48

In this thesis focus is on combining the abovementioned satellite systems with GPS for precise positioning, which are all based on Code Division Multiple Access (CDMA) frequencies. GLONASS is not considered as it currently (2014) only has one satellite transmitting a CDMA frequency that, moreover, does not overlap the GPS frequencies in Table 1.1. The main benefit of combining systems is the increase in redundancy (the number of observations minus the numbers of estimable unknowns) of the models when solving the unknown GNSS parameters by least-squares. This can consequently provide for more precise and robust GNSS receiver-positioning performance. By making use of several GNSSs one also can protect the surveyor from satellite outages or system failures, which is particular important in safety-of-life applications such as precise aircraft and maritime navigation.

1. 2 Literature review

BDS results based on simulation can be found in, e.g., Grelier et al. (2007), Chen et al. (2009), and Yang et al. (2011). In Grelier et al. (2007) the BDS signals were described, and the Positional Dilution of Precision (PDOP) for a full constellation of GPS, BDS, GPS+Galileo and GPS+Galileo+BDS was presented to illustrate the improved receiver-satellite geometry one can achieve when combining the systems in the future. A similar analysis was conducted in Yang et al. (2011), but they included GLONASS and considered satellite elevation cut-off angles between 10 to 40 degrees as well. Chen et al. (2009) simulated similarly the PDOP for BDS+GPS, but in contrast to Grelier et al. (2007) and Yang et al. (2011) they focused their analysis on the Asia-Pacific region. The main conclusions were that the number of satellites for the combined satellite systems will become more than double the

number of GPS satellites, and that the Asia-Pacific region will potentially have a better positioning performance capability in comparison to other parts of the world because of the regional BDS GEO and IGSO satellites that will be available.

Simulation of BDS ambiguity resolution performance can be found in, e.g., Cao et al. (2008a). Their main focus was to compute the single-baseline RTK formal ambiguity bootstrapped success rate (Teunissen, 1998a), which is the probability of correct integer ambiguity estimation – the key to precise positioning. The formal bootstrapped success rate is an accurate lower bound to the integer least-squares (ILS) (Teunissen, 1995) success rate (Teunissen 1998a; 1999), and can thus be used to infer whether integer ambiguity resolution can be expected to be successful. The simulation was based on a location in Calgary, Canada, and a global BDS constellation. It was concluded that dual-frequency BDS-only RTK will most likely have a somewhat worse ambiguity resolution performance than GPS and Galileo, due to the poorer code noise and larger multipath effects for the BDS signals.

None of the abovementioned authors, however, considered the current (2014) regional BDS constellation in Figure 1.2 and real data. Real data results were presented in, e.g., Shi et al. (2013) for BDS SPP, RPP, and single-baseline RTK based on an initial BDS constellation of 3 GEO and 3 IGSO satellites. The main conclusion was that the BDS-only positioning performance is somewhat poorer as compared to GPS-only, but when combining the systems a better positioning performance than for GPS was achievable. Some first BDS-only positioning results outside of China can also be found in Montenbruck et al (2013) when using 4 GEO and 5 IGSO satellites. It was illustrated that the BDS-only single-baseline RTK performance can be comparable to the GPS-only performance. However, this conclusion was based on a limited data set of 6 hours and not a full regional BDS constellation that are currently available for positioning.

Initial results on combined GIOVE+GPS single-baseline RTK were presented in Odijk and Teunissen (2013a). It was shown that the between-receiver differential inter-system biases (ISBs) for the overlapping GPS frequencies L1, L5 and GIOVE E1, E5a, respectively, are zero for similar receiver types, but indeed exist for mixed receiver types. Fortunately however the code and phase ISBs were found to be time-constant, which is very promising for calibration purposes. The GIOVE-GPS ISBs nature and behaviour were also investigated in Montenbruck et al. (2011) and for

IOV-GPS ISBs in Melgard et al. (2013) and Odijk and Teunissen (2013b), which all confirmed the results of Odijk and Teunissen (2013a). The main conclusion in Odijk and Teunissen (2013a) was then that the ILS success rate increases accordingly when combining GIOVE with GPS and as compared to using GPS as a standalone system, particularly if the ISBs can be calibrated to maximize the redundancy of the model. However, single-baseline RTK positioning results have not yet been illustrated using the Galileo IOV-satellites when combined with GPS and the other satellite systems.

1. 3 Thesis objectives and outline

The main objectives of this thesis are to formulate multi-GNSS functional and stochastic models for fast and precise positioning, and evaluate the positioning performance when combining the different satellite systems depicted in Figure 1.2. The shortcomings of other studies on this topic are that only limited data sets have been used and/or have been based on a preliminary regional BDS constellation. Moreover, there are no studies that focused on Australia in particular and/or on combining all the four satellite systems for single-baseline RTK, based on real data. Single-baseline RTK positioning results have been illustrated for Galileo GIOVE satellites (Odijk and Teunissen, 2013a), but not for the IOV satellites in combination with the other satellite systems. Moreover there are no studies on single-baseline RTK for longer baselines when combining the systems, and when the relative atmospheric errors cannot be neglected.

The GNSSs models derived throughout this thesis are formulated by using the S-system theory (Teunissen, 1985; Teunissen et al., 2010) to solve for rank deficiencies. The number of rank deficiencies is the number of linear combinations of the column vectors of the design matrix that produces the zero vectors. These combinations are said to span the null space of the design matrix. S-system theory then implies null space identification, S-basis constraining to eliminate the rank deficiencies, and interpretation of the estimable unknowns.

The following Chapters include papers that cover the following objectives. The conclusions of each chapter can be found in the respective papers, whereas the thesis conclusions can be found at the end of this Chapter as to bind the publications into a collective piece of work.

Chapter 2: BDS+GPS single-receiver and relative code-only positioning

This chapter is covered by the following publication:

- First combined COMPASS/BeiDou-2 and GPS positioning results in Australia. Part I: single-receiver and relative code-only positioning (Odolinski et al., 2014a)

In this contribution focus is on code-only measurements for single point positioning (SPP) and relative point positioning (RPP). The goal is to give Australian GNSS users indications of what BDS can bring in terms of satellite availability, positioning precision and robustness, both as a stand-alone system and when combined with GPS. SPP and RPP are investigated to give us a first idea of the quality of the BDS data and have the advantage that cheap code-only receivers can be used. Comparisons of the positioning performance are made between single- and multiple-frequencies when one ignores and estimates the ionospheric delays (SPP), respectively, as well as when the ionospheric delays can be eliminated by using two receivers separated by a short distance (RPP). A good code-only precision is moreover a prerequisite for successful instantaneous carrier-phase integer ambiguity resolution and precise RTK positioning, which is investigated in the subsequent Chapters 3-9 for short as well as long baselines.

Chapter 3: Single- and multiple-frequency BDS+GPS RTK positioning

This chapter is covered by the following publication:

- First combined COMPASS/BeiDou-2 and GPS positioning results in Australia. Part II: Single- and multiple-frequency single-baseline RTK positioning (Odolinski et al., 2014b)

In this contribution BDS+GPS *instantaneous* single-baseline RTK results will be presented, since it is the most challenging mode and has the advantage that the system becomes independent of cycle-slips. The baseline length will be short so that the relative atmospheric errors can be neglected, also referred to as the “atmosphere-fixed” model. The goal is to investigate whether successful instantaneous single-frequency RTK becomes feasible when combining the systems, as well as comparing the RTK positioning performance between the systems when using multiple-

frequencies. Dual- and triple-frequency BDS, and dual-frequency GPS observations will be analysed. A first indication in Australia of the achievable formal bootstrapped success rate and empirical integer least-squares (ILS) ambiguity success rates will be given. The LAMBDA method will be used for ambiguity resolution (Teunissen, 1995), and integer validation techniques (Teunissen and Verhagen, 2009; Verhagen and Teunissen, 2013a) to validate the resolved ambiguities. The emphasis will be on comparing the RTK performance between the systems when using a customary elevation cut-off angle of 10 degrees. An evaluation of the formal bootstrapped success rate for an elevation cut-off angle of 25 degrees will, however, be given as well. The use of higher cut-off angles can be of particular benefit in urban canyon environments, open pit mines, or when low-elevation multipath is present.

Chapter 4: On the reliability and performance of a BDS+GPS RTK model

This chapter is covered by the following publication:

- Quality Analysis of a Combined COMPASS/BeiDou-2 and GPS RTK Positioning Model (Odolinski et al., 2013a)

In this contribution single-baseline RTK ambiguity success rates and positioning precisions for higher than customary satellite elevation cut-off angles between 10 to 35 degrees, will be presented. The use of higher cut-off angles is motivated by the initial bootstrapped success rate analysis conducted in Chapter 3. The time-to-correct fix will also be computed for a particular case when instantaneous-RTK is not possible, i.e. by using a Kalman filter solution and assuming the ambiguities as time constant in the dynamic model. The emphasis will be on the reliability as well, which is the robustness of the underlying model. Internal reliability is the ability of the system to test the observations of modelling errors, and external reliability is the consequence on the estimated parameters if such modelling errors remain undetected. The internal reliability will be presented by minimal detectable biases (MDBs) and the external reliability by bias-to-noise-ratios (BNRs) (Teunissen, 1998b), and comparisons will be made between the single-systems and the combined BDS+GPS RTK model.

Chapter 5: Instantaneous BDS+GPS RTK positioning with high elevation cut-off angles

This chapter is covered by the following publication:

- Instantaneous BeiDou+GPS RTK positioning with high cut-off elevation angles (Teunissen et al., 2014)

In this contribution further analyses are made on the combination of BDS and GPS for single- and multiple-frequency instantaneous RTK. This analysis is based on satellite elevation cut-off angles ranging between 10 to 40 degrees. In this contribution the BDS+GPS formal bootstrapped success rates will be computed for different parts of the world as well, whereas in the previous two Chapters the focus is on the RTK performance in Australia. The ambiguity dilution of precision (ADOP) will moreover be derived and explained by a closed-form analytical expression for a single-system and combined BDS+GPS model. This is done as to quantify the intrinsic precision of the ambiguities, and to illustrate and explain the gain one can achieve by combining the systems. Comparisons will then be made between a single-frequency BDS+GPS RTK model to the dual-frequency single-systems, in terms of ambiguity resolution and positioning performance. It will further be stressed and demonstrated that the performance of positioning and ambiguity resolution do not always go hand-in-hand.

Chapter 6: BDS+Galileo+QZSS+GPS instantaneous single-frequency RTK

This chapter is covered by the following publication:

- Combined GPS, BeiDou, Galileo, and QZSS single-epoch, single-frequency RTK Performance Analysis (Odolinski et al., 2013b)

In this contribution use is made of four Galileo IOV and a single QZSS satellite (Figure 1.2) as well, as to investigate the further improvement one can achieve by combining all four systems in comparison to the RTK positioning models analysed in Chapters 3-5. A different functional model will however be derived here as some of the frequencies overlap between the systems, in contrast to the BDS and GPS frequencies that currently do not overlap. Emphasis is on the E1 frequency of Galileo that overlaps GPS L1 and QZSS L1 respectively (Table 1.1). This allows for a parameterization of the so called between-receiver differential inter-system biases

(ISBs), referred to as the “ISBs-float” model. If the ISBs can be calibrated the “ISBs-fixed” model can be obtained. The latter model implies that every satellite added to GPS can then function as if it was an additional satellite from the same system, thus truly maximizing the redundancy of the model. The ISBs-fixed model also allows for the use of a common pivot satellite when parameterizing the double-differenced ambiguities. The performance of the ISBs-float/ISBs-fixed four-system instantaneous (atmosphere-fixed) RTK models will be evaluated by formal/empirical integer ambiguity success rates and positioning precisions, for satellite elevation cut-off angles between 10 to 40 degrees.

Chapter 7: Performance of a BDS+Galileo+QZSS+GPS single-frequency RTK model

This chapter is covered by the following publication:

- Combined BDS, Galileo, QZSS and GPS single-frequency RTK (Odolinski et al., 2014c)

In this contribution use is made of the same functional models as in Chapter 6, but the analyses will instead of one day (as in Odolinski et al., 2013b) be based on four days of real data to illustrate the ambiguity success rate repeatability between days. Time-series of the ISBs will also be explicitly analysed as to answer the question whether the ISBs can be neglected for similar receiver types, in analogy to the GIOVE-GPS ISBs in Odijk and Teunissen (2013a). Single-baseline RTK results are then given for the ISBs-fixed and ISBs-float models. This in terms formal/empirical ambiguity success rates and positioning precisions. ADOPs will be presented (for the first time) for a four-system RTK model, and in addition to Chapter 6 that focus on instantaneous RTK, non-instantaneous RTK will be investigated here as well by using a Kalman filter with a dynamic model. The comparisons are made between the four systems to the single-systems and different combinations of the systems, for satellite elevation cut-off angles ranging between 10 to 40 degrees.

Chapter 8: Long baseline BDS+Galileo+QZSS+GPS RTK positioning

This chapter is covered by the following publication:

- Combined GPS+BDS+Galileo+QZSS for Long Baseline RTK Positioning (Odolinski et al., 2014d)

In this contribution an analysis of the combination of BDS, Galileo, QZSS and GPS for long baseline RTK positioning will be conducted. With long baseline we refer to the necessity to estimate the slant ionospheric delays as well as the Zenith Tropospheric Delay (ZTD), by the so called "ionosphere-float" and "ZTD-float" model respectively. This in contrast to Chapters 6-7, where the baseline is short so that the atmospheric delays can be neglected. The ionosphere-float, ISBs-float and ISBs-fixed functional models will be derived and explained. It will be shown that the interpretation of the estimable unknowns changes when one has to rely on the ionosphere-float model and in comparison to when the relative ionospheric delays can be neglected. It will be predicted by means of the ADOP whether successful, instantaneous RTK is possible when the ionosphere-float, ZTD-float model is used. A Kalman filter is subsequently used with a dynamic model for some of the unknown parameters. The formal/empirical analysis then consists of Kalman-filter based ADOPs, bootstrapped success rates and positioning precisions. Their improvement with respect to the accumulated time in the Kalman filter will be investigated as well. Focus will be on the precision improvement when going from ambiguity-float to ambiguity-fixed positioning, and comparing the combined four-system RTK model to the single-, dual- and triple-systems.

Chapter 9: BDS+GPS RTK positioning for short, medium and long baselines

This chapter is covered by the following publication:

- Combined GPS+BDS for short to long baseline RTK positioning (Odolinski et al., 2014e)

In this contribution emphasis is on short, medium and long baseline BDS+GPS RTK. This contribution is the ending Chapter of this PhD thesis, and it will illustrate the RTK performance one can expect for various baseline lengths when combining the systems. With short baseline we refer to when the baseline length is of at most a few kilometres so that the relative atmospheric delays can be assumed absent, whereas with medium baseline we refer to when the uncertainty of the slant ionospheric delays can reliably be modelled as a function of the baseline length. With long baseline we refer to the necessity to parameterize the ionospheric delays and (wet) ZTD as completely unknown. The functional models of these three cases will be

derived and their differences explained. It will be investigated by real data whether single-frequency instantaneous RTK is feasible for short/medium baselines, and when dual-frequencies are required. Emphasis is then on analysing the ionosphere-float, ZTD-float model by means of ADOPs, bootstrapped success rates, ambiguity/positioning convergence times, and the formal/empirical positioning performance. Special attention will be given on analysing the positioning precisions as a function of the time accumulated in the Kalman filter, and higher than customary elevation cut-off angles.

1. 4 Conclusions

The research objectives of this PhD thesis are to derive and evaluate the multi-GNSS functional and stochastic models for fast and precise positioning. These objectives are all covered by Chapters 2-9. The conclusions from these Chapters can briefly be summarized as follows.

The multi-GNSS functional/stochastic models for SPP, RPP, short, medium and long single-baseline RTK were derived, and the model differences were explained. Emphasis was on calibration of differential ISBs for overlapping frequencies, as to enable RTK functional models with the highest possible redundancy. It was demonstrated that combining GPS with the other systems (BDS, Galileo and QZSS) improves the reliability, integer ambiguity success rates, positioning availability and performance. The improvements were shown to become more significant for higher than customary elevation cut-off angles, because of the relatively larger number of visible satellites when compared to using GPS separately. It was further established that successful, instantaneous single-frequency RTK is achievable when at least two systems are combined (BDS+GPS) and the atmospheric errors can be neglected, whereas when any of the systems are used separately (or the atmospheric delays are present) at least two frequencies are required. It was also predicted that a Kalman filter with a dynamic model on certain parameters is required when the atmospheric errors need to be estimated as completely unknown, as to achieve successful ambiguity resolution. In conclusion it was shown for this latter functional model that the accumulated times needed in the Kalman filter were smaller for the combined systems in comparison to using the systems separately, as to obtain successful, ambiguity-fixed, mm-cm level RTK positioning precisions and ambiguity-float positions with a precision at the decimetre-level, respectively.

2 BDS+GPS SINGLE-RECEIVER AND RELATIVE CODE-ONLY POSITIONING

This chapter is covered by the following publication:

Odolinski R, Teunissen PJG, Odijk D (2014a) First combined COMPASS/BeiDou-2 and GPS positioning results in Australia. Part I: single-receiver and relative code-only positioning. Published in: Journal of Spatial Science, vol. 59, no. 1, p. 3-24, doi:10.1080/14498596.2013.840865

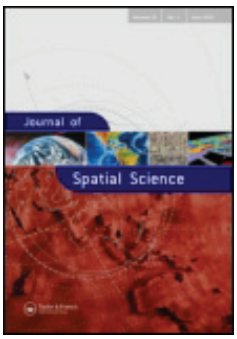

Journal of Spatial Science
Publication details, including instructions for authors and subscription information:
http://www.tandfonline.com/loi/tjss20

First combined COMPASS/BeiDou-2 and GPS positioning results in Australia. Part I: single-receiver and relative code-only positioning

R. Odolinski[a], P.J.G. Teunissen[ab] & D. Odijk[a]
[a] Department of Spatial Sciences, Curtin University, GPO Box U1987, Perth 6845, Australia
[b] Delft University of Technology, Delft, The Netherlands
Published online: 05 Dec 2013.

Journal of Spatial Science, 2014
Vol. 59, No. 1, 3–24, http://dx.doi.org/10.1080/14498596.2013.840865

Taylor & Francis
Taylor & Francis Group

First combined COMPASS/BeiDou-2 and GPS positioning results in Australia. Part I: single-receiver and relative code-only positioning

R. Odolinski[a]*, P.J.G. Teunissen[a,b] and D. Odijk[a]

[a]*Department of Spatial Sciences, Curtin University, GPO Box U1987, Perth 6845, Australia*
[b]*Delft University of Technology, Delft, The Netherlands*

China's BeiDou-2/COMPASS is expected to deliver global Positioning, Navigation and Timing (PNT) services by 2020. Australia is already a beneficiary of the regional BeiDou configuration, as enough satellites are available to perform PNT. The present contribution is Part I out of two parts that consider first combined BeiDou + GPS positioning results in Australia. In Part II, we will focus our attention on the single-baseline RTK model performance and the integer ambiguity success rates. Part I considers code-only single- and multiple-frequency single-receiver and relative point positioning. Our results show that the increased strength of the combined model allows for improved positioning robustness and accuracy over the BeiDou- and GPS-only solutions.

Keywords: GNSS; BeiDou; GPS; positioning navigation and timing (PNT); multipath; single-point positioning (SPP); relative point positioning (RPP)

1. Introduction

China's BeiDou (COMPASS) Navigation Satellite System attained initial regional operational status in the end of December 2011 (Langley 2011; CSNO 2011). The future BeiDou constellation will consist of five Geostationary Earth Orbit (GEO), three Inclined Geo-Synchronous Orbit (IGSO) and 27 Medium Earth Orbit (MEO) satellites (CSNO 2012). At this stage BeiDou is capable of providing Positioning, Navigation and Timing (PNT) services in the whole of the Asia-Pacific region, and will deliver global PNT services by 2020. With modern GNSS receivers tracking BeiDou on multiple frequencies, BeiDou data can be used for positioning, timing and navigation in various modes.

To date, there are some BeiDou results in the literature. Besides BeiDou simulation results in Grelier *et al.* (2007), Huang and Tsai (2008), Cao *et al.* (2008), Chen *et al.* (2009), Zhang *et al.* (2010), and Yang *et al.* (2011), we have real data results in Shi *et al.* (2012a), who processed BeiDou Single-Point Positioning (SPP), relative code positioning, and relative carrier-phase positioning (Real-Time-Kinematic (RTK)). Shi *et al.* (2012b) further evaluated orbit determination for BeiDou and combined BeiDou + GPS Precise Point Positioning (PPP). First positioning results using BeiDou outside of China are reported in Montenbruck *et al.* (2012a, 2012b) and Steigenberger *et al.* (2012, 2013). These later studies considered satellite

*Corresponding author. Email: robert.odolinski@curtin.edu.au

Table 1. Functional models and results to be presented for single-receiver and relative code-only positioning

Positioning	Section	Eq.	Unknowns
Single frequency SPP	3		Receiver coordinates, and clock
BeiDou/GPS		(1)	
Combined		(2)	
Multiple-frequency SPP	4		Receiver coordinates, clock, ionosphere
BeiDou/GPS		(6)	
Combined		(8)	
Single- and multiple- frequency RPP	5		Relative receiver coordinates and clock
BeiDou/GPS		(10)	
Combined		(12)	

orbit and clock determination, PPP, and RTK positioning.

This contribution presents first combined BeiDou + GPS positioning results in Australia, and consists of two parts. Part I considers combined BeiDou + GPS SPP and Relative Point Positioning (RPP), based on the code observables and single as well as multiple frequencies. In Part II carrier-phase positioning with ambiguity resolution will also be evaluated. The goal with these two parts is to give Australian GNSS users indications of what BeiDou can give in terms of positioning accuracy, both as a stand-alone system and when combined with GPS. The positioning model considered for RPP is of single-baseline type using two receivers separated by a short distance. With 'short distance' we refer to the assumptions that the single-differenced GNSS observables are insensitive to orbit errors and residual ionospheric and tropospheric delays.

SPP and RPP are investigated to give us a first idea of the quality of the data and have the advantage that cheap code-only receivers can be used. No external information such as precise orbits and clocks is further needed and only the broadcast data is necessary. SPP provides positioning accuracies at meter level and can be used for maritime navigation on the open sea, aircraft navigation en route, car navigation, and by hikers and backpackers. RPP can provide dm to meter-level positioning accuracy, and can be used for precise aircraft applications, harbor entry by ships, GIS, and many other applications (Misra & Enge 2006). A good code-only precision is moreover a prerequisite for successful instantaneous carrier-phase integer ambiguity resolution, the key to precise mm-cm-level positioning.

This contribution is organised as follows. The first section presents the current status of the BeiDou satellite constellation and the available signals. Then we describe the GNSS observation equations and the positioning models used for single- and multiple-frequency SPP and RPP (see Table 1). Following the description of each functional model, we also give the corresponding results. We conclude with a summary and discussion.

2. BeiDou system description

A fully operational BeiDou satellite constellation is shown to the left in Figure 1 (Astronautica Encyclopedia 2012), and to the right is a 24 h ground track of the operational BeiDou satellites available for positioning at 7 July 2012. The satellites' corresponding location is presented at UTC 04:25 as a dot, as observed from station CUT0, in Western Australia, Perth.

The operational satellite constellation (July 2012) consists of four Geostationary Earth Orbit (GEO) satellites in orbit at an altitude of 35,786 km, and five Inclined Geo-Synchronous Orbit (IGSO) satellites in two orbits at an altitude of 35,786 km as well with 55 degree inclination to the equatorial plane (CSNO 2012).

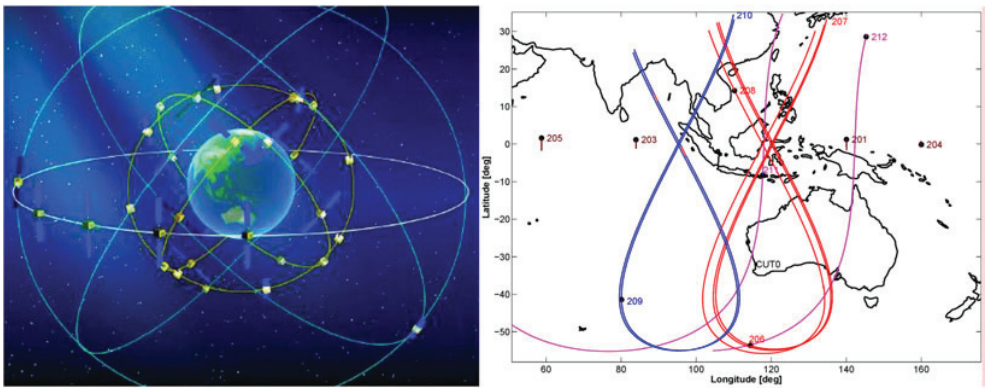

Figure 1. (Left) Full operational BeiDou satellite constellation (Astronautica 2012). (Right) Current BeiDou ground track from Perth station CUT0, where the satellite locations are given at 7 July 2012, UTC 04:25.

The Medium Earth Orbit (MEO) satellites are operated in orbit at an altitude of 21,528 km and 55 degree inclination to the equatorial plane (CSNO 2012) and are comparable to the GPS, GLONASS and Galileo satellites. In Figure 1 we see that some satellites are located to the South of CUT0 for some periods, whereas the remaining GEO satellites always remain stationary in the North and along the equator. The IGSO satellites describe two figure-of-eight loops and the GEO satellites are controlled in longitude but not latitude and thus reach peak inclinations of about 2 degrees (Montenbruck *et al.* 2012b).

The BeiDou satellites currently transmit at three frequencies, B1, B2 and B3, in Quadrature phase-shift keying (QPSK) modulation as shown in Table 2. In the Table we also show the L1, L2 and L5 GPS frequencies.

Table 2. COMPASS/BeiDou-2 (Han *et al.* 2011) and GPS signals

Sat. system	Band (component)	Frequency [MHz]	Wavelength [cm]
BeiDou	B1 (I/Q)	1561.098	19.20
	B2 (I/Q)	1207.140	24.83
	B3 (I/Q)	1268.520	23.63
GPS	L1	1575.42	19.03
	L2	1227.60	24.42
	L5	1176.45	25.48

The BeiDou signals are based on Code Division Multiple Access (CDMA), similar to GPS and Galileo. We also see that no BeiDou frequencies (currently) overlap the GPS frequencies. In this contribution we can only compare triple-frequency BeiDou results with those of dual-frequency GPS, since the third GPS L5 frequency is currently (2013) only available from PRN 1, 24 and 25.

3. Single-frequency single-point positioning

In this section we present the functional and stochastic models used for single-frequency single-receiver code-only positioning, also referred to as SPP. This is followed by some SPP results.

3.1 Functional model

The functional model describes the functional relation between the observations and the unknowns. Let us consider the receiver r, tracking the GPS or BeiDou satellites $s_* = 1_*, \ldots, m_*$, where m_* is the number of satellites of one GNSS system $*$ (G for GPS and C for COMPASS). We have no overlapping frequencies between GPS and BeiDou, thus we define the frequencies as $j_* = 1_*, \ldots, f_*$ frequencies, where f_* is the number of frequencies

for system $*$. Corrections for satellite orbits and clocks are provided from e.g. IGS and are assumed known. The Saastamoinen troposphere model (dry part) and the Klobuchar ionosphere model, which gives approximately 50 percent root-mean-square ionospheric range error reduction (Klobuchar 1987), can be applied as well. Any remaining residual ionosphere and (wet) tropospheric delays are ignored. The *single-system* (linearised) full-rank SPP observation equations then follow as,

$$p^{s*}_{r,j*} = -c_r^{s*\,T}\Delta x_r + \mathrm{d}\tilde{t}_{r,j*} \tag{1}$$

where $p^{s_*}_{r,j_*}$ is the code observable, with Δx_r the receiver coordinate increments, $\mathrm{d}\tilde{t}_{r,j_*}$ the estimable receiver clock biased by a frequency-dependent hardware (HW) code delay, and $c_r^{s_*T} = (x^{s_*} - x_r)^{\mathrm{T}}/\|x^{s_*} - x_r\|$ the line-of-sight unit vector from the receiver r to the satellites as obtained from linearising the observation equations with respect to the vector of receiver coordinates x_r, where x^{s_*} is the vector of satellite coordinates. For a *combined system* and in vector form we have on single-frequencies j_G and j_C,

$$y_{p;j} = \begin{bmatrix} G_r^G \\ G_r^C \end{bmatrix}\Delta x_r + \begin{bmatrix} e_{m_G} & 0 \\ 0 & e_{m_C} \end{bmatrix}\begin{bmatrix} \mathrm{d}\tilde{t}^G_{r,j_G} \\ \mathrm{d}\tilde{t}^C_{r,j_C} \end{bmatrix} \tag{2}$$

where $y_{p;j} = \left[y^{GT}_{p;j_G}, y^{CT}_{p;j_C}\right]^{\mathrm{T}}$ contains code observables of the two systems, with $y^{*}_{p;j_*} = \left[p^{1_*}_{r,j_*}, \ldots, p^{m_*}_{r,j_*}\right]^{\mathrm{T}}$, $G^{*}_r = \left[-c_r^{1_*}, \ldots, -c_r^{m_*}\right]^{\mathrm{T}}$ contains the unit vectors, and e_{m_*} is a column vector with only ones of size $m_* \times 1$. The estimable receiver clocks read $\mathrm{d}\tilde{t}^G_{r,j_G}$ for GPS and $\mathrm{d}\tilde{t}^C_{r,j_C}$ for BeiDou respectively, where the GPS clock is with respect to GPS time and the BeiDou clock to the BeiDou navigation satellite system Time (CSNO 2012). The possible shared parameters between the systems are the receiver coordinates.

The redundancy is computed as the number of observations minus the number of estimable unknowns. In Table 3 we give the number of observations, the number of estimable unknowns and the redundancy for the SPP models that we have presented. We also give in the last column a *solvability condition*, which is the number of satellites required to solve unbiased coordinate parameters. This follows from looking into the rank of the resulting system of observation Equations (1)–(2), and if it is not of full-rank more satellites are needed.

It is interesting to note that for instance $m_G = 3$ and $m_C = 2$ number of satellites are enough for positioning with a combined system, whereas with the same numbers it is impossible to position the receiver using the systems separately ($m_* \geq 4$ satellites required). A combined system thus gives the user more flexibility since the positioning requirements are less stringent. In order to illustrate this, we depict in Figure 2 the number of satellites for BeiDou, GPS and a combined system with 40 degrees cut-off elevation angle from our station CUTA in Perth, Western Australia, 7 July 2012. This is a reasonable cut-off angle in difficult areas such as urban canyons or open pit mines.

We see that with BeiDou and GPS only we will be able to position ourselves approximately 78 and 69 percent of the time respectively, whereas with the combined system we have the required number of satellites almost 100 percent of the time.

Table 3. Single-frequency SPP and the number of observations, unknowns, redundancy and solvability condition

Model/equation	# of observations	# of unknowns	Redundancy	Solvability condition
Single system (1)	m_*	4	$m_* - 4$	$m_* \geq 4$
Combined (2)	$m_G + m_C$	5	$m_G + m_C - 5$	$m_G + m_C \geq 5$

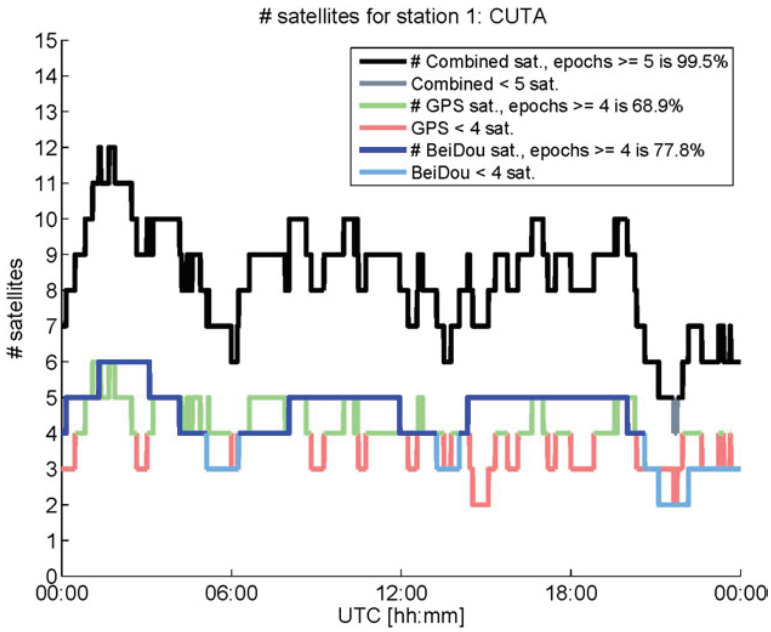

Figure 2. Satellite visibility for BeiDou, GPS and combined with 40 degree elevation cut-off angle for CUTA in Perth and 7 July 2012. Percentages given as the number of epochs above or equal to the required number of satellites as given in Table 3. Light green and dark blue represent GPS and BeiDou above or equal to four satellites respectively, light red and light blue are for below four satellites, and finally black and light grey is for the combined system above or equal to and below five satellites respectively.

3.2 SPP stochastic model

The stochastic model refers to the stochastic properties of the observables. We assume that the pseudorange observables are normally distributed and mutually uncorrelated; the variability of the observations can then be fully captured by its dispersion and be described by a diagonal variance-covariance (VCV) matrix. The following VCV-matrix will be used for a single-system SPP (1),

$$Q_0^* = \mathrm{diag}(f(E^1*), \ldots, f(E^m*)) \qquad (3)$$

where Q_0^* is the single-system VCV-matrix, 'diag' is a diagonal matrix, $f(E^{s*}) = (\sigma_0^*(1.02/(\sin(\mathrm{E}^{s*}) + 0.02)))^2$ the sine elevation-weighting function multiplied by σ_0^* the a-priori (known) range accuracy in zenith, and finally E^{s*} is the elevation angle of satellite $s* = 1*, \ldots, m*$ in degrees. For a combined system (2) we have the following VCV-matrix,

$$Q_0 = \mathrm{blkdiag}(Q_0^G, Q_0^C) \qquad (4)$$

where 'blkdiag' denotes a blockdiagonal matrix.

3.3 Single-frequency SPP results

In this section, SPP results are presented. Data from a static receiver named CUTA, one of Curtin's Continuously Operating Reference Stations, is analysed. The station is equipped with Trimble NetR9 multi-frequency multi-GNSS receiver.

Five days of data will be analysed, namely 7–11 July 2012, with 30 sec intervals between

Figure 3. Curtin CUTA (Left) and CUT0 (Right) GNSS antennas used.

consecutive measurements and 10 degrees of elevation cut-off angle. The BeiDou satellite orbit and clock products are provided by the GNSS centre of Wuhan University for this period, since broadcast data was not yet available. For GPS standard broadcast ephemerides are used, and the estimated positions are compared to very precise station benchmarks. The CUTA antenna is shown in Figure 3, together with a second receiver, CUT0, that we will use for RPP. CUT0 is equipped with a Trimble NetR9 receiver similar to CUTA. A typical sky plot, number of visible satellites and Positional Dilution Of Precision (PDOP), for GPS, BeiDou and combined BeiDou + GPS, are given in Figure 4.

The stochastic model settings for SPP are given in Table 4. The range accuracy in (3) holds for zenith and is dependent on the contributing error sources such as atmospheric errors, the code precision, type of receiver and frequency, the precision of the (broadcast) satellite coordinates and clocks, the precision of the Klobuchar ionospheric model, the Saastamoinen tropospheric model and satellite geometry. We used one day of data to find these stochastic settings in Table 4 by fitting the formal 95 percent confidence ellipse to the corresponding empirical ellipse; see further Figure 5. Then we applied these settings onto other days to independently check the validity of the stochastic model used.

In Figure 5 single-frequency B1 BeiDou, L1 GPS and B1 + L1 combined SPP results are given for CUTA and 7–11 July 2012, based on (2). In the figure we apply the Saastamoinen tropospheric model but ignore the ionosphere. Horizontal scatter plots are given with 95 percent confidence ellipses derived from the empirical and formal VCV-matrix of the positions. The empirical VCV-matrix is given by the positioning errors as derived from comparing the estimated positions to the precise benchmark coordinates, whereas the formal VCV-matrix is given from the mean of all single-epoch least-squares VCV-matrices of the entire observation time-span. All results are given in local North, East and Up. A good match between the two ellipses imply realistic assumptions on the stochastic model as given in Table 4, and that as a result we have a minimum variance estimator (Teunissen *et al.* 2008).

We see in Figure 5 that a larger standard deviation is obtained in North as compared to East when using BeiDou, due to the satellite geometry as depicted in Figure 4. Particularly the GEO satellites are all stationary over the day and located along the equator (Figure 1), and only a few satellites are located to the South for some periods. Since we ignore the ionosphere, we also see that the vertical positions are more biased as compared to GPS and we have large mean errors in the horizontal components of several meters for BeiDou, which are mitigated for the combined system. In other words errors from ionospheric delays are more prominent in the BeiDou data, due to the satellite geometry.

To further illustrate this we depict in Figure 6 (b) the ionosphere-estimated BeiDou positioning results using triple-frequency code-only measurements for 7 July 2012. The corresponding functional model is given and described in the next section and Equation (6). In Figure 6(a)

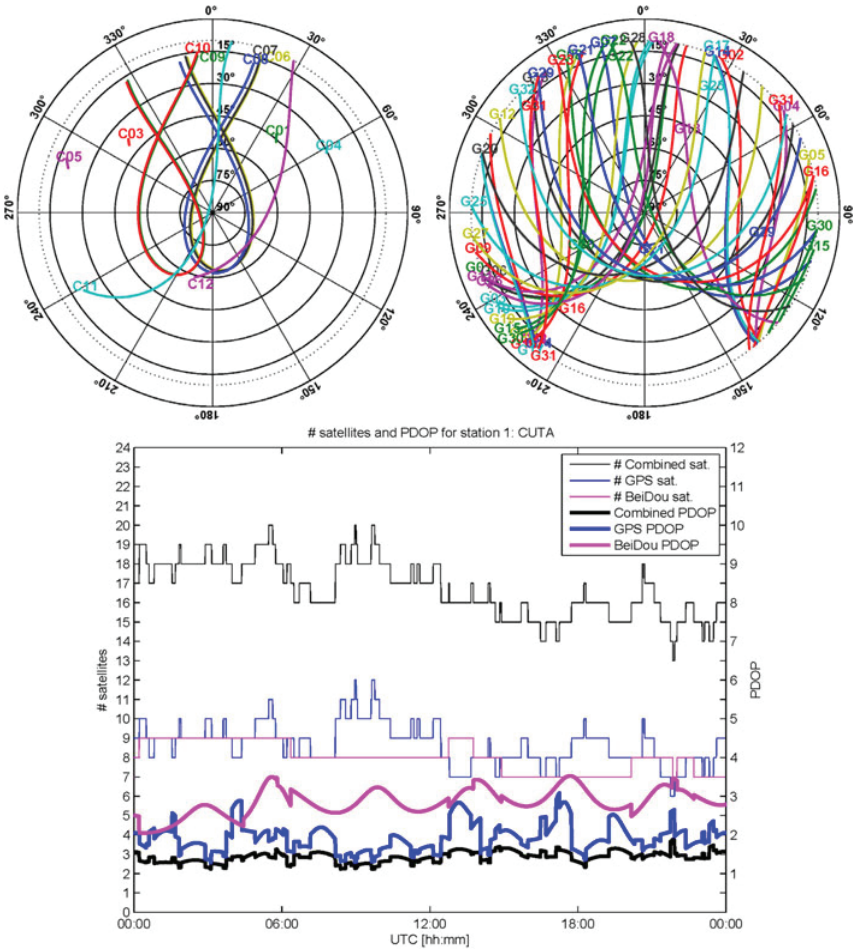

Figure 4. Satellite visibility for a combined system (Bottom) and skyplot of BeiDou (Left) and GPS (Right) with 10 degree elevation cut-off angle for CUTA in Perth and 7 July 2012.

the number of satellites, the North, East and Up formal standard deviations for each epoch (top), and single-frequency SPP results (without estimating ionosphere) (bottom) are depicted as well. The time is given in local Perth time UTC +8 h. We use a satellite elevation-weighting strategy in (3) and the resulting formal standard deviations thus mostly depend on the satellite geometry, number of satellites and the magnitude of the ignored slant ionospheric delays.

Table 4. Stochastic model settings for single-frequency SPP in (3)

System	Frequency	Range accuracy σ_0 [m]
GPS	L1	0.74
BeiDou	B1	1.63

In Figure 6(a) we see that the empirical B1 Up positioning error reached its largest peak during day time (around 13:00–14:00),

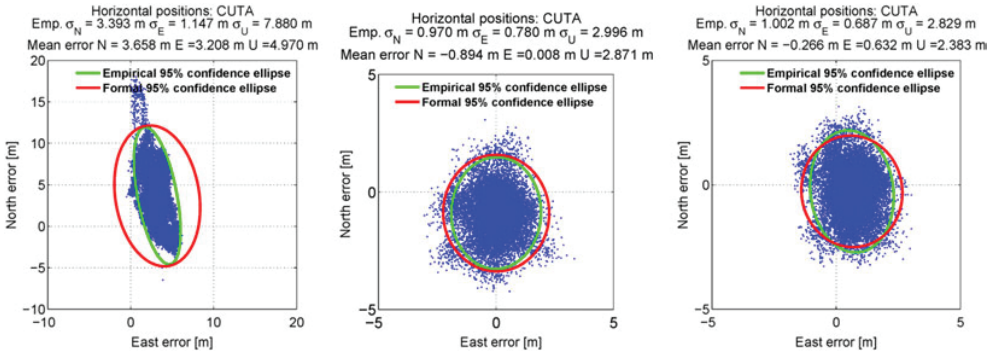

Figure 5. Ionosphere ignored SPP results (Left) B1 BeiDou, (Middle) L1 GPS, and (Right) B1,L1 BeiDou + GPS combined, based on (2). Empirical local North, East and Up mean and standard deviations, and 95 percent formal and empirical confidence ellipses, are given as well.

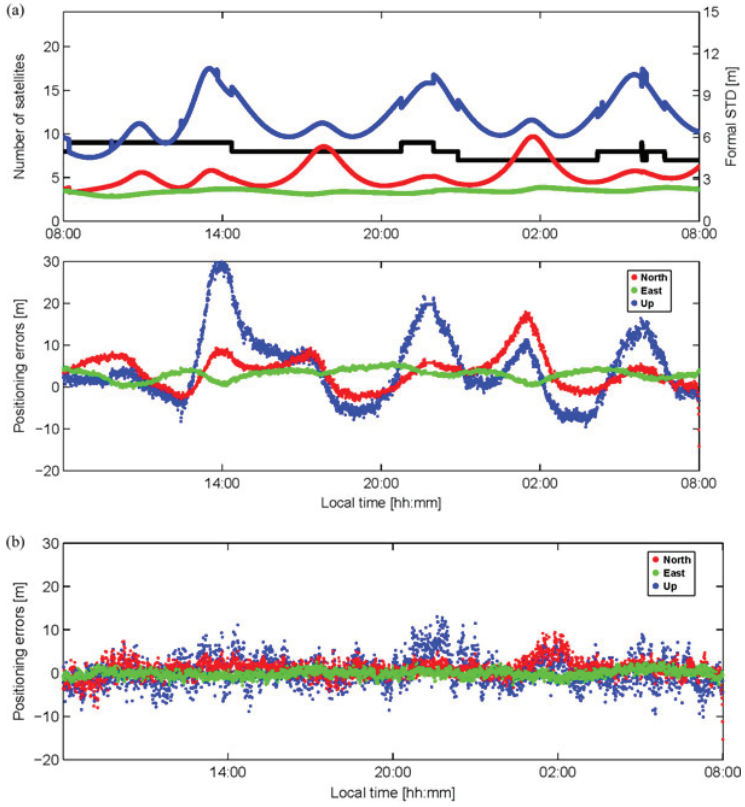

Figure 6. **B1** SPP results, number of satellites, formal standard deviations (a), and triple-frequency ionosphere-estimated (6) BeiDou positioning results (b) for CUTA and 7 July, UTC +8 h (local Perth time).

when we also expect more ionospheric activity as compared to night time. More importantly we see that the B1 positioning errors are well-reflected by the corresponding formal standard deviations, where the Up and North components vary more with larger magnitudes than the East component. In fact, the maximum peak of positioning errors is given when the formal standard deviations reach their maximum values. The ionosphere-estimated positioning model in Figure 6(b) reduces these effects significantly, and any remaining errors can be due to e.g. satellite clock and orbit errors (and multipath). In other words, when the satellite geometry becomes poor and the model is weak, the receiver becomes more sensitive to errors such as ionosphere. This effect is mitigated for the combined system (Figure 5) with the larger number of satellites and more robust satellite geometry with respect to our receivers (Figure 4).

All empirical SPP results are summarised in Table 5. When we applied the Klobuchar model we slightly improved the Up component for all systems as compared to ignoring it (not shown here). We have also looked at other receivers and we achieved similar SPP performance. However, we see in Table 5 larger biases in the East component for the combined system as compared to GPS, related to the ionospheric delays. We verify this in the ionosphere-estimated model in the next section (and Table 8), where the combined system and the East component become better than the corresponding GPS one.

4. Multi-frequency SPP with ionosphere estimation

In this section we present the functional model of SPP using multiple frequencies, and give the corresponding results based on the same data as in the previous section. The stochastic model that will be used has already been given in the previous section in (3) and (4).

4.1 Functional model

The ionosphere is a dispersive medium and the ionospheric range delay can be given as $I_r^{s_*} = 40.3\mathrm{TEC}/f_{j_*}^2$, where TEC is the line-of-sight total electron content. Using this fact one can either estimate the ionospheric delays on the first frequency and use μ_{j_*} to scale it to other frequencies, or form the dual-frequency (first-order) ionosphere-free code combination, where $\mu_{j_*} = f_{1_*}^2/f_{j_*}^2$.

The model when we estimate the ionospheric delays is also referred to as the 'ionosphere-float' model. We assume that satellite clocks, orbits and HW code delays on frequency $j_* = 1_*, 2_*$ are known. The system of observation equations, given in textbooks such as Teunissen and Kleusberg (1998), is, however, still rank defect. The number of rank defects is the number of linear combinations of the column vectors of the design matrix that produces the zero vector, of which the combinations are said to span the null space of the design matrix. These rank defects can be eliminated through an application of S-system theory (Teunissen 1984; Teunissen *et al.* 2010), implying null-space

Table 5. Single-frequency SPP results for BeiDou/GPS and combined

System/frequency	Mean error N [m]	STD N [m]	Mean error E [m]	STD E [m]	Mean error U [m]	STD U [m]
BeiDou B1, iono ignored	3.658	3.393	3.208	1.147	4.970	7.880
GPS L1, iono ignored	−0.894	0.970	0.008	0.780	2.871	2.996
COMBINED B1,L1 iono ignored	−0.266	1.002	0.632	0.687	2.383	2.829

Note: Positioning error results are for CUTA and 7–11 July 2012, with empirical mean and standard deviations in local North, East and Up.

identification, S-basis constraining and proper interpretation of the estimable parameters. We have the following number of rank deficiencies for a single-system,

$$\#\text{ of rank defects is } f_* \tag{5}$$

To eliminate these rank deficiencies we choose to fix the receiver HW code delays on all frequencies f_*. We get for $j_* = 2_*, \ldots, f_*$ frequencies and for a *single-system* the following full-rank system of observation equations,

$$p^{s*}_{r,j*} = -c_r^{s*\,T}\Delta x_r + \mathrm{d}\tilde{t}_r + \mu_{j*}\tilde{I}_r^{s*} \tag{6}$$

where the estimable unknowns are, from left to right: receiver coordinates Δx_r, a receiver clock $\mathrm{d}\tilde{t}_r$ and ionospheric delays $\tilde{I}_r^{s*}$ that are biased by receiver HW code delays on the first and second frequency (see e.g. Zhang *et al.* (2011)). We assume the third frequency and beyond estimable satellite HW code delays to be zero (for their interpretation see e.g. Henkel *et al.* (2011)), but as we will see in the results section there is a slight improvement if we parameterise them. The number of rank deficiencies and S-basis for a combined system are obtained by taking (5) for GPS and BeiDou as,

$$\#\text{ of rank defects is } f_G + f_C \tag{7}$$

For a *combined system* we then have the following compact form of system of observation equations, with the vector of ionospheric delays $\tilde{I}_r^* = [\tilde{I}_r^{1*}, \ldots, \tilde{I}_r^{m_*}]^{\mathrm{T}}$ that gives,

$$y_p = B_1 \cdot \Delta x_r + B_2 \cdot \begin{bmatrix} \mathrm{d}\tilde{t}_r^G \\ \mathrm{d}\tilde{t}_r^C \end{bmatrix} + B_3 \cdot \begin{bmatrix} \tilde{I}_r^G \\ \tilde{I}_r^C \end{bmatrix} \tag{8}$$

where $y_p = \left[y_p^{GT}, y_p^{CT}\right]^{\mathrm{T}}$ contains code observables of the two systems on multiple frequencies $y_p^* = \left[y_{p;1*}^{*T}, \ldots, y_{p;f*}^{*T}\right]^{\mathrm{T}}$, $B_1 = \begin{bmatrix} e_{f_G} \otimes G_r^G \\ e_{f_C} \otimes G_r^C \end{bmatrix}$ corresponds to the partial design matrix of the receiver coordinates, $B_2 = \begin{bmatrix} e_{f_G} \otimes e_{m_G} & 0 \\ 0 & e_{f_C} \otimes e_{m_C} \end{bmatrix}$ to the receiver clocks, and $B_3 = \begin{bmatrix} \mu_G \otimes I_{m_G} & 0 \\ 0 & \mu_C \otimes I_{m_C} \end{bmatrix}$ to the ionospheric delays, where e_{f_*}, e_{m_*} is the f_* and m_* dimensional column vectors with all elements of 1, $\otimes$ is the Kronecker product as given by Rao (1973), μ_* is a column vector of size $f_* \times 1$ that contains all μ_{j_*} for $j_* = 1_*, \ldots, f_*$, and I_{m_*} is the identity matrix of size m_*. We emphasise again that we can parameterise the satellite HW code delays on the third frequency and beyond as well, but here assume them to be zero.

The redundancy and solvability condition of the systems of Equations (6) and (8) are given in Table 6. We see that when we have

Table 6. Multiple-frequency ionosphere-float SPP and the number of observations, unknowns, redundancy and solvability condition

Model/equation	# of observations	# of unknowns	Redundancy	Solvability condition
				$f_* \geq 2$
Single system (6)	$f_* m_*$	$4 + m_*$	$f_* m_* - (4 + m_*)$	$m_* \geq 4$
Parameterise satellite HW delays for $f_* \geq 3$	$f_* m_*$	$4 - m_* + f_* m_*$	$m_* - 4$	$m_* \geq 4$
Combined system (8)	$f_G m_G + f_C m_C$	$5 + m_G + m_C$	$f_G m_G + f_C m_C - (5 + m_G + m_C)$	$m_G + m_C \geq 5$
Parameterise satellite HW delays for $f_* \geq 3$	$f_G m_G + f_C m_C$	$5 - m_G - m_C + f_G m_G + f_C m_C$	$m_G + m_C - 5$	$m_G + m_C \geq 5$

three or more frequencies and if we parameterise the satellite HW code delays, we reduce the redundancy with $(f_* - 2)m_*$ for the single-system, and $(f_G - 2)m_G + (f_C - 2)m_C$ for the combined system. In other words, there is a tradeoff between redundancy and estimating the satellite HW code delays (which might bias our estimated positions).

Table 7. Stochastic model settings for multiple-frequency SPP in (3)

System	Frequency	Range accuracy σ_0 [m]
GPS	L1	0.50
	L2	0.50
BeiDou	B1	0.35
	B2	0.35
	B3	0.35

4.2 Ionosphere-float positioning results

In this section we will evaluate the ionosphere-float positioning models. The stochastic settings for these scenarios are given in Table 7.

We give positioning results when we estimate the ionosphere in Figure 7, based on (6) and (8) respectively.

All coordinate component standard deviations improve as compared to those of GPS and BeiDou for the combined system. Moreover we have a better fit of the empirical ellipses to the estimated positions as compared to the single-frequency SPP results in Figure 5, since the ionospheric delays have now been estimated. The ionosphere-float BeiDou standard deviations are now even better than the corresponding GPS results, and this is due to the satellite clock and orbit products used (BeiDou is based on precise post-processed products and GPS on broadcast data). This is also reflected in our stochastic model settings in Table 7 and verified in the following section for RPP. We note though that if the BeiDou navigation data had been available as of July 2012, with comparable accuracy to the GPS orbits and clocks, the ionosphere-float positioning accuracy would have been better for GPS. This is because the number of visible GPS satellites is here larger and the satellite geometry stronger as compared to BeiDou (Figure 4) together with comparable code precision (Table 10). Nevertheless, we see large biases in particularly the North and Up components for BeiDou and the combined system of several dm, and this is due to multipath effects (see RPP and the discussion in relation to Figures 9–11).

We summarise all ionosphere-float positioning results in Table 8, and in parenthesis

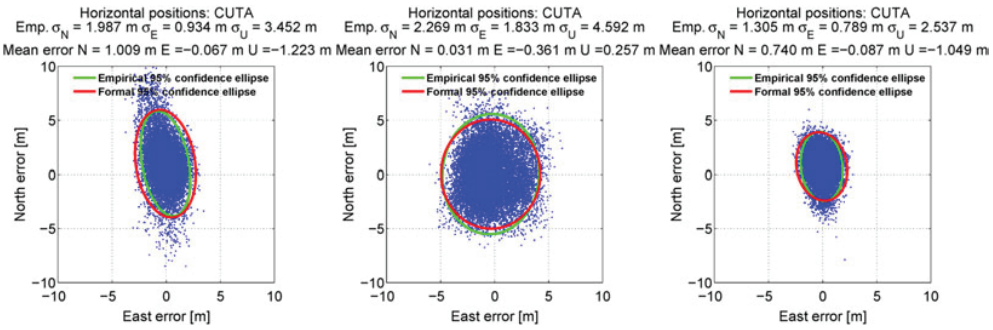

Figure 7. Ionosphere-float positioning for (Left) Triple-frequency BeiDou, (Middle) dual-frequency GPS and (Right) BeiDou + GPS combined, based on (8). Empirical local North, East and Up mean and standard deviations, and 95 percent formal and empirical confidence ellipses, are given as well.

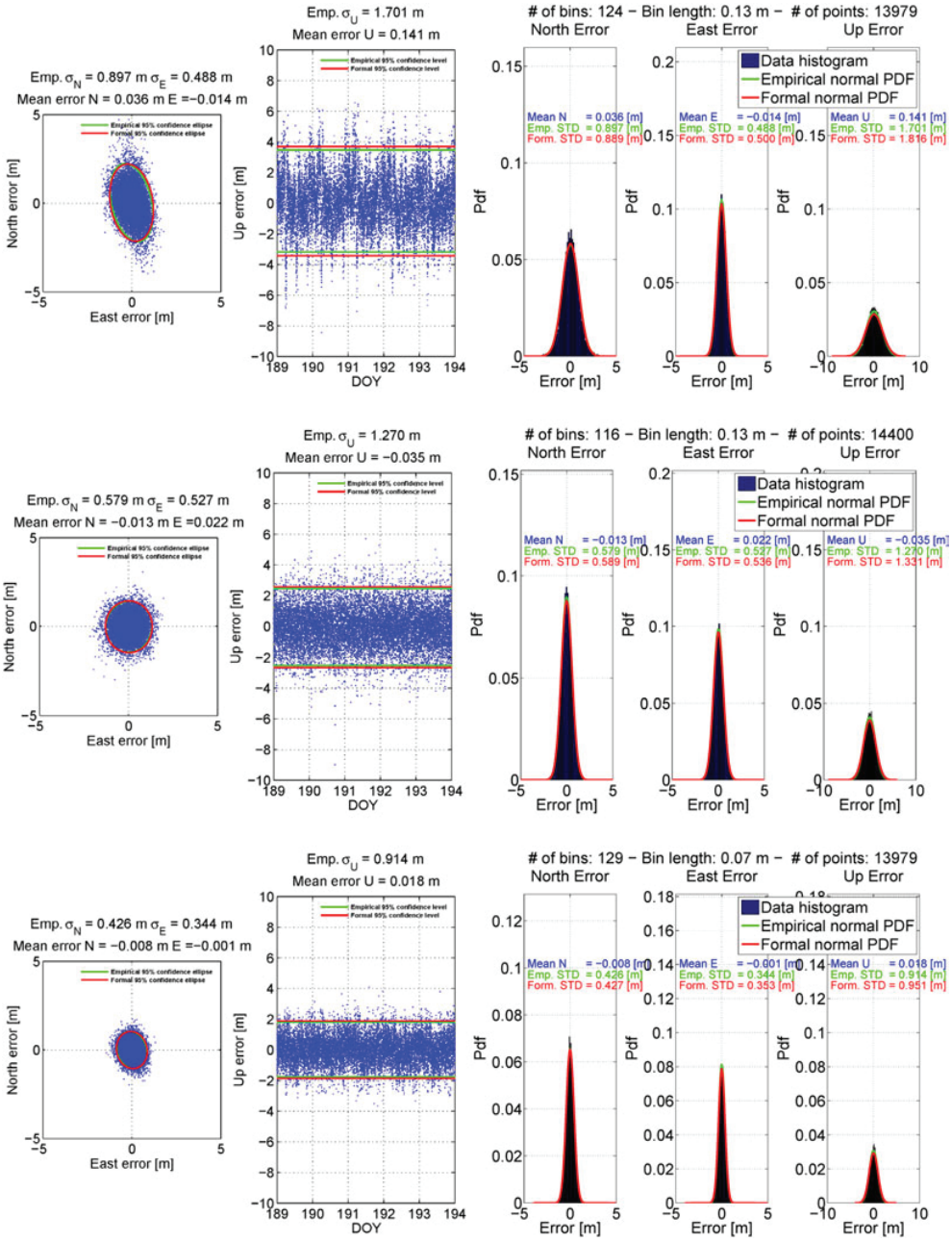

Figure 8. **Between-receiver SD** B1 BeiDou (Top), L1 GPS (Middle), and B1, L1 BeiDou + GPS combined (Bottom) positioning results for CUT0-CUTA based on (12). Empirical local North, East and Up mean and standard deviations, with 95 percent formal and empirical confidence ellipses/levels.

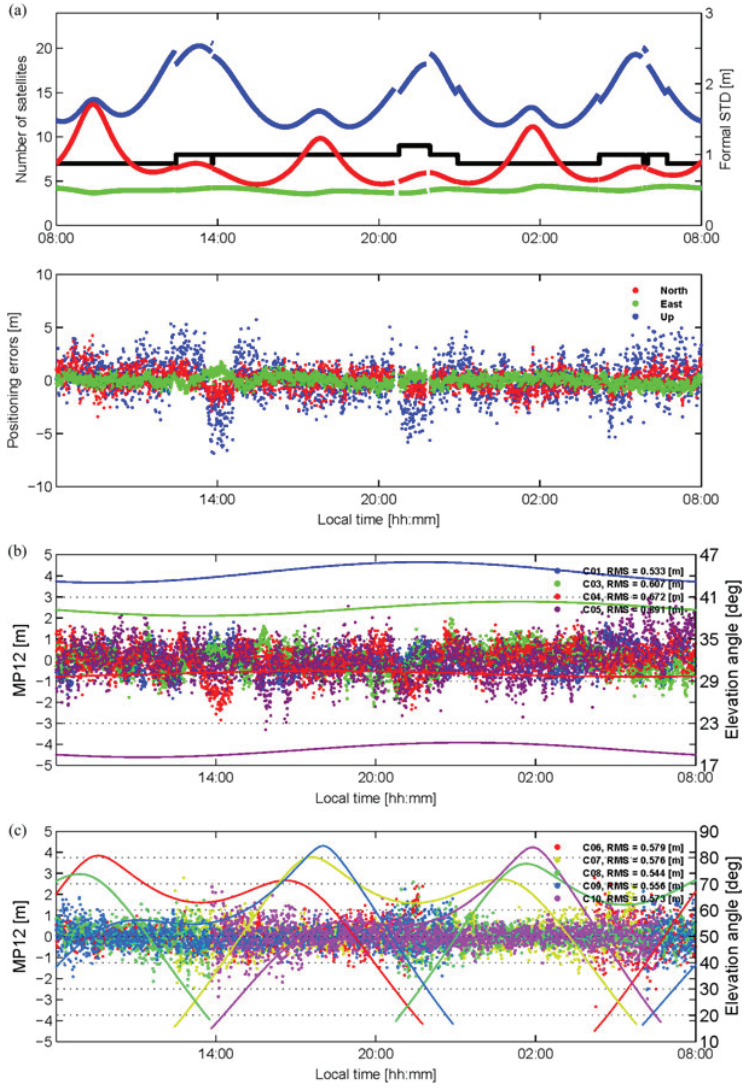

Figure 9. SD B1 BeiDou positioning results and formal standard deviations (a) together with the SD multipath combination (b) and (c) for 7 July 2012.

we give positioning results based on day-differences between coordinates as well, using the stochastic model settings in Table 10. By performing these day-differences with a time separation of 23 h and 56 min, similar to the GPS satellite constellation repeatability period (Axelrad *et al.* 2005), the multipath effects can be significantly reduced. The IGSO satellites have the same repeatability as GPS (Jiang *et al.* 2011), and the GEO satellites are (almost) stationary. It is, however, still an approximation as different satellites can have repeatability period shifts other than 4 min (Axelrad *et al.* 2005). Any daily repeatability caused by

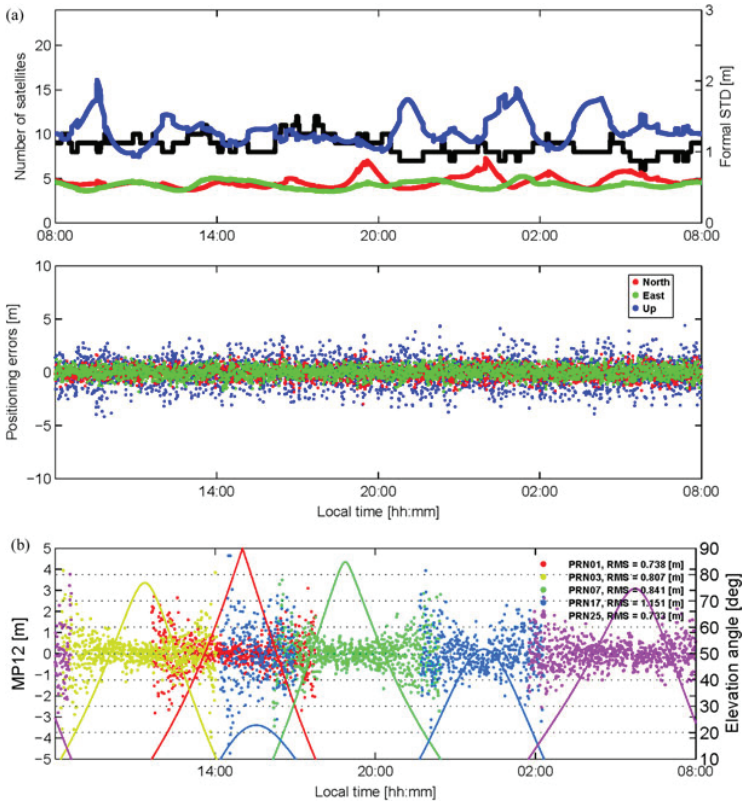

Figure 10. **SD L1 GPS** positioning results and formal standard deviations (a) together with SD multipath combination (b) for 7 July 2012.

satellite orbit/clock errors and third-frequency estimable satellite HW delays will then also be removed. Results when parameterising the third-frequency estimable satellite HW code delays in (6) and (8) are also given in Table 8.

The mean errors are reduced by the day-differences from several dm with multipath effects, down to a few cm for all systems without, and the standard deviations decrease for almost all coordinate components and all systems. The BeiDou and combined system Up and North errors slightly improve up to a few dm when parameterising the satellite HW delays for the undifferenced case. The combined system further provides us standard deviation improvements of approximately 48 percent as an average of North, East and Up components and as compared to GPS. Corresponding values compared to BeiDou are 22 percent.

5. Between-receiver single-differenced relative positioning for short baselines (RPP)

In this section we assume that we have two receivers observing the same satellites at the same time instant, with external products for satellite orbits available. We give the corresponding results as well.

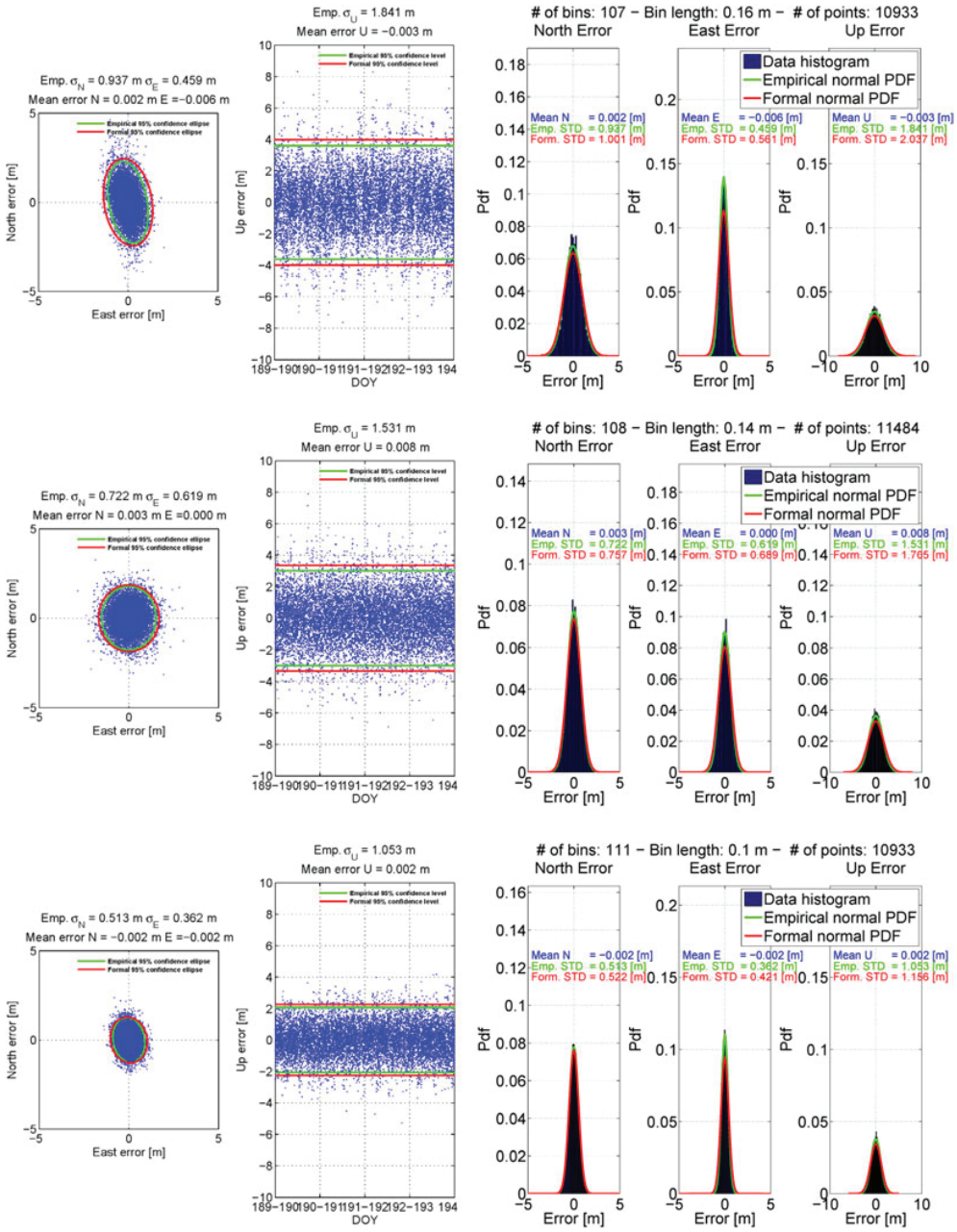

Figure 11. Day-differences on between-receiver SD B1 BeiDou (Top), L1 GPS (Middle), and B1, L1 BeiDou + GPS combined (Bottom) results for CUT0-CUTA based on (12). Empirical local North, East and Up mean and standard deviations, with 95 percent formal and empirical confidence ellipses/levels.

Table 8. Multiple-frequency ionosphere-float results for BeiDou/GPS and combined

System	Mean error N [m]	STD N [m]	Mean error E [m]	STD E [m]	Mean error U [m]	STD U [m]
BeiDou triple frequency	1.009 (−0.013)	1.987 (1.717)	−0.067 (0.046)	0.934 (0.895)	−1.223 (0.031)	3.452 (3.298)
GPS dual frequency	0.031 (−0.030)	2.269 (1.575)	−0.361 (−0.018)	1.833 (1.421)	0.257 (0.031)	4.592 (3.831)
COMBINED	0.740 (0.000)	1.305 (1.091)	−0.087 (0.016)	0.789 (0.761)	−1.049 (0.008)	2.537 (2.424)
Parameterise $f_* \geq 3$ satellite HW delays						
BeiDou triple frequency	0.921 (−0.011)	1.942 (1.701)	−0.174 (0.045)	0.919 (0.884)	0.248 (0.034)	3.142 (3.251)
COMBINED	0.577 (−0.001)	1.312 (1.089)	−0.165 (0.015)	0.802 (0.761)	−0.048 (0.009)	2.457 (2.419)

Note: Positioning error results are for CUTA and 7–11 July 2012, with empirical mean and standard deviations in local North, East and Up. In parenthesis day-difference statistics are given.

5.1 Functional model

The between-receivers single differences (SDs) that we will use in this section will be with respect to a pivot receiver 1. The relative atmospheric delays for significantly short baselines of a few km can then be considered negligibly small. Consequently parameterisation of these delays is not necessary, and we will accordingly improve the model strength with increased redundancy by omitting them. Any remaining errors from satellite orbits/clocks and HW delays are also eliminated. We refer to this model as the Relative Point Positioning (RPP) functional model. We have the following number of rank deficiencies for a single system,

$$\#\text{ of rank defects is } 5 + f_* \tag{9}$$

All rank deficiencies are eliminated by fixing pivot receiver 1 clock, coordinates and HW code delays on all frequencies, and receiver 2 HW code delays on the first frequency. We then have full-rank observation equations for the *single system* given as,

$$p^{s*}_{12,j*} = -c_2^{s*\,T}\Delta x_{12} + \mathrm{d}\tilde{r}_{12} \tag{10}$$

where $(\cdot)_{12} = (\cdot)_2 - (\cdot)_1$ is the notation for between-receiver SDs for receivers 1 and 2, and the estimable unknowns' corresponding interpretation is given in detail in e.g. Odijk *et al.* (2012). From left to right in (10) we have: relative receiver coordinates Δx_{12} and a relative receiver clock $\mathrm{d}\tilde{r}_{12}$ biased by receiver HW code delays on $j_* = 1_*$. We can also parameterise relative receiver Differential Code Biases (DCBs) in (10) for $f_* \geq 2$ frequencies, and the effect on the positioning results when doing so will be described in the following results section. For the combined system we share the three receiver coordinates and thus get the number of rank deficiencies and S-basis by taking (9) for GPS and BeiDou

Table 9. Between-receivers SDs (RPP) and the number of observations, unknowns, redundancy and solvability condition for two receivers

Model/equation	# of observations	# of unknowns	Redundancy	Solvability condition
Single system (10)	$f_* m_*$	4	$f_* m_* - 4$	$m_* \geq 4$
Parameterise DCBs	$f_* m_*$	$4 + f_* - 1$	$f_*(m_* - 1) - 3$	$m_* \geq 4$
Combined system (12)	$f_G m_G + f_C m_C$	5	$f_G m_G + f_C m_C - 5$	$m_G + m_C \geq 5$
Parameterise DCBs	$f_G m_G + f_C m_C$	$5 + f_G - 1 + f_C - 1$	$f_G(m_G - 1) + f_C(m_C - 1) - 3$	$m_G + m_C \geq 5$

and subtract 3,

$$\#\text{ of rank defects is } 7 + f_G + f_C \tag{11}$$

After solving the rank deficiencies we have the following compact form of the full-rank observation equations for a *combined system*,

$$y_{p_{12}} = B_1 \cdot \Delta x_{12} + B_2 \cdot \begin{bmatrix} \mathrm{d}\tilde{t}_{12}^{G} \\ \mathrm{d}\tilde{t}_{12}^{C} \end{bmatrix} \tag{12}$$

with $y_{p_{12}}$ the SD code observables on single or multiple frequencies, B_1 contains the line-of-sight unit vectors of receiver 2, and B_2 is the partial design matrix for the system-specific receiver clocks as already described in relation to (8). We see a resemblance between (10) and (12) and the functional model in (1) and (2) for single-frequency SPP, with the difference that in (10) and (12) we estimate relative receiver coordinates and clock and that all atmospheric delays, satellite orbit/clock errors and HW delays have been eliminated.

The number of observations, unknowns, redundancy and solvability condition are given in Table 9. We see that we decrease the redundancy by $(f_* - 1)$ if we parameterise DCBs for a single system, and with $(f_G - 1) + (f_C - 1)$ for the combined system.

5.2 RPP results

The second receiver we will use in addition to CUTA is named CUT0, and the distance between the stations is 8 m (Figure 3). The stochastic model settings for SDs (12) are given in Table 10. In the table we include day-differences (epoch-differences (ED)) as well, which reduce multipath effects, and the remaining noise is then dominated by receiver code noise.

Single-frequency B1, L1 and B1 + L1 SD results are depicted in Figure 8, together with the vertical positions and 95 percent formal and empirical confidence levels as well. We also give positioning histograms together with the theoretical empirical and formal normal distributions. The theoretical normal distributions and the vertical confidence levels are computed by the standard deviations from the formal and empirical VCV-matrices, and the mean is taken as the mean of the positioning errors.

Larger standard deviations are depicted in Figure 8 for North as compared to the East component for BeiDou, again related to the large fraction of GEO satellites along the equator. The Up component is further biased with a mean error of approximately 1.4 dm for BeiDou (and 3.5 cm for GPS), and we have a

Table 10. Stochastic model settings for SDs and ED (day-differences) for CUT0 and CUTA in (3)

System	Frequency	Range accuracy SD σ_0 [m]	Range accuracy SD + ED σ_0 [m]
GPS	L1	0.30	0.28
	L2	0.22	0.20
BeiDou	B1	0.27	0.21
	B2	0.27	0.21
	B3	0.22	0.16

periodic behaviour that repeats between days (for BeiDou) as well, due to multipath effects.

We therefore depict a single-channel linear geometry- and atmosphere-free code and phase multipath combination (see Equations (2) and (3) in de Bakker *et al.* (2011)) in Figure 9(b)–(c) for BeiDou, and Figure 10(b) for GPS, and 7 July 2012 (in local Perth time). The multipath combinations are given on the between-receiver SD level together with their corresponding root-mean-square (RMS) and satellite elevation angles. We further show in Figures 9(a) and 10(a) the number of satellites, North, East and Up formal standard deviations and the SD single-frequency B1 and L1 empirical positioning results respectively. Any gaps visible in the time series are due to the same-satellites-in-view restriction between the receivers. The multipath combinations are dominated by B1 and L1 code noise and multipath errors.

The multipath combinations show large fluctuations when the corresponding satellites reach a low elevation angle (e.g. C10 in Figure 9(c) and PRN17 in Figure 10(b) and around 14:00 local time). Moreover the C04 and C05 satellites, with the lowest elevations of all GEO satellites (see Figure 4), also give the largest RMS values among all BeiDou satellites in Figure 9(b). Most importantly and similarly to Figure 6 in the single-frequency SPP results, when there is a maximum peak of the BeiDou formal standard deviations we have the largest corresponding positioning errors in Figure 9(a). Specifically we see these peaks at approximately 14:00, 21:00 and 05:00 local Perth time, when some IGSO satellites rise or set with respect to the receiver. For GPS in Figure 10(a) on the other hand, the formal standard deviations are smaller since the satellite geometry is better than for BeiDou with respect to our receivers, and the influence of multipath effects on the positioning results is thus mitigated significantly.

We take day-differences on the SD results in Figure 8 and depict them in Figure 11. These day-differences can give us a more honest description of the BeiDou performance (without multipath effects). We see in Figure 11 mean positioning errors of at most a few mm as compared to several cm for the SD results in Figure 8. More importantly we see more similar empirical standard deviations for BeiDou and GPS as compared to the SDs in Figure 8. This implies that once we have more BeiDou satellites and thus a better satellite geometry, the positioning performance can be more fairly compared to that of GPS.

In Table 11 we summarise the SD results for varying numbers of frequencies, and in parenthesis we give the corresponding day-differenced statistics as well (to remove multipath effects). In the table we do not give results with parameterisation of DCBs in (12), since we could not see any difference in the positioning results as compared to ignoring them. This is because we have the same receiver types and expect the between-receiver differenced DCB to be so small that the relatively large redundancy mitigates the impact from them. The between-receiver DCBs for the receiver-types we use in this contribution are expected to reach a few mm (Steigenberger *et al.* 2012). However, we see in Table 11 that the positioning results well reflect our stochastic model settings in Table 10 and that the combined system with triple-frequency BeiDou and dual-frequency GPS gives the best precision of all combinations, due to the highest possible redundancy (Table 9).

6. Summary and conclusions

In this Part I we have studied the use of BeiDou, GPS and combined BeiDou + GPS for single- and multiple-frequency (single-receiver and relative) code-only positioning. We recall the single-receiver model as Single-Point Positioning (SPP), and the model with two receivers as Relative Point Positioning (RPP). In Part II, we will focus our attention on the single-baseline RTK model performance. We can summarise our findings and conclusions as follows.

Table 11. Between-receivers SD positioning (RPP) results for BeiDou/GPS and combined

System	Mean error N [m]	STD N [m]	Mean error E [m]	STD E [m]	Mean error U [m]	STD U [m]
Single frequency						
BeiDou						
B1	0.036 (0.002)	0.897 (0.937)	−0.014 (−0.006)	0.488 (0.459)	0.141 (−0.003)	1.701 (1.841)
B2	−0.037 (−0.006)	0.836 (0.909)	−0.097 (0.011)	0.513 (0.440)	−0.164 (−0.024)	1.600 (1.555)
B3	−0.212 (−0.010)	0.614 (0.671)	0.097 (−0.001)	0.324 (0.321)	−0.051 (−0.031)	1.160 (1.096)
GPS						
L1	−0.013 (0.003)	0.579 (0.722)	0.022 (0.000)	0.527 (0.619)	−0.035 (0.008)	1.270 (1.531)
L2	0.004 (0.002)	0.430 (0.531)	−0.040 (−0.002)	0.409 (0.466)	0.015 (0.002)	0.964 (1.202)
COMBINED						
B1 + L1	−0.008 (−0.002)	0.426 (0.513)	−0.001 (−0.002)	0.344 (0.362)	0.018 (0.002)	0.914 (1.053)
B2 + L2	0.005 (0.000)	0.347 (0.417)	−0.061 (0.003)	0.311 (0.315)	−0.038 (−0.002)	0.769 (0.878)
B3 + L2	−0.055 (0.000)	0.322 (0.383)	0.013 (−0.002)	0.259 (0.262)	0.092 (−0.009)	0.676 (0.780)
Multiple frequency						
BeiDou						
B1 + B2	0.000 (−0.002)	0.604 (0.683)	−0.056 (0.003)	0.349 (0.326)	−0.012 (−0.014)	1.183 (1.247)
B1 + B2 + B3	−0.089 (−0.006)	0.507 (0.587)	0.008 (0.001)	0.296 (0.281)	−0.029 (−0.022)	0.964 (1.001)
GPS						
L1 + L2	−0.002 (0.002)	0.360 (0.449)	−0.018 (−0.001)	0.336 (0.390)	−0.003 (0.004)	0.798 (0.993)
COMBINED						
B1,B2 + L1,L2	0.000 (−0.001)	0.278 (0.339)	−0.036 (0.001)	0.235 (0.247)	−0.013 (−0.001)	0.608 (0.694)
B1,B2,B3 + L1,L2	−0.031 (−0.001)	0.261 (0.329)	−0.009 (0.000)	0.214 (0.223)	0.023 (−0.006)	0.557 (0.638)

Note: Positioning error results are for CUT0-CUTA and 7–11 July 2012, with empirical mean and standard deviations in local North, East and Up. In parenthesis day-difference statistics are given.

6.1 Satellite availability

We found that with a 40 degree elevation cut-off angle (reasonable in urban canyons or open pit mines) a combined BeiDou + GPS system made it possible to position our CUTA receiver in Perth almost 100 percent of the time over the day (Figure 2). For BeiDou and GPS separately, on the other hand, we could only position the receiver approximately 78 and 69 percent of the time respectively.

6.2 Single-frequency single-point positioning

The single-frequency SPP results (Table 5), with 10 degrees of cut-off elevation angle, revealed larger biases in the horizontal components and Up component for BeiDou, as compared to GPS and the combined system (Figure 5). These effects were due to ionospheric delays and the large fraction of satellites located to the North and along the equator (four GEO satellites), with only a few satellites to the South of our Perth stations for some periods (Figure 1). This satellite geometry also gives less precise BeiDou North component as compared to East. The poorer the satellite geometry the more sensitive the receiver becomes to the presence of errors such as ionosphere effects, and when estimating the ionosphere with multiple frequencies we decreased these effects significantly (Figure 6).

6.3 Multiple-frequency ionosphere-float SPP

The BeiDou ionosphere-estimated (ionosphere-float) empirical positioning standard deviations turned out to be even better than the corresponding GPS ones, and this was due to the satellite clock and orbit products used (BeiDou was based on precise post-processed products and GPS on broadcast data). The combined system provided standard deviation improvements of approximately 48 percent as an average of North, East and Up components and as compared to GPS (Table 8). The corresponding value as compared to BeiDou was 22 percent. We also showed that a parameterisation of the third-frequency satellite HW code delays for BeiDou can improve the North and Up components by up to a few dm.

6.4 Relative point positioning

For short baselines and between-receivers SD relative positioning (RPP), only the relative receiver coordinates and clock (and optionally receiver Differential Code Biases (DCBs)) need to be estimated. The improvements for single-frequency B1 + L1 and a combined system (Table 11) were, as an average for all coordinate component standard deviations, 30 percent as compared to GPS and 43 percent as compared to BeiDou. The multiple-frequency combined system, with the highest possible redundancy, gave as expected the best possible accuracy of all positioning modes. A periodic and daily repeatable behaviour was, however, seen in the BeiDou Up positioning results due to multipath effects (Figures 8 and 9). We significantly reduced these effects by taking day-differences between coordinates with a time separation of 23 h and 56 min, similar to the satellite constellation repeatability period, and we decreased our mean errors from cm-dm level down to at most a few mm for all systems (Figure 11).

We can shortly summarise our findings in terms of obtainable BeiDou/GPS positioning accuracies as follows:

1. We can expect several meters in positioning error standard deviations for single-frequency SPP, with larger horizontal and vertical standard deviations and mean errors for BeiDou as compared to GPS due to the satellite geometry in combination with ionospheric delays. The combined system mitigates these effects significantly (Table 5).
2. If we estimate the ionosphere with multiple-frequency SPP, we can expect

more comparable BeiDou and GPS results and standard deviations at the level of 1–2 m in the horizontal and 3–4 m in the vertical component (Table 8). The combined system improves these standard deviations to approximately 1 m in the horizontal and 2.5 m in the vertical.

3. For single-frequency RPP we can expect standard deviations below 1 m in the horizontal components and in the range of 1–2 m in the vertical for GPS and BeiDou separately. For a combined system these values are below 0.5 m in the horizontal components and below 1 m in the vertical (Table 11).
4. For multiple-frequency RPP we reached standard deviations around 0.5 m in the horizontal components and around 1 m in the vertical for the single systems, whereas for a combined system these values are below 0.3 m in the horizontal and slightly above 0.5 m in the vertical (Table 11).

In 2020 a full constellation of BeiDou will be a reality, and a combined BeiDou + GPS system will then most certainly improve the accuracy and positioning robustness even further. The regional BeiDou system is already suitable as a complementary or stand-alone positioning system for Australia. In Part II we will investigate single-baseline RTK positioning performance and instantaneous carrier-phase integer ambiguity resolution, which also depend on the number of satellites, satellite geometry and the code quality.

References

Astronautica Encyclopedia (2012) Beidou. *Encyclopedia Astronautica*. Available from: http://www.astronautix.com/craft/beidou.htm, (accessed 27 December 2012).

Axelrad, P., Larson, K., & Jones, B. (2005) Use of the correct satellite repeat period to characterize and reduce site-specific multipath errors, *Proceedings of ION GNSS*, Long Beach, CA, 13–16 September 2005.

Cao, W., O'Keefe, K., & Cannon, M.E. (2008) Evaluation of COMPASS ambiguity resolution performance using geometric-based techniques with comparison to GPS and Galileo, *Proceedings of ION GNSS*, Savannah, GA, 16–19 September 2008.

Chen, H., Huang, Y., Chiang, K., Yang, M., & Rau, R. (2009) The performance comparison between GPS and BeiDou-2/COMPASS: a perspective from Asia. *Journal of the Chinese Institute of Engineers*, vol. 32, no. 5, pp. 679–689.

CSNO (2011) *BeiDou Navigation Satellite System Signal In Space Interface Control Document (Test Version) by China Satellite Navigation Office (CSNO)*. Technical report, December. 9 pages, 2011.

CSNO (2012) *BeiDou Navigation Satellite System Signal In Space Interface Control Document by China Satellite Navigation Office (CSNO)*. Open service signal B1I (Version 1.0). Technical report, December. 77 pages, 2012.

de Bakker, P.F., Tiberius, C.C.J.M., van der Marel, H., & van Bree, R.J.P. (2011) Short and zero baseline analysis of GPS L1 C/A, L5Q, GIOVE E1B, and E5aQ signals. *GPS Solutions*, vol. 16, no. 1, pp. 53–64.

Grelier, T., Ghion, A., Dantepal, J., Ries, L., DeLatour, A., Issler, J.-L., Avila-Rodriguez, J., Wallner, S., & Hein, G. (2007) Compass signal structure and first measurements, *Proceedings of ION GNSS*, pp. 3015–3024, Fort Worth, TX, September 2007.

Han, C., Yang, Y., & Cai, Z. (2011) Beidou navigation satellite system and its time scales. *Metrologia*, vol. 48, no. 4, pp. S213–S218, doi:10.1088/0026-1394/48/4/S13.

Henkel, P., Wen, Z., & Gunther, C. (2011) Method for determining code and phase biases of satellite signals. *European Patent Application Applicant: Technische Universität München*, European patent office, 22 June 2011.

Huang, Y.-S., & Tsai, M.-L. (2008) The impact of Compass/Beidou-2 on future GNSS: A perspective from Asia, *Proceedings of ION GNSS*, pp. 2227–2238, Savannah, GA, September 2008.

Jiang, Y., Yang, S., Zhang, G., & Li, G. (2011) Coverage performance analysis on combined-GEO-IGSO satellite constellation. *Journal of Electronics*, vol. 2, pp. 28.

Klobuchar, J.A. (1987) Ionospheric time-delay algorithm for single-frequency GPS users.

IEEE Transactions on Aerospace and Electronic Systems, vol. AES-23, no. 3, pp. 325–331.

Langley, R.B. (2011) Beidou/Compass declared operational, test ICD released. GPS World, *GNSS News*, Available from: http://www.gpsworld.com/, published 27 December 2011, accessed 28 December 2011, December 2011.

Misra, P., & Enge, P. (2006) *Global Positioning System: Signals, Measurements and Performance*, Ganga-Jumana Press, Lincoln, MA.

Montenbruck, O., Hauschild, A., Steigenberger, P., Hugentobler, U., & Riley, S. (2012a) A COMPASS for Asia: first experience with the BeiDou-2 regional navigation system, *Proceedings of IGS Workshop*, July 23–27, Olsztyn, Poland, 2012.

Montenbruck, O., Hauschild, A., Steigenberger, P., Hugentobler, U., Teunissen, P.J.G., & Nakamura, S. (2012b) Initial assessment of the COMPASS/BeiDou-2 regional navigation satellite system. *GPS Solutions*, vol. 17, no. 2, pp. 211–222.

Odijk, D., Teunissen, P.J.G., & Zhang, B. (2012) Single-frequency integer ambiguity resolution enabled precise point positioning. *Journal of Surveying Engineering*, vol. 138, no. 4, pp. 193–202.

Rao, C.R. (1973). *Linear Statistical Inference and its Applications*, 2nd ed. Wiley, New York.

Shi, C., Zhao, Q., Hu, Z., & Liu, J. (2012a) Precise relative positioning using real tracking data from COMPASS GEO and IGSO satellites. *GPS Solutions*, vol. 17, no. 1, pp. 103–119.

Shi, C., Zhao, Q., Li, M., Tang, W., Hu, Z., Lou, Y., Zhang, H., Niu, X., & Liu, J. (2012b) Precise orbit determination of Beidou satellites with precise positioning. *Science China Earth Sciences*, vol. 55, no. 7, pp. 1079–1086, doi: 10.1007/s11430-012-4446-8.

Steigenberger, P., Hauschild, A., Hugentobler, U., & Montenbruck, O. (2012) Performance analysis of Compass orbit and clock determination and Compass only PPP, *Proceedings of IGS Workshop*, July 23–27, Olsztyn, Poland, 2012.

Steigenberger, P., Hugentobler, U., Hauschild, A., & Montenbruck, O. (2013) Orbit and clock analysis of COMPASS GEO and IGSO satellites. *Journal of Geodesy*, vol. 87, no. 6, pp. 515–525.

Teunissen, P.J.G., & Kleusberg, Alfred, eds. (1998) *GPS for Geodesy: Second Completely Revised and Extended Edition*, Springer-Verlag, Berlin.

Teunissen, P.J.G. (1984) Generalized inverses, adjustment the datum problem and S-transformations. *Lecture notes in the International School of Geodesy, 3rd course: Optimization and design of geodetic networks*., 1984. Erice-Trapani-Sicilys, April 25–10 May 1984, Italy.

Teunissen, P.J.G., Odijk, D., & Zhang, B. (2010) PPP-RTK: results of CORS network-based PPP with integer ambiguity resolution. *Journal of Aeronautics, Astronautics and Aviation, Series A*, vol. 42, no. 4, pp. 223–230.

Teunissen, P.J.G., Simons, D.G., & Tiberius, C.C.J. M. (2008) Probability and Observation Theory. *Lecture Notes AE2-E01, Faculty of Aerospace Engineering, Delft University of Technology, 2008, The Netherlands*.

Yang, Y., Li, J., Xu, J., Tang, J., Guo, H., & He, H. (2011) Contribution of the Compass satellite navigation system to global PNT users. *Chinese Science Bulletin*, vol. 56, no. 26, pp. 2813–2819.

Zhang, B., Teunissen, P.J.G., & Odijk, D. (2011) A novel un-differenced PPP-RTK concept. *The Journal of Navigation*, vol. 64, no. S1, pp. S180–S191, doi:10.1017/S0373463311000361.

Zhang, S., Guo, J., Li, B., & Rizos, C. (2010) An analysis of satellite visibility and relative positioning precision of COMPASS, *Proceedings of Symposium for Chinese Professionals in GPS, Shanghai, China*, 18–20 August, pp. 41–46.

3 SINGLE- AND MULTIPLE-FREQUENCY BDS+GPS RTK POSITIONING

This chapter is covered by the following publication:

Odolinski R, Teunissen PJG, Odijk D (2014b) First combined COMPASS/BeiDou-2 and GPS positioning results in Australia. Part II: Single- and multiple-frequency single-baseline RTK positioning. Published in: Journal of Spatial Science, vol. 59, no. 1, p. 25-46. doi:10.1080/14498596.2013.866913

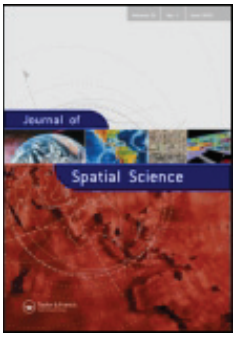

Journal of Spatial Science

Publication details, including instructions for authors and subscription information:
http://www.tandfonline.com/loi/tjss20

First combined COMPASS/BeiDou-2 and GPS positioning results in Australia. Part II: Single- and multiple-frequency single-baseline RTK positioning

R. Odolinski[a], P.J.G. Teunissen[ab] & D. Odijk[a]

[a] Department of Spatial Sciences, Curtin University, GPO Box U1987, Perth 6845, Australia

[b] Delft University of Technology, Delft, The Netherlands

Published online: 17 Jan 2014.

To cite this article: R. Odolinski, P.J.G. Teunissen & D. Odijk (2014) First combined COMPASS/BeiDou-2 and GPS positioning results in Australia. Part II: Single- and multiple-frequency single-baseline RTK positioning, Journal of Spatial Science, 59:1, 25-46, DOI: 10.1080/14498596.2013.866913

To link to this article: http://dx.doi.org/10.1080/14498596.2013.866913

Journal of Spatial Science, 2014
Vol. 59, No. 1, 25–46, http://dx.doi.org/10.1080/14498596.2013.866913

Taylor & Francis
Taylor & Francis Group

First combined COMPASS/BeiDou-2 and GPS positioning results in Australia. Part II: Single- and multiple-frequency single-baseline RTK positioning

R. Odolinski[a]*, P.J.G. Teunissen[a,b] and D. Odijk[a]

[a]*Department of Spatial Sciences, Curtin University, GPO Box U1987, Perth 6845, Australia;*
[b]*Delft University of Technology, Delft, The Netherlands*

Australia is a beneficiary of the current regional BeiDou configuration, as enough satellites are available for Positioning, Navigation and Timing (PNT). The present contribution is Part II out of two parts that consider first combined BeiDou + GPS results in Australia. In Part I we analysed the code-only single-receiver and relative point positioning performance. In this Part II we will evaluate the single- and multiple-frequency single-baseline RTK model. The performance is evaluated by ambiguity success-rates and by comparing the estimated positions to very precise benchmark coordinates. It will be shown that the increased strength of the combined model allows for improved ambiguity resolution performance and positioning robustness over the BeiDou- and GPS-only solutions.

Keywords: GNSS; BeiDou; GPS; Positioning, Navigation and Timing (PNT); single-baseline Real Time Kinematic (RTK); LAMBDA; success rates; Fixed-Failure rate Ratio Test (FFRT)

1. Introduction

The BeiDou-2 (COMPASS) Navigation Satellite System attained initial regional operational status in the end of December 2011, and can provide Positioning, Navigation and Timing (PNT) services in the whole Asia-Pacific region. Australia is a beneficiary of the current regional BeiDou configuration, as enough satellites are available for PNT. The full BeiDou constellation is expected in 2020, and will consist of five Geostationary Earth Orbit (GEO), three Inclined Geo-Synchronous Orbit (IGSO) and 27 Medium Earth Orbit (MEO) satellites (CSNO 2012).

Some BeiDou results can be found in the literature, where we have simulation results in Grelier *et al.* (2007), Huang and Tsai (2008), Cao *et al.* (2008), Chen *et al.* (2009), Feng and Li (2010), Zhang *et al.* (2010), Guo *et al.* (2011), Yang *et al.* (2011) and Qu *et al.* (2012). Real data results were presented by Shi *et al.* (2013), who evaluated BeiDou-only Single Point Positioning (SPP), relative code positioning and Real-Time-Kinematic (RTK). Shi *et al.* (2012) further evaluated orbit determination and combined BeiDou + GPS Precise Point Positioning (PPP). The first results using BeiDou outside China were reported in Montenbruck *et al.* (2012, 2013) and Steigenberger *et al.* (2012, 2013), which considered orbit determination, PPP and single-baseline RTK positioning.

*Corresponding author. Email: robert.odolinski@curtin.edu.au

This contribution presents the first combined BeiDou + GPS positioning results in Australia, and consists of two parts. The goal is to give Australian GNSS users indications of what BeiDou can bring in terms of positioning accuracy, both as a stand-alone system and when combined with GPS. In Part I (Odolinski *et al.* 2013) we considered combined BeiDou + GPS SPP and Relative Point Positioning (RPP), based on the code observables and single as well as multiple frequencies. This was to give an initial idea of the quality of the data and with the advantage that cheap code-only receivers can be used. We concluded that the regional BeiDou system is now suitable as a complementary or stand-alone positioning system for Australia.

In this Part II we present combined BeiDou + GPS single-baseline carrier-phase RTK positioning results, and compare the performance with the systems separately. In order to gain experimental experience and prove the potential of a combined system, the model considered for relative positioning is of the single-baseline type using two receivers separated by a short distance. The GNSS observables are then insensitive to residual ionospheric and tropospheric delays as well as satellite orbit errors. We will focus on single-epoch ambiguity resolution since it is the most challenging mode and has the advantage that the system becomes independent of cycle-slips. The positioning accuracy is evaluated by comparing the estimated positions to very precise benchmark coordinates, and for ambiguity resolution use is made of the LAMBDA method in combination with the Fixed Failure-rate Ratio Test.

In Part I (Odolinski *et al.* 2013) we described the BeiDou system and the frequencies available. The BeiDou satellites currently transmit at three frequencies, B1, B2 and B3, in Quadrature phase-shift keying (QPSK) modulation as shown in Table 1 and given together with the L1, L2 and L5 GPS frequencies.

The BeiDou signals are based on Code Division Multiple Access (CDMA) similar to GPS and Galileo. We see that no BeiDou frequencies overlap the GPS frequencies.

We begin by describing the GNSS observation equations and the models and methods used for positioning, ambiguity resolution and integer validation. Results of our analyses are then given, and we conclude with a summary and discussion.

2. System of GNSS observation equations

Let us consider the receivers $r = 1, \ldots, n$, where n is the number of receivers tracking the GPS or BeiDou satellites $s_* = 1_*, \ldots, m_*$, where m_* is the number of satellites of one GNSS system $*$ (G for GPS and C for BeiDou). We have no overlapping frequencies between GPS and BeiDou, thus we define the frequencies as $j_* = 1_*, \ldots, f_*$ frequencies, where f_* is the number of frequencies for system $*$. The single-system observation

Table 1. BeiDou-2/COMPASS (Han *et al.* 2011) and GPS signals

Sat. system	Band (component)	Frequency [MHz]	Wavelength [cm]
BeiDou	B1 (I/Q)	1561.098	19.20
	B2 (I/Q)	1207.140	24.83
	B3 (I/Q)	1268.520	23.63
GPS	L1	1575.42	19.03
	L2	1227.60	24.42
	L5	1176.45	25.48

equations are given as follows in units of range, and we omit time stamps for brevity,

$$
\begin{aligned}
p^{s*}_{r,j*} &= l^{s*}_{r} + dt_r + d_{r,j*} - dt^{s*} - d^{s*}_{j*} \\
&\quad + g^{s*}_{r}\,\tau_r + \mu_{j*} I^{s*}_{r} + \varepsilon_{p^{s*}_{r}} \\
\Phi^{s*}_{r,j*} &= l^{s*}_{r} + dt_r + \delta_{r,j*} - dt^{s*} - \delta^{s*}_{j*} \\
&\quad + g^{s*}_{r}\,\tau_r - \mu_{j*} I^{s*}_{r} \\
&\quad + \lambda_{j*} \underbrace{\left[N^{s*}_{r,j*} + \varphi_{r,j*}(t_0) - \varphi^{s*}_{j*}(t_0)\right]}_{M^{s*}_{r,j*}} \\
&\quad + \varepsilon_{\Phi^{s*}_{r}}
\end{aligned}
\tag{1}
$$

where the phase and code observable is denoted by $\Phi^{s*}_{r,j*}$ and $p^{s*}_{r,j*}$ respectively, and the receiver-satellite range is $l^{s*}_{r} = \|x^{s*} - x_r\|$, where $\|\cdot\|$ denotes the length, or norm, where x^{s*} is a vector that contains the satellite X, Y, Z coordinates, and x_r a vector with the corresponding receiver ones. The receiver and satellite clock errors are denoted by dt_r, dt^{s*} respectively, while $d_{r,j*}$, d^{s*}_{j*} are the frequency-dependent receiver and satellite hardware code delays and $\delta_{r,j*}, \delta^{s*}_{j*}$ the frequency-dependent receiver and satellite hardware phase delays. We use a mapping function g^{s*}_{r} to map the slant tropospheric delays from all satellites to station-wise wet Zenith Tropospheric Delays (ZTD) τ_r. Further $\mu_{j*} = \lambda^2_{j*}/\lambda^2_{1*} = f^2_{1*}/f^2_{j*}$ is the conversion of the first-order approximation ionospheric delay from the first frequency to a chosen frequency $j*$, and I^{s*}_{r} the ionospheric delay, the impact of which on the code and phase has opposite signs. Moreover, $M^{s*}_{r,j*}$ is the non-integer ambiguity due to initial phase delays for the receiver $\varphi_{r,j*}(t_0)$ and satellite $\varphi^{s*}_{j*}(t_0)$ that originate from the frequency oscillators (Blewitt 1989), where $N^{s*}_{r,j*}$ is the integer ambiguity, and λ_{j*} the wavelength corresponding to frequency $j*$. Finally $\varepsilon_{p^{s*}_{r}}, \varepsilon_{\Phi^{s*}_{r}}$ is the random observation noise and other unmodelled effects such as multipath. In the following we will refrain from carrying through the noise terms $\varepsilon_{p^{s*}_{r}}, \varepsilon_{\Phi^{s*}_{r}}$ explicitly for notational convenience.

For a combined BeiDou + GPS system with multiple frequencies we have in vector form $2f_G nm_G + 2f_C nm_C$ number of code and phase observations collected in y as,

$$
y = \left[y^{GT}_{p}, y^{GT}_{\Phi}, y^{CT}_{p}, y^{CT}_{\Phi}\right]^T \tag{2}
$$

where $(.)^T$ is the transpose of a vector, $y^*_p = \left[y^{*T}_{p;1*}, \ldots, y^{*T}_{p;f*}\right]^T$ with $y^*_{p;j*} = \left[p^{1*}_{1,j*}, \ldots, p^{m*}_{1,j*}, \ldots, p^{1*}_{n,j*}, \ldots, p^{m*}_{n,j*}\right]^T$, and $y^*_{\Phi} = \left[y^{*T}_{\Phi;1*}, \ldots, y^{*T}_{\Phi;f*}\right]^T$ with $y^*_{\Phi;j*} = \left[\Phi^{1*}_{1,j*}, \ldots, \Phi^{m*}_{1,j*}, \ldots, \Phi^{1*}_{n,j*}, \ldots, \Phi^{m*}_{n,j*}\right]^T$, respectively. The system of equations is not of full-rank, i.e. the parameters are not uniquely estimable. In the following we will present a single-baseline RTK positioning model that results in a full-rank system of observation equations.

Single-baseline RTK functional model

For the single-baseline RTK model we use two receivers and external products for satellite orbits. Between-receivers single differences (SD) is then performed on the system of observation equations (1) with respect to the 'pivot' receiver 1. The satellite delays common to both receivers are then eliminated, such as satellite clocks and hardware code/phase delays, and any remaining errors from the provided satellite orbits. If we assume that we have short baselines of a few km, the relative ZTD and ionosphere can be ignored since we have $\tau_1 \approx \tau_2$ and $I^{s*}_{1} \approx I^{s*}_{2}$ respectively.

The system of equations is, however, still rank deficient after the SD. The number of rank defects is the number of linear combinations of the column vectors of the design matrix that produces the zero vector, the combinations of which are said to span the null space of the

design matrix. These rank defects can be eliminated through an application of S-system theory (Teunissen 1984; Teunissen *et al.* 2010), implying null-space identification, S-basis constraining and proper interpretation of the estimable parameters. We have the following number of rank deficiencies for a single-system,

$$\#\text{of rank defects is } 4 + f_* m_* + 2f_* + 1 + f_* \tag{3}$$

three rank deficiencies of which stem from the fact that for short baselines the line-of-sight unit vectors become $c_1^{s_*T} = c_2^{s_*T}$, where $c_r^{s_*T} = (x^{s_*} - x_r)^T / \|x^{s_*} - x_r\|$ is the line-of-sight unit vector from the receiver r to the satellites obtained from linearising (1) with respect to the receiver coordinates. To eliminate these rank deficiencies we choose to fix the pivot receiver 1 coordinates (3), receiver clock (1), ambiguities ($f_* m_*$) and receiver code and phase hardware delays ($2f_*$), receiver 2 hardware code delays on the first frequency (1), and pivot satellite 1_* ambiguities observed from receiver 2 (f_*). We then have the *single system*, SD, and (linearised) full-rank observation equations expressed as,

$$\begin{aligned} p_{12,j*}^{s*} &= -c_2^{s*T} \Delta x_{12} + d\tilde{t}_{12} + \tilde{d}_{12,j*} \\ \Phi_{12,j*}^{s*} &= -c_2^{s*T} \Delta x_{12} + d\tilde{t}_{12} + \tilde{\delta}_{12,j*} + \lambda_{j*} \tilde{M}_{12,j*}^{1s*} \end{aligned} \tag{4}$$

where $(\cdot)_{12} = (\cdot)_2 - (\cdot)_1$ is the notation for between-receiver SD. The estimable unknowns are expressed as follows,

$$\Delta x_{12} = \Delta x_2 - \Delta x_1$$

relative receiver coordinates,

$$d\tilde{t}_{12} = dt_2 + d_{2,1_*} - \left(dt_1 + d_{1,1_*}\right)$$

relative receiver clock with code delays on $j_* = 1_*$,

$$\tilde{d}_{12,j*} = d_{2,j*} - d_{2,1_*} - \left(d_{1,j*} - d_{1,1_*}\right)$$

relative Differential Code Bias (DCB), $j_* = 2_*, \ldots, f_*$,

$$\tilde{\delta}_{12,j*} = \delta_{2,j*} - \delta_{1,j*} - \left(d_{2,1_*} - d_{1,1_*}\right) + \lambda_{j*} M_{12,j*}^{1*}$$

relative receiver hardware phase delays,

$$\tilde{M}_{12,j*}^{1s*} = M_{2,j*}^{s*} - M_{1,j*}^{s*} - M_{2,j*}^{1*} + M_{1,j*}^{1*}$$

double − differenced ambiguities, $s_* \geq 2$.

We have three baseline coordinate components, one receiver clock, $(f_* - 1)$ relative receiver DCBs on the second frequency and beyond, f_* receiver hardware phase delays, and $f_*(m_* - 1)$ double-differenced *integer* ambiguities. The integer nature of the ambiguities has been recovered from (1) since they are now expressed in double-differenced form and thus without receiver/satellite initial phase delays, i.e. $\varphi_{r,j_*}(t_0)$ and $\varphi_{j,*}^{s_*}(t_0)$ respectively.

For the combined system only the three receiver coordinates can be shared. The number of rank deficiencies and S-basis for a combined system is thus obtained by taking (3) for GPS and BeiDou, respectively, and subtracting 3 for the receiver coordinates in common, and we have,

$$\begin{aligned} \#\text{of rank defects is } & 5 + f_G m_G + f_C m_C \\ & + 2(f_G + f_C + 1) + f_G + f_C \end{aligned} \tag{5}$$

The full-rank system of observation equations for a *combined system* can then be expressed as follows, in vector form,

$$y_{12} = Bb + Aa \tag{6}$$

where y_{12} contains the SD code and phase observables on multiple frequencies, $B = [B_1\ B_2\ B_3]$ contains the unknowns b corresponding design matrices, where $B_1 = \begin{bmatrix} e_2 \otimes e_{f_G} \otimes G_2^G \\ e_2 \otimes e_{f_C} \otimes G_2^C \end{bmatrix}$, $B_2 = \text{blkdiag}\left(e_2 \otimes e_{f_G} \otimes e_{m_G}, e_2 \otimes e_{f_C} \otimes e_{m_C}\right)$,

$$B_3 = \begin{bmatrix} \text{blkdiag}\left(C_{f_G}, I_{f_G}\right)\otimes e_{m_G} & 0 \\ 0 & \text{blkdiag}(\end{bmatrix}$$

$C_{f_C}, I_{f_C})\otimes e_{m_C}]$, and with the respective vectors of unknowns in $b = \left[b_1^T, b_2^T, b_3^T\right]^T$, with $b_1 = \Delta x_{12}$, $b_2 = \begin{bmatrix} d\tilde{t}_{12}^G & d\tilde{t}_{12}^C \end{bmatrix}^T$, $b_3 = \begin{bmatrix} \overline{d}_{12,G}^T & \overline{\delta}_{12,G}^T & \overline{d}_{12,C}^T & \overline{\delta}_{12,C}^T \end{bmatrix}^T$, with $\bar{d}_{12,*} = \left[\tilde{d}_{12,2_*}, \ldots, \tilde{d}_{12,f_*}\right]^T$, $\bar{\delta}_{12,*} = \left[\tilde{\delta}_{12,1_*}, \ldots, \tilde{\delta}_{12,f_*}\right]^T$, and the ambiguity design matrix $A = \text{blkdiag}\left(\begin{bmatrix} 0 \\ \Lambda_G\otimes C_{m_G} \end{bmatrix}, \begin{bmatrix} 0 \\ \Lambda_C\otimes C_{m_C} \end{bmatrix}\right)$ with ambiguities in $a = \begin{bmatrix} a_{12}^{GT} & a_{12}^{CT} \end{bmatrix}^T$, with $a_{12}^* = \left[a_{12,1_*}^{*T}, \ldots, a_{12,f_*}^{*T}\right]^T$ and $a_{12,j_*}^* = \left[\tilde{M}_{12,j_*}^{12_*}, \ldots, \tilde{M}_{12,j_*}^{1m_*}\right]^T$. We have e_2, e_{f_*} and e_{m_*} as the column vectors with only ones of size 2×1, $f_*\times 1$ and $m_*\times 1$ respectively, G_2^* contains the line-of-sight unit vectors of receiver 2, $\otimes$ is the Kronecker product as given by Rao (1973), 'blkdiag' denotes a blockdiagonal matrix, I_{f_*} the identity matrix of size f_*, $C_{f_*} = \begin{bmatrix} 0_{1\times(f_*-1)} \\ I_{(f_*-1)} \end{bmatrix}$, $C_{m_*} = \begin{bmatrix} 0_{1\times(m_*-1)} \\ I_{(m_*-1)} \end{bmatrix}$, and $\Lambda_* = diag(\lambda_{1_*}, \ldots, \lambda_{f_*})$ the diagonal wavelength matrix. We have the same interpretation of the estimable unknowns as in (4), where the GPS clock is with respect to GPS time and the BeiDou clock to the BeiDou navigation satellite system time (CSNO 2012).

Single-baseline RTK stochastic model

The variance-covariance (VCV) matrix of the code and phase observables in SD form and for a single system (4) is given as,

$$Q_{yy}^* = \text{blkdiag}\left(C_p^*, C_\Phi^*\right)\otimes\left(D_n^T D_n\otimes W_{m*}^{-1}\right) \tag{7}$$

where D_n^T is the between-receivers SD operator (Teunissen 1997a), with -1 for the pivot receiver and a 1 for the second receiver, and the code and phase observable a priori variance factors are given in the sub-matrices $C_p^* = diag\left(\sigma_{p,1_*}^2, \ldots, \sigma_{p_{f_*}}^2\right)$ and $C_\Phi^* = diag\left(\sigma_{\Phi,1_*}^2, \ldots, \sigma_{\Phi_{f_*}}^2\right)$ respectively. Here we assume no cross-correlation between code and phase or between frequencies, otherwise the non-diagonal elements of C_p^* and C_Φ^* would be populated accordingly with covariances between the observables. Further $W_{m_*}^{-1}$ contains the exponential elevation-weighting function defined as

$$W_{m*}^{-1} = \text{blkdiag}\left(\left(1 + a_{j*}\, e^{-E^{1}*/E_0}\right)^2, \ldots, \left(1 + a_{j*}\, e^{-E^{m}*/E_0}\right)^2\right) \tag{8}$$

where the diagonal elements correspond to the elevation-dependent weighting function as given by Euler and Goad (1991), where E^{s_*} is the elevation to the satellites $s_* = 1_*, \ldots m_*$ from the receivers in degrees, a_{j_*} is the amplification factor dependent on observation type and frequency, and E_0 is the reference elevation angle in degrees. The combined system (6) VCV-matrix is given as,

$$Q_{yy} = \text{blkdiag}\left(Q_{yy}^G, Q_{yy}^C\right). \tag{9}$$

Redundancy and solvability

The redundancy is computed as the number of observations minus the number of estimable unknowns. In Table 2 we give the number of observations, the number of estimable unknowns and the redundancy for the single-baseline RTK

Table 2. Single-baseline RTK, number of observations, unknowns, redundancy and solvability condition

Model/equation	# of observations	# of unknowns	Redundancy	Solvability condition
Single system (4)	$2f_* m_*$	$3 + f_* + f_* m_*$	$f_*(m_* - 1) - 3$	$m_* \geq 4$
Combined system (6)	$2f_G m_G + 2f_C m_C$	$3 + f_G + f_G m_G + + f_C + f_C m_C$	$f_G(m_G - 1) + + f_C(m_C - 1) - 3$	$m_G + m_C \geq 5$

models that we have presented. We also give in the last column a *solvability condition*, which is the number of satellites required to solve unbiased coordinate parameters. This follows from looking into the rank of the resulting system of observation equations, and if it is not of full-rank more satellites are needed.

Satellite availability for single-baseline RTK success rates

We emphasise that according to Table 2, for example, $m_G = 3$ and $m_C = 2$ number satellites are enough for positioning with a combined system, whereas with the same numbers it is impossible to position the receiver using the systems separately ($m_* \geq 4$ satellites required). In Part I (Odolinski *et al.* 2013) we depicted the satellite availability when positioning a receiver in Perth with an elevation cut-off angle of 40 degrees (suitable in e.g. urban canyons or open pit mines). With a combined system we were then able to position our receiver approximately 100 percent of the time over the day, whereas we could do this with the systems separately only 70 percent of the time.

In order to not only position the receiver but also successfully fix the integer ambiguities – the key to high-precision positioning – more than four (for the single system) or five (for the combined system) satellites are needed. We set this bound to $m_* \geq 8$ for the single system and $m_G + m_C \geq 9$ for the combined system, since it is deemed reasonable by Figure 1. In Figure 1 we also depict the corresponding bootstrapped success rates for a 25 degree elevation cut-off angle and instantaneous single-baseline RTK ambiguity resolution for single-frequency B1 BeiDou, L1 GPS and B1 + L1 combined BeiDou + GPS. The bootstrapped success rate is an accurate lower bound to the Integer Least-Squares (ILS) success rate (Teunissen 1997b, 1998b) and can thus be used to infer whether integer ambiguity resolution can expected to be successful. This success rate can be computed without actual measurements, i.e. only the (decorrelated) VCV-matrix (Teunissen 1995) of the float ambiguities is needed. In other words, the success rate can be used for planning purposes and to decide whether to fix the ambiguities to the integers in real time or post-processing mode (Verhagen *et al.* 2013). Success-rate evaluation software 'Ps-LAMBDA' is available via http://gnss.curtin.edu.au/research/lambda.cfm; see further Verhagen *et al.* (2013). The stochastic model settings used to compute the bootstrapped success rates are given in Table 3.

We see in Figure 1 that when we have eight or more satellites for BeiDou we can expect (taken as a mean value of these epochs) approximately 98 percent probability of successful integer ambiguity resolution (dotted green line), and the corresponding number for GPS is a 92 percent success rate. It should be noted though that the availability of epochs with $m_* \geq 8$ satellites only holds approximately 14 percent of the time over the day for BeiDou, whereas the corresponding number for GPS is 2 percent. The bootstrapped success rates when we do not have a sufficient number of satellites are approximately 55 percent and 26 percent for BeiDou and GPS respectively (dotted red lines). We also see that over the entire day we have an approximately 61 percent success rate for BeiDou and 27 percent for GPS, whereas the corresponding number

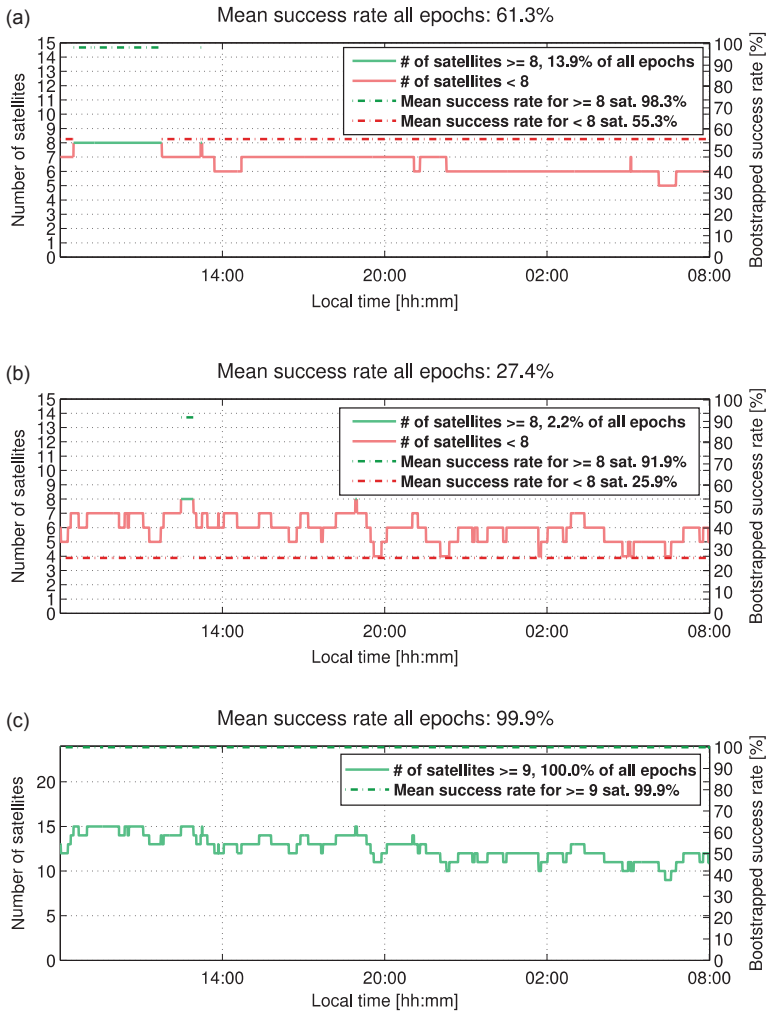

Figure 1. Bootstrapped success rates (Teunissen 1998b) for instantaneous single-baseline RTK integer ambiguity resolution for combined **B1 + L1 BeiDou + GPS**. Success rates for **25 degree** elevation cut-off angle for CUTA in Perth on 7 July 2012. Light green represents GPS L1 (b) and BeiDou B1 (a) with 8 or more satellites and for the combined system (c) 9 satellites; the corresponding red is for fewer than 8 satellites. Bootstrapped success rates are taken as a mean of all epochs above/equal and below these satellite limits.

for the combined system is close to 100 percent all the time. In other words, with a combined system we can have higher elevation cut-off angles as compared to when we use the single systems and still guarantee a sufficient number of satellites to allow successful integer ambiguity resolution.

3. Float and fixed baseline least-squares solution

In the following we describe how we solve our parameters and the integer ambiguities. A prerequisite for fast precise positioning is that we have estimated the correct integers, thus integer ambiguity validation will be

Table 3. Stochastic model settings for single-baseline RTK (7)

System	Frequency	Code $\sigma_{p_{j*}}$ [cm]	Phase $\sigma_{\phi_{j*}}$ [mm]
GPS	L1	37	1.7
	L2	27	1.8
BeiDou	B1	31	1.4
	B2	30	1.6
	B3	25	1.7

described as well. Consider the observation equations in (4) or (6), where we have the unknowns in vector b of say size $p \times 1$ and (double-differenced) ambiguities in vector a of size $q \times 1$. We will solve the following ILS problem (Teunissen 1995),

$$\min_{b,a} \|y - Bb - Aa\|^2_{Q_{yy}}, \text{with } b \in R^p, a \in Z^q, \tag{10}$$

where $\|\cdot\|^2_{Q_{yy}} = (\cdot)^T Q_{yy}^{-1}(\cdot)$, R^p is p-dimensional space of real numbers and Z^q the q-dimensional space of integers. The parameter estimation is divided into three steps, float solution, integer ambiguity estimation, and fixed solution.

Float solution

In the float solution we replace the integer constraint Z^q in (10) with R^q, i.e. both the ambiguities and baseline components will be estimated as real-valued parameters. The system of normal equations is formulated as,

$$\begin{bmatrix} B^T Q_{yy}^{-1} B & B^T Q_{yy}^{-1} A \\ A^T Q_{yy}^{-1} B & A^T Q_{yy}^{-1} A \end{bmatrix} \begin{bmatrix} \hat{b} \\ \hat{a} \end{bmatrix} = \begin{bmatrix} B^T Q_{yy}^{-1} y \\ A^T Q_{yy}^{-1} y \end{bmatrix}. \tag{11}$$

This can be solved as follows (Teunissen 2003),

$$\hat{a} = \left(\overline{A}^T Q_{yy}^{-1} \overline{A}\right)^{-1} \overline{A}^T Q_{yy}^{-1} y \tag{12}$$

with $\hat{a}$ the least-squares solution of the ambiguities. By the variance propagation law we have,

$$Q_{\hat{a}\hat{a}} = \left(\bar{A}^T Q_{yy}^{-1} \bar{A}\right)^{-1} \tag{13}$$

as the corresponding VCV-matrix, where $\bar{A} = P_B^{\perp} A$, $P_B^{\perp} = (I - P_B)$, and $P_B = B\left(B^T Q_{yy}^{-1} B\right)^{-1} B^T Q_{yy}^{-1}$ is a projector that projects onto the range space of B, while $P_B^{\perp}$ projects onto the orthogonal complement of the range space of B. The float baseline solutions follow as,

$$\hat{b} = \left(B^T Q_{yy}^{-1} B\right)^{-1} B^T Q_{yy}^{-1} \left(y - A\hat{a}\right) \tag{14}$$

The VCV-matrix of the baseline components is derived by the variance propagation law and given as

$$Q_{\hat{b}\hat{b}} = \left(\bar{B}^T Q_{yy}^{-1} \bar{B}\right)^{-1} \tag{15}$$

where $\bar{B} = P_A^{\perp} B$, $P_A^{\perp} = I - P_A$, and $P_A = A\left(A^T Q_{yy}^{-1} A\right)^{-1} A^T Q_{yy}^{-1}$ is a projector that projects onto the range space of A, while $P_A^{\perp}$ projects onto the orthogonal complement of the range space of A.

Integer ambiguity estimation

It can be shown that the integer solution of (10) is given by the integer minimiser,

$$\breve{a} = \arg\min_{a \in Z^q} \|\hat{a} - a\|^2_{Q_{\hat{a}\hat{a}}} \tag{16}$$

which can efficiently be computed with the LAMBDA method (Teunissen 1995). The ILS estimator is optimal in the sense that it results in the highest possible success rates of all integer estimators (Teunissen *et al.* 1996; Teunissen 1999, 2002).

Fixed baseline solution

The fixed baseline solution $\breve{b}$ of the (integer) constrained linear model (Teunissen *et al.* 2008) is given as,

$$\breve{b} = \hat{b} - Q_{\hat{b}\hat{a}} Q_{\hat{a}\hat{a}}^{-1} (\hat{a} - \breve{a}) \tag{17}$$

If we ignore the uncertainty in $\breve{a}$, the corresponding VCV-matrix reads,

$$Q_{\breve{b}\breve{b}} = Q_{\hat{b}\hat{b}} - Q_{\hat{b}\hat{a}} Q_{\hat{a}\hat{a}}^{-1} Q_{\hat{a}\hat{b}} \tag{18}$$

where $Q_{\hat{b}\hat{a}}, Q_{\hat{a}\hat{b}}$ are the covariance matrices between baseline components and ambiguities. The uncertainty in $\breve{a}$ can be ignored if the probability of correct integer estimation is sufficiently high. Ensuring that the integer ambiguity solution has a sufficiently high probability of being correct is the task of the integer validation step.

Integer validation: fixed failure rate ratio test

The ILS solution $\breve{a}$ is the integer minimiser of $\|\hat{a} - a\|^2_{Q_{\hat{a}\hat{a}}}$, and we let $\breve{a}'$ be the solution that gives the second smallest value of the quadratic form $\|\hat{a} - a'\|^2_{Q_{\hat{a}\hat{a}}}$. The idea with the Fixed Failure rate Ratio Test (FFRT) (Teunissen & Verhagen 2009; Verhagen & Teunissen 2013) is to let the user define the acceptable failure rate, i.e. the probability that the accepted integer solution is incorrect, P_f. For this failure rate P_f one can compute a threshold c given by tabulated values based on simulation and the VCV-matrix of the float ambiguities. The validation test reads,

$$\text{accept } \breve{a} \text{ if } \frac{(\hat{a} - \breve{a})^T Q_{\hat{a}\hat{a}}^{-1} (\hat{a} - \breve{a})}{(\hat{a} - \breve{a}')^T Q_{\hat{a}\hat{a}}^{-1} (\hat{a} - \breve{a}')} \leq c \tag{19}$$

i.e. it tests the closeness of the float solution to its nearest integer vector, and if it is close enough it leads to acceptance of the integer solution $\breve{a}$. The smaller the user-defined failure rate P_f the smaller is the threshold c, and thus the smaller the size of the aperture pull-in region (Teunissen & Verhagen 2009). The aperture pull-in region is symmetric with respect to the origin and its shape is governed by the VCV-matrix of the float solution. A value of $c = 1$ would imply an aperture pull-in region equal to the ILS pull-in region (Teunissen 1998a) and all integer solutions are accepted.

If we denote the probability of correct integer estimation as P_s, the probability of acceptance as $P_s + P_f$, we then have the probability of successful fixes as,

$$P_{sf} = \frac{P_s}{P_s + P_f} \tag{20}$$

In other words, when the failure rate is small or set close to zero by the user, the probability of successful fixes will be close to 1, thus we become very confident about the correctness of the integer solutions that are accepted by this test.

In current practice one often still uses test (19) with a fixed critical value c. This is not recommended as the Fixed Critical-value Ratio Test (FCRT) has the drawback that then the fail rate may change from epoch to epoch, thus not guaranteeing a constant user-defined quality in the produced results (Teunissen & Verhagen 2009).

4. Results

In this section single-baseline RTK positioning results for combined BeiDou + GPS and BeiDou- and GPS-only are presented. Data from static receivers CUT0 and CUTA in Curtin's Continuously Operating Reference Stations are analysed. The stations are equipped with Trimble NetR9 multi-frequency multi-GNSS receivers.

Five days of data will be analysed, namely 7–11 July 2012, with a 30 sec interval between consecutive measurements and 10 degrees of elevation cut-off angle. The BeiDou satellite orbit and clock products are provided by the GNSS centre of Wuhan University for this

period. For GPS standard broadcast ephemerides are used. The estimated receiver positions are compared to very precise station benchmarks. We make use of the Detection, Identification and Adaptation (DIA) procedure to eliminate outliers (Teunissen 1990). The CUT0 and CUTA antennas are shown in Figure 2. Typical skyplot, number of satellites and Positional Dilution Of Precision (PDOP) for a combined BeiDou + GPS system are given in Figure 3 for 7 July, UTC +0 hours.

Single-baseline RTK stochastic settings

The stochastic model settings for the RTK positioning are given in Table 3. We used one day of data to find the a priori accuracy by fitting the formal 95 percent confidence ellipse to the corresponding empirical ellipse; see further description in relation to Figure 4. We then applied these settings to the other days to independently check the validity of the stochastic model.

Single-epoch RTK positioning results

In this section we will evaluate the positioning performance of single-baseline RTK for a combined BeiDou + GPS system as well as for the single systems separately. We can only compare triple-frequency BeiDou results with those of dual-frequency GPS, since the third GPS frequency is currently (2013) only available from PRN 1, 24 and 25.

Figure 2. CUTA (left) and CUT0 (right) GNSS antennas.

Single-frequency RTK positioning results are depicted in Figure 4 with epoch-by-epoch (instantaneous) ambiguity resolution. Horizontal and vertical scatter plots are given with 95 percent confidence ellipses/levels as computed by the empirical and formal VCV-matrix of the positions. The empirical VCV-matrix is given by the positioning errors as derived by comparing the estimated positions to the precise benchmark coordinates, whereas the formal VCV-matrix is given from the mean of all single-epoch formal VCV-matrices of the entire observation span. All results are given in local North, East and Up. A good match between the two ellipses imply realistic assumptions on the stochastic model as given in Table 3, and that as a result we have a minimum variance estimator (Teunissen *et al.* 2008). Figure 5 gives the corresponding positioning error histograms with (Top) float solution and (Bottom) fixed solution. The given empirical and formal theoretical normal distributions are based on the empirical mean and empirical and formal standard deviations (STDs) of the position errors respectively.

We can see in Figure 4 that the combined system gives approximately 25 percent improvement in North, 30 percent in East, and 23 percent in Up empirical standard deviations as compared to GPS-only fixed solutions. The corresponding improvements as compared to BeiDou are 54 percent, 30 percent and 59 percent in North, East and Up respectively. The improvements are computed as,

$$\text{Improvement} = \frac{\text{STD}_* - \text{STD}_{\text{combined}}}{\text{STD}_*} \cdot 100\,[\%] \tag{21}$$

where STD is the standard deviation of system $*$ (C for BeiDou, G for GPS) and a combined system for North/East/Up. We read in Figure 5 that the total number of points to form the fixed solution histograms is 12,044 out of 14,400 epochs (84 percent) for BeiDou, also referred to

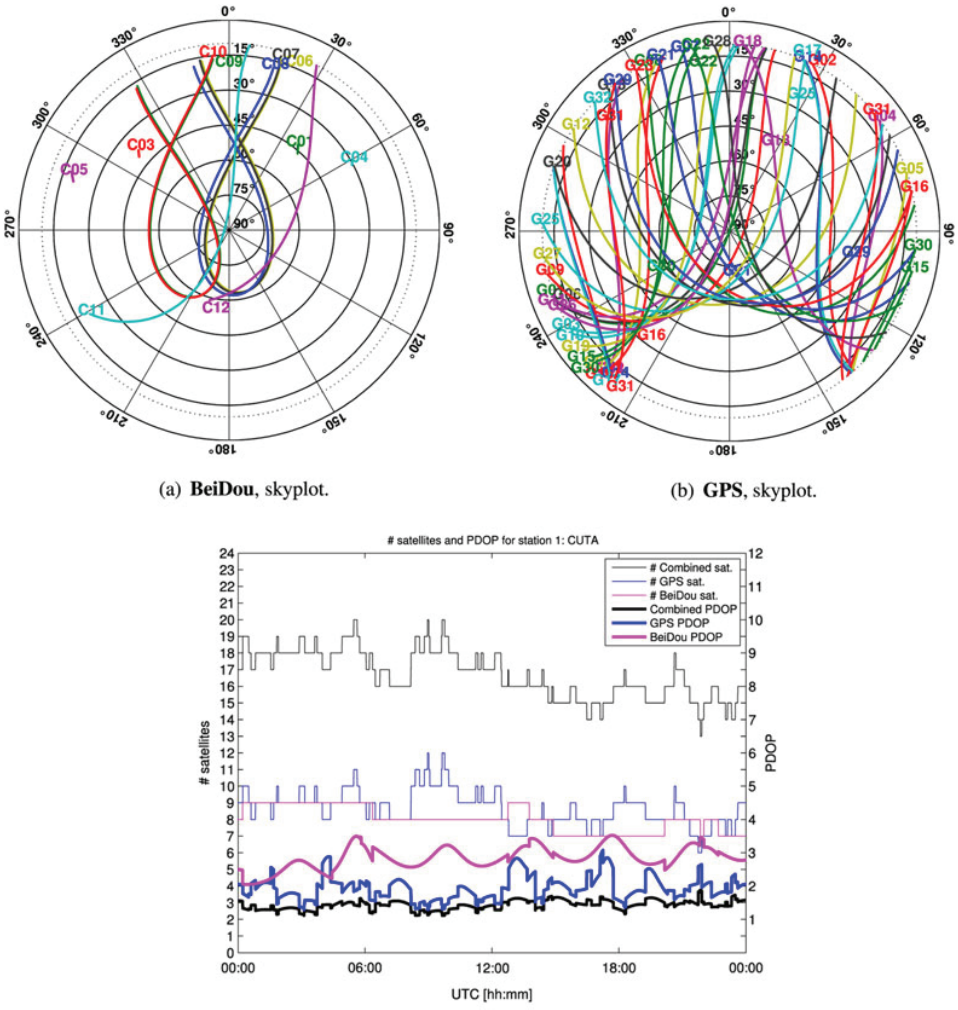

(a) **BeiDou**, skyplot.

(b) **GPS**, skyplot.

(c) **Combined BeiDou+GPS** number of satellites and PDOP.

Figure 3. Satellite visibility for a combined system (Bottom) and skyplot of BeiDou (Left) and GPS (Right) with 10 degree elevation cut-off angle for CUTA in Perth on 7 July 2012.

as the empirical success rate (see further (22)). For GPS we have 12,988 out of 14,400 epochs (90 percent) and for the combined system all 14,400 epochs (100 percent) were used. These numbers were determined by comparing the fixed ambiguities to a set of 'true' reference ambiguities solved by using a combined system with multiple frequencies and a Kalman filter over the whole time-span, assuming the ambiguities to be time constant. Epochs with fixed integer solutions deviating from the reference ones (wrongly fixed ambiguities) are not used here in our fixed solution positioning results. However, positioning results including the wrongly fixed integer ambiguities are given in the following Section.

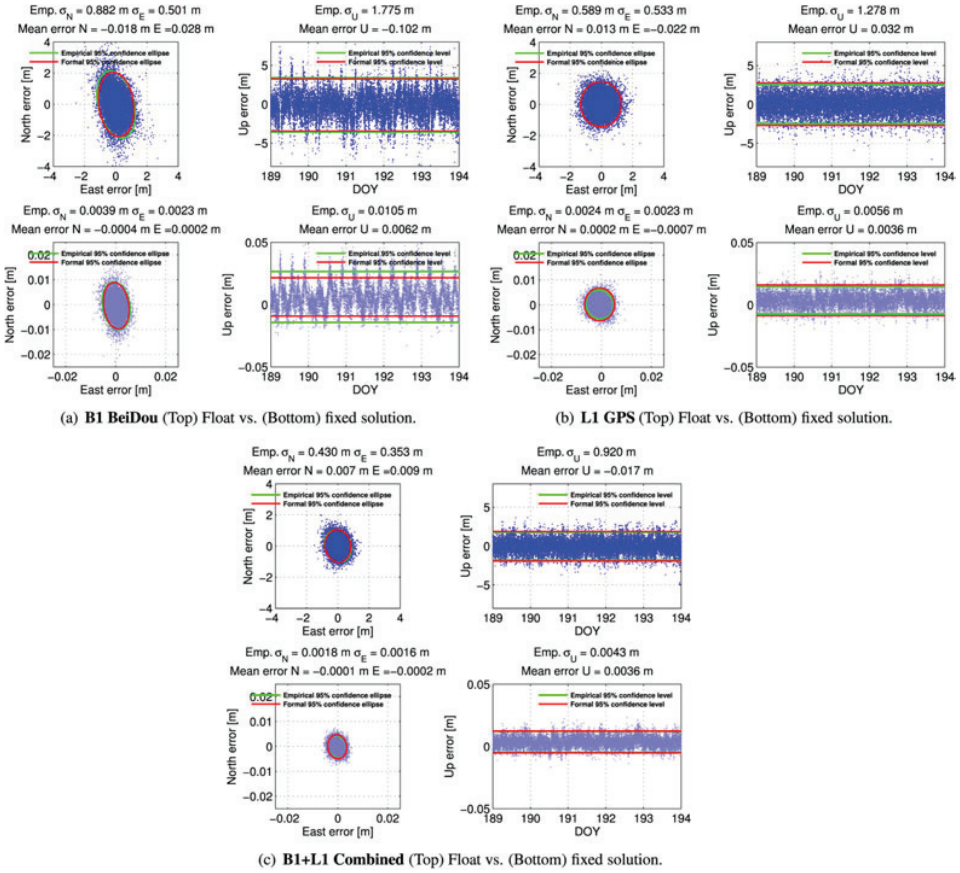

(a) **B1 BeiDou** (Top) Float vs. (Bottom) fixed solution.

(b) **L1 GPS** (Top) Float vs. (Bottom) fixed solution.

(c) **B1+L1 Combined** (Top) Float vs. (Bottom) fixed solution.

Figure 4. B1 + L1 BeiDou + GPS single-epoch and single-baseline RTK combined (6) positioning scatter for CUT0-CUTA.

We can see in Figures 4 and 5 that the North component is worse than the East for BeiDou. This is related to the satellite geometry (Figure 3) and the large fraction of GEO satellites around the equator (Odolinski *et al.* 2013), and is also verified by Figure 6, where we plot the number of satellites (Top), fixed BeiDou B1 positioning errors (Middle), and North, East and Up fixed solution formal standard deviations (Bottom). We restrict all days to track the same satellites to give comparable results between days.

We see a correlation between the formal standard deviations and the fixed solution positioning errors. This formal standard deviation variation in combination with multipath effects is believed to cause the periodic behaviour of the positioning errors that are visible in Figures 4 and 6, particularly for the Up component. The behaviour is also repeated between days. We elaborated more on these multipath effects in Part I (Odolinski *et al.* 2013). In Figure 7 we give the positioning errors based on day-differences with a time separation of 23 hours and 56 minutes, similar to the GPS and BeiDou constellation repeatability period (Jiang *et al.* 2011; Axelrad *et al.* 2005). Any gaps visible in the time-series are

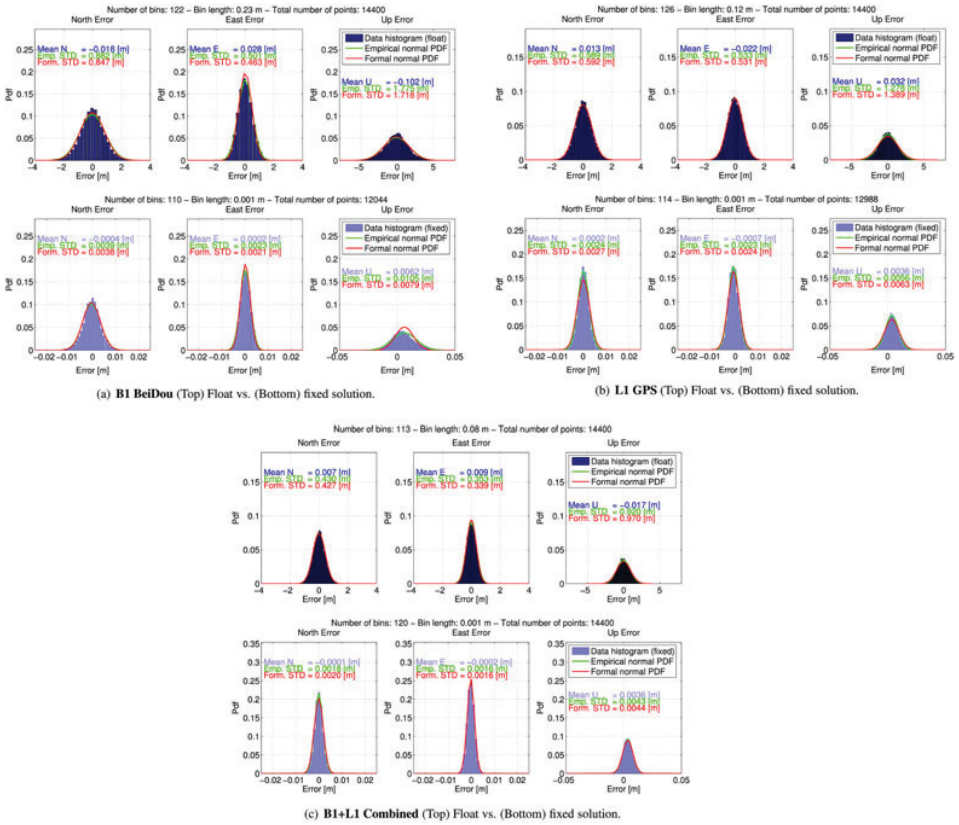

(a) **B1 BeiDou** (Top) Float vs. (Bottom) fixed solution.

(b) **L1 GPS** (Top) Float vs. (Bottom) fixed solution.

(c) **B1+L1 Combined** (Top) Float vs. (Bottom) fixed solution.

Figure 5. B1 + L1 BeiDou + GPS single-epoch and single-baseline RTK combined (6) positioning histograms CUT0-CUTA.

due to wrongly fixed ambiguities for one/both of the days.

The periodic behaviour due to multipath effects has been eliminated in Figure 7, and the mean errors are close to zero. The corresponding histograms of the positioning errors fit reasonably well with the empirical theoretical normal distribution. We can also compare this with Figure 5 without day-differences (and with multipath effects), where the histogram of the Up-component and BeiDou does not fit as well with the empirical theoretical normal distribution as when taking differences. BeiDou + GPS single-frequency RTK empirical positioning statistics are given in Table 4, and dual-/triple-frequency in Table 5.

In Table 4 we see that the single-epoch-based float solutions (which depend on the code noise) positioning standard deviations are overall larger for L1 and B1, due to the corresponding higher code noise (Table 3) as compared to B2 and L2. In Table 5 we see an improvement for the standard deviations of the dual-frequency combined system compared to those of GPS fixed solutions of approximately 20 percent, 26 percent and 20 percent in North, East and Up respectively, whereas for BeiDou the corresponding improvements are 58 percent, 39 percent and 61 percent respectively.

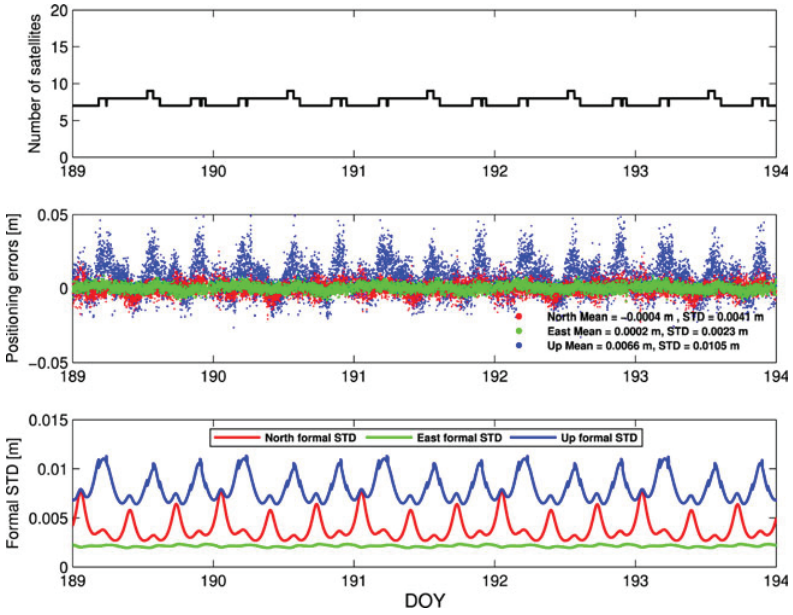

Figure 6. BeiDou B1. (Top) Number of satellites, (Middle) fixed solution positioning errors, and (Bottom) North, East and Up fixed solution formal standard deviations for single-baseline RTK.

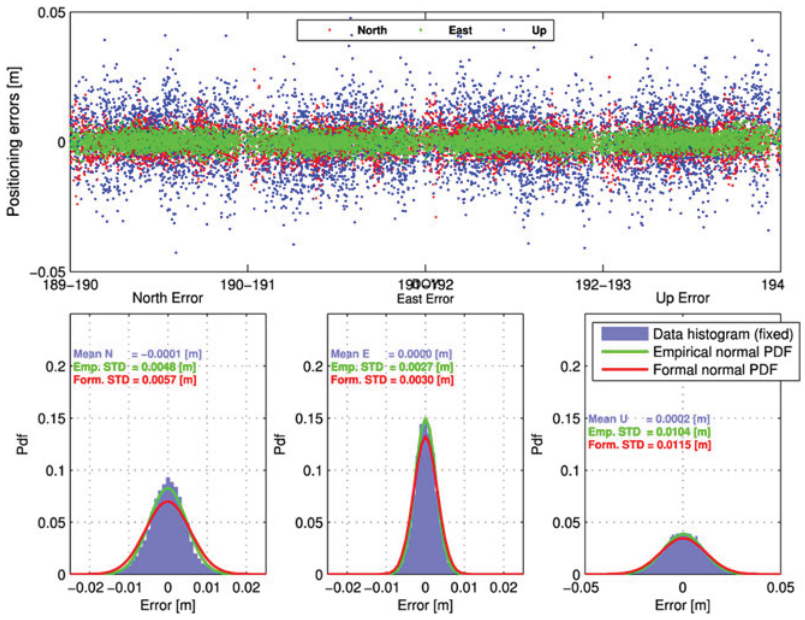

Figure 7. BeiDou B1 day-differences. (Top) fixed solution positioning errors, and (Bottom) corresponding fixed solution histograms.

Table 4. BeiDou/GPS and combined single-frequency RTK positioning results for CUT0-CUTA 7–11 July 2012. Improvement of the combined system is compared to GPS, and in brackets compared to BeiDou

System/freq.	Mean error N [m]	STD N [m]	Mean error E [m]	STD E [m]	Mean error U [m]	STD U [m]	Improvement STD [percent]		
							N	E	U
BeiDou B1 float	−0.018	0.882	0.028	0.501	−0.102	1.775	–	–	–
BeiDou B2 float	0.008	0.813	0.101	0.523	0.142	1.597	–	–	–
GPS L1 float	0.013	0.589	−0.022	0.533	0.032	1.278	–	–	–
GPS L2 float	−0.007	0.433	0.041	0.410	−0.016	0.978	–	–	–
Combined B1 + L1 float	0.007	0.430	0.009	0.353	−0.017	0.920	27 (51)	34 (30)	28 (48)
Combined B2 + L2 float	−0.009	0.349	0.064	0.319	0.040	0.773	19 (57)	22 (39)	21 (52)
	Mean error N [mm]	STD N [mm]	Mean error E [mm]	STD E [mm]	Mean error U [mm]	STD U [mm]			
BeiDou B1 fixed	−0.4	3.9	0.2	2.3	6.2	10.5	–	–	–
BeiDou B2 fixed	−0.5	4.1	−0.5	2.5	5.5	11.0	–	–	–
GPS L1 fixed	0.2	2.4	−0.7	2.3	3.6	5.6	–	–	–
GPS L2 fixed	0.8	2.5	−0.9	2.4	4.3	6.0	–	–	–
Combined B1 + L1 fixed	−0.1	1.8	−0.2	1.6	3.6	4.3	25 (54)	30 (30)	23 (59)
Combined B2 + L2 fixed	0.4	2.0	−0.7	1.6	3.9	4.6	20 (51)	33 (36)	23 (58)

Wrongly fixed integer solutions

In the previous Section we only showed the correctly fixed integer solutions' corresponding positioning results. These correct solutions were deemed by comparing the estimated ambiguities to reference ambiguities as computed from multiple-frequency measurements and a Kalman filter assuming the ambiguities time-constant. For a surveyor collecting measurements in real time, reference ambiguities are usually not available beforehand. This is where integer validation techniques play an important role.

In order to illustrate the positioning results when we do not use integer validation, in Figure 8 we give the corresponding single-frequency B1 and L1 BeiDou and GPS positioning results if all integer solutions were to be accepted in Figure 4. The fixed solution (green) is given together with the float solution (grey), and the wrongly fixed solutions (red) (Top). We also give (Bottom) the number of satellites equal to or above 8 and the bootstrapped success rates (similar to Figure 1).

In Figure 8 we see that the correctly fixed positioning errors are very small (mm level), and the Figure illustrates well the need for integer validation techniques since wrong fixing can directly lead to an even worse positioning performance as compared to taking the float solution (meter level). More specifically, the wrongly fixed solutions' standard deviations become almost twice as big as the corresponding values for the float solutions. We also see a correlation between epochs with the number of satellites below 8 and when the wrong integer solutions are given during the day, where the corresponding bootstrapped success rates reach approximately 58 percent for BeiDou and 46 percent for GPS.

Success rates and integer validation

In this section we evaluate the success rate performance of single-baseline RTK for a combined BeiDou + GPS system and the single systems separately. We compute the

Table 5. BeiDou/GPS and combined multiple-frequency RTK positioning results for CUT0-CUTA 7–11 July 2012. Improvement of the combined system is compared to GPS, and in brackets compared to BeiDou

System/freq.	Mean error N [m]	STD N [m]	Mean error E [m]	STD E [m]	Mean error U [m]	STD U [m]	Improvement STD [percent]		
							N	E	U
BeiDou B1,B2 float	−0.005	0.586	0.066	0.354	0.018	1.175	–	–	–
BeiDou B1,B2,B3 float	0.078	0.517	0.002	0.305	0.016	0.998	–	–	–
GPS L1,L2 float	0.002	0.377	0.010	0.349	0.007	0.832	–	–	–
Combined B1,B2 + L1,L2 float	−0.001	0.285	0.038	0.242	0.019	0.623	24 (51)	31 (32)	25 (47)
Combined B1,B2,B3 + L1,L2 float	0.029	0.271	0.009	0.225	−0.019	0.583	28 (48)	36 (26)	30 (42)
	Mean error N [mm]	STD N [mm]	Mean error E [mm]	STD E [mm]	Mean error U [mm]	STD U [mm]			
BeiDou B1,B2 fixed	−0.4	3.8	−0.1	2.3	5.8	10.2	–	–	–
BeiDou B1,B2,B3 fixed	−0.3	3.8	−1.1	2.2	4.8	10.5	–	–	–
GPS L1,L2 fixed	0.5	2.0	−0.8	1.9	3.9	5.0	–	–	–
Combined B1,B2 + L1,L2 fixed	0.1	1.6	−0.5	1.4	3.7	4.0	20 (58)	26 (39)	20 (61)
Combined B1,B2,B3 + L1,L2 fixed	0.1	1.7	−1.0	1.5	3.3	4.2	15 (55)	21 (32)	16 (60)

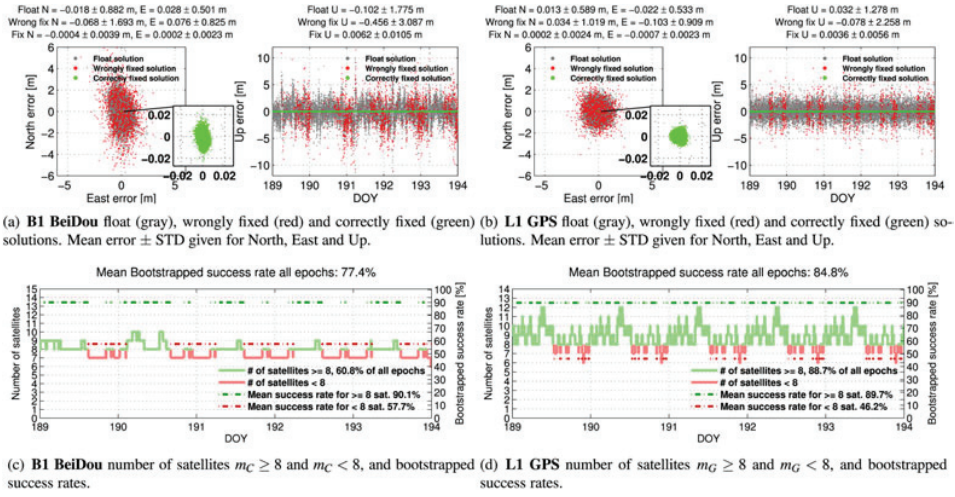

(a) **B1 BeiDou** float (gray), wrongly fixed (red) and correctly fixed (green) solutions. Mean error ± STD given for North, East and Up.

(b) **L1 GPS** float (gray), wrongly fixed (red) and correctly fixed (green) solutions. Mean error ± STD given for North, East and Up.

(c) **B1 BeiDou** number of satellites $m_C \geq 8$ and $m_C < 8$, and bootstrapped success rates.

(d) **L1 GPS** number of satellites $m_G \geq 8$ and $m_G < 8$, and bootstrapped success rates.

Figure 8. Float (grey), correctly fixed (green) and **wrongly fixed (red) solutions** at top for single-epoch single-baseline RTK (6) **B1 BeiDou and L1 GPS** positioning scatter for CUT0-CUTA. At bottom light green represents GPS and BeiDou with 8 or more satellites; the corresponding red is for fewer than 8 satellites. Bootstrapped success rates are taken as a mean of all epochs above/equal and below these satellite limits.

empirical success rates by comparing the single-epoch estimated ambiguities to reference ambiguities. The empirical success rate is then defined as,

$$P_{s_E} = \frac{\#\text{of correctly fixed epochs}}{\text{total \# of epochs}} \tag{22}$$

The empirical failure rate is given as the complement,

$$P_{f_E} = 1 - P_{s_E} \tag{23}$$

These two measures are evaluated without any integer validation, i.e. it is the outcome if we accept all integer ambiguities. We give the empirical success and failure rates in Table 6 for single- and multiple-frequency RTK, together with the bootstrapped success rates, denoted as $P_{s,BS}$ and taken as a mean of all epochs over 5 days.

The solutions accepted by the FFRT (19) can also be compared to the reference ambiguities accordingly. The empirical success rate for the FFRT test is defined as,

$$P_{s,\text{FFRT}} = \frac{\#\text{accepted and correctly fixed epochs}}{\text{total \# of epochs}} \tag{24}$$

The empirical FFRT failure rate is defined as,

$$P_{f,\text{FFRT}} = \frac{\#\text{accepted and incorrectly fixed epochs}}{\text{total \# of epochs}} \tag{25}$$

This empirical failure rate should, in theory, be at most or equal to the user-defined failure rate. The empirical number of successful fixes for the FFRT can then be computed similarly to (20) as,

$$P_{sf,\text{FFRT}} = \frac{P_{s,\text{FFRT}}}{P_{s,\text{FFRT}} + P_{f,\text{FFRT}}} \tag{26}$$

The FFRT statistics are presented in Table 7, with an a priori user-defined failure rate set to

Table 6. Empirical success, failure and bootstrapped success rates for CUT0-CUTA. Number of epochs 14,400

System/freq.	Empirical success rate P_{s_E} [percent]	Failure rate P_{f_E} [percent]	Bootstrapped success rate $P_{s,BS}$ [percent]
BeiDou			
B1	83.6	16.4	77.4
B2	91.9	8.1	91.0
GPS			
L1	90.2	9.8	84.8
L2	97.3	2.7	96.1
Combined			
B1 + L1	100.0	0.0	100.0
B2 + L2	100.0	0.0	100.0
BeiDou			
B1,B2	100.0	0.0	100.0
B1,B2,B3	100.0	0.0	100.0
GPS			
L1,L2	100.0	0.0	100.0
Combined			
B1,B2 + L1,L2	100.0	0.0	100.0
B1,B2,B3 + + L1,L2	100.0	0.0	100.0

$P_f = 0.1\%$. We also give the corresponding Fixed Critical-value Ratio Test (FCRT) with standard values in (19) of $c = 1/2$ and $c = 1/3$ respectively. We substitute the subscript 'FFRT' for the success rates with '$c = 1/2$' or '$c = 1/3$', respectively.

In Table 6 we see (as expected) that the single-frequency single systems with the largest code noise (Table 3) and smallest wavelengths (Table 1) have the highest fractions of empirical failure rates P_{f_E} (BeiDou B1 and GPS L1). For single-frequency positioning even up to 16.4 percent of the epochs were wrongly fixed (BeiDou B1). However the combined system show significant improvement in terms of empirical success rates P_{s_E} and failure rates P_{f_E}, where all epochs were successfully fixed in all cases. All epochs were also successfully fixed for the single system with multiple frequencies. This was all without integer validation.

With validation (Table 7), the FFRT provides the highest number of successful fixes $P_{sf,\mathrm{FFRT}}$ equal or close to 100 percent in all cases, as compared to the FCRT, with values reaching below 97 percent (96.7) for BeiDou B1 and $c = 1/2$. Moreover, The FFRT gives a failure rate equal to or smaller than the user-defined value of 0.1 percent in all cases, except for BeiDou B2 (0.2 percent), and gives smaller failure rates compared to the FCRTs. In other words, the FFRT yields the best protection against wrongly fixed ambiguities.

5. Summary and conclusions

BeiDou is the third satellite system (in addition to GPS and GLONASS) that offers continuous navigation in the Asia-Pacific region. Australia is a beneficiary of the regional BeiDou configuration as enough satellites are available to perform PNT. In this contribution we have analysed single-epoch single-baseline RTK performance in Perth, Western Australia, of a combined BeiDou + GPS system, and for the systems separately. We summarise our main findings and conclusions as follows.

Table 7. Empirical FFRT statistics with user-defined $P_f = 0.1\%$ and FCRT with $c = 1/2$ and $c = 1/3$, all for CUT0-CUTA. Number of epochs 14,400

System/freq.	FFRT empirical			FCRT $c = 1/2$ empirical			FCRT $c = 1/3$ empirical		
	Success–ful fix	Success rate	Failure rate	Success–ful fix	Success rate	Failure rate	Success–ful fix	Success rate	Failure rate
	$P_{sf,\mathrm{FFRT}}$ [percent]	$P_{s,\mathrm{FFRT}}$ [percent]	$P_{f,\mathrm{FFRT}}$ [percent]	$P_{sf,c=1/2}$ [percent]	$P_{s,c=1/2}$ [percent]	$P_{f,c=1/2}$ [percent]	$P_{sf,c=1/3}$ [percent]	$P_{s,c=1/3}$ [percent]	$P_{f,c=1/3}$ [percent]
BeiDou									
B1	99.8	34.9	0.1	96.7	55.4	1.9	98.5	35.8	0.5
B2	99.6	57.9	0.2	98.7	72.1	1.0	99.4	54.1	0.3
GPS									
L1	100.0	45.1	0.0	98.5	70.0	1.0	99.5	51.5	0.3
L2	100.0	79.5	0.0	99.6	89.1	0.3	99.9	78.4	0.1
Combined									
B1 + L1	100.0	100.0	0.0	100.0	100.0	0.0	100.0	100.0	0.0
B2 + L2	100.0	100.0	0.0	100.0	100.0	0.0	100.0	100.0	0.0
BeiDou									
B1,B2	100.0	100.0	0.0	100.0	100.0	0.0	100.0	100.0	0.0
B1,B2,B3	100.0	100.0	0.0	100.0	100.0	0.0	100.0	100.0	0.0
GPS									
L1,L2	100.0	100.0	0.0	100.0	100.0	0.0	100.0	100.0	0.0
Combined									
B1,B2 + L1,L2	100.0	100.0	0.0	100.0	100.0	0.0	100.0	100.0	0.0
B1,B2,B3 + L1,L2	100.0	100.0	0.0	100.0	100.0	0.0	100.0	100.0	0.0

Satellite availability and bootstrapped success rates for instantaneous integer ambiguity resolution

The bootstrapped success rate is suitable as a lower bound to the Integer-Least-Squares (ILS) success rate and can thus be used to infer whether integer ambiguity resolution can be expected to be successful (Teunissen 1997b, 1998b). We found that with an elevation cut-off angle of up to 25 degrees, a combined B1 + L1 BeiDou + GPS system provided a sufficient number of satellites over the whole day – with a corresponding bootstrapped success rate of 100 percent (Figure 1). For BeiDou and GPS separately we could only achieve corresponding success rates of approximately 61 percent and 27 percent respectively, due to the lack of a sufficient number of visible satellites over the day. In other words, we have shown for the first time that a combined system allows for higher satellite elevation angles than with a single system, and as a result it makes the system less susceptible for low-elevation multipath effects.

Single-baseline RTK positioning

The single-epoch single-baseline RTK results showed that the fixed solution positioning standard deviation improvements for a single frequency and a combined system were on average, for all coordinate components, approximately 26 percent as compared to GPS. The corresponding value was 48 percent as compared to BeiDou (Table 4). The corresponding dual-frequency (Table 5) improvements were 22 percent and 53 percent for GPS and BeiDou respectively.

Wrongly fixed integer solutions for RTK positioning

For a surveyor collecting measurements in real time, integer validation is of high importance. We illustrated (without validation) that the wrongly fixed solutions corresponding to North, East and Up standard deviations can become almost twice as large as for the float solution (Figure 8).

Success rates and integer validation

The empirical success rates (Table 6) were approximately 84–97 percent for single-frequency, single-baseline RTK and BeiDou- and GPS-only solutions. The combined system dramatically improved these numbers to 100 percent. This was all without integer validation. With validation (Table 7), the FFRT provided us with almost 100 percent successful fixes for all these cases, which implies that it does indeed make a correct decision most of the time. More specifically, we can compare the FFRT failure rate of at most 0.2 percent with that of the traditional Fixed Critical-value Ratio Test (FCRT) of up to 0.5–2 percent, and conclude that FFRT yields the best protection against wrongly fixed ambiguities.

BeiDou has already at this stage been shown to be suitable as a complementary or stand-alone GNSS system for Australia. More BeiDou MEO satellites are upcoming and will improve the current satellite geometry with respect to the location of our Australian receivers.

Acknowledgements

This work and Part I (Odolinski et al. 2013) have been executed in the framework of the Positioning Program Project 1.01 “New carrier phase processing strategies for achieving precise and reliable multi-satellite, multi-frequency GNSS/RNSS positioning in Australia” of the Cooperative Research Centre for Spatial Information (CRC-SI). The second author is the recipient of an Australian Research Council (ARC) Federation Fellowship (project number FF0883188). Post processed orbit and clock products were kindly provided by the GNSS centre of Wuhan University China. Observation data was provided by Noor Raziq and Boris Padovan at the GNSS Research Centre of Curtin University. All this support is gratefully acknowledged.

References

Axelrad, P., Larson, K., & Jones, B. (2005) Use of the correct satellite repeat period to characterize and reduce site-specific multipath errors. In *Proceedings of ION GNSS*, Long Beach, CA, 13–16 September 2005.

Blewitt, G. (1989) Carrier phase ambiguity resolution for the global positioning system applied to geodetic baselines up to 2000 km. *Journal of Geophysical Research*, vol. 94, no. B8, pp. 10187–10203.

Cao, W., O'Keefe, K., & Cannon, M.E. (2008) Evaluation of COMPASS ambiguity resolution performance using geometric-based techniques with comparison to GPS and Galileo, *Proceedings of ION GNSS*, Savannah, GA, 16–19 September 2008.

Chen, H.C., et al. (2009) The performance comparison between GPS and BeiDou-2/COMPASS: a perspective from Asia. *Journal of the Chinese Institute of Engineers*, vol. 32, no. 5, pp. 679–689.

CSNO BeiDou Navigation Satellite System Signal In Space Interface Control Document by China Satellite Navigation Office (CSNO). Open service signal B1I (Version 1.0). Technical report, 77 pages, 2012.

Euler, H.J., & Goad, C.G. (1991) On optimal filtering of GPS dual frequency observations without using orbit information. *Bulletin Géodésique*, vol. 65, no. 2, pp. 130–143.

Feng, Y., & Li, B. (2010) Wide area real time kinematic decimetre positioning with multiple carrier GNSS signals. *Science China Earth Sciences*, vol. 53, no. 5, pp. 731–740.

Grelier, T., et al. (2007) Compass signal structure and first measurements. In *Proc. of ION GNSS*, pp. 3015–3024, Fort Worth, TX, September 2007.

Guo, H., et al. (2011) Estimation and mitigation of the main errors for centimetre-level COMPASS RTK solutions over medium-long baselines. *Journal of Navigation*, vol. 64, no. S1, pp. S113–S126 doi:10.1017/S0373463311000324.

Han, C., Yang, Y., & Cai, Z. (2011) BeiDou navigation satellite system and its time scales. *Metrologia*, vol. 48, no. 4, pp. S213–S218 doi:10.1088/0026-1394/48/4/S13.

Huang, Y.-S., & Tsai, M.-L. (2008) The impact of Compass/Beidou-2 on future GNSS: A perspective from Asia, *Proceedings of ION GNSS*, pp. 2227–2238, Savannah, GA, September 2008.

Jiang, Y., et al. (2011) Coverage performance analysis on combined-GEO-IGSO satellite constellation. *Journal of Electronics*, vol. 28, no. 2, pp. 2011.

Montenbruck, O., et al. (2012) A COMPASS for Asia: First experience with the BeiDou-2 Regional Navigation System. In *Proceedings of IGS Workshop*, July 23–27, Olsztyn, Poland, 2012.

Montenbruck, O., et al. (2013) Initial assessment of the COMPASS/BeiDou-2 regional navigation satellite system. *GPS Solutions*, vol. 17, no. 2, pp. 211–222.

Odolinski, R., Teunissen, P.J.G., & Odijk, D. (2013) First combined COMPASS/BeiDou-2 and GPS positioning results in Australia Part I: Single-receiver and relative code-only positioning. *Journal of Spatial Science*, 22 pages, http://dx.doi.org/10.1080/14498596.2013.840865.

Qu, J., Yuan, H., Zhang, X., & Ouyang, G. (2012) Single-epoch COMPASS carrier-phase ambiguous resolution using three civil frequencies and special constellations. *Proceedings of ION GNSS*, Nashville TN, September 17–21, 2012.

Rao, C.R. (1973). *Linear statistical inference and its applications*, 2nd ed. Wiley, New York.

Shi, C., et al. (2012) Precise orbit determination of Beidou Satellites with precise positioning. *Science China Earth Sciences*, vol. 55, no. 7, pp. 1079–1086 doi:10.1007/s11430-012-4446-8.

Shi, C., et al. (2013) Precise relative positioning using real tracking data from COMPASS GEO and IGSO satellites. *GPS Solutions*, vol. 17, no. 1, pp. 103–119.

Steigenberger, P., et al. (2012) Performance analysis of Compass orbit and clock determination and Compass only PPP. In *Proceedings of IGS Workshop*, July 23–27, Olsztyn, Poland, 2012.

Steigenberger, P., et al. (2013) Orbit and clock analysis of COMPASS GEO and IGSO satellites. *Journal of Geodesy*, vol. 87, no. 6, pp. 515–525.

Teunissen, P.J.G. (1984) Generalized inverses, adjustment the datum problem and S-transformations. *Lecture Notes in the International School of Geodesy, 3rd Course: Optimization and Design of Geodetic Networks* Erice-Trapani-Sicilys, April 25–10 May, 1984, Italy.

Teunissen, P.J.G. (1990) An integrity and quality control procedure for use in multi sensor integration. In *Proc. of ION GPS*, pages 513–522, Colorado Spring, CO, September 1990. Also published in: Volume VII of the GPS Red Book Series: Integrated systems, ION Navigation, 2012.

Teunissen, P.J.G. (1995) The least-squares ambiguity decorrelation adjustment: a method for

fast GPS integer ambiguity estimation. *Journal of Geodesy*, vol. 70, no. 1-2, pp. 65–82.

Teunissen, P.J.G. (1997a) A canonical theory for short GPS baselines. Part I: The baseline precision. *Journal of Geodesy*, vol. 71, no. 6, pp. 320–336.

Teunissen, P.J.G. (1997b) A canonical theory for short GPS baselines. Part IV: Precision versus reliability. *Journal of Geodesy*, vol. 71, no. 9, pp. 513–525.

Teunissen, P.J.G. (1998a) On the integer normal distribution of the GPS ambiguities. *Artifical Satellites*, vol. 33, no. 2, pp. 49–64.

Teunissen, P.J.G. (1998b) Success probability of integer GPS ambiguity rounding and bootstrapping. *Journal of Geodesy*, vol. 72, no. 10, pp. 606–612.

Teunissen, P.J.G. (1999) An optimality property of the integer least-squares estimator. *Journal of Geodesy*, vol. 73, no. 11, pp. 587–593.

Teunissen, P.J.G. (2002) The parameter distributions of the integer GPS model. *Journal of Geodesy*, vol. 76, no. 1, pp. 41–48.

Teunissen, P.J.G. (2003) Adjustment Theory – An Introduction, *Series on Mathematical Geodesy and Positioning, Faculty of Aerospace Engineering*, Delft University of Technology, The Netherlands.

Teunissen, P.J.G., de Jonge, P.J., & Tiberius, C.C.J. M. (1996) The volume of the GPS ambiguity search space and its relevance for integer ambiguity resolution. *Proceedings of ION GPS*, vol. 9, pp. 889–898.

Teunissen, P.J.G., Odijk, D., & Zhang, B. (2010) PPP-RTK: Results of CORS network-based PPP with integer ambiguity resolution. *Journal of Aeronautics, Astronautics and Aviation, Series A*, vol. 42, no. 4, pp. 223–230.

Teunissen, P.J.G., Simons, D.G., & Tiberius, C.C.J. M. (2008) Probability and observation theory. *Lecture Notes AE2-E01, Faculty of Aerospace Engineering*, Delft University of Technology, The Netherlands, 2008.

Teunissen, P.J.G., & Verhagen, S. (2009) The GNSS ambiguity ratio-test revisited: a better way of using it. *Survey Review*, vol. 41, no. 312, pp. 138–151.

Verhagen, S., Li, B., & Teunissen, P.J.G. (2013) Ps-LAMBDA: Ambiguity success rate evaluation software for interferometric applications. *Computers and Geosciences*, vol. 54, pp. 361–376.

Verhagen, S., & Teunissen, P.J.G. (2013) The ratio test for future GNSS ambiguity resolution. *GPS Solutions*, vol. 17, no. 4, pp. 535–548.

Yang, Y.X., et al. (2011) Contribution of the compass satellite navigation system to global PNT users. *Chinese Science Bulletin*, vol. 56, no. 26, pp. 2813–2819.

Zhang, S., et al. (2010) An analysis of satellite visibility and relative positioning precision of COMPASS. In *Proceedings of Symposium for Chinese Professionals in GPS*, pp. 41–46. Shanghai, China, 18-20 August.

4 ON THE RELIABILITY AND PERFORMANCE OF A BDS+GPS RTK MODEL

This chapter is covered by the following publication:

Odolinski R, Teunissen PJG, Odijk D (2013a) Quality analysis of a combined COMPASS/BeiDou-2 and GPS RTK positioning model. Published in: Proceedings of the International Global Navigation Satellite System Society (IGNSS) Symposium, Golden Coast, Australia, July 16-18, 2013 (see Appendix C for proof of peer-review)

International Global Navigation Satellite Systems Society
IGNSS Symposium 2013

Outrigger Gold Coast, Qld Australia
16-18 July, 2013

Quality Analysis of a Combined COMPASS/BeiDou-2 and GPS RTK Positioning Model

Robert Odolinski (1)
GNSS Research Centre, Curtin University of Technology, Australia
+61 8 9266 3157 & +61 8 9266 2703, email: robert.odolinski@curtin.edu.au
Peter J.G. Teunissen (2)
GNSS Research Centre, Curtin University of Technology, Australia, and Delft University of Technology, the Netherlands
+61 8 9266 7676 & +61 8 9266 2703, email: P.Teunissen@curtin.edu.au
Dennis Odijk (3)
GNSS Research Centre, Curtin University of Technology, Australia
+61 8 9266 3157 & +61 8 9266 2703, email: D.Odijk@curtin.edu.au

ABSTRACT

The Chinese COMPASS/BeiDou-2 full constellation is expected by year 2020 with more than 30 satellites, and will provide global coverage. Australia is already a beneficiary of the regional Beidou system as enough satellites are available for Positioning, Navigation and Timing (PNT). A combined Beidou+GPS system increases the redundancy, which allows for higher accuracy and improved integrity. In this contribution we will compare a combined system performance with the Beidou- and GPS-only systems. The comparisons will involve integer ambiguity success rates and measures of precision of the estimated GNSS parameters and their reliability. Comparisons will involve single-frequency vs. multiple-frequencies and various satellite elevation cut-off angles. The results will show that the combined system allows for improved integer ambiguity success rates, satellite visibility and reliability as compared to the systems separately.

KEYWORDS: COMPASS/BeiDou-2, GPS, RTK, precision, variance matrix, reliability, Minimal Detectable Bias (MDB), integer ambiguity success rates

1. INTRODUCTION

The COMPASS satellite system, commonly known as BeiDou-2, attained initial regional operational status in the end of December 2011. Australia is a beneficiary of the current Beidou configuration located in the Asia-Pacific region, as enough satellites are available for Positioning, Navigation and Timing (PNT). Information about the navigation message was released to the public domain in December 2012 (CSNO, 2012). The full Beidou constellation is expected in 2020, and will consist of five Geostationary Earth Orbit (GEO), three Inclined Geo-Synchronous Orbit (IGSO) and 27 Medium Earth Orbit (MEO) satellites (CSNO, 2012). Beidou simulation results can be found in e.g. Grelier et al. (2007); Chen et al. (2009); Yang et al. (2011); Qu et al. (2012). Real data results were presented in Shi et al. (2012a) and Shi et al. (2012b) that evaluated Beidou-only Single Point Positioning (SPP), relative code

positioning, Real-Time-Kinematic (RTK), orbit determination and combined Beidou+GPS Precise Point Positioning (PPP). First real data Beidou results outside of China are reported in Montenbruck et al. (2012a, b) and Steigenberger et al. (2012, 2013). These later studies considered orbit determination, PPP, and single-baseline RTK positioning.

In this contribution we compare a combined system single-baseline RTK performance with the Beidou- and GPS-only systems. The comparisons will be made on measures of integer ambiguity success rates and on precision of the estimated GNSS parameters and their reliability. Reliability is a measure of robustness of the underlying model, and can be categorized into internal and external reliability. Internal reliability concerns the ability of the system to test the observations for modelling errors, and external reliability is referred to as the consequences on the estimated parameters when such model misspecifications are left undetected. For ambiguity resolution use is made of the LAMBDA method. The goal is to give Australian GNSS users indications of what Beidou can bring, both as a stand-alone system and when combined with GPS.

We start with a Beidou and GPS system overview, and describe the models and methods used for positioning and integer ambiguity resolution. Then we describe the reliability measures, and results are given. We conclude with a summary and discussion.

2. BEIDOU AND GPS FREQUENCIES AND WAVELENGTHS

The Beidou satellites currently transmit at three frequencies, B1, B2 and B3 in Quadrature phase-shift keying (QPSK) modulation as shown in Table 1, given together with the L1, L2 and L5 GPS frequencies. The Beidou signals are based on Code Division Multiple Access (CDMA) similar to GPS, Galileo and QZSS. We see that no Beidou frequencies overlap the GPS frequencies, and thus no Inter-system-bias parameterizations are needed (Odijk and Teunissen, 2013).

Table 1: COMPASS/BeiDou-2 and GPS signals.

Sat. system	Band (component)	Frequency [MHz]	Wavelength [cm]
BEIDOU	B1 (I/Q)	1561.098	19.20
	B2 (I/Q)	1207.140	24.83
	B3 (I/Q)	1268.520	23.63
GPS	L1	1575.42	19.03
	L2	1227.60	24.42
	L5	1176.45	25.48

3. METHODOLOGY

This section briefly describes the float and fixed baseline least-squares solution and integer ambiguity resolution. Then we describe the internal and external reliability measures that will be analyzed in the results section.

3.1 Float and fixed baseline least-squares solution

In the following we describe how we solve our unknown parameters and the integer ambiguities. Consider a single-baseline RTK model and GNSS observations collected in the m-vector y, where we divide the unknowns into baseline components in vector b including receiver position increments, receiver clock, etc., of say size $p \times 1$ with partial design matrix B, and (double-differenced) ambiguities in vector a of size $q \times 1$ with design matrix A. We

will solve the following Integer Least-Squares (ILS) problem (Teunissen, 1995),

$$\min_{b,a} \| y - Bb - Aa \|^2_{Q_{yy}}, \; b \in \mathbf{R}^p, a \in \mathbf{Z}^q \tag{1}$$

where $\| \cdot \|^2_{Q_{yy}} = (\cdot)^T Q_{yy}^{-1} (\cdot)$, Q_{yy} is the GNSS observations' variance-covariance (VCV) matrix, $\mathbf{R}^p$ the p-dimensional space of real numbers and $\mathbf{Z}^q$ the q-dimensional space of integers. The parameter estimation is divided into three steps, *1)* float solution, *2)* integer ambiguity estimation, and *3)* fixed solution.

3.1.1 Float solution

In the float solution we replace the integer constraint $\mathbf{Z}^q$ in (1) with $\mathbf{R}^q$, i.e. both the ambiguities and baseline components will be estimated as real-valued parameters. The unknown parameters can be solved by least-squares as follows (Teunissen et al., 2006),

$$\begin{bmatrix} \hat{b} \\ \hat{a} \end{bmatrix} = \begin{bmatrix} Q_{\hat{b}\hat{b}} & Q_{\hat{b}\hat{a}} \\ Q_{\hat{a}\hat{b}} & Q_{\hat{a}\hat{a}} \end{bmatrix} \begin{bmatrix} B^T Q_{yy}^{-1} y \\ A^T Q_{yy}^{-1} y \end{bmatrix} \tag{2}$$

$$\begin{bmatrix} Q_{\hat{b}\hat{b}} & Q_{\hat{b}\hat{a}} \\ Q_{\hat{a}\hat{b}} & Q_{\hat{a}\hat{a}} \end{bmatrix} = \begin{bmatrix} B^T Q_{yy}^{-1} B & B^T Q_{yy}^{-1} A \\ A^T Q_{yy}^{-1} B & A^T Q_{yy}^{-1} A \end{bmatrix}^{-1} \tag{3}$$

where $\hat{a}$, $\hat{b}$ are the least-squares solution of the ambiguities and baseline components respectively, and $Q_{\hat{a}\hat{a}}$, $Q_{\hat{b}\hat{b}}$, $Q_{\hat{a}\hat{b}}$ and $Q_{\hat{b}\hat{a}}$ are the corresponding (co-)variance matrices.

3.1.2 Integer ambiguity estimation

It can be shown that the integer solution of (1) is given by the integer minimizer,

$$\breve{a} = \underset{a \in \mathbf{Z}^q}{arg\,min} \| \hat{a} - a \|^2_{Q_{\hat{a}\hat{a}}} \tag{4}$$

which can efficiently be computed with the LAMBDA method (Teunissen, 1995). The ILS estimator in the LAMBDA method results in the highest possible success rates of all integer estimators (Teunissen et al., 1996, Teunissen 1999, 2002).

3.1.3 Fixed baseline solution

The fixed baseline solution $\breve{b}$ of the (integer) constrained linear model (Teunissen et al., 2006) then reads,

$$\breve{b} = \hat{b} - Q_{\hat{b}\hat{a}} Q_{\hat{a}\hat{a}}^{-1} (\hat{a} - \breve{a}) \tag{5}$$

If we neglect the uncertainty in $\breve{a}$, the corresponding VCV-matrix is given as,

$$Q_{\breve{b}\breve{b}} = Q_{\hat{b}\hat{b}} - Q_{\hat{b}\hat{a}} Q_{\hat{a}\hat{a}}^{-1} Q_{\hat{a}\hat{b}} \tag{6}$$

The uncertainty in $\breve{a}$ can be neglected if the probability of correct integer estimation is sufficiently high. Ensuring that the used integer ambiguity solution has a sufficiently high probability of being correct is the task of integer validation, see e.g. the Fixed Failure rate Ratio Test (FFRT) in (Teunissen and Verhagen, 2009), and (Verhagen and Teunissen, 2012).

3.2 Reliability, detection and identification of outliers

Reliability is a measure of robustness of the underlying model. We consider the following two composite hypotheses (Teunissen et al., 2006),

$$H_0 : E(y) = Ax, \tag{7}$$

and,

$$H_a : E(y) = Ax + C_y \nabla \tag{8}$$

In the null hypothesis H_0 in (7) we have $E(.)$ as the expectation operator, y as the m-vector

of observations, A the $m \times n$ (full-rank) design matrix and x the n-vector of unknowns. Further in the alternative hypothesis H_a in (8) we have C_y as an $m \times q$ (full-rank) matrix relating the outliers in the q-vector ∇ ($\nabla \neq 0$) to the observations y, where $1 \leq q \leq m-n$. In the absence of outliers (7) should be taken to estimate the unknown parameters x, otherwise (8). We emphasize that A should not be confused with the one in equation (1), i.e. the design matrix now also contains columns for the baseline components in addition to the ambiguities.

In order to describe the relevance of internal and external reliability, we need to introduce the Detection, Identification and Adaptation (DIA) procedure that can be used to identify and eliminate outliers (Teunissen, 1990). We focus on the Detection and Identification steps.

3.2.1 Detection

The Detection step in the DIA procedure concerns testing the model in (7) for all kinds of errors on all observations without any specific error signature in mind, i.e. it considers a full C_y in (8) of size q=m-n. The test statistic used is referred to as the Local Overall Model (LOM) test, see (Teunissen et al., 2006), and follows a central F-distribution with $m-n, \infty$ degrees of freedom (Figure 1). If the LOM test is exceeding a critical value as defined by a lookup table of the F-distribution for a certain level of significance, the Identification step should be taken since our assumed model in (7) then might be affected by outliers or anomalies.

3.2.2 Identification

Identification concerns constructing the C_y matrix in (8) to identify, if any, outliers ∇. Since many different alternative hypotheses can be taken, we usually restrict us to the case of one outlier per observation $q = 1$ for practical applications. Hence we formulate m number of alternative hypotheses by m number of c_{y_i} canonical vectors in (8), i.e. a vector of size $m \times 1$ with a 1 at the i:th position, with $i = 1,2,\ldots,m$, and the remaining zeros. This way of screening the observations is referred to as data snooping (Baarda, 1968), and can be tested by the so called w-test statistic, see (Teunissen et al., 2006). The w-test is standard normally distributed under H_0 (Figure 1).

3.2.3 Minimal Detectable Bias and internal reliability

Reliability of the LOM and w-test can be controlled by the power of test γ, i.e. the probability of rejecting H_0 in (7) when the alternative hypothesis H_a (8) is indeed true. The power of the test is a function of α the level of significance, i.e. the probability of rejecting H_0 when it is true (false alarm), the number of degrees of freedom q, and the non-centrality parameter λ. By fixing the power of the tests we can make sure that both tests detect a certain size of a bias with the same probability. Recall this probability as γ_0, and the non-centrality parameter λ_0 can then be fixed according to the following inverse power-function (Baarda, 1968),

$$\lambda_0 = \lambda(\alpha, m-n, \gamma_0) = \lambda(\alpha_0, 1, \gamma_0) \tag{9}$$

This implies that if we fix the power of the test for both the LOM and w-test, and as well fix α_0 for the w-test, we achieve the same size of the non-centrality parameter and thus same reliability for both tests. This quantity can for the F-distributed LOM-test and the normally distributed w-test be considered as an offset between the two modes of the corresponding distributions, see Figure 1.

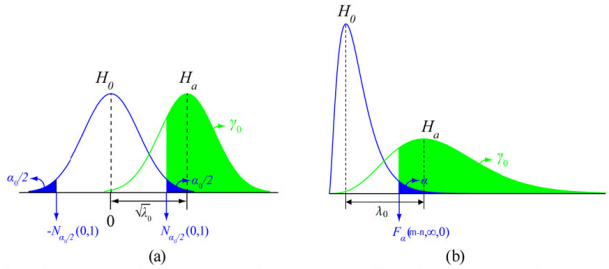

Figure 1: Linking the power of the LOM and w-test as well as the non-centrality parameter.

From this non-centrality parameter one can already in the design stage, before taking actual measurements, compute the Minimum Detectable Bias (MDB). We have $\lambda = \nabla^T c_y^T Q_{yy}^{-1} Q_{\hat{e}\hat{e}} Q_{yy}^{-1} c_y \nabla$ as the non-centrality parameter for the one-dimensional outlier case, with Q_{yy} as the observations' VCV-matrix, $Q_{\hat{e}\hat{e}} = P_A^{\perp} Q_{yy} P_A^{\perp T}$ as the VCV-matrix of the least-squares residuals and $P_A^{\perp} = \left(I_m - A\left(A^T Q_{yy}^{-1} A\right)^{-1} A^T Q_{yy}^{-1}\right)$ as a projector that projects onto the orthogonal complement to the range space of A. We then get,

$$|\nabla| = \sqrt{\frac{\lambda_0}{c_y^T Q_{yy}^{-1} Q_{\hat{e}\hat{e}} Q_{yy}^{-1} c_y}} \tag{10}$$

as the MDB (Teunissen, 1998a). One can also besides the MDB consider the following scalar squared Bias-to-Noise Ratio (BNR), with a specific outlier in $\nabla y = c_y \nabla$ in case of data snooping,

$$\lambda_y = \nabla y^T Q_{yy}^{-1} \nabla y \tag{11}$$

A small value of λ_y indicates that the bias is small as compared to the observation noise, whereas a large value indicates that the bias is significantly large.

3.2.4 External reliability

We can then compute the impact the bias ∇y has on the estimated unknown parameters $\hat{x}$ as obtained by taking (7), when (8) is actually true. The probability that the bias is not detected is also referred to as the probability of missed detection $1\text{-}\gamma_0$. With the bias propagation law and the difference of the hypotheses in (7) and (8) given as $E(y|H_a) - E(y|H_0) = \nabla y = C_y \nabla$, we get,

$$\nabla \hat{x} = (A^T Q_{yy}^{-1} A)^{-1} A^T Q_{yy}^{-1} \nabla y \tag{12}$$

This vector $\nabla \hat{x}$ represents the impact a bias in ∇y will have on the least-squares estimates under the null hypothesis (7) in case of a missed detection. We can also compute the squared BNR for the unknown parameters, similar to (11), as,

$$\lambda_{\hat{x}} = \nabla \hat{x}^T Q_{\hat{x}\hat{x}}^{-1} \nabla \hat{x} \tag{13}$$

where $Q_{\hat{x}\hat{x}} = (A^T Q_{yy}^{-1} A)^{-1}$ is the VCV-matrix of the unknown parameters. It can be shown (Teunissen, 2006) that the relation between λ_y, λ_0 and $\lambda_{\hat{x}}$ is,

$$\lambda_{\hat{x}} = \lambda_y - \lambda_0 \tag{14}$$

In other words, once the internal BNR (11) has been computed, the external BNR follows by subtracting the non-centrality parameter (9) from equation (11).

4 RESULTS

Data from one static receiver CUTA in Curtin's Continuously Operating Reference Stations and one experimental receiver CUTT are evaluated. The stations are equipped with Trimble NetR9 multi-frequency multi-GNSS receivers. One day of data was processed, namely April 21, 2013, with 30 sec interval between consecutive measurements. The distance between the stations is approximately 964 m. The Beidou (CSNO 2012) and GPS satellite orbits and clocks are given by the broadcast ephemerides. The estimated receiver positions are compared to very precise station benchmarks, and we make use of the DIA procedure to detect, identify and adapt for outliers. The CUTA antenna is shown to the left of Figure 2, whereas CUTT is given to the right. Typical skyplot, number of satellites and Positional Dilution Of Precision (PDOP) for a combined Beidou+GPS system is given in Figure 3 for April 21, UTC +0 hours. We see in Figure 3 that the current Beidou constellation overall provides us with a larger number of satellites over the day as compared to GPS.

Figure 2: CUTA (Left) and CUTT (Right) GNSS antennas, baseline distance 964 m.

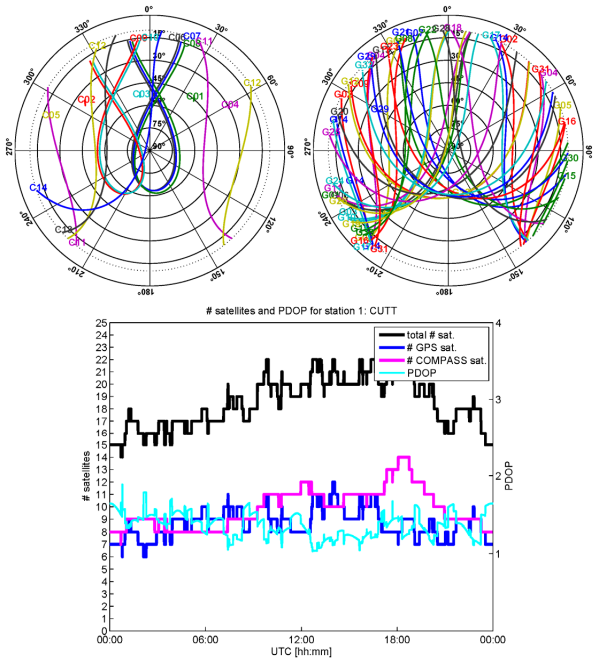

Figure 3: Satellite visibility and PDOP for a combined system (Bottom) with skyplot of Beidou (Top left) and GPS (Top right), with **10 degrees** elevation cut-off angle for CUTT in Perth and April 21, 2013.

4.1 Single-baseline RTK stochastic settings

The stochastic model settings in Q_{yy} for single-baseline RTK positioning are given in Table 2. We used data from other days than presented in this contribution to find these settings. We then applied these settings to the daily data to be analyzed to independently check the validity of the stochastic model used. The stochastic model is the exponential elevation weighting function as defined in (Euler and Goad, 1991). We restrict our analyses to Beidou B1 and B2 frequencies (not B3) to fairly compare the results to dual-frequency GPS L1 and L2.

Table 2: Stochastic model settings for single-baseline RTK, with a priori standard deviations for code and phase.

Sat. system	Frequency	Code [cm]	Phase [mm]
BEIDOU	B1	31	2.5
	B2	30	3.3
GPS	L1	37	2.5
	L2	27	2.6

4.2 Single-baseline RTK positioning results

Single-frequency RTK positioning results are shown in Figure 4 with epoch-by-epoch (instantaneous) integer ambiguity resolution for 10 degrees elevation cut-off angle and a combined B1+L1 Beidou+GPS system. Only the correctly fixed solutions are shown at bottom as determined by comparing the ambiguities to a set of reference ambiguities, see the description in relation to equation (15). Horizontal and vertical scatter plots are given with 95% confidence ellipses/levels derived from the empirical and formal VCV-matrix of the positions. The empirical VCV-matrix is given by the positioning errors as obtained from comparing the estimated positions to precise benchmark coordinates. The benchmark coordinates for our experimental receiver CUTT was obtained by using a combined Beidou+GPS RTK-system with multiple frequencies. The formal VCV-matrix is given from the mean of all single-epoch formal VCV-matrices of the entire observation span. All results are given in local North, East and Up and local Perth time, UTC +8 hours. Λ good match between the two ellipses implies realistic assumptions on the stochastic model and that we as a result have a minimum variance estimator (Teunissen et al., 2006).

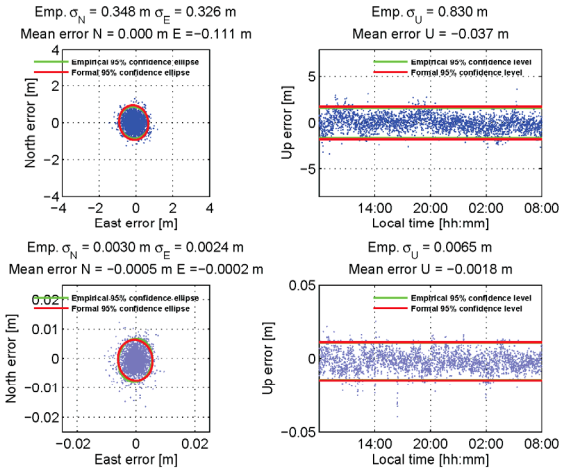

Figure 4: B1+L1 combined Beidou+GPS single-epoch and single-baseline RTK positioning scatter for CUTA-CUTT and April 21, 2013 and **10 degrees** cut-off angle. Float solutions (Top) and fixed solutions (Bottom), where empirical positioning mean errors and standard deviations are given in local North, East and Up.

We see in Figure 4 a good match between the formal and empirical ellipses/confidence levels, which implies that we have realistic stochastic settings in Table 2. We also see that the precision of the float solutions go from dm-meter level, down to a few mm standard deviations for the fixed solutions.

4.3 Integer ambiguity success rates and time-to-fix

The success rate, i.e. the probability of correct integer estimation, cannot be computed exactly for ILS. Fortunately however, the so called bootstrapped success rate can be used as an accurate lower bound to the ILS success rate (e.g. Teunissen, 1997, 1998b). We will denote this probability as $P_{s,B}$. This success rate can be computed without actual measurements i.e. only the (decorrelated) VCV-matrix (Teunissen, 1995) of the float ambiguities is needed.

We can also compute the so called ILS empirical success rates by comparing the estimated ambiguities to reference ambiguities. These reference ambiguities are estimated by using a combined Beidou+GPS system over the whole time-span with multiple-frequencies and a Kalman filter, assuming the ambiguities time-constant. The empirical success rate is given as,

$$P_{s_E} = \frac{\#\text{correct integer amb.}}{\text{total}\,\#\text{of integer amb.}} \tag{15}$$

The empirical failure rate is given as the complement,

$$P_{f_E} = 1 - P_{s_E} \tag{16}$$

4.3.1 Single-epoch success rates for various elevation cut-off angles

Empirical ILS success, failure and bootstrapped success rates for elevation cut-off angles ranging between 10-35 degrees are given in Table 3 for single- and multiple-frequency RTK. The higher elevation cut-off angles are taken as to mimick conditions with obstructed satellite availability such as in urban canyons or open pit mines. The bootstrapped success rates are computed as the mean of all single-epochs over the day. We denote all success rates of 100% with bold and in green color, whereas non-zero failure rates are denoted with red color.

The bootstrapped success rates in Table 3 are indeed good lower bounds to the ILS solutions, except for the combined system B1+L1 (98.1% vs. 100%) that is related to some epochs with poor quality signals from low elevation satellites (see e.g. a 15 degree cut-off angle, where the empirical success rate instead reach 100%). As expected the single-frequency single-system with the largest code noise (Table 2), smallest wavelength (Table 1) and number of satellites (Figure 3), also give the highest fractions of empirical failure rates (GPS L1). All epochs were however successfully fixed for all elevation angles for the combined-system when using multiple-frequencies. The GPS single-frequency system performs considerably worse than Beidou due to the smaller number of visible satellites at high elevations (see e.g. Figure 5). Very promisingly though is that the single-frequency combined system gives close to 100% success rates for elevation cut-off angles up to 30 degrees, and even 97%-98% at an elevation cut-off angle of 35 degrees. Compare these numbers to Beidou- and GPS-only success rates, with values down to 9% for GPS L1 and 52% for Beidou B1, and 35 degrees.

4.3.2 The wrongly fixed solutions single-epoch positioning results

For a surveyor collecting measurements in real-time, reference ambiguities are usually not available beforehand. This is where integer validation plays an important role (Teunissen and Verhagen, 2009). In Figure 5, B1 Beidou, L1 GPS and B1+L1 combined positioning results, with an elevation cut-off angle of 35 degrees, are given. The float solution is given in gray, correctly fixed solution in green, and the wrongly fixed solutions in red. We also give at bottom the number of satellites equal/above and below 8 for a single-system, and 9 for a

combined system, and the corresponding bootstrapped success rates (SR). The number of satellites lower bound for the combined system is set to 9 due to parameterization of different receiver clocks between the systems (one additional unknown). The GPS clock is given with respect to GPS time and the Beidou clock to BeiDou navigation satellite system time (CSNO, 2012). Gaps are seen in the GPS results since less than 4 satellites are visible for these epochs and thus the receiver coordinates are not (unbiased) estimable.

Table 3: Empirical ILS success, failure and bootstrapped success rates for single- and multiple-frequency RTK, CUTA-CUTT and elevation cut-off angles of **10, 15, 20, 25, 30 and 35 degrees** (from left to right respectively). Number of epochs 2880 (30 sec interval).

System/ frequency	**Empirical Success rate** P_{s_E} [%], cut-off [deg]						**Failure rate** P_{f_E} [%], cut-off [deg]						**Bootstrapped Success rate** $P_{s,BS}$ [%], cut-off [deg]					
	10	15	20	25	30	35	10	15	20	25	30	35	10	15	20	25	30	35
BEIDOU																		
B1	96.4	96.1	86.9	83.4	66.8	51.5	3.6	3.9	13.1	16.6	33.2	48.5	93.1	92.8	80.7	77.1	60.0	42.4
B2	97.6	97.5	87.5	84.6	72.6	59.4	2.4	2.5	12.5	15.4	27.4	40.6	96.0	95.8	86.9	83.7	67.1	52.1
GPS																		
L1	79.4	68.9	52.6	33.4	19.3	9.0	20.6	31.1	47.4	66.6	80.7	91.0	67.9	54.8	37.8	21.4	11.0	4.4
L2	93.3	87.3	73.5	50.6	32.5	16.9	6.7	12.7	26.5	49.4	67.5	83.1	90.0	82.3	67.3	45.6	28.3	14.5
COMBINED																		
B1+L1	98.1	**100**	**100**	**100**	99.4	97.0	1.9	0.0	0.0	0.0	0.6	3.0	**100**	**100**	**100**	99.9	98.7	94.4
B2+L2	**100**	**100**	**100**	**100**	99.7	97.6	0.0	0.0	0.0	0.0	0.3	2.4	**100**	**100**	**100**	**100**	99.6	97.5
BEIDOU																		
B1,B2	**100**	**100**	**100**	**100**	99.9	99.7	0.0	0.0	0.0	0.0	0.1	0.3	**100**	**100**	**100**	**100**	99.8	98.9
GPS																		
L1,L2	**100**	**100**	**100**	99.1	97.6	96.0	0.0	0.0	0.0	0.9	2.4	4.0	**100**	**100**	99.9	98.2	94.8	90.4
COMBINED																		
B1,B2+L1,L2	**100**	**100**	**100**	**100**	**100**	**100**	0.0	0.0	0.0	0.0	0.0	0.0	**100**	**100**	**100**	**100**	**100**	**100**

In Figure 5 we see that the correctly fixed positioning errors are very small (mm-level), and the Figure illustrates well the need of integer validation since the wrongly fixed solutions standard deviations become even larger than the corresponding values for the float solutions (meter-level). The number of satellites above/equal 8 (single-system) and 9 (combined-system) is shown to be a good indication whether single-frequency integer ambiguity resolution can be successful. This number of satellites (for 35 degree cut-off angle) is, however, only available approximately 18% of the time for Beidou and *never* for GPS, whereas 9 satellites (or more) are available approximately 92% of all epochs for the combined system. The insufficient number of satellites is also reflected in the float and wrongly fixed positioning results, particularly for GPS with errors of several tens of meters in the Up component. We see more specifically six large peaks of the Up errors that are related to poor satellite geometry, thus we depict the number of satellites and PDOP for GPS in Figure 6. By inspecting Figure 6 we have indeed PDOP peaks at the same time as for the float and wrongly fixed solutions in Figure 5. This implies that the combined system does not only dramatically improve the success rates (from 9% L1 GPS and 52% B1 Beidou, to 97% empirical success rate for a combined system), but also the satellite geometry and positioning availability.

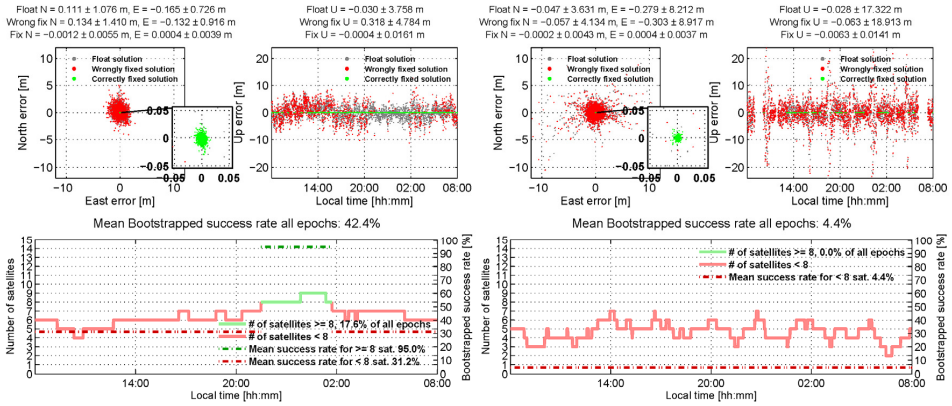

(a) B1 Beidou positioning and bootstrapped SR (35 deg). (b) L1 GPS positioning and bootstrapped SR (35 deg).

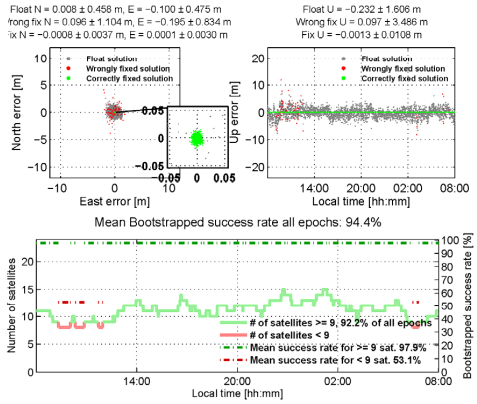

(c) B1+L1 Combined positioning and bootstrapped SR (35 deg).

Figure 5: Float (gray), correctly fixed (green) and wrongly fixed (red) solutions for single-epoch single-baseline RTK B1 Beidou (a), L1 GPS (b), and combined B1+L1 (c) positioning scatter for CUTA-CUTT and an elevation cut-off angle of **35 degrees**. Mean positioning errors ± standard deviations given in local North, East and Up. At the bottom of each positioning scatter plot light green represents number of satellites above or equal 8 (9 for combined) satellites, red corresponding color is for below 8 (9 for combined) satellites. Bootstrapped success rates are taken as a mean of all epochs above/equal and below these satellite limits.

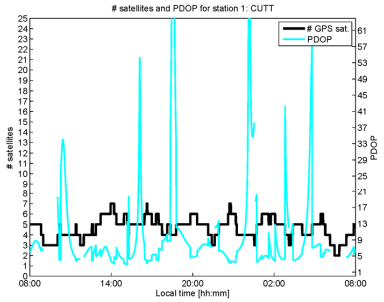

Figure 6: PDOP and number of satellites for GPS and an elevation cut-off angle of **35 degrees**.

4.3.3 Time-to-fix for single-frequency solutions

We conclude this section by giving the most demanding RTK scenario with single-frequency data and elevation cut-off angle of 35 degrees, but now instead of epoch-by-epoch solutions

we accumulate epochs by a Kalman filter assuming the ambiguities time-constant. This procedure goes as follows; The filter is initialized (at the first epoch) and based on the (filtered) set of float ambiguities, integer ambiguity resolution is attempted. The fixed ambiguities are then compared to the true reference ambiguities, and if they are not correct another epoch is included in the filter, and so on, until the estimated integer ambiguities are correct. When this is true, the filter is re-initialized at the second epoch, and the whole process is repeated again. In this way it is decided how many epochs that are needed for successful ambiguity resolution (time-to-fix). The time-to-fix results with mean ± standard deviation over the day are depicted in Figure 7 for B1 Beidou, L1 GPS and a B1+L1 combined system. Gaps are again seen in the GPS results since less than 4 satellites are visible for these epochs (Figure 6).

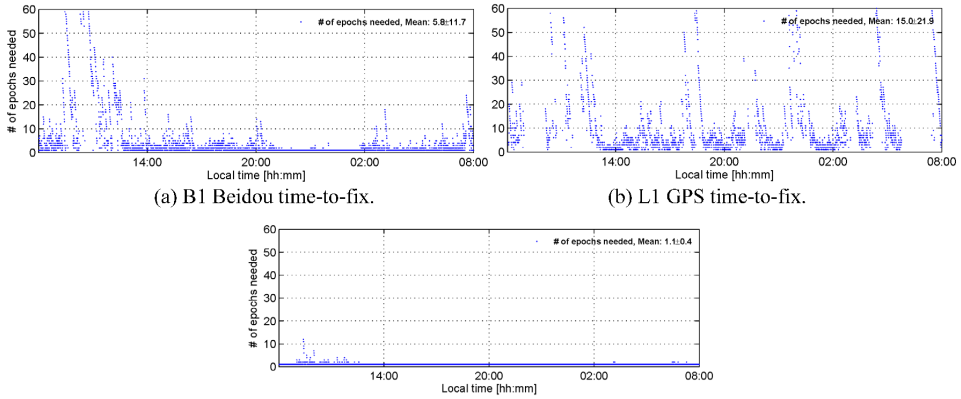

(a) B1 Beidou time-to-fix.

(b) L1 GPS time-to-fix.

(c) B1+L1 combined time-to-fix.

Figure 7: Time-to-fix (1 epoch = 30 sec) with mean ± standard deviation over the day for an elevation cut-off angle of **35 degrees** and single-baseline RTK B1 Beidou (a), L1 GPS (b) and B1+L1 combined (c) for CUTA-CUTT.

The combined system needs (estimated as a mean value) 1.1 epochs for successful ambiguity resolution, with a standard deviation of 0.4 epochs. Corresponding value for the single-systems are approximately 6 epochs (3 min) for Beidou B1 (standard deviation 6 min), and 15 epochs (7.5 min) for GPS L1 (standard deviation 11 min). When comparing Figure 7 to Figure 5, we see overall that the number of required epochs is one (instantaneous ambiguity resolution) when the number of satellites is sufficient (equal/above 8/9 satellites). This holds true for most of the epochs from approximately 9/10 p.m. to slightly before 2 a.m. local Perth Time for Beidou, and at all times for the combined system, except for some epochs before 12 a.m. For GPS however the number of satellites *never* reaches the sufficient number of satellites and thus we need (for 91% of the time, see Table 3) more than one epoch to successfully fix the ambiguities.

4.4 Internal and external reliability

The robustness of the GPS, Beidou and combined models against model errors is analyzed for single-frequency RTK. Two types of model errors have been assumed: i) outliers in the code data, and ii) cycle-slips in the phase data. Outliers affect the code observations of one single epoch, while cycle-slips shift the phase observations from a certain epoch by an integer amount of cycles. For both types of model errors we compute code outlier and phase slip MDBs and BNRs in a systematic way (by data snooping) for all observations during the day. While the code outlier MDBs/BNRs can be computed based on one single epoch, the phase

slip MDBs/BNRs are based on two consecutive epochs, for which the ambiguities are treated as time constant between them. The BNRs are taken as the square root of equation (13). We computed MDBs and BNRs as daily mean values for each satellite. In Table 4 and 5 we present the ranges (minimum to maximum) of these daily means for all satellites. In order to make a comparison between the 10-degree (Table 4) and 35-degree (Table 5) cases possible, the MDB time series time-span, from which the per-satellite mean MDB was computed, was in both cases confined to the 35-degree cut-off angle. The redundancy will however still be different between scenarios, since (other) visible satellites below 35 degrees are also contributing in the 10-degree case. In other words, we expect larger values of MDBs/BNRs in the 35-degree case, due to the less redundancy as compared to the 10-degree case. The MDBs are computed based on a significance level of 0.001 and a power of 0.80, such that the non-centrality parameter is 17.07. Large deviating values of MDBs/BNRs are given within brackets.

Table 4: Range of daily mean of code outlier (single-epoch) and phase slips (two-epochs) MDBs/BNRs for single-frequency B1 Beidou, L1 GPS, and B1+L1 combined, for an elevation cut-off angle of **10 degrees**.

Model	**System/ frequency**	**Code outlier (1 epoch) MDB [m]**	**BNR**	**Phase slip (2 epochs) MDB [cyc]**	**BNR**
SINGLE-SYSTEM	BEIDOU B1	2-5	6-8	0.07-0.2	0.2-0.8
	GPS L1	3-4	6-8	0.08-0.1	0.3-1.1
COMBINED	BEIDOU B1	2-3	5-8	0.07-0.08	0.2-0.4
	GPS L1	2-3	5-6	0.07-0.09	0.2-0.8

Table 5: Range of daily mean of code outlier (single-epoch) and phase slips (two-epochs) MDBs/BNRs for single-frequency B1 Beidou, L1 GPS, and B1+L1 combined, for an elevation cut-off angle of **35 degrees**.

Model	**System/ frequency**	**Code outlier (1 epoch) MDB [m]**	**BNR**	**Phase slip (2 epochs) MDB [cyc]**	**BNR**
SINGLE-SYSTEM	BEIDOU B1	2-24	5-76	0.08-1.1 (some MDBs > 9)	0.3-0.8 (some BNRs > 100)
	GPS L1	4-38	10-160	0.2-9.0 (some MDBs > 15)	0.9-110 (some BNRs > 1000)
COMBINED	BEIDOU B1	2-4	6-8	0.07-0.1	0.2-0.5 (some BNRs > 10)
	GPS L1	3-4	6-8	0.08-0.1	0.3-0.9 (some BNRs > 6)

It can be seen from Table 4 that with a cut-off of 10 degrees the code outliers MDBs lie in the range of 2-5 m for Beidou-only and 3-4 m for GPS-only. The Beidou MDBs are generally smaller than those of GPS, because of the lower noise of the Beidou B1 code data (see Table 2) and (on average) the larger number of Beidou satellites tracked (see Figure 3). The corresponding BNRs are in the range of 6-8 for both Beidou and GPS. When the constellations are combined the values for the code outlier MDBs/BNRs are decreased as compared to the single-system MDBs/BNRs, this since the combined model is stronger and has higher redundancy. The phase slip MDBs lie in the range of 0.07-0.2 cycles for Beidou-only and 0.08-0.1 cycles for GPS-only. These are slightly improved in the combined solution to values ranging between 0.07-0.09 cycles. The corresponding BNRs, which are up to 0.8 for Beidou-only and up to 1.1 for GPS-only, are also slightly improved when the two are combined.

The results using the much higher cut-off elevation of 35 degrees are as follows. From Table 5 it can be seen that the mean code outlier MDBs are in the range of 2-24 m for Beidou, and those for GPS in the range of 4-38 m. These much larger ranges as compared to the 10-degree

cut-off scenario are due to the low redundancy when using a 35 degree cut-off angle (see Figure 5). The corresponding single-system BNRs can take on very large values as well: up to 160 for GPS. In other words, the reliability becomes poorer when we decrease the number of satellites. A significant improvement in code outlier robustness can however be observed for a combined Beidou+GPS system: the MDBs reduce to low values below 4 m and the BNRs are not larger than 8 for both systems. With an elevation cut-off angle of 35 degrees, the phase slip MDBs can also be very large: MDBs larger than 9 cycles are observed for Beidou-only and even larger values (more than 15 cycles) for GPS-only. This implies that cycle slips smaller than these values may not be detected, which can inhibit (non-instantaneous) integer ambiguity resolution. This is also visible from the corresponding BNR values, which can be more than 100 for Beidou-only and even more than 1000 for GPS-only. However, the results improve significantly when the two constellations are combined: all phase slip MDBs become at most 0.1 cycles, while the corresponding BNR has some sporadic outliers of 10 at most. By comparing the 35-degree MDBs/BNRs for the combined system with the corresponding 10-degree, we see a much less degradation of the reliability as compared to the single-system cases. This is promising, since a combined system does then not only allow for high success rates for large elevation angles (Table 3), but also preserves the reliability of the model.

5. CONCLUSIONS

In this contribution we have studied the third satellite system Beidou that in addition to GPS and GLONASS provides continuous PNT in the Asia-Pacific region. We focused our attention on positioning in Perth, Western Australia and a combined Beidou+GPS single-baseline RTK model, the integer ambiguity success rates and the internal/external reliability of the model. The comparisons were made to the systems separately. We can summarize our findings and conclusions as follows.

5.1 Integer ambiguity success rates for various satellite elevation cut-off angles

In Table 3 we summarized (single-epoch) ILS empirical success rates results for single- and multiple-frequency Beidou, GPS and combined Beidou+GPS RTK. This was given for several different satellite cut-off elevation angles (10-35 degrees), where higher cut-off angles are suitable in e.g. urban canyons or open pit mines. Our main conclusion is that with an elevation cut-off angle of up to 35 degrees, a combined single-frequency Beidou+GPS system can provide us with empirical success rates of 97%-98%. The corresponding number for 30 degrees was 100%. If we compare the 35 degree results to the single-systems, with success rates ranging between 9% (for L1 GPS) to at most 59% (for B2 Beidou), it is indeed a dramatic and promising improvement. We also concluded that the Beidou-only system currently has, during a 24 hour period, more satellites at higher elevation angles as compared to GPS and with respect to our receivers, which allows for larger Beidou success rates for different cut-off angles.

5.2 Time-to-fix

When looking into the most demanding scenario with an elevation cut-off angle of 35 degrees and single-frequency (B1 and L1) data, we found by using a Kalman filter that the time-to-fix was (almost) only one epoch for the combined system, taken as mean over the day. The corresponding numbers for Beidou and GPS were 6 epochs (3 min) and 15 epochs (7.5 min) respectively (Figure 7). The time-to-fix results were also found to be correlated to the number of satellites as depicted in Figure 5, and the corresponding (single-epoch) bootstrapped success rates.

5.3 Internal and external reliability

When the constellations were combined, the values of the code outlier MDBs/BNRs were slightly decreased for a 10 degree of elevation cut-off angle (Table 4), with a significant improvement for the 35 degree angle (Table 5). More specifically, in the latter case the code MDBs were decreased from several tens of meters down to a few meters. With an elevation cut-off angle of 35 degrees, the single-system phase slip MDBs also become very large. We obtained MDBs larger than 9 cycles for Beidou, and more than 15 cycles for GPS. This implies that cycle slips smaller than these values might not be detected for a single-system, which can seriously inhibit (non-instantaneous) integer ambiguity resolution. However, the results improve significantly when the two constellations are combined, where all phase slip MDBs become at most 0.1 cycles, while the corresponding BNR has some sporadic outliers of 10. Comparing 35-degree MDBs/BNRs (Table 5) with the corresponding 10-degree results (Table 4), we can also conclude that a combined system preserves the reliability of the model.

Beidou has already been shown to be suitable as a complementary or standalone GNSS system for Australia. More satellites are upcoming and will improve the Beidou and combined Beidou+GPS system even further.

ACKNOWLEDGEMENTS

This work has been executed in the framework of the Positioning Program Project 1.01 "New carrier phase processing strategies for achieving precise and reliable multi-satellite, multi-frequency GNSS/RNSS positioning in Australia" of the Cooperative Research Centre for Spatial Information (CRC-SI). The second author is the recipient of an Australian Research Council (ARC) Federation Fellowship (project number FF0883188). Data was provided by Noor Raziq and Boris Padovan, and help was provided from Nandakumaran Nadarajah with the Beidou navigation message, all at the GNSS Research Centre of Curtin University. All this support is gratefully acknowledged.

REFERENCES

Baarda, W. (1968) A testing procedure for use in geodetic networks. Netherlands Geodetic Commission, Publ. on Geodesy, New Series, 2(5), 1968.

Chen, H.C., Huang, Y.S., Chiang, K.W., Yang, M. and Rau, R.J. (2009) The performance comparison between GPS and BeiDou-2/COMPASS: A perspective from Asia. *J. of the Chinese institute of engineers*, 32(5):679–689, 2009.

CSNO (2012). BeiDou Navigation Satellite System Signal In Space Interface Control Document by China Satellite Navigation Office (CSNO). Open service signal B1I (Version 1.0). Technical report, December 2012. 77 pages., 2012.

Euler, H. J. and Goad, C. g. (1991) On optimal filtering of GPS dual frequency observations without using orbit information. *Bulletin Geodesique*, 65:130–143, 1991.

Grelier, T., Ghion, A., Dantepal, J., Ries, L., DeLatour, A., Issler, J-L., Avila-Rodriguez, JA., Wallner, S. and Hein, GW. (2007) Compass signal structure and first measurements. In *Proc. of ION GNSS-2007*, pages 3015–3024, Fort Worth, TX, September 2007.

Montenbruck, O., Hauschild, A., Steigenberger, P., Hugentobler, U., Teunissen, P.J.G. and Nakamura, S. (2012a) Initial assessment of the COMPASS/BeiDou-2 regional navigation satellite system. *GPS Solutions*, 2012. DOI 10.1007/s10291-012-0272-x.

Montenbruck, O., Hauschild, A., Steigenberger, P., Hugentobler, U. and Riley, S. (2012b) A COMPASS for Asia: First experience with the BeiDou-2 Regional Navigation System. In *Proc. of IGS Workshop 2012, July 23-27, Olsztyn, Austria*, 2012.

Odijk, D. and Teunissen, P.J.G. (2013) Characterization of between-receiver GPS-Galileo

inter-system biases and their effect on mixed ambiguity resolution. *GPS Solutions*, Springer-Verlag, p. 1-13, DOI 10.1007/s10291-012-0298-0, 2013.

Qu, J., Yuan, H., Zhang, X. and Ouyang, G. (2012) Single-epoch COMPASS carrier-phase ambiguous resolution using three civil frequencies and special constellations. In *25th ITM of the Satellite Division of the Institute of Navigation, Nashville TN, September 17-21*, 2012.

Shi, C., Zhao, Q., Li, M., Tang, W., Hu, Z., Lou, Y., Zhang, H., Niu, X. and Liu, J. (2012a) Precise orbit determination of Beidou Satellites with precise positioning. *Science China Earth Sciences*, 55:1079–1086, 2012. doi: 10.1007/s11430-012-4446-8.

Shi, C., Zhao, Q., Hu, Z. and Liu, J. (2012b) Precise relative positioning using real tracking data from COMPASS GEO and IGSO satellites. *GPS Solutions*, pages 1–17, 2012. DOI 10.1007/s10291-012-0264-x.

Steigenberger, P., Hauschild, A., Hugentobler, U. and Montenbruck, O. (2012) Performance analysis of Compass orbit and clock determination and Compass only PPP. In *Proc. of IGS Workshop 2012, July 23-27, Olsztyn, Austria*, 2012.

Steigenberger, P., Hugentobler, U., Hauschild, A., Montenbruck, O., (2013). Orbit and clock analysis of COMPASS GEO and IGSO satellites. *J. of Geodesy* doi:10.1007/s00190-013-0625-4.

Teunissen, P. J. G. (1990) An integrity and quality control procedure for use in multi sensor integration. In *Proc. of the 3rd ITM of the Satelllite Division of the Institute of Navigation (ION GPS 1990)*, pages 513–522, Colorado Spring, CO, September 1990. Also published in: Volume VII of the GPS Red Book Series: Integrated systems, *ION Navigation*, 2012.

Teunissen, P. J. G. (1995) The least squares ambiguity decorrelation adjustment: a method for fast GPS integer estimation. *J. of Geodesy*, 1995. 70: 65-82.

Teunissen, P. J. G. (1997) A canonical theory for short GPS baselines. Part IV: Precision versus reliability. *J. of Geodesy*, 1997. 71: 513-525.

Teunissen, P. J. G. (1998a) Minimal detectable biases of GPS data. *J. of Geodesy*, 1998. 72: 236-244.

Teunissen, P. J. G. (1998b) Success probability of integer GPS ambiguity rounding and bootstrapping. *J. of Geodesy*, 1998. 72: 606-612.

Teunissen, P. J. G. (1999) An optimality property of the integer least-squares estimator. *J. of Geodesy*, 1999. 73: 587-593.

Teunissen, P. J. G. (2002) The parameter distributions of the integer GPS model. *J. of Geodesy*, 2002. 76: 41-48.

Teunissen, P. J. G. (2006). Testing theory - an introduction. Series on Mathematical Geodesy and Positioning, Delft University of Technology, 2006, The Netherlands.

Teunissen, P. J. G., de Jonge, P.J., and Tiberius, C.C.J.M. (1996) The volume of the GPS ambiguity search space and its relevance for integer ambiguity resolution. *Proc. of ION GPS*. Volume 9, pages 889-898, 1996.

Teunissen, P. J. G., Simons, D.G. and Tiberius, C.C.J.M. (2006) Probability and Observation Theory. *Lecture Notes AE2-E01, Delft University of Technology, The Netherlands*, 2006.

Teunissen, P. J. G. and Verhagen, S. (2009) The GNSS ambiguity ratio-test revisited: a better way of using it. *Survey Review Vol. 41, No. 312*, pages 138–151, 2009.

Verhagen, S. and Teunissen, P. J. G. (2012) The ratio test for future GNSS ambiguity resolution. *GPS Solutions*, 2012. DOI 10.1007/s10291-012-0299-z.

Yang, Y.X., Li, J.L., Xu, J.Y., Tang, J., Guo, H.R. and He, H.B. (2011) Contribution of the Compass satellite navigation system to global PNT users. *Chinese Science Bulletin*, 56(26):2813–2819, 2011.

5 INSTANTANEOUS BDS+GPS RTK POSITIONING WITH HIGH ELEVATION CUT-OFF ANGLES

This chapter is covered by the following publication:

Teunissen PJG, **Odolinski R**, Odijk D (2014) Instantaneous BeiDou+GPS RTK positioning with high cut-off elevation angles. Published in: Journal of Geodesy, vol. 88, no. 4, p. 335-350. doi:10.1007/s00190-013-0686-4

J Geod (2014) 88:335–350
DOI 10.1007/s00190-013-0686-4

ORIGINAL ARTICLE

Instantaneous BeiDou+GPS RTK positioning with high cut-off elevation angles

P. J. G. Teunissen · R. Odolinski · D. Odijk

Received: 30 August 2013 / Accepted: 3 December 2013 / Published online: 20 December 2013

Abstract As the Chinese BeiDou Navigation Satellite System (BDS) has become operational in the Asia-Pacific region, it is of importance to better understand as well as demonstrate the capabilities that a combination of BeiDou with GPS brings to positioning. In this contribution, a formal and empirical analysis is given of the single-epoch RTK positioning capabilities of such a combined system. This will be done for the single- and dual-frequency case, and in comparison with the BDS- and GPS-only performances. It will be shown that with the combined system, when more satellites are available, much larger than the customary cut-off elevations can be used. This is important, as such measurement set-up will significantly increase the GNSS applicability in constrained environments, such as e.g. in urban canyons or when low-elevation multipath is present.

Keywords BeiDou (BDS) · GPS · Multi-GNSS · Integer ambiguity resolution · Real time kinematic (RTK) Positioning · Cut-off elevation

P. J. G. Teunissen (✉) · R. Odolinski · D. Odijk
Department of Spatial Sciences, GNSS Research Centre, Curtin University of Technology, Perth, Australia
e-mail: p.teunissen@curtin.edu.au

R. Odolinski
e-mail: Robert.Odolinski@curtin.edu.au

D. Odijk
e-mail: D.Odijk@curtin.edu.au

P. J. G. Teunissen
Mathematical Geodesy and Positioning, Delft University of Technology, Delft, The Netherlands

1 Introduction

The BeiDou Navigation Satellite System (BDS) attained initial regional operational status at the end of December 2011, and can now provide positioning, navigation and timing (PNT) services in the whole Asia-Pacific region. The full BDS constellation is expected to be operational in 2020, and will consist of five Geostationary Earth Orbit (GEO), three Inclined Geo-Synchronous Orbit (IGSO) and 27 Medium Earth Orbit (MEO) satellites (CSNO 2012).

Simulation results for BDS can be found in Grelier et al. (2007), Huang and Tsai (2008), Cao et al. (2008b), Chen et al. (2009), Zhang et al. (2010), Guo et al. (2011), Yang et al. (2011), Qu et al. (2012), Verhagen and Teunissen (2013). Real data results were presented in e.g. Shi et al. (2012, 2013), Li et al. (2013) evaluating BDS single point positioning, orbit determination and combined BDS+GPS precise point positioning (PPP). First results using BDS outside of China are reported in Montenbruck et al. (2012, 2013), Steigenberger et al. (2012, 2013), Nadarajah et al. (2013).

In this contribution, we use real data to analyse the real-time kinematic (RTK) positioning capabilities of the single- and dual-frequency combined BDS+GPS system under different cut-off elevation angles, ranging from 10° to 40°. We will show that with the combined system much higher than customary cut-off elevations can be used. This is important, since such capability increases the GNSS applicability in constrained environments (e.g. urban canyon, open pits) and allows one to avoid low-elevation multipath in general.

In our analyses, the emphasis is on instantaneous ambiguity resolution as this is the most challenging case to study. Hence, all our results of ambiguity resolution as well as positioning are based on the use of single-epoch data. This approach has the added advantage that the results will be insensitive to the occurrences of carrier-phase cycle slips.

This contribution is organized as follows. After a brief description in Sect. 2 of BDS in the Asia-Pacific region, the combined GPS+BDS model, together with its integer least-squares (ILS) solution, is formulated in Sect. 3. A formal analysis of the expected performance of the combined GPS+BDS model is given in Sect. 4. It provides for an analytical expression of the ambiguity dilution of precision (ADOP), followed by an integer bootstrapped (IB) success-rate analysis of single- and dual-frequency GPS and BDS, both as stand-alone single systems as well as a combined system. This analysis is done for different cut-off elevation angles, ranging from 10° to 40°. We also present a formal analysis of the positioning precision, whereby we stress and demonstrate that the performance of positioning and ambiguity resolution do not always go hand-in-hand. In Sect. 5, we complement the formal analysis with an empirical performance analysis of GPS+BDS covering 5 days over a 10-day period. This analysis is based on empirically determined positioning precision and ambiguity success-rates. These results show the markedly different performance of the systems when increasing the cut-off elevations. They also show, importantly, that with the combined GPS+BDS system, much larger than the customary cut-off elevations can be used. A summary of the work and conclusions is given in Sect. 6.

2 BeiDou in the Asia-Pacific region

The BeiDou Navigation Satellite System attained initial regional operational status at the end of December 2011, and can now provide PNT services in the whole of the Asia-Pacific region. Figure 1a shows a 24-h ground track of the operational BDS satellites available for positioning at June 26, 2013. The positions of the satellites at UTC 10.54 pm are indicated with a dot.

The operational satellite constellation consists of five GEO satellites in orbit at an altitude of 35, 786 km, and five IGSO satellites at an altitude of 35, 786 km as well as with 55° inclination to the equatorial plane (CSNO 2012). The MEO satellites are operated in orbit at an altitude of 21, 528 km and 55° inclination to the equatorial plane (CSNO 2012) and are comparable to the GPS, GLONASS and Galileo satellites. The IGSO satellites describe figure-of-eight loops, while the GEO satellites are controlled in longitude, but not latitude and thus reach peak inclinations of about 2° (Montenbruck et al. 2013).

The BDS satellites currently transmit on three frequencies, B1, B2 and B3, in quadrature phase-shift keying (QPSK) modulation as shown in Table 1. In the Table, we also depict the L1, L2 and L5 GPS frequencies. The BDS signals are based on code division multiple access (CDMA) similar to GPS and Galileo. The signals are referred to as "I" and "Q", where I components are likely to be available for an open service, and the Q components for a restricted or authorized

Table 1 BDS (Han et al. 2011) and GPS signals

Sat.system	Band (component)	Frequency (MHz)	Wavelength (cm)
BDS	B1 (I/Q)	1,561.098	19.20
	B2 (I/Q)	1,207.140	24.83
	B3 (I/Q)	1,268.520	23.63
GPS	L1	1,575.42	19.03
	L2	1,227.60	24.42
	L5	1,176.45	25.48

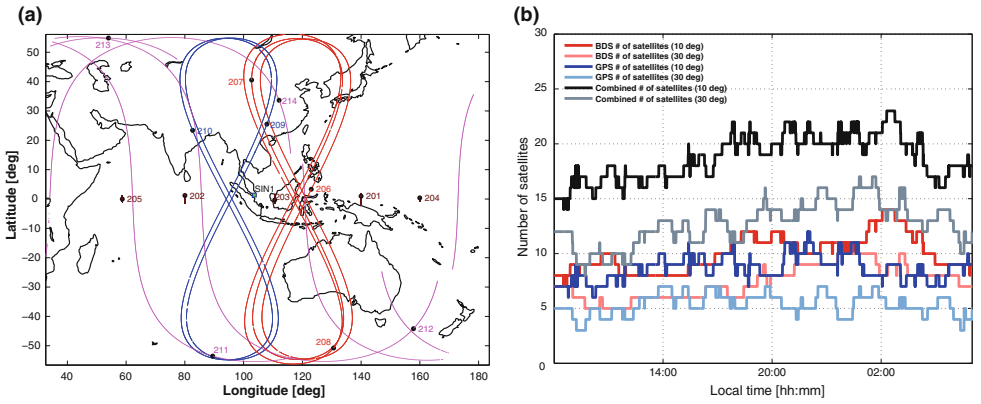

Fig. 1 **a** BeiDou System (BDS) ground tracks with satellite locations (*black dots*) given for June 26, 2013, UTC 10:54pm; **b** Satellite visibility of GPS and BDS with 10° and 30° elevation cut-off angle for Perth station CUT0, April 21, 2013

service (Cao et al. 2008a). In this contribution, we only compare the BDS results with that of single- and dual-frequency GPS, since the third GPS L5 frequency is currently (2013) only available from PRNs 1, 24, 25, and 27.

As the Table shows, there is no overlap between the BDS and GPS frequencies [note: there are plans to shift the B1 signal to L1, Gibbons (2013)]. This implies that in the double-differencing (DD) formulation system-specific pivot satellites can be taken, i.e. one reference satellite per system.

Figure 1b provides time series of the number of GPS and BDS satellites that can be tracked under a 10° and a 30° cut-off elevation angle. From this figure alone, one can already predict that the availability of high-precision positioning capabilities will increase significantly when both systems, GPS and BDS, are combined. For instance, if one would assume that, say, eight or more satellites are needed for a high-precision solution, then for a ten degree elevation cut-off angle, GPS and BDS would provide this as stand-alone systems 84 and 95 % of the time, respectively, while this would be 100 % for a combined GPS+BDS system. For higher elevation cut-off angles, this difference between the single systems and the combined system increases rapidly. For a 30° cut-off elevation angle, only fewer than eight satellites are tracked with GPS, while with BDS and the combined system the eight or more satellites are still tracked 41 and 100 % of the time, respectively.

3 The GPS+BDS GNSS model

In this section, we present the GNSS model for combining GPS and BDS, together with its ILS solution.

3.1 The model

We assume that $s_G + 1$ GPS-satellites are tracked on f_G frequencies and $s_B + 1$ BDS satellites on f_B frequencies. We apply system-specific double-differencing (DD) and thus have one reference (or pivot) satellite per system. The total number of DD phase and code observations per epoch equals therefore $2f_G s_G + 2f_B s_B$. No cross-correlation between code and phase, nor between frequencies, will be assumed. The combined short-baseline GPS+BDS model can then be defined as follows.

Definition (*Combined GPS+BDS model*) Let the system-specific DD phase and code observation vectors be denoted as ϕ_* and p_*, respectively, with $* = \{G, B\}$ (G = GPS, B = BDS). Then, the single-epoch linear(ized) GNSS model of the combined system is given as

$$\mathrm{E}\begin{bmatrix}\phi\\ p\end{bmatrix} = \begin{bmatrix}\Lambda & A\\ 0 & A\end{bmatrix}\begin{bmatrix}a\\ b\end{bmatrix}, \quad \mathrm{D}\begin{bmatrix}\phi\\ p\end{bmatrix} = \begin{bmatrix}Q_{\phi\phi} & 0\\ 0 & Q_{pp}\end{bmatrix} \tag{1}$$

in which E[.] and D[.] denote the expectation and dispersion operator, respectively, $\phi = [\phi_G^T, \phi_B^T]^T \in \mathbb{R}^{f_G s_G + f_B s_B}$ the combined phase vector, $p = [p_G^T, p_B^T]^T \in \mathbb{R}^{f_G s_G + f_B s_B}$ the combined code vector, $a = [a_G^T, a_B^T]^T \in \mathbb{Z}^{f_G s_G + f_B s_B}$ the combined integer ambiguity vector, $b \in \mathbb{R}^v$ the real-valued baseline vector, and with the entries of the design matrix given as

$$\Lambda = \mathrm{blkdiag}[\Lambda_G, \Lambda_B], \quad \Lambda_* = \mathrm{diag}[\lambda_{1_*}, \ldots, \lambda_{f_*}] \otimes I_{s_*}$$
$$A = [A_G^T, A_B^T]^T, \qquad A_* = [e_{f_*} \otimes D_{s_*}^T G_*]$$

where I_{s_*} is the $s_* \times s_*$ unit matrix, e_{f_*} is the $f_* \times 1$ vector of 1's, and $D_{s_*}^T = [-e_{s_*}, I_{s_*}]$ is the $s_* \times (s_* + 1)$ differencing matrix, and with the entries of the positive definite variance matrix given as

$$Q_{\phi\phi} = \mathrm{blkdiag}[Q_{\phi_G\phi_G}, Q_{\phi_B\phi_B}], \; Q_{\phi_*\phi_*} = C_{\phi_*\phi_*} \otimes 2Q_*$$
$$Q_{pp} = \mathrm{blkdiag}[Q_{p_G p_G}, Q_{p_B p_B}], \; Q_{p_* p_*} = C_{p_* p_*} \otimes 2Q_*$$
$$C_{\phi_*\phi_*} = \mathrm{diag}[\sigma^2_{\phi_{1_*}}, \ldots, \sigma^2_{\phi_{f_*}}], \; C_{p_* p_*} = \mathrm{diag}[\sigma^2_{p_{1_*}}, \ldots, \sigma^2_{p_{f_*}}]$$
$$Q_* = D_{s_*}^T W_*^{-1} D_{s_*}, \; W_* = \mathrm{diag}[w_{1_*}, \ldots, w_{s_*+1}]$$

where w_{i_*} denotes the satellite elevation dependent weight.

In the above definition, the diagonal matrix Λ contains the wavelengths of the observed frequencies and the geometry-matrices G_G and G_B contain the undifferenced receiver-satellite unit direction vectors for GPS and BDS, respectively. The Kronecker product is denoted as $\otimes$. As first shown in (Teunissen 1997), it allows for a compact respresentation of general GNSS models. As the above model applies to short baselines, the ionospheric delays are assumed absent (Goad 1998). The zenith tropospheric delay (ZTD), however, may be present. If it is included, then $v = 4$ instead 3, and G_G and G_B will have a fourth column containing the ZTD mapping functions. Our numerical and empirical analyses are based on $v = 3$. For the weights w_{i_*}, we take the elevation-dependent weighting function as given in Euler and Goad (1991). For the zenith-referenced undifferenced phase- and code standard deviations, $\sigma_{\phi_{j_*}}$ and $\sigma_{p_{j_*}}$ ($j_* = 1_*, \ldots, f_*$), we use the values of Table 2. They were estimated using data that are independent from the data used in the following sections. The method of estimation is described in Odolinski et al. (2013).

We assume the design matrix of (1) to be of full column rank. Its *redundancy* is then equal to the number of DD

Table 2 Zenith-referenced code- and phase standard deviations

	Frequency	Code $\sigma_p(cm)$	Phase $\sigma_\phi(mm)$
GPS	L1	37	2.5
	L2	27	2.6
BDS	B1	31	2.5
	B2	30	3.3

observables minus the number of unknowns. For the combined system, this gives

$$\text{redundancy} = s_G f_G + s_B f_B - \nu \tag{2}$$

It is the sum of the redundancies of the single systems plus ν, the number of parameters the two systems have in common. Hence, the redundancy increases by $s_* f_*$ if one goes from a single system to a combined system.

From (2), the *solvability* condition of the combined system follows as

$$\text{solvability} : s_G + s_B \geq \nu \tag{3}$$

This demonstrates the increase in availability that a combination of the two systems brings. For a single system, the system is only solvable if $s_* \geq \nu$ (at least four satellites are needed if $\nu = 3$). For the combined system however, this single-system condition can be relaxed as now also the satellites of the second system contribute. Instead of a minimum of four satellites when $\nu = 3$, the combined system only requires the total number of satellites to be not smaller than five. Hence, where three GPS satellites ($s_G = 2$) and three BDS satellites ($s_B = 2$) would not be sufficient for single-system solvability when $\nu = 3$, it does suffice for the combined case.

3.2 The integer least-squares solution

The (mixed) integer least-squares solution of model (1) is defined as

$$\{\check{a}, \check{b}\} = \arg \min_{a \in \mathbb{Z}^n, b \in \mathbb{R}^\nu} \left(||\phi - \Lambda a - Ab||^2_{Q_{\phi\phi}} + ||p - Ab||^2_{Q_{pp}} \right) \tag{4}$$

with $n = f_G s_G + f_B s_B$ and $||.||^2_Q = (.)^T Q^{-1}(.)$ denoting the weighted squared norm. The solution of this ILS problem can be obtained in three steps (Teunissen 1995). First, the so-called float solution $\hat{a}, \hat{b}$ is obtained by discarding the integer constraints on the ambiguities. Then, the float ambiguities are used to estimate their integer values as $\check{a}$. This integer ambiguity vector is then finally used to obtain the fixed baseline solution $\check{b}$ from its float counterpart $\hat{b}$.

The least-squares (LS) float solution $\hat{a}$, $\hat{b}$ of the single-epoch model (1) is given as

$$\begin{aligned} \hat{b} &= Q_{\hat{b}\hat{b}} A^T Q_{pp}^{-1} p, \;\; Q_{\hat{b}\hat{b}} = (A^T Q_{pp}^{-1} A)^{-1} \\ \hat{a} &= \Lambda^{-1}(\phi - A\hat{b}), \;\; Q_{\hat{a}\hat{a}} = \Lambda^{-1}(Q_{\phi\phi} + A Q_{\hat{b}\hat{b}} A^T)\Lambda^{-1} \end{aligned} \tag{5}$$

Note that the float solution of b is only driven by the code observables. Due to the single-epoch nature of model (1), the phase observables do not contribute to $\hat{b}$.

Using the ILS-principle, the integer ambiguity vector is estimated from $\hat{a}$ as

$$\check{a} = \arg \min_{z \in \mathbb{Z}^n} ||\hat{a} - z||^2_{Q_{\hat{a}\hat{a}}}, \;\; n = f_G s_G + f_B s_B \tag{6}$$

As proven in Teunissen (1999), ILS-estimators have the highest success-rate, i.e. the highest probability of correct integer estimation of all admissible integer estimators.

Once the integer solution is accepted, the fixed baseline solution $\check{b}$ follows as

$$\begin{aligned} \check{b} \;\; &= Q_{\check{b}\hat{b}} A^T [Q_{pp}^{-1} p + Q_{\phi\phi}^{-1}(\phi - \Lambda\check{a})] \\ Q_{\check{b}\check{b}} &= (A^T (Q_{pp}^{-1} + Q_{\phi\phi}^{-1}) A)^{-1} \end{aligned} \tag{7}$$

Note that $Q_{\check{b}\check{b}} << Q_{\hat{b}\hat{b}}$ if $Q_{\phi\phi} << Q_{pp}$. The latter condition is indeed satisfied, since the phase measurements of both GPS and BDS are about two orders of magnitude more precise than their corresponding code counterparts. Hence, if matrix $Q_{\check{b}\check{b}}$ can be considered to describe the precision of $\check{b}$, the fixed solution will be about two orders of magnitude more precise than the float solution. This is what one tries to achieve with ambiguity resolution. However, matrix $Q_{\check{b}\check{b}}$ is only the variance matrix of $\check{b}$ if one may neglect the uncertainty in $\check{a}$. This therefore requires very high success-rates.

In the next sections we show, first formally and then empirically, what a combination of GPS and BDS brings in terms of improved ambiguity resolution and positioning performance.

4 GPS+BDS formal analysis

4.1 Ambiguity dilution of precision

The ADOP was introduced in Teunissen (1997) as an easy-to-compute scalar diagnostic to measure the *intrinsic* model strength for successful ambiguity resolution. The ADOP is defined as

$$\text{ADOP} = \sqrt{|Q_{\hat{a}\hat{a}}|}^{\frac{1}{n}} \quad \text{(cycle)} \tag{8}$$

with n the dimension of the ambiguity vector and where $|.|$ denotes the determinant. The ADOP has the important property that it is invariant against the choice of ambiguity parametrization. Since all admissible ambiguity transformations can be shown to have a determinant of one, the ADOP does not change when one changes the definition of the ambiguities. It therefore measures the intrinsic precision of the ambiguities. It is also a measure of the volume of the ambiguity confidence ellipsoid (Teunissen et al. 1996). As a rule-of-thumb, an ADOP smaller than about 0.12 cycle corresponds to an ambiguity success-rate larger than 0.999 (Odijk and Teunissen 2008).

The following lemma gives an easy-to-interpret analytical closed-form formula for the single-system ADOP.

Lemma (Single-system ADOP) *The single-epoch, single-system ADOP of model* (1) *is given as*

$$\text{ADOP}_* = \sqrt{2}\left[\frac{\bar{c}_{\phi_*}}{\bar{\lambda}_*}\right]\left[\frac{\sum_{i=1}^{s_*+1} w_{i_*}}{\prod_{i=1}^{s_*+1} w_{i_*}}\right]^{\frac{1}{2s_*}}\left[1+\frac{1}{\epsilon_*^2}\right]^{\frac{\nu}{2f_*s_*}} \quad (9)$$

with

$$\bar{c}_{\phi_*} = \sqrt{|C_{\phi_*\phi_*}|}^{\frac{1}{f_*}},\ \bar{\lambda}_* = \prod_{i=1}^{f_*}\lambda_{i_*}^{\frac{1}{f_*}},\ \epsilon_*^2 = \frac{e_{f_*}^T C_{p_*p_*}^{-1} e_{f_*}}{e_{f_*}^T C_{\phi_*\phi_*}^{-1} e_{f_*}} \quad (10)$$

Proof The proof can be found in (Teunissen 1997). □

This ADOP-expression clearly shows how the different factors contribute to the success of ambiguity resolution. In the ratio $\bar{c}_{\phi_*}/\bar{\lambda}_*$, the role played by the phase precision and the wavelengths is shown (note: $\bar{c}_{\phi_*}$ and $\bar{\lambda}_*$ are the geometric averages of the phase standard deviations and wavelengths, respectively). The expression containing the w_{i_*}'s shows the contribution of the different elevations, while the important last term in (9) shows the relative contribution of the code precision in relation to the number of frequencies used (f_*) and number of satellites tracked (s_*+1). With $C_{p_*p_*} \approx \sigma_p^2 I$ and $C_{\phi_*\phi_*} \approx \sigma_\phi^2 I$, this last term can be approximated as

$$\left[1+\frac{1}{\epsilon_*^2}\right]^{\frac{\nu}{2f_*s_*}} \approx \left[\frac{\sigma_p}{\sigma_\phi}\right]^{\frac{\nu}{f_*s_*}} \quad (11)$$

thus showing how a relatively poor code precision can be compensated by an increase in frequencies and satellites. For instance, changing from a single-frequency model ($f_* = 1$) to a dual-frequency model ($f_* = 2$) reduces the ADOP, as the dual-frequency ADOP equals $\sqrt{\sigma_\phi/\sigma_p}^{\nu/s_*}$ times its single-frequency counterpart.

We now show how the ADOP improves when the two GNSS systems are combined. We have the following result.

Table 3 ADOP rule-of-thumb for single and combined systems (f_* = # frequencies, s_*+1 = # satellites, ν = # common parameters, σ_ϕ/σ_p = phase-code standard deviation ratio)

$\text{ADOP}_* \propto \left[\frac{\sigma_p}{\sigma_\phi}\right]^{\frac{\nu}{f_*s_*}}$	$\text{ADOP}_{G+B} \approx \text{ADOP}_* \left[\frac{\sigma_\phi}{\sigma_p}\right]^{\frac{\nu}{2f_*s_*}}$ (cycle)

Theorem (Combined-system ADOP) *The single-epoch, combined-system ADOP of model (1) is given as*

$$\text{ADOP}_{G+B} = \text{ADOP}_G^{\frac{1}{1+\frac{n_B}{n_G}}}\ \text{ADOP}_B^{\frac{1}{1+\frac{n_G}{n_B}}}\ \Gamma^{\frac{-1}{2(n_G+n_B)}} \quad (12)$$

with gain factor

$$\Gamma = \frac{|Q_{\hat{b}_G\hat{b}_G} + Q_{\hat{b}_B\hat{b}_B}|}{|Q_{\check{b}_G\check{b}_G} + Q_{\check{b}_B\check{b}_B}|} \quad (13)$$

and

$$Q_{\hat{b}_*\hat{b}_*} = 2\sigma_{\hat{\rho}_*}^2[G_*^T P_{D_{s_*}} W_* G_*]^{-1};\ \sigma_{\hat{\rho}_*}^2 = [e_{f_*}^T C_{p_*p_*}^{-1} e_{f_*}]^{-1}$$
$$Q_{\check{b}_*\check{b}_*} = 2\sigma_{\check{\rho}_*}^2[G_*^T P_{D_{s_*}} W_* G_*]^{-1};\ \sigma_{\check{\rho}_*}^2 = [e_{f_*}^T (C_{\phi_*\phi_*}^{-1} + C_{p_*p_*}^{-1}) e_{f_*}]^{-1}$$

where $n_* = f_*s_*$, $P_{D_{s_*}} = D_{s_*}[D_{s_*}^T W_*^{-1} D_{s_*}]^{-1} D_{s_*}^T W_*^{-1}$, *and* ADOP_* *denotes a single-system ADOP.*

Proof see Sect. 7. □

This result shows that it is primarily the determinant ratio (13) that drives the ADOP-improvement. With the approximation $\sigma_{\hat{\rho}_G}^2/\sigma_{\check{\rho}_G}^2 \approx \sigma_{\hat{\rho}_B}^2/\sigma_{\check{\rho}_B}^2$, the determinant ratio (13) simplifies to $\Gamma \approx (1+1/\epsilon_*^2)^\nu$, which together with $\text{ADOP}_G \approx \text{ADOP}_B$ and $n_G \approx n_B$, gives the approximation

$$\text{ADOP}_{G+B} \approx \text{ADOP}_* \sqrt{\left[1+\frac{1}{\epsilon_*^2}\right]^{\frac{-\nu}{2f_*s_*}}} \quad (14)$$

Compare this expression with that of (9). It shows how the phase-code variance ratio (ϵ_*^2), the number of frequencies (f_*), the number of satellites (s_*+1), and the number of common parameters between the two systems (ν), contribute in reducing the ADOP. The two ADOP approximations are summarized in Table 3.

In Fig. 2, we show ADOP time-series, over a three-day time period, for L1 GPS, B1 BDS, L1+L2 GPS and L1 GPS+B1 BDS. Instances where the ADOP-values get below the 0.12 cycle level (indicated by the dashed red line) can be taken as indication of successful ambiguity resolution. The figure shows that the ADOPs of L1 GPS and B1 BDS are generally too large to expect instantaneous ambiguity resolution successful. Note that the ADOPs of L1 GPS are larger,

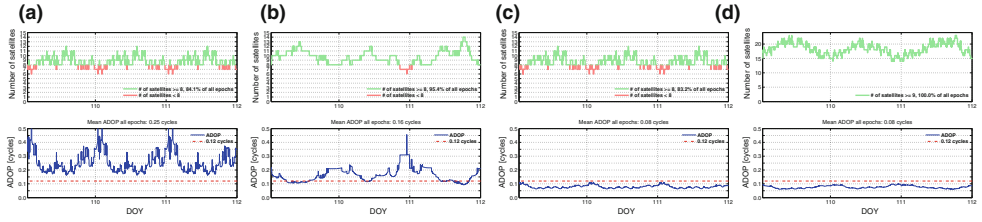

Fig. 2 Single-epoch ADOP time-series (in *blue*) and number of visible satellites (in *red* when less than 8) for GPS, BDS and GPS+BDS, using ten degrees cut-off elevation (Perth, Australia, April 19-21, 2013). **a** L1 GPS. **b** B1 BDS. **c** L1+L2 GPS. **d** L1 GPS + B1 BDS

and fluctuate more, than those of B1 BDS. This is due to the fewer tracked GPS satellites, the more frequent changes in their tracking and the somewhat poorer precision of the L1 GPS code when compared with that of B1 BDS (see Table 2).

The figure also shows that dual-frequency GPS clearly outperforms both single-frequency L1 GPS and single-frequency B1 BDS. The L1+L2 GPS ADOP time-series shows much less fluctuations and it remains below the 0.12 cycle level all the time. Importantly though, this is also true for the single-frequency combined system L1 GPS + B1 BDS (Fig. 2d). The ADOP time-series of this single-frequency combined system has an almost identical behaviour as that of dual-frequency GPS. This similarity is explained by the ADOP expressions given in Table 3. As a consequence of this similarity, one can expect the single-frequency combined system to also have a good instantaneous success-rate performance.

The fact that the performance of the single-frequency combined system is close to that of dual-frequency GPS, can also be explained from the structure of model (1). By taking $f_G = f_B = 1$ and assuming $G_G = G_B$, one effectively obtains the dual-frequency single-system model from the single-frequency combined-system model. This observation is also important in light of the BeiDou Phase III plan for shifting the B1 civil signal to the L1 frequency similar to the modernized GPS civil signal (L1C) and the Galileo L1 Open Service signal (Gibbons 2013). With frequency overlap, calibration of inter system biases (ISBs) requires one reference (or pivot) satellite less in the double-differencing, thus resulting in a further strengthening of the combined model (Odijk and Teunissen 2013).

4.2 GPS and BDS bootstrapped success-rates

4.2.1 Using 10° cut-off elevation

To further analyse the ambiguity resolution performance of the combined system, we now consider the ambiguity success-rates. For our formal analyses, we make use of the success-rate formula of Teunissen (1998),

$$\mathrm{P}[\check{z}_{\mathrm{IB}} = z] = \prod_{i=1}^{n} \left[2\Phi\left(\frac{1}{2\sigma_{\hat{z}_{i|I}}} \right) - 1 \right] \tag{15}$$

where $\mathrm{P}[\check{z}_{\mathrm{IB}} = z]$ denotes the probability of correct integer estimation of the integer bootstrapped estimator $\check{z}_{\mathrm{IB}}$, $\Phi(x) = \int_{-\infty}^{x} \frac{1}{\sqrt{2\pi}} \exp\{-\frac{1}{2}v^2\}\mathrm{d}v$ and $\sigma_{\hat{z}_{i|I}}$, $i = 1, \ldots, n$, $I = \{1, \ldots, (i-1)\}$, denote the conditional standard deviations of the decorrelated ambiguities.

We use the bootstrapped success-rate (15) not only because it is easy to compute, but also since it is a sharp lower bound of the ILS success-rate (Teunissen 1999). In fact, the bootstrapped success-rate is currently the sharpest lower bound available to the ILS success-rate (Verhagen et al. 2013).

It is important that the bootstrapped success-rate is computed for the decorrelated ambiguities and not for the original DD ambiguities. As the DD ambiguities have a rather poor precision, their corresponding bootstrapped success-rate would be low as well. In Teunissen (1995), it is shown how the required $\sigma_{\hat{z}_{i|I}}$ can be obtained from the triangular decomposition of the decorrelated ambiguity variance matrix $Q_{\hat{z}\hat{z}} = Z^T Q_{\hat{a}\hat{a}} Z$.

In Fig. 3, we show the instantaneous spectra of conditional standard deviations for both the DD ambiguities ($\sigma_{\hat{a}_{i|I}}$) and the decorrelated ambiguities ($\sigma_{\hat{z}_{i|I}}$). This is done for the four cases L1 GPS, B1 BDS, L1+L2 GPS and L1 GPS + B1 BDS.

As the figure shows, all transformed spectra are flat and start at a much lower level than their DD counterpart (note the vertical logarithmic scale). The different levels of the four transformed spectra also show the difference between the four cases, in particular, indicating the good performance one can expect from L1 GPS + B1 BDS.

Figure 4 shows the mean bootstrapped success-rates, taken over a three-day period, versus the number of tracked satellites, indeed confirming the excellent performance that one can expect from the single-frequency combined system. As 14 or more satellites are visible all the time with the combined system, the figure predicts that instantaneous ambiguity resolution will be possible on a continuous basis with L1 GPS + B1 BDS. This is not possible with the single systems as their number of visible satellites varies between 6 and 14.

4.2.2 Using higher cut-off elevations

As the combined system results of Fig. 4 are very promising, the question comes up whether a combined system processing would allow the use of higher cut-off elevations. If possible, such processing would increase the GNSS applicability in constrained environments enormously, such as e.g. in urban canyons or when significant low-elevation multipath is present.

In Fig. 5, the single-epoch success-rates are shown as function of the cut-off elevation. The figure clearly shows the benefit that a combination of GPS and BDS brings. Particularly for the single-frequency case, the differences are remarkable. Where the single-frequency, single system success-rates get rapidly smaller when the cut-off elevation angle gets larger, the single-frequency combined success-rates remain large up to a 30° cut-off elevation. For the dual-frequency case shown in Fig. 5b, the success-rates of the combined system even remain close to 100 % up to 40°.

To illustrate that these results are representative for the region, we have computed the success-rates for different cut-off elevations also for two other locations, namely for a station north of CUTA (Singapore) and a station east of CUTA

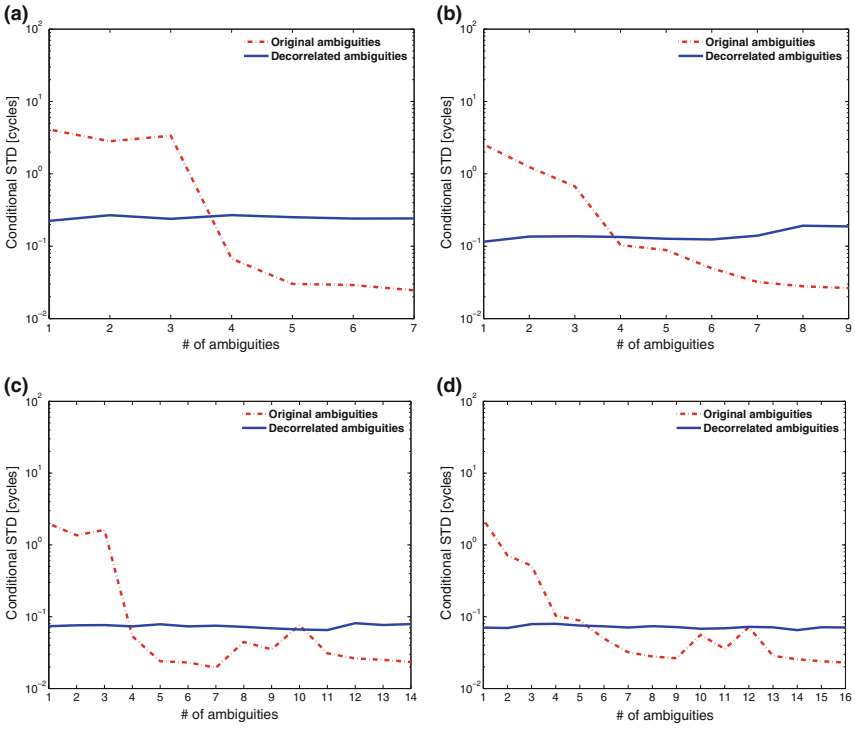

Fig. 3 Spectrum of instantaneous conditional standard deviations (cycles) of double-differenced (*red dashed line*) and decorrelated (*full blue line*) ambiguities for GPS, BDS and GPS+BDS [10° cut-off; #BDS = 10, #GPS = 8; 02:00 local Perth time (UTC +0 hours18:00)]. **a** L1 GPS. **b** B1 BDS. **c** L1+L2 GPS. **d** L1 GPS + B1 BDS

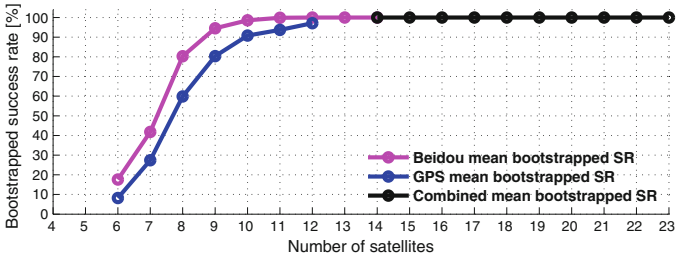

Fig. 4 Mean single-epoch, single-frequency bootstrapped success rates vs. number of satellites for L1 GPS, B1 BDS, and L1 GPS + B1 BDS (10° cutoff, Perth April 19–21, 2013). The mean values were obtained from averaging the single-epoch success-rates of all epochs for the corresponding number of visible satellites

(Swan Hill). As Fig. 6 shows, the success-rates of the combined system again remain high for large cut-off elevations. In case of Singapore, even BDS alone achieves high success-rates for large cut-off elevation angles. This is due to the fact that the regional BDS configuration of the GEO and IGSO satellites is almost perfectly symmetric with respect to Singapore's location.

4.3 GPS and BDS positioning

Ambiguity resolution is not a goal in itself. The goal is to have positioning profit from the integer ambiguity constraints through successful ambiguity resolution. Table 4 provides information on the expected positioning precision. It provides the formal standard deviations (North, East, Up)

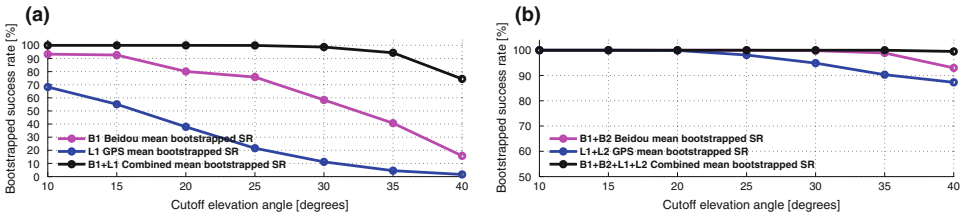

Fig. 5 Single-frequency (**a**) and dual-frequency (**b**), single-epoch bootstrapped success rates vs. different cutoff elevation angles (10°–40° cutoff, Perth, April 19–21, and April 29–30, 2013). The bootstrapped success rates are taken as a mean over all 5 days. **a** B1 BDS, L1 GPS, and B1 BDS+L1 GPS. **b** B1+B2 BDS, L1+L2 GPS, and (B1+B2) BDS + (L1+L2) GPS

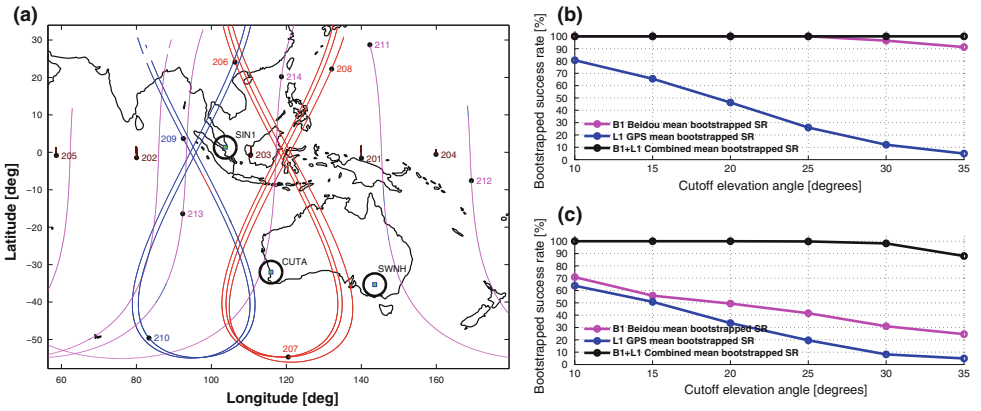

Fig. 6 Single-frequency, single-epoch, mean bootstrapped success-rates as function of cut-off elevation angle for Singapore and Swan Hill. **a** Regional BDS with satellite locations at UTC 06:04 pm, **b** Singapore, **c** Swan Hill (East Australia)

of float and fixed single-epoch positioning for BDS, GPS and BDS+GPS. It clearly shows the two orders of magnitude improvement when going from ambiguity-float positioning to ambiguity-fixed positioning. It also shows the improvement, both for float and fixed, that a combined system achieves. Since the fixed solutions are already driven by the very-precise carrier-phase data, their improvement from combining the two systems is of course less spectacular.

The results of Table 4 hold true for a 10° cut-off elevation angle. Since the ambiguity resolution results of the previous section predict that much larger cut-off elevations are possible when combining GPS and BDS, it is of interest to see what larger cut-off elevations do to the PDOP. Figure 7 shows the PDOP as function of the cut-off elevation angle for the single-frequency single systems and for the combined system. In all three cases, the PDOP gets larger as the cut-off elevation angle gets larger. Importantly though, the PDOP of the combined system remains small for large cut-off elevation angles. Also note, although the BDS-PDOP starts somewhat poorer than that of GPS, for large cut-off elevation angles it is much smaller than its GPS counterpart. This is due to the fact that more BDS satellites than GPS satellites are visible at large elevation angles.

Table 4 Formal standard deviations (STD) for float/fixed single-epoch positioning (North, East, Up)

System/frequency	STD N (cm)	STD E (cm)	STD U (cm)
BDS B1	64/0.5	44/0.4	134/1.0
GPS L1	60/0.4	52/0.4	142/0.9
B1+L1	40/0.3	32/0.3	91/0.7
BDS B1+B2	44/0.4	30/0.3	93/0.9
GPS L1+L2	37/0.3	32/0.3	88/0.7
B1,B2+L1,L2	26/0.2	21/0.2	60/0.5

The values are mean values over period April 19-21, 2013, with 10° cut-off elevation

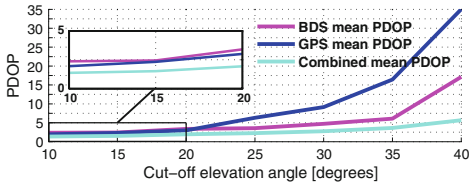

Fig. 7 Mean PDOP versus cut-off elevation angle, at Perth, for B1 BDS, L1 GPS and B1 BDS + L1 GPS. The mean is taken over the period April 19–21 and April 29–30, 2013

4.4 Ambiguity resolution and positioning

Although the above results are very promising, one should be aware of the fact that a good ambiguity resolution performance not necessarily implies a good positioning performance (Teunissen 1997). Ambiguity resolution and positioning are namely driven by different contributing factors of the GNSS model. Figure 8 (top) shows an example of an ADOP and PDOP time series for the same period and same satellites. It shows that the ADOP behaviour can really be different from that of the PDOP. This is clearly shown in the second graph of Fig. 8 (bottom). Here, we see that the ADOP remains practically unchanged over the period, while the PDOP changes dramatically over this period of time.

This difference in behaviour can be understood by considering how the different variance matrices, $Q_{\hat{a}\hat{a}}$ and $Q_{\hat{b}\hat{b}}$, are impacted by changes in the relative receiver-satellite geometry and thus by changes in the design matrix A (cf. 5). From the structure of the ambiguity variance matrix,

$$Q_{\hat{a}\hat{a}} = \Lambda^{-1}(Q_{\phi\phi} + A(A^T Q_{pp}^{-1} A)^{-1} A^T)\Lambda^{-1} \tag{16}$$

it follows that it is only the range space of A, $\mathcal{R}(A)$, that impacts the ambiguity variance matrix. The same variance matrix $Q_{\hat{a}\hat{a}}$ is namely obtained, when A in (16) is replaced by AX, with X an arbitrary invertible matrix. Hence, $Q_{\hat{a}\hat{a}}$ is invariant for such transformation, whereas $Q_{\hat{b}\hat{b}}$ is not. This is also the explanation to what is seen in Fig. 8 (bottom). In this case the change in the receiver-satellite geometry makes the conditioning of matrix A poorer (i.e. less spread in the column vector directions), while still the same range space is spanned by its columns.

5 GPS+BDS empirical analysis

5.1 Success-rates and positioning with 10° cut-off

A 5 day, single-baseline RTK analysis was performed to verify the formal claims of the previous section and to study the actual BDS+GPS performance. The 5 days were April 19–21, 2013, and 10 days later, April 29–30. The data were collected at the Curtin University Bentley campus over a one kilometre baseline, with Trimble NetR9 multi-frequency multi-GNSS receivers using 30 s sampling. The standard broadcast ephemerides were used to provide for the BDS and GPS satellite orbits and clocks.

We start with the success-rate analysis. The empirical success-rates were computed by comparing the single-epoch ILS estimated ambiguities to reference ambiguities obtained from a 5-day, baseline known, batch solution of the multi-frequency combined system, assuming the ambiguities time-

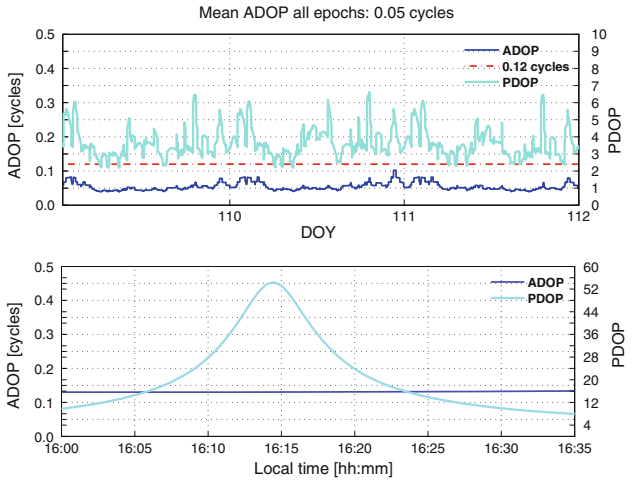

Fig. 8 *Top* ADOP and PDOP times series for dual-frequency combined BDS+GPS over a three-day period (35° cut-off elevation); *Bottom* ADOP and PDOP time series for dual-frequency GPS over a particular short time span (35° cut-off elevation)

Table 5 Single-epoch, empirical integer least-squares (ILS) and formal integer bootstrapped (IB) success-rates, for single- and dual-frequency, single and combined BDS and GPS, for days April 19–21 and 29–30, 2013 (10° cut-off elevation)

System/freq.	Empirical ILS					Formal IB				
	Success rate P_{s_E} (%)					Success rate $P_{s,IB}$ (%)				
April:	19	20	21	29	30	19	20	21	29	30
B1	97.1	*90.3*	96.2	97.2	97.8	96.3	*86.7*	93.8	93.5	96.3
B2	98.6	*93.6*	97.4	97.1	98.4	98.0	*90.7*	96.4	96.4	98.2
L1	81.7	79.5	79.4	83.9	82.0	69.7	68.0	67.9	67.9	67.8
L2	93.7	93.5	93.3	94.1	93.9	91.0	89.9	90.0	89.9	89.8
B1+L1	98.6	*97.8*	98.1	98.5	98.3	**100**	*100*	**100**	**100**	**100**
B2+L2	**100**	*100*	**100**	**100**	**100**	**100**	*100*	**100**	**100**	**100**
B1,B2	**100**	*100*	**100**	**100**	**100**	**100**	*100*	**100**	**100**	**100**
L1,L2	**100**	**100**	**100**	**100**	**100**	**100**	**100**	**100**	**100**	**100**
B1,B2 + L1,L2	**100**	*100*	**100**	**100**	**100**	**100**	*100*	**100**	**100**	**100**

Data of BDS satellite C07 was not logged for most of the day on April 20th

constant. The empirical ILS success rate is then defined as,

$$P_{s_E} = \frac{\text{Number of correctly fixed epochs}}{\text{total number of epochs}} \tag{17}$$

The empirical single-epoch success-rates are given in Table 5 for the single- and dual-frequency single systems as well as combined system, using a ten degree cut-off elevation angle. The success-rates have been computed for each of the 5 days separately so as to demonstrate their repeatability. As the observations of the BDS satellite C07 were not logged for one of the receivers for most of the day on April 20th, the affected success-rates of this day are denoted italic. The unaffected success rates of 100 % are given in bold.

Table 5 shows good repeatability over the 5 days. It also shows excellent results for all dual-frequency cases as well as for the single-frequency combined system's case B2+L2. In all these cases, the single-epoch ambiguity resolution has been successful for every epoch of the complete five-day period.

The table also shows the mean values of the single-epoch bootstrapped success-rates for each of the 5 days. Note that in all cases except one, the IB success-rates are smaller than their empirical ILS counterparts. Although the IB success-rate should be smaller than the ILS success-rate, this is not the case for the 5 days of the single-frequency combined system B1+L1. The explanation for this discrepancy lies in the presence of multipath. Analysis of the data has shown that every day, during the same short period of time, the ambiguities of GPS satellites G14 (setting) and G21 (rising) were wrongly resolved as a consequence of low-elevation multipath. As a result, the empirical success-rate fails to achieve the full hundred percent as predicted by the bootstrapped success-rate.

The results of the table also show that single-frequency, single-system ambiguity resolution is not possible instantaneously. The reason for the regional BDS to have a better single-frequency ambiguity resolution performance than GPS, lies mainly in its larger number of visible satellites. Finally note that of the single-frequency, single-systems, the one with smallest wavelengths and largest code noise (cf. Tables 1, 2) indeed has the lowest success-rates (BDS B1, GPS L1).

As an illustration of the achievable positioning accuracy, Fig. 9 shows the repeatability of the float and fixed single-epoch B1+L1 solutions. The empirical and formal confidence ellipses/intervals have been computed from the empirical and formal position variance matrices. The empirical variance matrix was estimated from the positioning errors as obtained from comparing the estimated positions to precise benchmark coordinates. The formal variance matrix used is determined from the mean of all single-epoch formal variance-matrices.

Table 6 provides information on the float and fixed instantaneous positioning performance for the single- and dual-frequency, single and combined system performance. Note that these results are in good agreement with the formal precision description as given in Table 4.

5.2 Success-rates with higher cut-off elevations

The success-rate results of Table 5 hold true for a ten degree cut-off elevation angle. To show how the success-rates change when the cut-off elevation angle changes, we have computed the single-epoch success-rates over the 5 days for seven different cut-off elevations. The results are shown in Table 7. As one would expect, the single-frequency, single-system success-rates all get smaller as the cut-off elevation

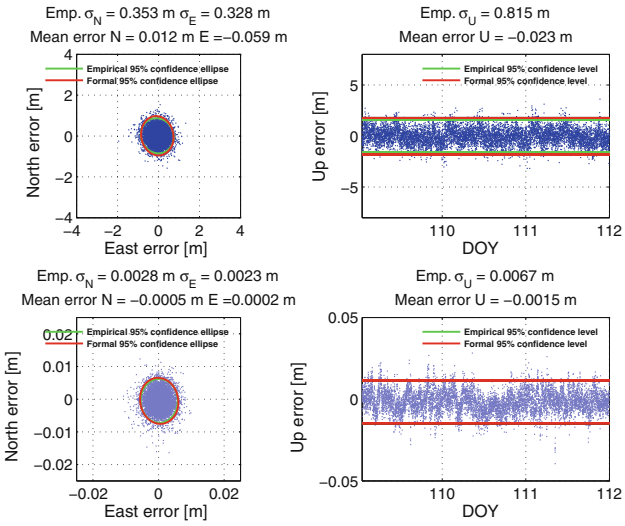

Fig. 9 Horizontal (N, E) position scatter and corresponding vertical (U) time series (April 19–21, 2013) of the float (*top*) and fixed (*bottom*) B1+L1 single-epoch solutions. Only the correctly fixed solutions and their float counterparts are shown. The 95 % empirical and formal confidence ellipse/interval are shown in *green* and *red*, respectively

Table 6 Empirical standard deviations (STD) for float/(correctly)-fixed single-epoch positioning (North, East, Up)

System/frequency	Empirical STD N (cm)	Empirical STD E (cm)	Empirical STD U (cm)
BDS B1	56/0.4	48/0.3	120/1.0
GPS L1	53/0.4	49/0.3	120/0.9
B1+L1	35/0.3	33/0.2	82/0.7
BDS B1+B2	42/0.4	33/0.3	94/1.0
GPS L1+L2	35/0.4	32/0.3	79/0.9
B1,B2+L1,L2	25/0.3	22/0.2	58/0.6

The values are mean values over period April 19–21 2013, with 10° elevation cut-off angle

gets larger. For GPS, they decrease more rapidly than for BDS. In the success-rate behaviour of the single-frequency, combined-system B1+L1, we recognize the earlier referenced presence of low-elevation multipath. As the cut-off elevation angle increases to 20°, the effect of the low-elevation multipath disappears and the success-rate increases to 100 %, as predicted by the corresponding bootstrapped success-rate. Thus here we see an important example of the advantage that successful-ambiguity resolution at higher cut-off elevation brings.

Just as the single-frequency, combined systems achieve successful ambiguity resolution at higher cut-off elevations (up to 25°), also the dual-frequency, single- and combined

Table 7 Single-epoch, empirical ILS and formal IB success-rates for 10°–40° cut-off elevation angles (April 19–21, 29–30 combined)

System/freq.	Empirical ILS							Formal IB						
	success rate $P_{s,E}$ (%)							success rate $P_{s,IB}$ (%)						
cut-off	10	15	20	25	30	35	40	10	15	20	25	30	35	40
B1	95.7	95.0	85.8	82.3	65.8	48.8	21.7	93.3	92.6	80.1	75.8	58.4	40.7	15.8
B2	97.0	96.7	87.8	84.0	70.8	56.4	27.7	95.9	95.4	86.3	82.8	66.1	50.0	22.2
L1	81.3	70.7	54.1	33.7	19.4	8.8	3.7	68.2	55.1	37.9	21.6	11.2	4.5	1.6
L2	93.7	87.0	73.5	51.0	32.7	17.1	8.1	90.1	82.4	67.3	45.9	28.6	14.7	6.9
B1+L1	98.3	99.7	**100**	**100**	99.5	96.9	81.7	**100**	**100**	**100**	99.9	98.7	94.3	74.4
B2+L2	**100**	**100**	**100**	**100**	99.7	98.1	84.5	**100**	**100**	**100**	**100**	99.6	97.5	82.5
B1,B2	**100**	**100**	**100**	**100**	**100**	99.8	97.7	**100**	**100**	**100**	**100**	99.8	98.9	93.0
L1,L2	**100**	**100**	**100**	99.1	97.5	95.9	95.2	**100**	**100**	99.9	98.1	94.9	90.3	87.3
B1,B2+L1,L2	**100**	**100**	**100**	**100**	**100**	**100**	99.9	**100**	**100**	**100**	**100**	**100**	**100**	99.5

systems achieve this at higher cut-off elevations, with the dual-frequency, combined system even being successful up to 35° cut-off elevation.

5.3 Positioning with higher cut-off elevations

Although the success-rate results of Table 7 are very exciting indeed, we should keep in mind that the ambiguity resolution performance and the positioning performance are not driven by the same contributing factors of the GNSS model (cf. Sect. 4.4). Hence, a good ambiguity resolution performance does not necessarily imply a good positioning performance. As will be shown, this becomes particularly apparent when one increases the cut-off elevation angles.

Table 8 shows the single-frequency empirical positioning performance of the correctly fixed solutions for different cut-off elevation angles. It includes the corresponding empirical ILS success-rates as well. The corresponding dual-frequency results are given in Table 9. The two tables also provide the *conditional* positioning performance and the corresponding *conditional* success-rates when the condition PDOP $\leq$ 10 is imposed. This conditioning is only applied to the correctly fixed solutions. Hence, by means of this conditioning, we achieve that poor receiver-satellite geometries (if they occur) are excluded from the set of correctly fixed solution, thus enabling us to show how such an exclusion affects the positioning and success-rate performance. Note, since all our results are single-epoch based, that the given success-rates can also be directly interpreted as an *availability* measure of ambiguity resolved positioning.

In support of better understanding the results of Tables 8 and 9, we also present some of the typical results graphically in Fig. 10. This figure consists of a 6×3 panel matrix, showing horizontal and vertical positioning results. The column-panels show results of BDS, GPS and BDS+GPS, respectively. The odd-numbered row-panels show horizontal (N, E) scatterplots, while the even-numbered row-panels show the corresponding vertical (U) time series over the three-day period. The horizontal scatterplots and the vertical times series show the float solutions in grey and the fixed solutions in red and green, with red referring to the wrongly fixed solutions and green to the correctly fixed solutions. Each of the horizontal scatterplots also has a zoom-in to better show the spread of the correctly fixed solutions.

Table 8 Single-frequency, single-epoch empirical STDs (N, E, U) of correctly fixed positions (B1, L1 and B1+L1), together with their ILS success-rates (SR), for 25°–40° cut-off elevations (April 19–21, 29–30 combined)

System/freq.	Empirical STDs (mm) and ILS SR (%)															
cut-off (°)	25				30				35				40			
	N	E	U	SR	N	E	U	SR	N	E	U	SR	N	E	U	SR
B1	5	3	12	82.3	5	4	13	65.8	6	4	16	48.8	6	5	22	21.7
PDOP $\leq$ 10													6	5	19	17.2
L1	4	3	10	33.7	4	4	12	19.4	4	4	16	8.8	5	5	21	3.7
PDOP $\leq$ 10					4	3	11	19.3	4	4	14	8.5	4	4	16	3.3
B1+L1	3	3	8	**100**	3	3	9	99.5	3	3	11	96.9	4	4	15	81.7
PDOP $\leq$ 10													4	4	14	80.5

The empirical STDs and success-rates conditioned on PDOP $\leq$ 10 are also given, when different from their unconditional counterpart

Table 9 Dual-frequency, single-epoch empirical STDs (N, E, U) of correctly fixed positions (B1+B2, L1+L2 and B1,B2+L1,L2), together with their ILS success-rates (SR), for 25°–40° cut-off elevations (April 19–21, 29–30 combined)

System/freq.	Empirical STDs (mm) and ILS SR (%)															
cut-off (°)	25				30				35				40			
	N	E	U	SR	N	E	U	SR	N	E	U	SR	N	E	U	SR
B1+B2	5	4	13	**100**	6	4	17	**100**	7	4	21	99.8	174	175	885	97.7
PDOP$\leq$ 10													7	5	22	45.3
L1+L2	38	37	80	99.1	354	188	163	97.5	47	124	246	95.9	56	152	351	95.2
PDOP$\leq$ 10	5	3	12	96.5	5	4	13	90.0	5	4	16	75.8	5	5	17	60.6
B1,B2,L1,L2	3	3	8	**100**	3	3	10	**100**	4	3	12	**100**	4	4	18	99.9
PDOP$\leq$ 10													4	4	15	94.7

The empirical STDs and success-rates conditioned on PDOP $\leq$ 10 are also given, when different from their unconditional counterpart

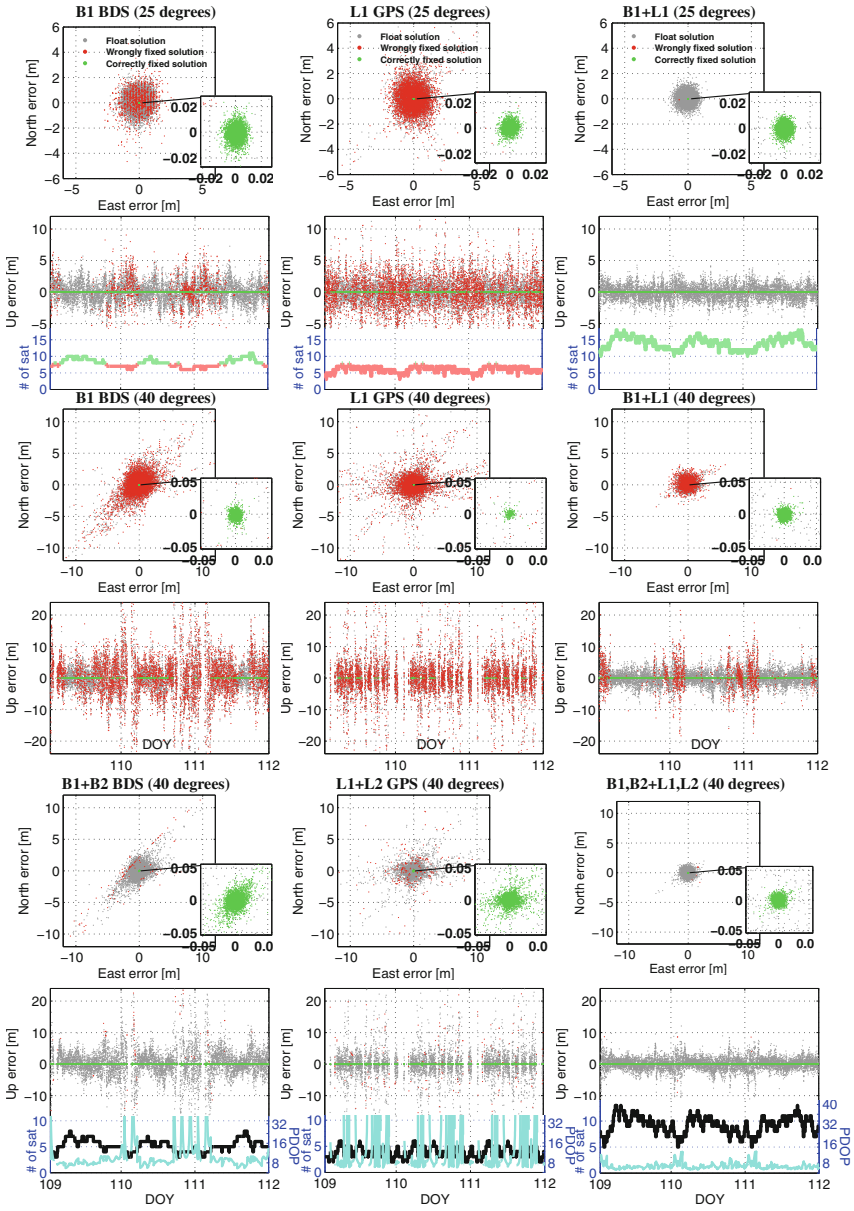

Fig. 10 Horizontal (N, E) scatterplots and vertical (U) time series of BDS (1st column), GPS (2nd column) and BDS+GPS (3rd column). *Top two rows* single-frequency B1 BDS, L1 GPS and B1+L1 with 25° cut-off. *Middle two rows* single-frequency B1 BDS, L1 GPS and B1+L1 with 40° cut-off. *Bottom two rows* dual-frequency B1+B2 BDS, L1+L2 GPS and B1,B2+L1,L2 with 40° cut-off.

Results are shown for different frequencies and different cut-off elevations. The first two rows show single-frequency results for a 25° cut-off elevation, while the 3rd and 4th row show single-frequency results for a 40° cut-off elevation. The last two rows correspond to dual-frequency results for a 40° cut-off elevation.

To illustrate how the occurence of wrongly fixed solutions is related to the number of tracked satellites, we added the number of tracked satellites to the time series of the 2nd row-panels, in red when less than eight satellites were tracked, otherwise in green. Likewise, we added to the time-series in the last row-panels, the PDOP time series (light blue) as well as the number of tracked satellites (black). This helps to illustrate how large excursions in positioning errors are related to the behaviour of the PDOP.

Table 8 clearly shows the excellent performance of the single-frequency combined system B1+L1. While maintaining a positioning accuracy that is comparable to that of the single systems, the combined system has a significantly higher success-rate and is therefore much longer available. In case of 25 degrees cut-off elevation, the fixed positions are continuously available with the combined system, while this is only 33.7 and 82.3 % of the time for GPS and BDS, respectively (see also the first two rows of Fig. 10). These differences become even more pronounced for larger cut-off elevations. At 40° cut-off elevation, the combined system still enables high precision positioning in about 80 % of the time, while this drops to around 20 % for BDS and to a mere 4 % for GPS. See also the third and fourth row of Fig. 10. Here, the single systems also clearly show data gaps in their time series due to the fact that the total number of their visible satellites then drops below four.

In Table 9, the dual-frequency results are given. A comparison between the two Tables 8 and 9, allows us to compare the relative effect of an added frequency versus an added system. If we take GPS L1 (25°) as an example, we see from Table 8 that the addition of BDS B1 increases the success-rates enormously, while maintaining a similar good positioning performance. A similar increase in success-rate is also achieved if L2 is added to GPS L1 (25°), see Table 9. The positioning performance, however, is now much worse. The explanation lies in the receiver-satellite geometry, i.e. for many of the epochs where integer ambiguity resolution is successful because of the additional second frequency, the PDOP is too poor. With the addition of BDS to GPS, the improved receiver-satellite geometry not only improves ambiguity resolution, but it also avoids that in the many more correctly fixed solutions (from 33.7 to 100 %) the geometry spoils positioning performance. With the addition of L2 to GPS L1, however, no such improved receiver-satellite geometry is present. Hence, although the success-rate again improves significantly (from 33.7 to 99.1 %), any poor GPS geometries of these 99.1 % fixed solutions will now not be compensated by the presence of a BDS geometry.

Note that this lack in improved geometry is even more felt for the higher cut-off elevations. Although both dual-frequency, single-systems still have a large success-rate at 40°, their positioning performance has become poorer. This positioning performance can be improved by conditioning on PDOP $\leq$ 10, i.e. by eliminating the poor geometries from the correctly fixed solutions. For dual-frequency BDS, for instance, this improves positioning performance significantly, but at the expense of availability, which drops from 97.7 to 45.3 %, which is far less than the about 80 % availability at 40 degrees of the single-frequency, dual-system B1+L1 (cf. Table 8).

As Table 9 shows, the dual-frequency, combined system has of course the best performance of all. It maintains successful ambiguity resolution up to a 35° cut-off elevation, while at 40° only about 5 % of the correctly fixed solutions have a PDOP larger than 10. This excellent performance of the dual-frequency, dual-system is also clearly visible from the last two rows of Fig. 10.

6 Summary and conclusions

In this contribution, the instantaneous RTK positioning capabilities of a combined GPS+BDS system were analysed for cut-off elevation angles ranging between ten and 40°. It was shown that with the combined system much larger than the customary cut-off elevations can be used. This is an important result, as such measurement set-up will significantly increase the GNSS applicability in constrained environments, such as e.g. in urban canyons or when low-elevation multipath is present.

The study consisted of a formal and an empirical analysis. In the formal analysis, the ADOP, the bootstrapped success-rate and the positioning precision were used to gain insight into the effect of combining the two systems. The given analytical ADOP provides good understanding of how the different factors of the combined model contribute to improved ambiguity resolution. It was also shown that the bootstrapped success-rates give a very good indication of the actual ambiguity resolution performance for varying cut-off elevations. They were found consistent with the empirically determined success-rates, computed from 5 days of GNSS data covering a 10-day period.

In our analysis of the positioning precision, we also explained and demonstrated that improved ambiguity resolution does not always go hand-in-hand with improved positioning. Ambiguity resolution and positioning are namely driven by different contributing factors of the GNSS model. This is particularly true when increasing the cut-off elevations.

Our formal and empirical results show that the single-frequency combined system has an ambiguity resolution performance that is similar to that of a dual-frequency single system. Its positioning capability, however, clearly outperforms that of the dual-frequency single system, in particular, for large cut-off elevation angles.

The best performance is of course realized by the dual-frequency combined system. The ambiguity resolution performance of such combination benefits from the presence of the two frequencies, while its positioning performance benefits from the increased spread in receiver-satellite geometry. It was shown that this combination has good high-precision positioning availability for up to fourty degrees cut-off elevation.

Acknowledgments This work has been executed in the framework of the Positioning Program of the Cooperative Research Centre for Spatial Information (CRC–SI). The first author is the recipient of an Australian Research Council (ARC) Federation Fellowship (Project number FF0883188). All this support is gratefully acknowledged.

7 Appendix

Proof of Theorem (*Combined-system ADOP*) The ambiguity variance matrix of the combined system can be expressed in the single-system variance matrices as

$$Q_{\hat{a}\hat{a}} = \begin{bmatrix} Q_{\hat{a}_G\hat{a}_G} & 0 \\ 0 & Q_{\hat{a}_B\hat{a}_B} \end{bmatrix} - \begin{bmatrix} Q_{\hat{a}_G\hat{b}_G} \\ Q_{\hat{a}_B\hat{b}_B} \end{bmatrix} [Q_{\hat{b}_G\hat{b}_G} + Q_{\hat{b}_B\hat{b}_B}]^{-1} \begin{bmatrix} Q_{\hat{a}_G\hat{b}_G} \\ Q_{\hat{a}_B\hat{b}_B} \end{bmatrix}^T$$

Upon taking the determinant, we get

$$|Q_{\hat{a}\hat{a}}| = |Q_{\hat{a}_G\hat{a}_G}||Q_{\hat{a}_B\hat{a}_B}||I - [Q_{\hat{b}_G\hat{a}_G} Q^{-1}_{\hat{a}_G\hat{a}_G} Q_{\hat{a}_G\hat{b}_G} + Q_{\hat{b}_B\hat{a}_B} Q^{-1}_{\hat{a}_B\hat{a}_B} Q_{\hat{a}_B\hat{b}_B}][Q_{\hat{b}_G\hat{b}_G} + Q_{\hat{b}_B\hat{b}_B}]^{-1}|$$

where we made use of the determinant property $|I_m - BC| = |I_n - CB|$ for $m \times n$ matrices B and C^T. With the use of

$$Q_{\check{b}_*\check{b}_*} = Q_{\hat{b}_*\hat{b}_*} - Q_{\hat{b}_*\hat{a}_*} Q^{-1}_{\hat{a}_*\hat{a}_*} Q_{\hat{a}_*\hat{b}_*}$$

we can then finally write

$$|Q_{\hat{a}\hat{a}}| = |Q_{\hat{a}_G\hat{a}_G}||Q_{\hat{a}_B\hat{a}_B}||\frac{Q_{\check{b}_G\check{b}_G} + Q_{\check{b}_B\check{b}_B}}{Q_{\hat{b}_G\hat{b}_G} + Q_{\hat{b}_B\hat{b}_B}}| \quad (18)$$

from which the expression (12) for the combined ADOP follows. □

References

Cao C, Jing G, Luo M (2008a) COMPASS satellite navigation system development. In: PNT challenges and opportunities symposium. Stanford, California

Cao W, O'Keefe K, Cannon M (2008b) Evaluation of COMPASS ambiguity resolution performance using geometric-based techniques with comparison to GPS and Galileo. In: Proceedings of the ION GNSS, Savannah

Chen H, Huang Y, Chiang K, Yang M, Rau R (2009) The performance comparison between GPS and BeiDou-2/COMPASS: a perspective from Asia. J Chin inst of eng 32(5):679–689

CSNO (2012) BeiDou navigation satellite system signal. In: Space interface control document by China satellite navigation office (CSNO). Open service signal B1I (Version 1.0). Tech. rep., December 2012

Euler HJ, Goad C (1991) On optimal filtering of GPS dual frequency observations without using orbit information. Bull Geod 65:130–143

Gibbons G (2013) GNSS News. Inside GNSS, p 1

Goad C (1998) Short distance GPS models (Chap. 11). In: Teunissen PJG, Kleusberg A (eds) GPS for geodesy, 2nd edn. Springer, Berlin, pp 457–482

Grelier T, Ghion A, Dantepal J, Ries L, DeLatour A, Issler JL, Avila-Rodriguez J, Wallner S, Hein G (2007) Compass signal structure and first measurements. In: Proceedings of the ION GNSS, Fort Worth, pp 3015–3024

Guo H, He H, Li J, Wang A (2011) Estimation and mitigation of the main errors for centimetre-level COMPASS RTK solutions over medium-long baselines. J Navig 64:S113–S126. doi:10.1017/S0373463311000324

Han C, Yang Y, Cai Z (2011) BeiDou navigation satellite system and its timescales. Metrol 48(4). doi:10.1088/0026-1394/48/4/S13

Huang YS, Tsai ML (2008) The impact of Compass/Beidou-2 on future GNSS: a perspective from Asia. In: Proceedings of the ION GNSS, Savannah, pp 2227–2238

Li W, Teunissen PJG, Zhang B, Verhagen S (2013) Precise point positioning using GPS and Compass observations. In: Sun et al. (eds) Lect Notes in Electr Eng, Chap. 33, vol 2, pp 367–378

Montenbruck O, Hauschild A, Steigenberger P, Hugentobler U, Riley S (2012) A COMPASS for Asia: first experience with the BeiDou-2 regional Navigation System. In: Proceedings of the IGS workshop 2012, Olsztyn, 23–27 July 2012

Montenbruck O, Hauschild A, Steigenberger P, Hugentobler U, Teunissen P, Nakamura S (2013) Initial assessment of the COMPASS/BeiDou-2 regional navigation satellite system. GPS Solut 17(2):211–222. doi:10.1007/s10291-012-0272-x

Nadarajah N, Teunissen PJG, Raziq N (2013) BeiDou inter-satellite-type bias evaluation and calibration for mixed receiver attitude determination. Sensors 13(7):9435–9463

Odijk D, Teunissen PJG (2008) ADOP in closed form for a hierarchy of multi-frequency single-baseline GNSS models. J Geod 82:473

Odijk D, Teunissen PJG (2013) Characterization of between-receiver GPS-Galileo inter-system biases and their effect on mixed ambiguity resolution. GPS Solut 17(4):521–533. doi:10.1007/s10291-012-0298-0

Odolinski R, Teunissen PJG, Odijk D (2013) An analysis of combined COMPASS/BeiDou-2 and GPS single- and multiple-frequency RTK positioning. In: Proceedings of the ION Pacific PNT, Honolulu, pp 69–90

Qu J, Yuan H, Zhang X, Ouyang G (2012) Single-epoch COMPASS carrier-phase ambiguous resolution using three civil frequencies and special constellations. In: Proceedings of the ION GNSS, Nashville

Shi C, Zhao Q, Li M, Tang W, Hu Z, Lou Y, Zhang H, Niu X, Liu J (2012) Precise orbit determination of Beidou Satellites with precise positioning. Sci China Earth Sci 55:1079–1086. doi:10.1007/s11430-012-4446-8

Shi C, Zhao Q, Hu Z, Liu J (2013) Precise relative positioning using real tracking data from COMPASS GEO and IGSO satellites. GPS Solut 17(1):103–119. doi:10.1007/s10291-012-0264-x

Steigenberger P, Hauschild A, Hugentobler U, Montenbruck O (2012) Performance analysis of Compass orbit and clock determination and

Compass only PPP. In: Proceedings of the IGS Workshop 2012, Olsztyn, 23–27 July 2012

Steigenberger P, Hugentobler U, Hauschild A, Montenbruck O (2013) Orbit and clock analysis of COMPASS GEO and IGSO satellites. J Geod. doi:10.1007/s00190-013-0625-4

Teunissen PJG (1995) The least squares ambiguity decorrelation adjustment: a method for fast GPS integer estimation. J Geod 70:65–82

Teunissen PJG (1997) A canonical theory for short GPS baselines. Part I: The baseline precision, Part II: The ambiguity precision and correlation, Part III: The geometry of the ambiguity search space, Part IV: Precision versus reliability. J Geod 71(6): 320–336, 71(7): 389–401, 71(8): 486–501, 71(9): 513–525

Teunissen PJG (1998) Success probability of integer GPS ambiguity rounding and bootstrapping. J Geod 72:606–612

Teunissen PJG (1999) An optimality property of the integer least-squares estimator. J Geod 73:587–593

Teunissen PJG, de Jonge P, Tiberius C (1996) The volume of the GPS ambiguity search space and its relevance for integer ambiguity resolution In:Proceedings of the ION GPS, vol 9, pp 889–898

Verhagen S, Teunissen PJG (2013) Ambiguity resolution performance with GPS and BeiDou for LEO formation flying. J Adv Space Res. http://dx.doi.org/10.1016/j.asr.2013.03.007

Verhagen S, Li B, Teunissen PJG (2013) Ps-LAMBDA: ambiguity success rate evaluation software for interferometric applications. Comput Geosci 54:361–376

Yang Y, Li J, Xu J, Tang J, Guo H, He H (2011) Contribution of the compass satellite navigation system to global PNT users. Chinese Sci Bull 56(26):2813–2819

Zhang S, Guo J, Li B, Rizos C (2010) An analysis of satellite visibility and relative positioning precision of COMPASS. In: Proceedings of the symposium for Chinese professionals in GPS, pp 41–46. Singhai, 18–20 August 2010

6 BDS+GALILEO+QZSS+GPS INSTANTANEOUS SINGLE-FREQUENCY RTK

This chapter is covered by the following publication:

Odolinski R, Teunissen PJG, Odijk D (2013b) Combined GPS, BeiDou, Galileo, and QZSS single-epoch, single-frequency RTK performance analysis. Published in: Proceedings of the International Association of Geodesy (IAG) symposium in Potsdam, Germany, September 1-6, 2013, accepted (see Appendix C for proof of peer-review and acceptance)

Noname manuscript No.
(will be inserted by the editor)

Combined GPS, BeiDou, Galileo, and QZSS single-epoch, single-frequency RTK Performance Analysis

Robert Odolinski · Peter J.G. Teunissen · Dennis Odijk

Received: date / Accepted: date

Abstract In this contribution we will focus on instantaneous (single-epoch) single-baseline Real-Time Kinematic (RTK) combining four CDMA satellite systems. We will combine the Chinese BeiDou, the European Galileo, the American GPS and the Japanese QZSS system. To further strengthen the underlying model and maximize the redundancy, attention will be given to overlapping frequencies between the systems. With calibrated Inter System Biases (ISBs), it enables one to use a common pivot satellite between the respective systems when parameterizing the double-differenced ambiguities. We make use of the LAMBDA method for ambiguity resolution, and the performance is evaluated by ambiguity success-rates and by comparing the estimated positions to very precise benchmark coordinates. This will be based on various elevation cut-off angles so as to mimic conditions with obstructed satellite visibility (such as in urban canyons). It will be shown by how much the increased strength of the combined models allow for improved ambiguity resolution performance and positioning robustness over the single-systems.

Keywords Multi-GNSS · BeiDou · Galileo · QZSS · GPS · Real Time Kinematic · cut-off angle

R. Odolinski
GNSS Research Centre, Curtin University of Technology, Australia
Tel.: +618 9266 3157
E-mail: Robert.Odolinski@curtin.edu.au

P.J.G Teunissen
GNSS Research Centre, Curtin University of Technology, Australia, and
Mathematical Geodesy and Positioning, Delft University of Technology, The Netherlands

D. Odijk
GNSS Research Centre, Curtin University of Technology, Australia

1 Introduction

The BeiDou Navigation Satellite System (BDS) attained Asia-Pacific regional operational status in the end of December 2011. The current (December 2013) BDS constellation consists of five Geostationary Earth Orbit (GEO), five Inclined Geo-Synchronous Orbit (IGSO) and four Medium Earth Orbit (MEO) satellites. BDS satellites currently transmit at three frequencies, B1, B2 and B3 in Quadrature phase-shift keying (QPSK) modulation, as is shown in Table 1 and given together with the L1, L2 and L5 GPS frequencies. Some first BDS positioning results based on real data can be found in e.g. Montenbruck et al (2013).

Two Galileo In-Orbit Validation Element (GIOVE) satellites have been in orbit since 2005 and 2008 respectively. The four In-Orbit Validation (IOV) MEO satellites that since 2012 are currently (December 2013) available for positioning broadcast signals at E1, E5a, E5b, and E6 frequencies (Table 1). The E6 frequency will only be received as part of Galileo's Commercial Service. Initial results on combined single-frequency Galileo+GPS single-baseline RTK were presented in Odijk and Teunissen (2013). It was shown that with overlapping frequencies and a-priori corrected Inter System Biases (ISBs), one maximizes the redundancy and each additional Galileo satellite to GPS then contributes to the solution. The nature and variation of GIOVE-GPS ISBs were also investigated in Montenbruck et al (2011).

The Quasi-Zenith Satellite System (QZSS) uses the same orbital period as a traditional equatorial geostationary orbit, however, they have a large orbital inclination and therefore move with respect to the Earth (JAXA, 2013). The system is designed to enable users in the coverage area to receive QZSS signals from a high

elevation angle at all times in East Asia and Japan. The QZSS L1, L2 and L5 signals all overlap the GPS signals (Table 1). Currently (December 2013) one satellite is in orbit named MICHIBIKI, or QZS-1, which was launched September 2010.

In this contribution we present four-system GPS +BDS+Galileo+QZSS instantaneous (single-epoch), single-frequency single-baseline RTK results. Special attention will be given to the overlapping frequencies between the systems. We will focus on the frequencies B1, E1 and L1 of GPS/QZSS (Table 1) in this contribution to maximize the number of available satellites as well as overlapping frequencies for single-frequency RTK.

Table 1 BDS, Galileo, QZSS and GPS signals.

Sat. system	Band	Freq. [MHz]	Wavelength [cm]
BDS	**B1**	1561.098	19.20
BDS/Galileo	B2/E5b	1207.140	24.83
BDS	B3	1268.520	23.63
QZSS, GPS/Galileo	**L1/E1**	1575.42	19.03
QZSS, GPS	L2	1227.60	24.42
QZSS, GPS/Galileo	L5/E5a	1176.45	25.48

We start with describing the between-receiver single-differenced (SD) GNSS observation equations in Section 2, and to make it brief we present them for a combination of Galileo and GPS. Results are then given for ambiguity success rates and RTK positioning in Section 3, and we conclude with a summary and discussion.

2 System of single-differenced GNSS observation equations

Let us consider the receivers $r = 1, 2$ tracking satellites $s_* = 1_*, \ldots, m_*$, where m_* is the number of satellites of one GNSS system $*$ (B for BDS, E for Europe/Galileo, Q for QZSS and G for GPS). When we have non-overlapping single-frequencies we define the frequency as 1_*, where 1_* is the frequency for system $*$, whereas for overlapping frequencies the symbol $*$ is omitted.

For the following single-baseline RTK model we use external products for satellite orbits, and between-receivers single-differences (SD) is subsequently performed on the system of observation equations with respect to the 'pivot' receiver 1. The satellite delays common to both receivers are then eliminated (satellite clocks, satellite hardware (HW) code and phase delays, and initial phase delays). For short baselines of a few km the relative atmospheric delays and any remaining orbit errors can be neglected as well.

We present the following dual-system combination of GPS (G) and Galileo (E) for notational convenience (combination of other satellite systems with overlapping frequencies goes along similar lines), where we share the receiver clock between the systems (the GPS-to-Galileo Time-Offset (GGTO) is eliminated by the SDs). The combined system can then be formulated in the following rank defect, (linearized) SD system of observation equations, in units of range and for *overlapping frequencies*, where we omit time stamps for brevity,

$$\begin{aligned}
p^{s_G}_{12,1} &= c_1^{s_G T}\Delta x_1 - c_2^{s_G T}\Delta x_2 + dt_{12} + d^G_{12,1}\\
\phi^{s_G}_{12,1} &= c_1^{s_G T}\Delta x_1 - c_2^{s_G T}\Delta x_2 + dt_{12} + \delta^G_{12,1} + \lambda_1 M^{s_G}_{12,1}\\
p^{s_E}_{12,1} &= c_1^{s_E T}\Delta x_1 - c_2^{s_E T}\Delta x_2 + dt_{12} + d^G_{12,1} + d^{GE}_{12,1}\\
\phi^{s_E}_{12,1} &= c_1^{s_E T}\Delta x_1 - c_2^{s_E T}\Delta x_2 + dt_{12} + \delta^G_{12,1} + \delta^{GE}_{12,1} +\\
&+ \lambda_1 M^{s_E}_{12,1}
\end{aligned} \tag{1}$$

where $(\cdot)_{12} = (\cdot)_2 - (\cdot)_1$ is the notation for between-receiver SDs, the SD code and phase observable is denoted $p^{s_*}_{12,1}$ and $\phi^{s_*}_{12,1}$ respectively, $c_r^{s_* T} = \frac{(x^{s_*} - x_r)^T}{||x^{s_*} - x_r||}$ is the line-of-sight unit vector from the receiver r to the satellites obtained from linearizing the system of equations with respect to the receiver coordinates, and λ_1 is the wavelength corresponding to frequency 1. The unknowns read,

x_r	vector with receiver X, Y, Z coordinates
dt_{12}	SD receiver clock error
$d^G_{12,1}$	SD GPS receiver HW code delay
$\delta^G_{12,1}$	SD GPS receiver HW phase delay
$d^{GE}_{12,1} = d^E_{12,1} - d^G_{12,1}$	SD differential code ISB
$\delta^{GE}_{12,1} = \delta^E_{12,1} - \delta^G_{12,1}$	SD differential phase ISB
$M^{s_*}_{12,1} = N^{s_*}_{12,1} +$ $+\varphi_{12,1}(t_0)$	SD non-integer ambiguity due to SD initial phase delay for the receiver $\varphi_{12,1}(t_0)$, where
$N^{s_*}_{12,1}$	is the SD integer ambiguity

We refrain from carrying through SD random observation noise and un-modeled effects such as multipath for notational convenience.

Note that we in (1) made use of the reparameterization such that $d^E_{12,1} = d^G_{12,1} + d^{GE}_{12,1}$ and $\delta^E_{12,1} = \delta^G_{12,1} + \delta^{GE}_{12,1}$, since the receivers are tracking the satellites on the same overlapping frequency. Thus if the differential ISBs can be assumed zero/corrected all receiver-dependent parameters in (1) can be shared between the systems, which increases the redundancy of the resulting full-rank model (see Section 2.3).

2.1 Rank deficiency elimination by S-system theory

The number of rank defects is the number of linear combinations of the column vectors of the design ma-

trix that produces the zero vector, of which the combinations are said to span the null space of the design matrix. These rank defects can be eliminated through an application of S-system theory (Teunissen, 1985; Teunissen et al, 2010), implying null-space identification, S-basis constraining and interpretation of the estimable parameters. The number of rank defects and S-basis choice for the model in (1) is given in Table 2.

Table 2 Single-epoch, single-frequency and single-baseline RTK S-basis choice and number of rank deficiencies.

Model	S-basis choice	# of rank defects
Eq. (1)	$\Delta x_1, dt_1, d^G_{2,1}, M^{s_*}_{1,1}, \delta^{s_*}_{1,1}, d^{s_*}_{1,1}, M^{1_*}_{2,1}$	$11 + m_G + m_E$

2.2 Full-rank RTK functional model - ISBs unknown

The SD, and (linearized) full-rank observation equations for *overlapping frequencies* and a combined GPS +Galileo system is then expressed as,

$$\begin{aligned}
p^{s_G}_{12,1} &= -{c_2^{s_G}}^T \Delta x_{12} + d\tilde{t}_{12} \\
\phi^{s_G}_{12,1} &= -{c_2^{s_G}}^T \Delta x_{12} + d\tilde{t}_{12} + \tilde{\delta}^G_{12,1} + \lambda_1 \tilde{M}^{1_G s_G}_{12,1} \\
p^{s_E}_{12,1} &= -{c_2^{s_E}}^T \Delta x_{12} + d\tilde{t}_{12} + \tilde{d}^{GE}_{12,1} \\
\phi^{s_E}_{12,1} &= -{c_2^{s_E}}^T \Delta x_{12} + d\tilde{t}_{12} + \tilde{\delta}^G_{12,1} + \tilde{\delta}^{GE}_{12,1} + \lambda_1 \tilde{M}^{1_E s_E}_{12,1}
\end{aligned} \tag{2}$$

The estimable unknowns are expressed as follows,

$\Delta x_{12} = \Delta x_2 - \Delta x_1$	Relative receiver coordinates,
$d\tilde{t}_{12} = dt_{12} + d^G_{12,1}$	Relative receiver clock with code delay of GPS
$\tilde{\delta}^G_{12,1} = \delta^G_{12,1} - d^G_{12,1} + \lambda_1 M^{1_G}_{12,1}$	GPS receiver HW phase delay
$\tilde{d}^{GE}_{12,1} = d^E_{12,1} - d^G_{12,1}$	Galileo-GPS code ISB
$\tilde{\delta}^{GE}_{12,1} = \delta^E_{12,1} - \delta^G_{12,1} + \lambda_1 M^{1_G 1_E}_{12,1}$	Galileo-GPS phase ISB
$\tilde{M}^{1_* s_*}_{12,1} = M^{s_*}_{12,1} - M^{1_*}_{12,1}$	Double-differenced integer ambiguities

One can see that the phase ISB is biased by double-differenced (integer) ambiguities of the pivot satellites of both GPS (1_G) and Galileo (1_E). One can also reparameterize the differential phase ISB into a Galileo-specific HW phase delay relative to the GPS HW code delay on frequency 1, as follows (the code ISB is already relative to the GPS HW code delay),

$$\tilde{\delta}^E_{12,1} = \tilde{\delta}^G_{12,1} + \tilde{\delta}^{GE}_{12,1} = \delta^E_{12,1} - d^G_{12,1} + \lambda_1 M^{1_E}_{12,1} \tag{3}$$

In other words, the model in (2) is equivalent (in terms of redundancy) to the one taken when one does not have overlapping frequencies and wants to estimate system-specific HW delays for frequency 1_*.

Note also in (2) that the Galileo-GPS code ISB is estimable on the first frequency, whereas for GPS the Differential Code Bias (DCB) is not estimable. One can thus prove that the functional model (2) is equivalent, in terms of redundancy, to the model when one takes different receiver clocks for each system (see e.g. Odolinski et al (2013)). This since the code ISB then plays the role as the additional unknown. The number of observations, estimable unknowns and redundancy for the model (2) is shown in Table 3.

2.3 Full-rank RTK functional model - ISBs corrected

We can express the phase ISB correction as follows (Odijk and Teunissen, 2013),

$$\begin{aligned}
\overline{\delta}^{GE}_{12,1} &= \delta^{GE}_{12,1} + \lambda_1 z_{12,1} = \\
&= \delta^{GE}_{12,1} + \lambda_1 M^{1_G 1_E}_{12,1} - \lambda_1 \left(M^{1_G 1_E}_{12,1} - z_{12,1} \right)
\end{aligned} \tag{4}$$

where $z_{12,1}$ is an integer ambiguity that originates from the observations that are used to determine the ISB corrections. This ambiguity is in principle different from $M^{1_G 1_E}_{12,1}$ in the observations (2) to be corrected.

Thus when we apply the correction in (4) to the Galileo phase observations in (2), the ambiguity difference part of the correction can be lumped into the ambiguities,

$$M^{1_E s_E}_{12,1} + \left(M^{1_G 1_E}_{12,1} - z_{12,1} \right) = M^{\mathbf{1_G} s_E}_{12,1} - z_{12,1} \tag{5}$$

i.e. the ambiguity becomes differenced with respect to the pivot satellite of GPS (1_G) minus the integer ambiguity that is lumped into the phase ISB correction (4). If we denote the code ISB correction as $\overline{d}^{GE}_{12,1} = d^{GE}_{12,1}$, we then have the following full-rank Galileo-part of the observation equations (the GPS part is equivalent to (2)),

$$\begin{aligned}
p^{s_G}_{12,1} &= -{c_2^{s_G}}^T \Delta x_{12} + d\tilde{t}_{12} \\
\phi^{s_G}_{12,1} &= -{c_2^{s_G}}^T \Delta x_{12} + d\tilde{t}_{12} + \tilde{\delta}^G_{12,1} + \lambda_1 \tilde{M}^{1_G s_G}_{12,1} \\
p^{s_E}_{12,1} - \overline{d}^{GE}_{12,1} &= -{c_2^{s_E}}^T \Delta x_{12} + d\tilde{t}_{12} \\
\phi^{s_E}_{12,1} - \overline{\delta}^{GE}_{12,1} &= -{c_2^{s_E}}^T \Delta x_{12} + d\tilde{t}_{12} + \tilde{\delta}^G_{12,1} + \lambda_1 \tilde{M}^{1_G s_E}_{12,1}
\end{aligned} \tag{6}$$

where $\tilde{M}^{1_G s_E}_{12,1} = M^{1_G s_E}_{12,1} - z_{12,1}$ is the estimable ambiguity as defined in (5). Note that this ambiguity will also be estimable for $s_E = 1_E$ (one additional unknown as compared to (2)). In other words, with a-priori corrected values for the two differential code and phase ISBs, the redundancy of this model increases with one as compared to the model in (2), see Table 3.

2.4 Redundancy and solvability

In Table 3 we give the number of observations, the number of estimable unknowns and the redundancy for the single-baseline RTK models (2) and (6), as well as for a four-system model assuming that all frequencies overlap between the systems. In the last column a *solvability condition* is defined, which is the number of satellites required to solve coordinate parameters. The single-system RTK model in the Table can be found in (2) for GPS, where BDS-/Galileo- or QZSS-only models will have a similar definition of the unknowns.

One can imply from Table 3 that with the ISBs corrected model (6) at least four satellites are needed for the combined systems for positioning, whereas if the ISBs are unknown (2) five satellites are required in case of a dual-system, and seven for the four-system model.

Table 3 Single-epoch, single-frequency, single-baseline RTK redundancy and solvability condition (overlapping frequencies).

Model	# of obs.	# of unknowns	Redundancy	Solvability condition
Single-system	$2m_*$	$4+m_*$	m_*-4	$m_*\geq 4$
GPS+Galileo (2)	$2m_G+2m_E$	$5+m_G+m_E$	m_G+m_E-5	$m_G+m_E\geq 5$
ISBs unknown				
GPS+Galileo (6)	$2m_G+2m_E$	$4+m_G+m_E$	m_G+m_E-4	$\mathbf{m_G+m_E\geq 4}$
ISBs corrected				
Four-system	$2m_G+2m_E$	$7+m_G+m_E$	m_G+m_E	m_G+m_E
ISBs unknown	$+2m_B+2m_Q$	$+m_B+m_Q$	$+m_B+m_Q-7$	$+m_B+m_Q\geq 7$
Four-system	$2m_G+2m_E$	$4+m_G+m_E$	m_G+m_E	$\mathbf{m_G+m_E}$
ISBs corrected	$+2m_B+2m_Q$	$+m_B+m_Q$	$+m_B+m_Q-4$	$\mathbf{+m_B+m_Q\geq 4}$

3 Results

Data from 29-30 April 2013 of CUTA and CUTT (both Trimble NetR9 receivers with an inter-distance of 1 km) at Curtin University, are evaluated, with a measurement interval of 30 seconds. The LAMBDA method is used for integer ambiguity resolution (Teunissen, 1995), and the Detection, Identification and Adaptation (DIA) procedure to eliminate outliers (Teunissen, 1990). The positioning results are evaluated by comparing the estimated positions to very precise benchmark coordinates. The number of satellites visible for CUTT for an elevation cut-off angle of 10 degrees is given in Figure 1.

We see similar number of satellites for BDS and GPS, and we have (December 2013) four Galileo satellites and one QZSS satellite visible. The stochastic RTK model settings are given in Table 4. This is based on the exponential elevation weighting function by Euler and Goad (1991), where $\sigma_{p,1_*}$ and $\sigma_{\phi,1_*}$ are the zenith-referenced a priori code and phase standard deviation (STD) respectively for undifferenced observations.

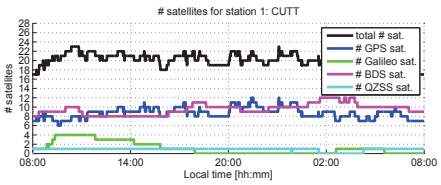

Fig. 1 Satellite visibility for CUTT April 29, 2013.

Table 4 Zenith-referenced code and phase STDs.

	Frequency	Code $\sigma_{p,1_*}$ [cm]	Phase $\sigma_{\phi,1_*}$ [mm]
GPS	L1	37	3
BDS	B1	30	3
Galileo	E1	30	2
QZSS	L1	30	3

3.1 Inter System Biases

We focus on Trimble-Trimble receivers throughout this contribution. To investigate whether the QZSS-GPS ISBs are zero for similar receiver types, we depict in Figure 2 the code and (fractional) phase differential ISBs for L1-L1 QZSS-GPS. This is based on single-epoch RTK for a zero baseline with fixed receiver positions of CUT0-CUT2 (at Curtin University), and an elevation cut-off angle of 10 degrees. The STDs are computed assuming the ISBs to be *constant in time* during the time span to illustrate the ISBs repeatability.

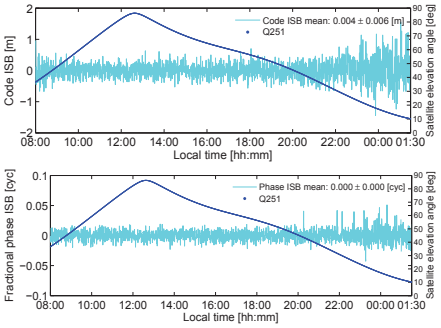

Fig. 2 L1-L1 QZSS-GPS code ISB (top), phase ISB (bottom) for a zero-baseline setup CUT0-CUT2 (both Trimble NetR9), 29 April 2013, and a cut-off angle of 10 degrees.

We see noisier behavior of the ISBs when the QZSS satellite sets at a low elevation angle that causes less precise observations. The phase ISB mean value is however zero and the code ISB is also close to zero (mean value of 4 mm), and the code and phase STDs (6 mm

and below 0.001 cycles respectively) also fall well within the code and phase measurement noise levels in Table 4, which makes it plausible to believe that they are time-constant. This was also concluded to be the case with the same data set for E1-L1 Galileo-GPS ISBs, with similar precision and close to zero mean values (not explicitly shown herein).

3.2 Bootstrapped success rates for large cut-off angles

The formal bootstrapped success rate (SR) is an accurate lower bound to the Integer Least-Squares (ILS) success rate (Teunissen, 1998, 1999) and can thus be used to infer whether integer ambiguity resolution can be expected to be successful. To compute the bootstrapped success rate we only need the variance covariance matrix of the (decorrelated) float ambiguities and we follow equation (19) in Teunissen (1998).

The bootstrapped success rates for CUTA-CUTT and different elevation cut-off angles between $10-40$ degrees are given in Figure 3 for B1 BDS in magenta, L1 GPS as blue, E1+L1 Galileo+GPS as green, B1+L1 BDS+GPS in cyan, and a combined B1+E1+L1+L1 four-system RTK model in black (full lines for ISBs corrected, dotted lines for ISBs unknown).

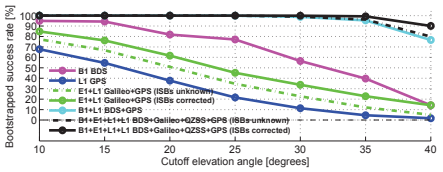

Fig. 3 Bootstrapped success rates for single-epoch, single-frequency RTK vs different elevation cut-off angles of 10-40 degrees.

We see in Figure 3 a dramatic decrease of the success rates with respect to increasing cut-off angles for the single-systems, whereas the success rate remains at stable values close to 100% for cut-off angles up to 35 degrees for the four-system with ISBs corrected. We also see the positive effect on the success rates when the differential ISBs are assumed zero/corrected.

3.3 Integer Least Squares ambiguity success rates

We compute the empirical ILS success rate by comparing the single-epoch estimated integer ambiguities to reference ambiguities. These reference ambiguities were estimated by using a combined system with multiple-frequencies and a Kalman filter over the entire observation time-span, assuming the ambiguities time-constant. The empirical success rate is defined as,

$$P_{s_E} = \frac{\#\text{correctly fixed epochs}}{\text{total } \#\text{ of epochs}} \tag{7}$$

The ILS success rates are presented in Table 5 for elevation cut-off angles of $10-40$ degrees, for different variations of satellite combinations.

Table 5 Empirical ILS success rate for single-epoch, single-frequency RTK and *full* ambiguity resolution, CUTA-CUTT and an elevation cut-off angle of $10-40$ degrees. April 29-30, 2013. The success rates corresponds to ISBs corrected when applicable (in brackets SRs are given when ISBs are unknown for overlapping frequencies).

System/ freq. cut-off	**Empirical Integer Least Squares SR** P_{s_E} [%] [deg] 10	20	25	30	35	40
B1 BDS	97.5	88.2	84.8	64.5	48.6	19.1
L1 GPS	82.9	55.7	34.8	19.9	9.1	3.7
E1+L1 Galileo+GPS	91.5 (87.1)	72.9 (65.3)	54.0 (45.8)	39.8 (31.3)	26.6 (18.7)	16.6 (9.4)
B1+L1 BDS+GPS	98.4	100	100	99.6	98.0	84.3
B1+E1+L1+L1 BDS+Galileo +QZSS+GPS	98.4 (98.4)	100 (100)	100 (100)	100 (99.7)	99.8 (98.2)	94.3 (85.9)

In Table 5 we see that the ILS success rates are consistent with the values of the Bootstrapped success rates in Figure 3, except for the 10 degree cut-off angle for B1+L1 and the four-system models with 98.4% ILS success rate (and 100% bootstrapped success rate). We investigated these instances and found that for both days (during the same short period of time) the ambiguities of two GPS satellites that were rising and setting were wrongly fixed, as a consequence of low elevation multipath. This thus illustrates one of the benefits of using larger cut-off angles for a combined system.

3.4 Positioning results for large cut-off angles

In order to illustrate the positioning results for a large elevation cut-off angle of 35 degrees, we give in Figure 4 the single-frequency B1 BDS, B1+L1 BDS+GPS and a four-system B1+E1+L1+L1 (with ISBs corrected) positioning results. The correctly fixed solution (green) is given together with the float solution (gray), and the wrongly fixed solutions (red).

Figure 4 illustrates that the correctly fixed positioning errors are at the mm-cm level and about two-orders of magnitude more precise than the float solution at dm-meter-level. It also illustrates the need of integer

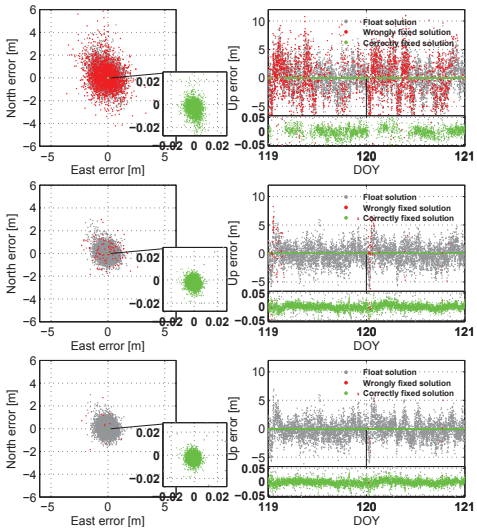

Fig. 4 B1 BDS (1st row), **B1+L1 BDS+GPS** (2nd row), and **B1+E1+L1+L1 ISBs corrected** (last row). Float (gray), correctly fixed (green), wrongly fixed (red) solutions for 35 degrees cut-off angle, single-epoch RTK, CUTA-CUTT.

validation techniques (Verhagen and Teunissen, 2013) since wrong fixing can lead to worse positioning performance compared to the float solution. Importantly an increase of availability of very precise positioning results can be seen in particular for the four-systems.

4 Conclusions

In this contribution we studied a four-system combination of B1 BDS, E1 Galileo, L1 QZSS and L1 GPS for instantaneous (single-epoch) single-frequency RTK positioning. We focused our attention on Inter System Biases (ISBs), on the integer ambiguity success rates as well as positioning for larger elevation cut-off angles.

The code and (fractional) phase differential ISB for L1-L1 QZSS-GPS were estimated with values close to zero mean and the standard deviations fall well within the code and phase measurement noise levels (Figure 2), which makes it plausible to believe that they are time-constant. Similar values were also observed for E1-L1 Galileo-GPS ISBs (not explicitly shown), and thus we conclude that one can safely neglect the ISBs for similar receiver types. Future studies will involve different receiver types and other overlapping frequencies.

The Integer Least Squares (ILS) empirical success rates were given for several satellite elevation cut-off angles between 10-40 degrees in Table 5, with larger angles suitable in e.g. urban canyons. We can conclude that the four-system model allows for *continuous* instantaneous RTK up to the 30 degree cut-off angle (100% success rate), which is not the case for the single-systems. Moreover the four-system model achieved larger success rates compared to Galileo+GPS and BDS+GPS, resulting in better precise positioning availability (Figure 4).

Acknowledgements This work has been executed in the framework of the Positioning Program Project 1.01 "New carrier phase processing strategies for achieving precise and reliable multi-satellite, multi-frequency GNSS/RNSS positioning in Australia" of the Cooperative Research Centre for Spatial Information (CRC-SI). The second author is the recipient of an Australian Research Council (ARC) Federation Fellowship (project number FF0883188). All this support is gratefully acknowledged.

References

Euler HJ, Goad Cg (1991) On optimal filtering of GPS dual frequency observations without using orbit information. Bull Geod 65:130–143

JAXA (2013) Japan Aerospace Exploration Agency (JAXA), Navigation Service Interface Specification for QZSS (IS-QZSS), V1.5. Tech. rep., 225 pages.

Montenbruck O, Hauschild A, Hessels U (2011) Characterization of GPS/GIOVE sensor stations in the CONGO network. GPS Solut 15(3):193–205

Montenbruck O, Hauschild A, Steigenberger P, Hugentobler U, Teunissen PJG, Nakamura S (2013) Initial assessment of the COMPASS/BeiDou-2 regional navigation satellite system. GPS Solut 17(2):211–222

Odijk D, Teunissen PJG (2013) Characterization of between-receiver GPS-Galileo inter-system biases and their effect on mixed ambiguity resolution. GPS Solut 17(4):521–533

Odolinski R, Teunissen PJG, Odijk D (2013) An analysis of combined COMPASS/BeiDou-2 and GPS single- and multiple-frequency RTK positioning. In: ION Pac PNT, Honolulu, HI, USA, pp 69–90

Teunissen (1990) An integrity and quality control procedure for use in multi sensor integration. In: Proc of ION GPS 1990, CO, pp 513–522, also in: Vol VII of GPS Red Book Ser: Integr syst, ION Navig, 2012

Teunissen PJG (1985) Generalized inverses, adjustment the datum problem and S-transformations. In: Optimization of geodetic networks Editors EW Grafarend and F Sanso, Springer-Verlag pp 11–55

Teunissen PJG (1995) The least squares ambiguity decorrelation adjustment: a method for fast GPS integer estimation. J Geod 70: 65-82

Teunissen PJG (1998) Success probability of integer GPS ambiguity rounding and bootstrapping. J Geod 72:606–612

Teunissen PJG (1999) An optimality property of the integer least-squares estimator. J Geod 73: 587-593

Teunissen PJG, Odijk D, Zhang B (2010) PPP-RTK: Results of CORS network-based PPP with integer ambiguity resolution. J Aeronaut, Astronaut and Aviat, Ser A 42(4):223–230

Verhagen S, Teunissen PJG (2013) The ratio test for future GNSS ambiguity resolution. GPS Solut (17):535–548

7 PERFORMANCE OF A BDS+GALILEO+QZSS+GPS SINGLE-FREQUENCY RTK MODEL

This chapter is covered by the following publication:

Odolinski R, Teunissen PJG, Odijk D (2014c) Combined BDS, Galileo, QZSS and GPS single-frequency RTK. Published in: GPS Solutions. doi: 10.1007/s10291-014-0376-6

GPS Solut
DOI 10.1007/s10291-014-0376-6

ORIGINAL ARTICLE

Combined BDS, Galileo, QZSS and GPS single-frequency RTK

Robert Odolinski · Peter J. G. Teunissen · Dennis Odijk

Received: 19 December 2013 / Accepted: 2 April 2014

Abstract We will focus on single-frequency single-baseline real-time kinematic (RTK) combining four Code Division Multiple Access (CDMA) satellite systems. We will combine observations from the Chinese BeiDou Navigation Satellite System (BDS), European Galileo, American Global Positioning System (GPS) and the Japanese Quasi-Zenith Satellite System (QZSS). To further strengthen the underlying model, attention will be given to overlapping frequencies between the systems. If one can calibrate the inter-system biases, a common pivot satellite between the respective systems can be used to parameterize double-differenced ambiguities. The LAMBDA method is used for ambiguity resolution. The instantaneous (single-epoch) single-frequency RTK performance is evaluated by a formal as well as an empirical analysis, consisting of ambiguity dilution of precision (ADOP), bootstrapped and integer least-squares success rates and positioning precisions. The time-to-correct-fix in some particular cases when instantaneous RTK is not possible will also be analyzed. To simulate conditions with obstructed satellite visibility or when low-elevation multipath is present, various elevation cut-off angles between 10 and 40° will be used. Four days of real data are collected in Perth, Western Australia. It will be shown that the four-system RTK model allows for improved integer ambiguity resolution and positioning performance over the single-, dual- or triple-systems, particularly for higher cut-off angles.

R. Odolinski (✉) · P. J. G. Teunissen · D. Odijk
GNSS Research Centre, Curtin University,
GPO Box U1987, Perth, WA 6845, Australia
e-mail: robert.odolinski@curtin.edu.au

P. J. G. Teunissen
Delft University of Technology, Delft, The Netherlands

Published online: 27 April 2014

Keywords Inter-system biases (ISBs) · Real-time kinematic (RTK) · Multi-global navigation satellite system (GNSS) · Integer ambiguity resolution · LAMBDA

Introduction

The next generations Global Navigation Satellite Systems (GNSSs) have the potential to enable a wide range of applications for positioning, navigation and timing. For positioning, the accuracy, reliability and satellite availability will be improved as compared to today's solutions, provided that a combination of the satellite systems is used. Since some of the frequencies overlap between the systems, one can also take full advantage of the measurements by applying a priori corrections for the receiver-dependent differential inter-system biases (ISBs) to maximize the redundancy (Odijk and Teunissen 2013a). This allows for a parameterization of double-differenced (DD) integer ambiguities with respect to a common "pivot" satellite between the systems. In this contribution, we will focus on the Global Positioning System (GPS), BeiDou Navigation Satellite System (BDS), Galileo and Quasi-Zenith Satellite System (QZSS) since they are all based on the Code Division Multiple Access (CDMA). GLONASS is not considered in this contribution as it currently (December 2013) only has one satellite transmitting a CDMA frequency (Mirgorodskaya 2013), which, moreover, does not overlap the GPS frequencies. Including this satellite would not result in a strengthening of our four-system (single-epoch) RTK model, as at least two CMDA GLONASS satellites would be needed (see also Table 3).

BDS attained Asia–Pacific regional operational status in the end of December 2011. The current (2013) BDS constellation has 5 Geostationary Earth Orbit (GEO), 5 Inclined Geo-Synchronous Orbit (IGSO) and 4 Medium

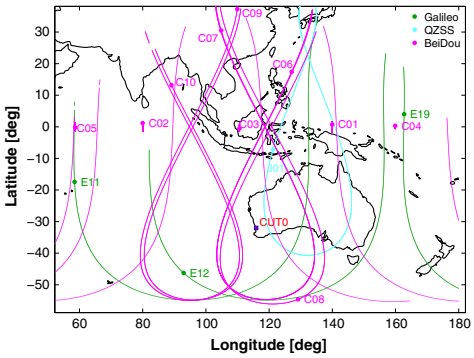

Fig. 1 BDS (*magenta*), Galileo (*green*) and QZSS (*cyan*) ground tracks with satellites location (*dots*) given at 10:05 a.m. local Perth time, April 29, 2013

Table 1 BDS, Galileo, QZSS and GPS signals

Satellite system	Band	Frequency (MHz)	Wavelength (cm)
BDS	**B1**	**1561.098**	**19.20**
BDS/Galileo	B2/E5b	1207.140	24.83
BDS	B3	1268.520	23.63
QZSS, GPS/Galileo	**L1/E1**	**1575.420**	**19.03**
QZSS, GPS	L2	1227.600	24.42
QZSS, GPS/Galileo	L5/E5a	1176.450	25.48

Frequencies that will be used are marked in bold

Earth Orbit (MEO) satellites available for positioning. Figure 1 shows a 24 h ground track of the operational BDS satellites in Perth, Western Australia at April 29, 2013. The positions of the satellites at 10.05 a.m. local Perth time (UTC +8 h) are indicated with a dot. BDS currently transmit at three frequencies, B1, B2 and B3 as is shown in Table 1. In the table, the L1, L2 and L5 GPS frequencies are given as well. BDS positioning results based on simulation can be found in, e.g., Grelier et al. (2007), Chen et al. (2009), and Yang et al. (2011) and BDS ambiguity resolution performance in, e.g., Cao et al. (2008). Real data results were presented in, e.g., Shi et al. (2012, 2013) and He et al. (2013a) for BDS single point and relative positioning, and precise orbit determination. Li et al. (2013a) and Li et al. (2013b) further evaluated BDS-only and combined BDS + GPS precise point positioning (PPP). Combined BDS + GPS RTK results can be found in Li et al. (2013c), Deng et al. (2013) and He et al. (2013b). Some first BDS-only results outside of China can be found in Montenbruck et al. (2013), Steigenberger et al. (2013) and Nadarajah et al. (2013). Combined BDS + GPS single-baseline RTK results can be found in, e.g., Odolinski et al. (2013) and Teunissen et al. (2013).

Since 2005 and 2008, respectively, two Galileo In-Orbit Validation Element (GIOVE) satellites have been in orbit. Moreover, four In-Orbit Validation (IOV) MEO satellites are currently available (since 2012) for positioning (Fig. 1) and broadcast signals at E1, E5a, E5b and E6 frequencies (Table 1). The E6 frequency will only be received as part of Galileo's Commercial Service. Initial results on combined GIOVE + GPS single-baseline RTK were presented in Odijk and Teunissen (2013a). It was shown that the ISBs between GPS and GIOVE are zero for similar receiver types, but indeed exist for mixed receiver types. The GIOVE-GPS ISBs nature and behavior were also investigated in Montenbruck et al. (2011) and for IOV-GPS ISBs in Melgard et al. (2013) and Odijk and Teunissen (2013b), which confirmed the results of Odijk and Teunissen (2013a).

QZSS uses the same orbital period as a traditional equatorial geostationary orbit but makes use of a large orbital inclination, see Fig. 1 (JAXA 2013). The system is designed to enable users to receive QZSS signals from a high elevation angle at all times in East Asia and Japan. The QZSS L1, L2 and L5 signals all overlap the GPS signals (Table 1). One satellite "MICHIBIKI", or "QZS-1", is currently in orbit and was launched September 2010.

We present a four-system BDS + Galileo + QZSS + GPS single-baseline RTK model, and we will compare its performance with the systems separately or some other combinations of them. The frequencies B1 of BDS, E1 and L1 of Galileo and GPS/QZSS, respectively, (bold in Table 1) will be used to maximize the number of available satellites with overlapping frequencies (note: B1 does currently not overlap any of the frequencies). L1 of GPS is used since at this time (December 2013) only four GPS satellites transmit the L5 signal.

The GNSS observation equations are introduced in Section "System of single-differenced GNSS observation equations", where the increased redundancy when calibrating the ISBs is demonstrated. Information about the 4 days of real data used to evaluate the RTK models is presented in Section "GNSS data collection and RTK stochastic model settings". In Section "Inter-system biases", we try to verify that the ISBs can be assumed zero for similar receiver types. This is followed by a single-baseline RTK analysis, formal as well as empirical, based on various cut-off elevation angles ranging between 10 and 40°. The higher elevation cut-off angles are used to simulate conditions with obstructed satellite visibility or when low-elevation multipath is present. The formal analysis is given in Section "Formal analysis of four-system RTK model", where ambiguity dilution of precision (ADOP), bootstrapped success rates and position precisions are given. The empirical analysis is then presented in Section

"Empirical analysis of four-system RTK model" based on real data. This to verify the conclusions made in the formal analysis. In this section, integer least-squares (ILS) success rates and statistics of the positioning performance, as obtained by comparing the estimated positions to precise benchmark coordinates, will be presented. We also look into the time-to-correct-fix in Section "Time-to-correct-fix using multiple-epoch solutions" for two special cases when single-epoch RTK is not possible. A summary and discussion is finally presented in "Conclusions".

System of single-differenced GNSS observation equations

Consider two receivers $r = 1, 2$ tracking the GPS (G) satellites $s_G = 1_G,\ldots,m_G$ and another GNSS system $s_* = 1_*,\ldots,m_*$, where m_G and m_* is the number of satellites of GPS and system $*$, respectively. The symbol $*$ is B for BDS, E for Europe/Galileo and Q for QZSS. Assume that we only track satellites on overlapping frequencies and we define the frequencies as $j = 1,\ldots, f$, where f is the corresponding number of frequencies. External products for satellite orbits are used and between-receivers single-differences (SDs) are subsequently performed on the system of observation equations with respect to the "pivot" receiver 1. Satellite delays common to both receivers are then eliminated, and for short baselines of a few km, the (relative) atmospheric delays and any remaining orbit errors can be neglected as well. The model presented assumes for notational convenience that *all frequencies overlap* with GPS and that the GPS receiver clock is shared among the systems. The time offsets, e.g., GPS-to-Galileo Time-Offset (*GGTO*), is then eliminated by the SDs.

Full-rank RTK functional model: ISBs-float

The system of observation equations is, however, not of full-rank after the SDs. These rank defects can be eliminated through an application of S-system theory (Teunissen 1985; Teunissen et al. 2010). This implies null-space identification, S-basis constraining and interpretation of the estimable parameters. The number of rank deficiencies and the S-basis choice are depicted in Table 2. We remark that many other S-basis choices are admissible but that they all give the same adjusted observations and least-squares residuals. Moreover, each minimum constrained solution can be transformed to another minimum constrained solution by means of an S-transformation (Teunissen 1985). From a precise GNSS positioning perspective, however, it is important that the particular S-basis choice results in estimable ambiguities that are integers (see Eq. 1). The "ISBs-float model" in (1) implies that the ISBs will be parameterized as unknowns.

Once the rank deficiencies in Table 2 have been solved, the combined RTK model can be formulated in the following full-rank, linearized, SD system of observation equations, in units of range and time stamps are omitted for brevity,

$$\begin{aligned} p^{s_G}_{12,j} &= -c_2^{s_G T}\Delta x_{12} + d\tilde{t}_{12} + \tilde{d}^{G}_{12,j} \\ \phi^{s_G}_{12,j} &= -c_2^{s_G T}\Delta x_{12} + d\tilde{t}_{12} + \tilde{\delta}^{G}_{12,j} + \lambda_j \tilde{M}^{1_G s_G}_{12,j} \\ p^{s_*}_{12,j} &= -c_2^{s_* T}\Delta x_{12} + d\tilde{t}_{12} + \tilde{d}^{G}_{12,j} + \tilde{d}^{G*}_{12,j} \\ \phi^{s_*}_{12,j} &= -c_2^{s_* T}\Delta x_{12} + d\tilde{t}_{12} + \tilde{\delta}^{G}_{12,j} + \tilde{\delta}^{G*}_{12,j} + \lambda_j \tilde{M}^{1_* s_*}_{12,j} \end{aligned} \quad (1)$$

where $(\cdot)_{12} = (\cdot)_2 - (\cdot)_1$ is the notation for between-receiver SDs, the SD code and phase observable is denoted $p^s_{12,j}$, $\phi^s_{12,j}$, respectively, $c_r^{sT} = (x^s - x_r)^T/\|x^s - x_r\|$ is the line-of-sight unit vector from the receiver r to the GNSS satellites obtained from linearizing the system of equations with respect to the receiver coordinates, where $(.)^T$ is the transpose of a vector, $\|.\|$ denotes the length, or norm, x^s is the vector of satellite coordinates and x_r the vector of receiver coordinates, λ_j is the wavelength corresponding to frequency j and * stands for systems B, E or Q, respectively. For notational convenience, we refrain from carrying through SD random observation noise and un-modeled effects such as multipath. The estimable unknowns are,

$\Delta x_{12} = \Delta x_2 - \Delta x_1$	relative receiver coordinates,
$d\tilde{t}_{12} = dt_{12} + d^G_{12,1}$	relative receiver clock with differential code delay of GPS,
$\tilde{d}^G_{12,j} = d^G_{12,j} - d^G_{12,1}$	relative GPS Differential Code Bias (DCB) for $f > 1$,
$\tilde{\delta}^G_{12,j} = \delta^G_{12,j} - d^G_{12,1} + \lambda_j M^{1_G}_{12,j}$	relative GPS receiver hardware (HW) phase delay,
$\tilde{d}^{G*}_{12,j} = d^*_{12,j} - d^G_{12,j}$	differential code ISB,
$\tilde{\delta}^{G*}_{12,j} = \delta^*_{12,j} - \delta^G_{12,j} + \lambda_j M^{1_G 1_*}_{12,j}$	differential phase ISB biased by DD ambiguity,
$\tilde{M}^{1_G s_G}_{12,j} = M^{s_G}_{12,j} - M^{1_G}_{12,j}$	DD GPS *integer* ambiguity,

Table 2 Single-epoch, single-baseline RTK S-basis choice and number of rank deficiencies

Model	S-basis choice	# of rank deficiencies
Four-system ISBs-float	Δx_1, dt_1, $d^G_{2,1}$, $d^G_{1,j}$, $d^*_{1,j}$, $\delta^G_{1,j}$, $\delta^*_{1,j}$, $M^{1_G}_{2,j}$, $M^{1_*}_{2,j}$, $M^{s_G}_{1,j}$, $M^{s_*}_{1,j}$	$5 + 12f + fm_G + fm_B + fm_E + fm_Q$

Table 3 Single-epoch, single-baseline RTK redundancy and solvability condition

Model	# of observations	# of unknowns	Redundancy	Solvability condition
Single-system	$2f_s m_*$	$3 + f_* + f_s m_*$	$f_s(m_*-1)-3$	$m_* \geq 4$
Four-system ISBs-float (1)	$2fm_G + 2fm_B + 2fm_E + 2fm_Q$	$3 + 4f + fm_G + fm_B + fm_E + fm_Q$	$f(m_G-1) + f(m_B-1) + f(m_E - 1) + f(m_Q - 1) - 3$	$m_G + m_B + m_E + m_Q \geq 7$
Four-system, ISBs-fixed *assuming* all freq. overlap (6)	$2fm_G + 2fm_B + 2fm_E + 2fm_Q$	$3 + f + fm_G + fm_B + fm_E + fm_Q$	$f(m_G - 1) + fm_B + fm_E + fm_Q - 3$	$m_G + m_B + m_E + m_Q \geq 4$
Four-system, ISBs-fixed for the overlapping freq. (bold in Table 1)	$2fm_G + 2f_B m_B + 2fm_E + 2fm_Q$	$3 + f + fm_G + f_B + f_B m_B + fm_E + fm_Q$	$f(m_G - 1) + f_B(m_B - 1) + fm_E + fm_Q - 3$	$m_G + m_B + m_E + m_Q \geq 5$

The last row corresponds to the ISBs-fixed four-system RTK model used in the following sections

$\tilde{M}^{1_* s_*}_{12,j} = M^{s_*}_{12,j} - M^{1_*}_{12,j}$ DD BDS, Galileo or QZSS *integer* ambiguity.

The DD ambiguities are integers since the initial receiver and satellite HW phase delays have been eliminated by the implicit double-differences. Note further that the differential phase ISB is biased by the inter-system DD (integer) ambiguities of the pivot satellites.

In case one wants to estimate system-specific HW delays for non-overlapping frequencies, we can make use of a reparameterization of the code and phase HW delays and ISBs, respectively, as follows,

$$\begin{aligned} \tilde{d}^{*}_{12,j*} &= \tilde{d}^{G*}_{12,j} + \tilde{d}^{G}_{12,j} = d^{*}_{12,j} - d^{G}_{12,1} \\ \tilde{\delta}^{*}_{12,j*} &= \tilde{\delta}^{G*}_{12,j} + \tilde{\delta}^{G}_{12,j} = \delta^{*}_{12,j} - d^{G}_{12,1} + \lambda_j M^{1_*}_{12,j} \end{aligned} \tag{2}$$

These system-specific HW delays are now biased by the GPS receiver HW code delay on the first frequency. In other words, the reparameterization in (2) shows that the model in (1) is equivalent (in terms of redundancy) to the model when one assumes system-specific HW delays for each system. Note also that the code ISB is estimable on the first frequency in (1), whereas the GPS DCB is only estimable on the second frequency and beyond. It thus implies that (1) also has an equivalent redundancy to the model when one takes different receiver clocks for each system (Odolinski et al. 2013), since the code ISBs on the first frequency then play the role as the additional unknowns instead of additional receiver clocks. The number of observations, estimable unknowns and redundancy of the model in (1) is shown in Table 3.

Full-rank RTK functional model: ISBs-fixed

In the previous section it was shown that if we for overlapping frequencies parameterize the ISBs, it does not strengthen the model as compared to a traditional model with system-specific receiver clocks/HW delays. However, if a priori knowledge of the ISBs is available we can strengthen the model accordingly. We will refer to the following model (6) as the "ISBs-fixed model". The phase ISB correction is defined as (Odijk and Teunissen 2013a),

$$\begin{aligned} \bar{\delta}^{G*}_{12,j} &= \delta^{*}_{12,j} - \delta^{G}_{12,j} + \lambda_j z_{12,j} \\ &= \delta^{G*}_{12,j} + \lambda_j M^{1_G 1_*}_{12,j} - \lambda_j (M^{1_G 1_*}_{12,j} - z_{12,j}) \end{aligned} \tag{3}$$

where $z_{I2,j}$ is an integer ambiguity that originates from the observations that are used to determine the ISB corrections. Since these observations are different from the observations to be corrected (1), the integer ambiguity $z_{I2,j}$ is in principle different from $M^{1_G 1_*}_{12,j}$. In other words, when the correction (3) is applied to the phase observations of system * in (1), the last ambiguity part of the correction will be lumped into the ambiguities,

$$\tilde{M}^{1_G s_*}_{12,j} = M^{1_* s_*}_{12,j} + (M^{1_G 1_*}_{12,j} - z_{12,j}) = M^{1_G s_*}_{12,j} - z_{12,j} \quad (4)$$

i.e., the ambiguity is now differenced with respect to the pivot satellite of GPS minus the integer ambiguity $z_{12,j}$ that is lumped into the phase ISB correction (3). If we denote the code ISB correction as,

$$\bar{d}^{G*}_{12,j} = d^{*}_{12,j} - d^{G}_{12,j} \quad (5)$$

the full-rank system * (*B, E* or *Q*) part of the observation equations can be expressed as (the GPS observation equations are still equivalent to (1)),

$$\begin{aligned} p^{s_G}_{12,j} &= -c_2^{s_G T}\Delta x_{12} + d\tilde{t}_{12} + \tilde{d}^{G}_{12,j} \\ \phi^{s_G}_{12,j} &= -c_2^{s_G T}\Delta x_{12} + d\tilde{t}_{12} + \tilde{\delta}^{G}_{12,j} + \lambda_j \tilde{M}^{1_G s_G}_{12,j} \\ p^{s_*}_{12,j} - \bar{d}^{G*}_{12,j} &= -c_2^{s_* T}\Delta x_{12} + d\tilde{t}_{12} + \tilde{d}^{G}_{12,j} \\ \phi^{s_*}_{12,j} - \bar{\delta}^{G*}_{12,j} &= -c_2^{s_* T}\Delta x_{12} + d\tilde{t}_{12} + \tilde{\delta}^{G}_{12,j} + \lambda_j \tilde{M}^{1_G s_*}_{12,j} \end{aligned} \quad (6)$$

Note that the ambiguity $\tilde{M}^{1_G s_*}_{12,j}$ (4) will also be estimable for $s_* = 1_*$, which gives us f additional unknowns for each system added to GPS in (6) as compared to Eq. (1). However, with a priori corrected values for differential code and phase ISBs ($2f$ corrections), the redundancy of the model increases with f as compared to (1) for each additional system to GPS. This is further clarified by Table 3.

Redundancy and solvability of the full-rank RTK models

In Table 3, the number of observations, estimable unknowns and redundancy of the presented single-baseline RTK models (1) and (6) are given (assuming that all frequencies overlap). A solvability condition is also defined, which is the number of satellites required to solve the models. The single-system RTK model in the table can be found in (1) for GPS, and we note that BDS-/Galileo- or QZSS-only models will have a similar definition of the unknowns.

One can imply from Table 3 that with the single-system or ISBs-fixed four-system model (6) at least four satellites are needed for positioning, whereas if all ISBs are unknown (1) at least seven satellites are needed. This thus illustrates that *each* satellite added to GPS will contribute to the solution in cases when all ISBs are corrected and when all frequencies overlap. Note, however, that since B1 of BDS currently (2013) does not overlap L1 of GPS (Table 1), one additional receiver clock for BDS will be parameterized in the following sections. This implies that at least five satellites will be needed to solve the BDS + GPS and four-system RTK model (assuming the other systems' ISBs corrected). We add this model to the last row of Table 3 as well since it is the model we will refer to as the "ISBs-fixed" four-system RTK model

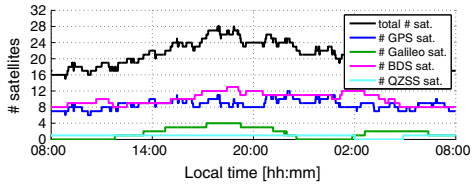

Fig. 2 Four-system satellite visibility for CUTT with an elevation cut-off angle of 10°, April 20, 2013

throughout this contribution. However, there are plans to shift the B1 signal to L1 (Gibbons 2013), and consequently then all frequencies analyzed in this research will overlap.

GNSS data collection and RTK stochastic model settings

Data from April 19–20 and, 10 days later, April 29–30, 2013 of CUT0 and CUTT (Trimble NetR9 receivers) at Curtin University, Perth Australia are evaluated. The measurement interval is set to 30 s, and the distance between the stations is approximately 1 km. We make use of the Detection, Identification and Adaptation (DIA) procedure to eliminate outliers (Teunissen 1990), and the LAMBDA method is used for integer ambiguity resolution (Teunissen 1995). The number of satellites visible over 24 h for an elevation cut-off angle of 10° and CUTT is given in Fig. 2.

A similar number of satellites for BDS and GPS can be seen in Fig. 2, and we have (2013) four Galileo satellites and one QZSS satellite visible. It is also evident that a combination of the four systems provides us with overall more than double the number of GPS satellites.

The stochastic RTK model settings are given in Table 4 based on the exponential elevation weighting function by Euler and Goad (1991). The zenith-referenced a priori code and phase standard deviation (STD), respectively, are given for undifferenced observations. These values were estimated using data that is independent from the data used in the following sections, and the procedure is further described in Odolinski et al. (2013).

Inter-system biases

Trimble NetR9 receivers are used throughout this contribution. Fortunately, the GIOVE-GPS ISBs have been shown to be zero for similar receiver types (Odijk and Teunissen 2013a). We want to confirm these results with Galileo IOV-GPS, as well as for the QZSS-GPS ISBs. If they turn out to be zero, we can safely neglect them and

Table 4 Zenith-referenced code and phase STDs for single-baseline RTK

Satellite system	Frequency	Code (cm)	Phase (mm)
BDS	B1	35	3
Galileo	E1	30	2
GPS	L1	37	3
QZSS	L1	30	3

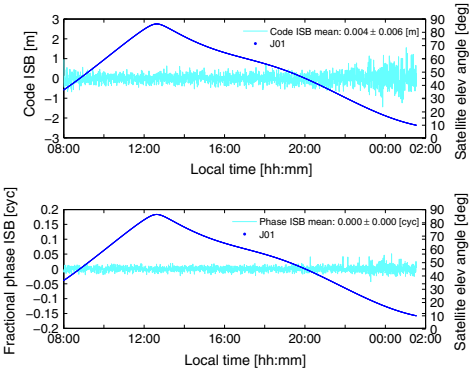

Fig. 3 L1-L1 QZSS-GPS code ISB at *top* and phase ISB at *bottom* for a zero-baseline setup CUT0-CUT2 (both Trimble NetR9), April 29, 2013, and for an elevation cut-off angle of 10°

maximize the redundancy of our RTK model. In Fig. 3, the code and (fractional) phase differential ISBs are depicted for L1-L1 QZSS-GPS. They are computed on an epoch-by-epoch basis for a zero-baseline setup and with fixed receiver positions of CUT0-CUT2 (Curtin University). The elevation cut-off angle is 10°, and the STDs are computed assuming the ISBs *time-constant* during the whole time-span to illustrate the ISBs repeatability.

When the QZSS satellite sets at a low elevation angle that causes less precise observations, we also see noisier behavior of the ISBs. The QZSS-GPS phase ISB mean value is, however, zero, and the mean value of the code ISB is also close to zero (4 mm). The ISB STDs fall well within the code and phase measurement noise levels in Table 4, which makes it plausible to believe that the ISBs are absent.

In Fig. 4, the corresponding E1-L1 Galileo-GPS ISBs are presented. The Galileo-GPS code and phase ISBs have a slightly better precision as compared to the ISBs of QZSS-GPS in Fig. 3, since, over the day, more satellites are tracked. More importantly, they also have close to zero mean values (4.3 cm and 0.001 cycles, respectively) and STDs (3 mm and below 0.001 cycles, respectively) that fall well within the code and phase measurement noise levels.

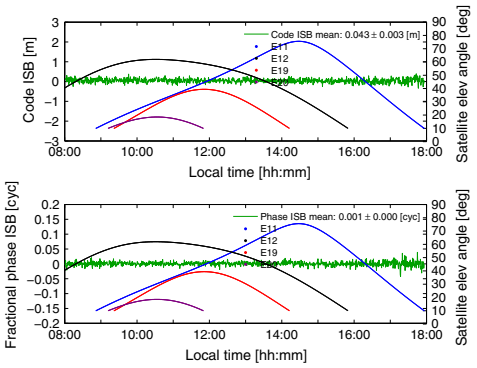

Fig. 4 E1-L1 Galileo-GPS code ISB at *top* and phase ISB at *bottom* for a zero-baseline setup CUT0-CUT2 (both Trimble NetR9), April 29, 2013, and for an elevation cut-off angle of 10°

Formal analysis of four-system RTK model

This section presents the formal analysis of the four-system RTK model. For the following computations we only need the design matrix and the variance–covariance (VCV) matrix of the observations, i.e., real data is not necessary.

Ambiguity dilution of precision

The ADOP is a scalar measure of the model strength for ambiguity resolution and was first introduced in Teunissen (1997). The ADOP is defined as,

$$\mathrm{ADOP} = \sqrt{|Q_{\hat{a}\hat{a}}|^{\frac{1}{n}}} \quad \text{(cycle)} \tag{7}$$

where $Q_{\hat{a}\hat{a}}$ is the VCV-matrix of the float ambiguities, n is the dimension of the ambiguity vector and $|\cdot|$ denotes the determinant. The ADOP measures the intrinsic precision of the ambiguities and is also a measure of the volume of the ambiguity confidence ellipsoid (Teunissen et al. 1996). In Fig. 5, we show the single-epoch ADOP time-series in blue over two days for L1 GPS, B1 BDS, B1 + L1 BDS + GPS and a 10 degree elevation cut-off angle. When the ADOP-values get below the 0.12 cycles is indicated by a dashed red line and can be taken as indication of successful ambiguity resolution, since it corresponds to an ambiguity success rate larger than 99.9 % (Odijk and Teunissen 2008). We also depict the number of satellites as green and when below 8 as red.

The ADOPs of B1 BDS and L1 GPS in Fig. 5 are generally too large to expect (successful) instantaneous ambiguity resolution. The ADOPs of L1 GPS are larger and fluctuate more than those of B1 BDS due to the fewer

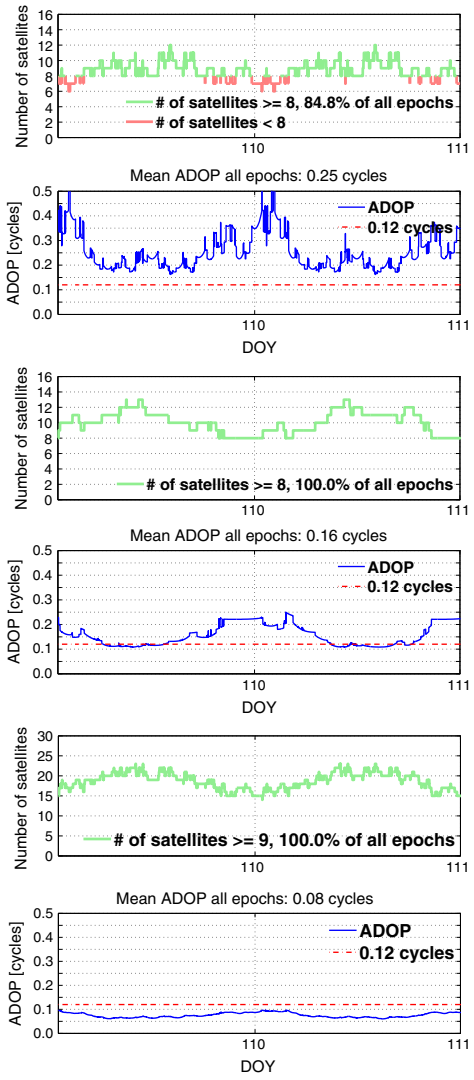

Fig. 5 Single-epoch ADOP (*blue*) and number of visible satellites in *green* (and in *red* when less than 8) for L1 GPS (*top*), B1 BDS (*middle*) and B1 + L1 BDS + GPS (*bottom*), 10° cut-off elevation angle (Perth, April 19–20, 2013)

tracked GPS satellites, more frequent changes in their tracking, as well as the poorer code precision (Table 4). Importantly, the BDS + GPS system shows less ADOP fluctuations and remains below 0.12 cycles all the time. In Teunissen et al. (2013), this is explained analytically,

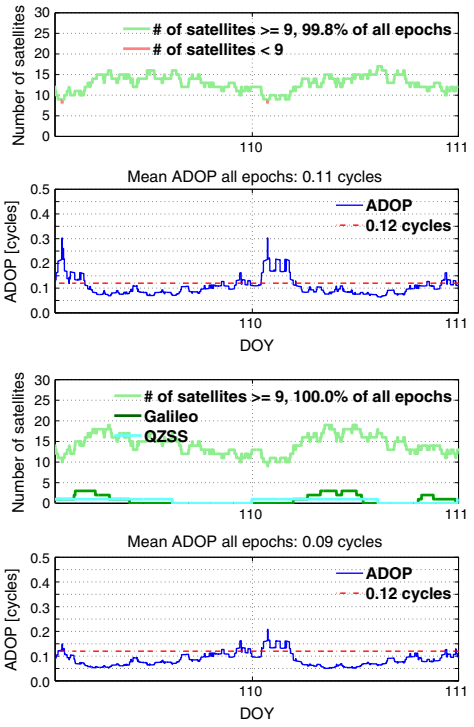

Fig. 6 Single-epoch ADOP (*blue*) and number of visible satellites in *light green* (and in *red* when less than 9) for B1 + L1 BDS + GPS (*top*) and B1 + E1 + L1 + L1 BDS + Galileo + QZSS + GPS with ISBs-fixed (*bottom*), 30° cut-off elevation angle (Perth, April 19–20, 2013)

where it was shown that the number of satellites, the phase-code variance ratio, the number of frequencies and the number of common parameters between the systems all contribute in reducing the ADOP.

Since the combined BDS + GPS system shows such promising results, it is of interest to see the expected ambiguity resolution improvement if we can include the Galileo and QZSS satellites as well. To get a more challenging case, we increase the elevation cut-off angle to 30°. In Fig. 6, the corresponding ADOP time-series is depicted for B1 + L1 BDS + GPS and a B1 + E1 + L1 + L1 BDS + Galileo + QZSS + GPS model with ISBs-fixed/assumed zero. The number of satellites is depicted dark green for Galileo and cyan for QZSS as well to illustrate the redundancy differences between the models.

With the combination of all four systems, we see in Fig. 6 a decrease in the ADOPs as compared to BDS + GPS and can thus expect the four-system model to have a better instantaneous success rate performance as

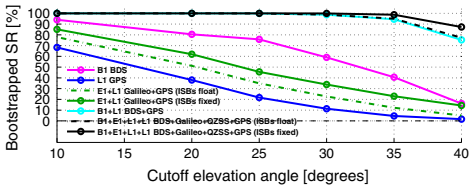

Fig. 7 Bootstrapped success rate for single-epoch, single-frequency RTK versus cut-off elevation angles of 10–40° (Perth, April 19–20 and April 29–30, 2013)

well. This since the ADOP time-series stays close to or below the 0.12 cycle level the entire two days. However, for BDS + GPS, quite some epochs reach values above 0.12 cycles.

Bootstrapped success rates

The formal bootstrapped success rate (SR) is an accurate lower bound to the integer least-squares (ILS) success rate (Teunissen 1998, 1999) and can thus be used to infer whether integer ambiguity resolution can be expected to be successful. To compute it, we only need the VCV-matrix of the (decorrelated) float ambiguities. The bootstrapped success rate is given as (Teunissen 1998),

$$P\left[\breve{z}_{IB} = z\right] = \prod_{i=1}^{n}\left[2\Phi\left(\frac{1}{2\sigma_{\hat{z}_{i|I}}}\right) - 1\right] \tag{8}$$

where $P[\breve{z}_{IB} = z]$ denotes the probability of correct integer estimation of the integer bootstrapped estimator $\breve{z}_{IB}$, $\Phi(x) = \int_{-\infty}^{x} \frac{1}{\sqrt{2\pi}} \exp\left(-\frac{1}{2}v^2\right)dv$ is the cumulative normal distribution, and $\sigma_{\hat{z}_{i|I}}$ with $i = 1,\ldots,n$, $I = \{1,\ldots,(i-1)\}$ is the conditional standard deviations of the decorrelated ambiguities.

The single-epoch bootstrapped success rate for different cut-off elevation angles between $10 - 40°$ are given in Fig. 7 for B1 BDS (magenta), L1 GPS (blue), E1 + L1 Galileo + GPS (green), B1 + L1 BDS + GPS (cyan) and a combined B1 + E1 + L1 + L1 four-system RTK model (black). Full and dotted lines are ISBs-fixed and ISBs-float models, respectively, provided that any of the frequencies overlap. The depicted success rates are based on the mean of all single-epoch bootstrapped success rates for April 19–20, as well as April 29–30, 2013. Note that when the ISBs are unknown, the single QZSS satellite does not contribute to the single-epoch solution. This implies that the ISBs-float four-system RTK model (dotted black line) is actually a three-system BDS + Galileo + GPS model.

In Fig. 7 we see a dramatic decrease in the success rates with respect to increasing cut-off angles for the single-systems. BDS is, however, more stable than GPS and Galileo + GPS due to more satellites tracked at higher cut-off angles. Most importantly, the success rate remains at stable values close to 100 % for cut-off angles up to 25° for BDS + GPS. The corresponding angle is even 30° for the four-system model with ISBs-fixed. The success rate differences between the ISBs-fixed four-system model (full black line), the ISBs-float counterpart (dotted black line) and BDS + GPS (cyan) increase more rapidly when reaching angles of 35–40°. We also see the positive effect on the success rates when the differential ISBs are fixed/assumed zero.

Table 5 Formal STDs for single-epoch, single-frequency RTK and an elevation cut-off angle of 10°, ambiguity-float/fixed solutions in North, East and Up (Perth, April 19–20, 2013)

System/freq.	Formal STDs float/fixed		
	N (cm)	E (cm)	U (cm)
B1 BDS	69/0.5	49/0.3	151/1.1
L1 GPS	60/0.4	52/0.4	141/0.9
E1 + L1 Galileo + GPS	56/0.4	47/0.3	128/0.8
	(58/0.4)	(49/0.3)	(133/0.8)
B1 + L1 BDS + GPS	41/0.3	35/0.2	96/0.7
B1 + E1 + L1 + L1	38/0.3	32/0.2	89/0.6
BDS + Galileo + QZSS + GPS	(41/0.3)	(33/0.2)	(93/0.6)

The STDs correspond to ISBs-fixed when applicable (in brackets STDs are given for ISBs-float)

Positioning

In Table 5, we provide information on the expected positioning precision in terms of formal standard deviations (local North, East, Up) of the float and fixed single-frequency, single-epoch solutions for all combination of satellite systems as depicted in Fig. 7. This is given for a 10 degree elevation cut-off angle.

We can see the two orders of magnitude improvement when going from ambiguity-float to ambiguity-fixed solutions, as well as the improvement which a combination of the systems brings.

Empirical analysis of four-system RTK model

In this section, an empirical analysis based on real data will be presented to verify the formal claims in the previous section and to show the actual performance of the four-system RTK model.

Integer least-squares ambiguity success rates

We compute the empirical ILS success rate by comparing the single-epoch estimated integer ambiguities to reference

Table 6 Empirical ILS success rate for single-epoch, single-frequency RTK and full ambiguity resolution, CUT0-CUTT and an elevation cut-off angle of 10°

Empirical integer least-squares success rate (%)				
System/freq. April:	19	20	29	30
B1 BDS	96.7	*94.8*	96.6	97.3
L1 GPS	83.0	79.3	82.8	81.1
E1 + L1 Galileo + GPS	91.4	88.2	92.3	89.4
	(87.5)	(84.5)	(87.4)	(84.8)
B1 + L1 BDS + GPS	98.6	*97.8*	98.5	98.4
B1 + E1 + L1 + L1	98.6	*97.8*	98.5	98.4
BDS + Galileo + QZSS + GPS	(98.6)	*(97.8)*	(98.5)	(98.4)

The success rates are given for April 19–20 and April 29–30, 2013, from left to right columns, respectively. The success rates correspond to ISBs-fixed when applicable (in brackets SRs are given for ISBs-float)

Table 7 Empirical ILS success rate for elevation cut-off angles of 10, 20, 25, 30, 35 and 40° (from left to right columns, respectively)

Empirical integer least-squares success rate (%)						
System/freq., cut-off (°):	10	20	25	30	35	40
B1 BDS	96.4	85.4	81.2	63.4	46.7	20.8
L1 GPS	81.6	53.9	32.4	17.7	7.5	3.3
E1 + L1 Galileo + GPS	90.3	72.6	53.9	39.8	27.5	19.1
	(86.0)	(63.9)	(43.8)	(29.3)	(16.7)	(8.2)
B1 + L1 BDS + GPS	98.3	**100**	**100**	99.4	96.5	81.7
B1 + E1 + L1 + L1	98.3	**100**	**100**	**100**	99.5	91.7
BDS + Galileo + QZSS + GPS	(98.3)	(100)	(100)	(99.5)	(96.7)	(83.1)

Success rates are given for single-epoch, single-frequency RTK and full ambiguity resolution for CUT0-CUTT, April 19–20 and April 29–30 combined, 2013. The success rates correspond to ISBs-fixed when applicable (in brackets SRs are given for ISBs-float)

ambiguities. The reference ambiguities were estimated by a batch solution using a combined system with multiple-frequencies and assuming the ambiguities time-constant over the whole time-span. The empirical success rate can be defined as,

$$P_{s_E} = \frac{\#\text{ of correctly fixed epochs}}{\text{total }\#\text{ of epochs}} \quad (9)$$

The empirical single-epoch ILS success rates are given in Table 6 for the single-frequency single and combined systems and for an elevation cut-off angle of 10°. The success rates are given for two days and then 10 days later another two days are included, as to demonstrate their repeatability. Satellite C07 was not logged for most of the day on April 20 and we thus denote the affected success rates with italics. The empirical ILS success rates for all four days combined and for elevation cut-off angles of 10, 20, 25, 30, 35 and 40° are further presented in Table 7.

Note the good repeatability of the success rates in Table 6. Moreover, note in Tables 6 and 7 for the 10° angle that the ILS success rates for BDS + GPS as well as the four-system models are *not consistent* with the bootstrapped success rates in Fig. 7. The bootstrapped success rates should in fact be lower than the ILS success rates. We analyzed these wrongly fixed instances in detail and found that every day, during the same short period of time, the ambiguities of some GPS satellites that were setting and rising were wrongly fixed as consequence of low-elevation multipath.

This thus illustrates one of the benefits of using a large cut-off angle for a combined system since one can avoid low-elevation multipath and still allow for instantaneous RTK. For BDS + GPS, we namely have 100 % ILS success rate for the 20 and 25 degree cut-off angles, and the corresponding angles are 20–30 (almost 35)° for the four-system model with ISBs-fixed.

Positioning

Table 8 provides information on the empirical float and correctly fixed instantaneous positioning performance for the single-frequency, single and all combined systems' performance for a 10 degree elevation cut-off angle. These results were obtained by comparing the estimated positions to precise benchmark coordinates and are in good agreement with the formal precision in Table 5.

Table 8 Empirical STDs for single-epoch, single-frequency RTK and an elevation cut-off angle of 10°, ambiguity-float/(correctly)-fixed solutions in North, East and Up, CUT0-CUTT. April 19–20, 2013

System/freq.	STDs float/(correctly)-fixed		
	N (cm)	E (cm)	U (cm)
B1 BDS	66/0.4	55/0.3	154/0.9
L1 GPS	57/0.3	48/0.3	121/0.9
E1 + L1 Galileo + GPS	52/0.3	43/0.3	107/0.9
	(54/0.3)	(45/0.3)	(112/0.9)
B1 + L1 BDS + GPS	40/0.3	35/0.2	85/0.7
B1 + E1 + L1 + L1	37/0.3	32/0.2	79/0.7
BDS + Galileo + QZSS + GPS	(39/0.3)	(34/0.2)	(81/0.7)

The STDs correspond to ISBs-fixed when applicable (in brackets STDs are given for ISBs-float)

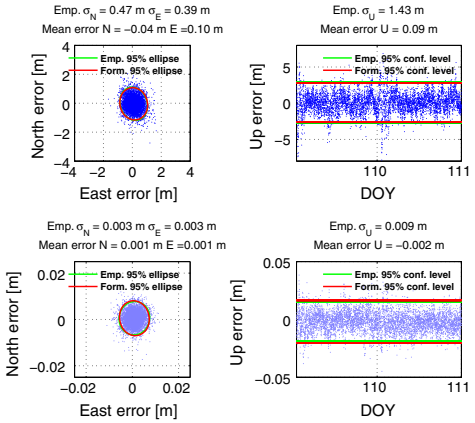

Fig. 8 Horizontal (N, E) position scatter and corresponding vertical (U) time-series (CUT0-CUTT, April 19–20, 2013) of the float (*top*) and fixed (*bottom*) B1 + E1 + L1 + L1 BDS + Galileo + QZSS + GPS (ISBs-fixed) single-epoch RTK solutions for an elevation cut-off angle of 30°. The 95 % empirical and formal confidence ellipse/interval is shown in *green* and *red*, respectively. All epochs are correctly fixed (Table 7)

Figure 8 further shows the repeatability (April 19–20, 2013) of float and fixed positioning for the single-epoch, single-frequency four-system (ISBs-fixed) model and an elevation cut-off angle of 30°. All epochs were correctly fixed for this cut-off angle (Table 7), as also predicted by the bootstrapped success rate in Fig. 7. The empirical and formal confidence ellipses/intervals have been computed from the empirical and formal position VCV-matrices. The empirical VCV-matrix was estimated from the positioning errors as obtained from comparing the estimated positions to precise benchmark coordinates. The formal VCV-matrix used is determined from the mean of all single-epoch formal VCV-matrices for both days.

To illustrate the positioning results for a higher elevation cut-off angle of 35°, we give in Fig. 9 the L1 GPS, B1 + L1 BDS + GPS and a four-system B1 + E1 + L1 + L1 (with ISBs-fixed) positioning results. The results are shown for April 19–20, 2013. The correctly fixed solution (green) is given together with the float solution (gray) and the wrongly fixed solutions (red). We also depict the number of satellites for GPS together with the positional dilution of precision (PDOP) as to demonstrate the large positioning errors' dependency on the satellite geometry. The combined systems do not suffer from very large PDOPs for this cut-off angle. For the combined systems, we therefore simply plot the number of satellites below nine as red, otherwise as green, as to illustrate the correctly fixed solutions' dependency on the number of satellites. The number of satellites is also depicted as dark green for Galileo and cyan for QZSS to illustrate the redundancy differences between the two models.

Figure 9 shows that the correctly fixed positioning errors are at the mm-cm level and that wrong fixing can lead to an even worse positioning performance as compared to taking the float solution at the decimeter-meter level. GPS have quite some epochs with positioning unavailability due to the insufficient number of satellites (should be at least four satellites). Most importantly, we see a dramatic increase in the number of satellites and thus availability of precise positioning for the combined systems, in particular for the four systems with ISBs-fixed and with the additional Galileo and QZSS satellites.

Time-to-correct-fix using multiple-epoch solutions

A case with an elevation cut-off angle of 40° will be analyzed in this section, but instead of epoch-by-epoch solutions we accumulate epochs by a Kalman filter assuming the ambiguities time-constant. This is done as to determine the time-to-correct-fix in cases when instantaneous RTK is not possible for the combined systems compared in Fig. 9.

The filter is initialized and based on the filtered set of float ambiguities, ambiguity resolution is attempted. The fixed ambiguities are then compared to the reference ambiguities, and if they are not correct a second epoch is included in the filter, and so on, until the estimated integer ambiguities are correct. When this is true, the filter is re-initialized at the second epoch and the whole process is repeated again. The time-to-correct-fix results with mean ± STD over a two day period are depicted in Fig. 10

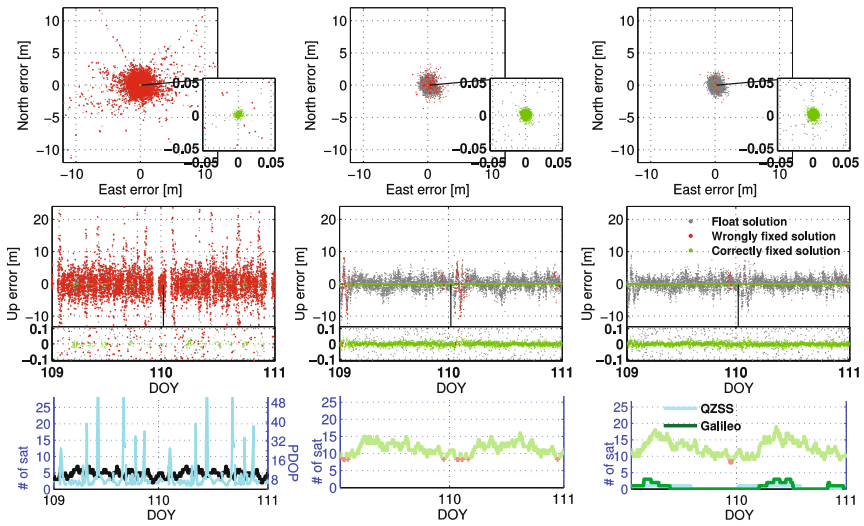

Fig. 9 L1 GPS (*left*), B1 + L1 BDS + GPS (*middle*), and four-system B1 + E1 + L1 + L1 ISBs-fixed model (*right*) for April 19–20, 2013. Float (*gray*), correctly fixed (*green*) and wrongly fixed (*red*) solutions at *top two rows*, and at *bottom* PDOP (*cyan*) for GPS and number of satellites for the combined systems are depicted as well (below 9 as *red*, otherwise as *light green*). This is given for 35° elevation cut-off angle, single-epoch RTK and CUT0-CUTT

for an elevation cut-off angle of 40° for B1 + L1 BDS + GPS and the B1 + E1 + L1 + L1 four-system, ISBs-fixed, RTK model. The total number of satellites is depicted in red when below nine, otherwise in green.

The number of epochs needed for successful integer ambiguity resolution is smaller when using a four-system model as compared to BDS + GPS combined. The mean value in Fig. 10 is namely reduced from 2.4 down to 1.2 epochs and with a standard deviation improvement from 7.1 down to 0.7 epochs. This indicates again the gain one achieves by combining all satellite systems and accounting for the ISBs to maximize the redundancy. Thus, the increase in number of satellites from combining the systems does not only improve *single-epoch* ambiguity resolution (see previous sections), but the time-to-correct-fix can also be improved significantly in case of a *multiple-epoch* solution.

Conclusions

In this contribution, we studied a combination of B1 BDS, E1 Galileo, L1 QZSS and L1 GPS for (short, atmosphere-fixed) single-baseline RTK. The inter-system biases (ISBs) were fixed/assumed zero whenever possible to maximize the redundancy. We could namely verify that the ISBs between L1 GPS, L1 QZSS and E1 Galileo can be safely neglected when using similar receiver types. Future ISB studies will involve different receiver types as well as other overlapping frequencies.

Our single-baseline RTK results consisted then of a formal and an empirical analysis. In the formal analysis, the ADOP, bootstrapped success rates and positioning precision were analyzed to illustrate the benefits of combining the systems. In the empirical analysis, the ILS success rates were computed and the positioning precision was determined by comparing the estimated positions to precise benchmark coordinates. It was shown that with combined systems much larger than customary elevation cut-off angles can be used. This is of importance in areas such as urban canyons or when low-elevation multipath is present.

The formal bootstrapped success rates were overall shown to be consistent with the empirically determined ILS success rates as computed from four days of GNSS data covering a 10 day period. The four-system ISB-fixed RTK model allows for continuous instantaneous RTK even for an elevation cut-off angle of 30°. This was not the case when the ISBs were estimated, for the single-systems or B1 + L1 BDS + GPS, for instance. We also showed that the ISB-fixed four-system model achieves significantly larger success rates for cut-off angles of 35–40°, as compared to, e.g., the ISB-float counterpart or BDS + GPS. This consequently results in better precise positioning

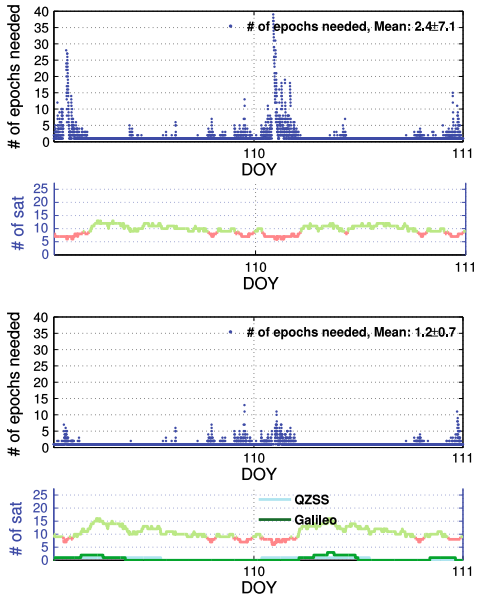

Fig. 10 Time-to-correct-fix (1 epoch = 30 s) with mean ± STD over April 19–20, 2013, for an elevation cut-off angle of 40° and single-baseline RTK for B1 + L1 BDS + GPS (*top*) and B1 + E1 + L1 + L1 BDS + Galileo + QZSS + GPS ISBs-fixed model (*bottom*), CUT0-CUTT. The number of satellites are depicted in *red* when below 9, and in *light green* otherwise

availability. The conclusion reads therefore that ISB calibration is particularly important in environments with obstructed satellite visibility, where every additional satellite to GPS can contribute to the solution.

We concluded by analyzing an elevation cut-off angle of 40° for two days of data using multiple-epoch solutions. This was done for the single-frequency four-system (ISBs-fixed) model and compared to B1 + L1 BDS + GPS. We found a significant improvement of the time-to-correct-fix for the combination of four systems, due to the additional Galileo and QZSS satellites tracked.

Acknowledgments This work has been executed in the framework of the Positioning Program of the Cooperative Research Centre for Spatial Information (CRC-SI). The second author is the recipient of an Australian Research Council (ARC) Federation Fellowship (project number FF0883188). All this support is gratefully acknowledged.

References

Cao W, O'Keefe K, Cannon M (2008) Evaluation of COMPASS ambiguity resolution performance using geometric-based techniques with comparison to GPS and Galileo. In: Proceedings of ION-GNSS-2008, Institute of Navigation, Savannah, GA, 16–19 September, pp 1688–1697

Chen H, Huang Y, Chiang K, Yang M, Rau R (2009) The performance comparison between GPS and BeiDou-2/COMPASS: a perspective from Asia. J Chin Inst Eng 32(5):679–689

Deng C, Tang W, Liu J, Shi C (2013) Reliable single-epoch ambiguity resolution for short baselines using combined GPS/BeiDou system. GPS Solut. doi:10.1007/s10291-013-0337-5

Euler HJ, Goad Cg (1991) On optimal filtering of GPS dual frequency observations without using orbit information. Bull Geod 65:130–143

Gibbons G (2013) GNSS News. Inside GNSS, p 1

Grelier T, Ghion A, Dantepal J, Ries L, DeLatour A, Issler JL, Avila-Rodriguez J, Wallner S, Hein G (2007) Compass signal structure and first measurements. In: Proceedings of ION-GNSS-2007, Institute of Navigation, Fort Worth, TX, September, pp 3015–3024

He L, Ge M, Wang J, Wickert J, Schuh H (2013a) Experimental study on the precise orbit determination of the BeiDou navigation satellite system. Sensors 13(3):2911–2928. doi:10.3390/s130302911

He H, Li J, Yang Y, Xu J, Guo H, Wang A (2013b) Performance assessment of single- and dual-frequency BeiDou/GPS single-epoch kinematic positioning. GPS Solut. doi:10.1007/s10291-013-0339-3

JAXA (2013) Japan Aerospace Exploration Agency (JAXA), navigation service interface specification for QZSS (IS-QZSS), V1.5 Tech. Rep., March 27, 2013

Li W, Teunissen PJG, Zhang B, Verhagen S (2013a) Precise point positioning using GPS and Compass observations. In: Sun et al (eds) Lect Notes in Electrical Engineering, Chap 33, vol 2, pp 367–378

Li X, Ge M, Zhang H, Nischan T, Wickert J (2013b) The GFZ real-time GNSS precise positioning service system and its adaption for COMPASS. J Adv Space Res 51(6):1008–1018

Li J, Yang Y, Xu J, He H, Guo H, Wang A (2013c) Performance analysis of single-epoch dual-frequency RTK by BeiDou navigation satellite system. In: Sun et al (eds) Lecture notes in Electrical Engineering, Chap 12, vol 3, pp 133–143

Melgard T, Tegedor J, de Jong K, Lapucha D, Lachapelle G (2013) Interchangeable integration of GPS and Galileo by using a common system clock in PPP. In: Proceedings of ION-GNSS-2013, Institute of Navigation, Nashville, TN, 16–20 September, pp 1198–1206

Mirgorodskaya T (2013) GLONASS government policy, status and modernization plans. In: Proceedings of international global navigation satellite systems (IGNSS) symposium, Golden Coast, 16–18 July

Montenbruck O, Hauschild A, Hessels U (2011) Characterization of GPS/GIOVE sensor stations in the CONGO network. GPS Solut 15(3):193–205

Montenbruck O, Hauschild A, Steigenberger P, Hugentobler U, Teunissen PJG, Nakamura S (2013) Initial assessment of the COMPASS/BeiDou-2 regional navigation satellite system. GPS Solut 17(2):211–222

Nadarajah N, Teunissen PJG, Raziq N (2013) BeiDou inter-satellite-type bias evaluation and calibration for mixed receiver attitude determination. Sensors 13(7):9435–9463

Odijk D, Teunissen PJG (2008) ADOP in closed form for a hierarchy of multi-frequency single-baseline GNSS models. J Geod 82:473–492

Odijk D, Teunissen PJG (2013a) Characterization of between-receiver GPS-Galileo inter-system biases and their effect on mixed ambiguity resolution. GPS Solut 17(4):521–533

Odijk D, Teunissen PJG (2013b) Estimation of differential inter-system biases between the overlapping frequencies of GPS,

Galileo, BeiDou and QZSS. In: 4th International colloquium scientific and fundamental aspects of the Galileo programme, 4–6 December, Prague, Czech Republic

Odolinski R, Teunissen PJG, Odijk D (2013) An analysis of combined COMPASS/BeiDou-2 and GPS single- and multiple-frequency RTK positioning. In: Proceedings of ION PNT 2013, Honolulu, Hawaii, April 23–25, pp 69–90

Shi C, Zhao Q, Li M, Tang W, Hu Z, Lou Y, Zhang H, Niu X, Liu J (2012) Precise orbit determination of Beidou Satellites with precise positioning. Sci China Earth Sci 55:1079–1086. doi:10.1007/819s11430-012-4446-8

Shi C, Zhao Q, Hu Z, Liu J (2013) Precise relative positioning using real tracking data from COMPASS GEO and IGSO satellites. GPS Solut 17(1):103–119. doi:10.1007/s10291-012-0264-x

Steigenberger P, Hugentobler U, Hauschild A, Montenbruck O (2013) Orbit and clock analysis of COMPASS GEO and IGSO satellites. J Geod 87(6):515–525. doi:10.1007/s00190-013-0625-4

Teunissen PJG (1985) Generalized inverses, adjustment, the datum problem and S-transformations. In: Grafarend EW, Sanso F (eds) Optimization of geodetic networks. Springer, Berlin, pp 11–55

Teunissen PJG (1990) An integrity and quality control procedure for use in multi sensor integration. In: Proceedings of ION-GPS-1990, Colorado Spring, CO, pp 513–522, also published in: vol VII of GPS Red Book Series: Integrated systems, ION Navigation, 2012

Teunissen PJG (1995) The least squares ambiguity decorrelation adjustment: a method for fast GPS integer estimation. J Geod 70:65–82

Teunissen PJG (1997) A canonical theory for short GPS baselines. Part I: the baseline precision, Part II: the ambiguity precision and correlation, Part III: the geometry of the ambiguity search space, Part IV: precision versus reliability. J Geod 71(6):320–336, 71(7):389–401, 71(8):486–501, 71(9):513–525

Teunissen PJG (1998) Success probability of integer GPS ambiguity rounding and bootstrapping. J Geod 72:606–612

Teunissen PJG (1999) An optimality property of the integer least-squares estimator. J Geod 73:587–593

Teunissen PJG, de Jonge P, Tiberius C (1996) The volume of the GPS ambiguity search space and its relevance for integer ambiguity resolution. In: Proceedings of ION-GPS-1996, vol 9, pp 889–898

Teunissen PJG, Odijk D, Zhang B (2010) PPP-RTK: results of CORS network-based PPP with integer ambiguity resolution. J Aeronaut Astronaut Aviation Ser A 42(4):223–230

Teunissen PJG, Odolinski R, Odijk D (2013) Instantaneous BeiDou+GPS RTK positioning with high cut-off elevation angles. J Geod. doi:10.1007/s00190-013-0686-4

Yang Y, Li J, Xu J, Tang J, Guo H, He H (2011) Contribution of the compass satellite navigation system to global PNT users. Chin Sci Bull 56(26):2813–2819

Robert Odolinski received his M.Sc. degree in Geodesy and Geoinformatics from the Royal Institute of Technology (KTH) Stockholm, Sweden, in 2009. He is since 2011 a Ph.D. Candidate in the GNSS Research Centre at Curtin University in Perth, Australia. His research topics include multi-GNSS integer ambiguity resolution, precise positioning and quality control.

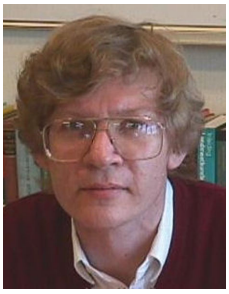

Peter Teunissen is a Federation Fellow of the Australian Research Council (ARC), Professor of Geodesy and Navigation and Head of Curtin's GNSS Research Centre. His current research focus is on modeling next-generation GNSSs for relative navigation and attitude determination in space and air.

Dennis Odijk is a research fellow in the GNSS Research Centre. His research is focused on high-precision GNSS positioning, with emphasis on integer ambiguity resolution enabled precise point positioning, ionospheric modeling, multi-GNSS interoperability, quality control and prototype software development.

8 LONG BASELINE BDS+GALILEO+QZSS+GPS RTK POSITIONING

This chapter is covered by the following publication:

Odolinski R, Teunissen PJG, Odijk D (2014d) Combined GPS+BDS+Galileo+QZSS Long Baseline RTK Positioning. Published in: Proceedings of the ION GNSS, Tampa, Florida, USA, September 8-12, 2014 (non-peer-reviewed)

Combined GPS+BDS+Galileo+QZSS for Long Baseline RTK Positioning

R. Odolinski[1], P.J.G Teunissen[1,2], D. Odijk[1]
1) *GNSS Research Centre, Department of Spatial Sciences*
Curtin University, Perth, Australia
2) *Mathematical Geodesy and Positioning*
Delft University of Technology, The Netherlands

BIOGRAPHY

Robert Odolinski received in 2009 his MSc degree in Geodesy at the Royal Institute of Technology (KTH), Stockholm, Sweden. In 2011 he started his PhD studies at Curtin University, Australia. His research topic is next generation multi-GNSS integer ambiguity resolution enabled precise positioning.

Peter J.G. Teunissen is a Federation Fellow of the Australian Research Council (ARC), Professor of Geodesy and Navigation and Head of Curtin's GNSS Research Centre. His current research focus is on modeling next-generation GNSS for improved parameter estimation and validation.

Dennis Odijk is a Research Fellow in the GNSS Research Centre at Curtin University. His research is focused on high-precision GNSS positioning, with an emphasis on integer ambiguity resolution enabled precise point positioning, ionospheric modeling, multi-GNSS interoperability, quality control and prototype software development.

ABSTRACT

In this contribution we will focus on long single-baseline real-time kinematic (RTK) positioning when combining the American GPS, Chinese BDS, European Galileo and Japanese QZSS. The main objective is to demonstrate the potential benefits for RTK when combining the next generation GNSSs, as compared to using the systems separately. With long baseline we refer to the necessity to model the slant ionospheric delays by the ionosphere-float strategy. The (wet) Zenith Tropospheric Delay (ZTD) will be estimated as well. The ionosphere-float model implies that the slant ionospheric delays are assumed completely unknown. We will focus on overlapping frequencies between the systems. The advantage with overlapping frequencies is that the redundancy of the model can be maximized if the inter-system biases (ISBs) can be calibrated. This also allows for a common pivot satellite between the systems when parameterizing the double-differenced integer ambiguities. It will be shown that with the ionosphere-float model at least two overlapping frequencies between the systems are required to benefit from calibration of ISBs. The GNSS real data is collected in Perth Australia, a country where the multi-system satellite visibility is almost at a global maximum. The single-baseline RTK performance is evaluated by a formal and empirical analysis, consisting of ambiguity dilution of precision (ADOP), bootstrapped success rates and positioning precisions. It will be shown that the combination of the four systems provides for shorter ambiguity/positioning convergence times, improved integer ambiguity resolution and positioning performance over the single-, dual- and triple-systems.

INTRODUCTION

Precise positioning applications using the next generation Global Navigation Satellite Systems (GNSSs) have the potential to improve, provided that a combination of the systems is used. This since already today (2014) we have 32 American Global Positioning System (GPS), 14 Chinese BeiDou Navigation Satellite System (BDS), 4 European Galileo, and 1 Quasi-Zenith Satellite System (QZSS) satellites available for positioning. In addition the Russian GLONASS is available with around 24 satellites [1]. But in contrary to the other Code Division Multiple Access (CDMA) systems, the majority part of the GLONASS satellites are based on the Frequency Division Multiple Access (FDMA) and will thus not be used in this contribution.

The 32 GPS satellites transmit on the L1, L2 frequencies, and currently six satellites also on the modernized L5 frequency (Table 1). BDS is an Asia-Pacific regional

constellation, but will by 2020 become global and consist of 5 Geostationary Earth Orbit (GEO), 3 Inclined Geo-Synchronous Orbit (IGSO) and 27 Medium Earth Orbit (MEO) satellites [2]. BDS broadcasts signals on the B1, B2 and B3 frequencies (Table 1). Since 2005 and 2008, respectively, two Galileo In-Orbit Validation Element (GIOVE) satellites have been in orbit, but they are currently not available for positioning. However at this moment (2014) four Galileo In-Orbit Validation (IOV) MEO satellites are available (since 2012) for positioning [3], which broadcast signals at the E1, E5a, E5b and E6 frequencies (Table 1). The E6 frequency will only be received as part of Galileos commercial service. Galileo is intended to be a global constellation once it reaches its full constellation by 2020, with 27 MEO and 3 spare satellites. The QZSS is to be developed as an Asia-Pacific regional constellation. QZSS uses the same orbital period as a traditional equatorial geostationary orbit and a large orbital inclination, as to enable Japanese users to receive QZSS signals from a high elevation angle at all times. The QZSS broadcasts signals on the L1, L2 and L5 frequencies (Table 1). One Highly-inclined Elliptical Orbit (HEO) satellite 'MICHIBIKI' (or 'QZS-1') is currently in orbit, and was launched in September 2010. By 2018 the QZSS constellation is planned to consist of 3 GEO and 4 HEO satellites [4].

Some first BDS-only results based on real data were presented in, e.g., [5] for BDS single point positioning (SPP) and single-baseline real-time kinematic (RTK) positioning based on an initial BDS constellation of 3 GEO and 3 IGSO satellites. Some first BDS-only RTK positioning results outside of China can be found in [6]. Single-baseline RTK contributions using the current regional BDS constellation that consists of 14 BDS satellites can be found in, e.g., [7–10]. Positioning results for combined GIOVE+GPS single-baseline RTK were presented in [11]. It was shown that the code/phase inter-system biases (ISBs) on the overlapping frequencies between those systems are zero for similar receiver types, but exist for mixed receiver types. The nature and behavior of the GIOVE-GPS ISBs were also investigated in [12], and for IOV-GPS ISBs in [13, 14], which confirmed the results of [11].

Table 1: GPS, BDS, Galileo and QZSS signals

Sat. system	Band	Freq. [MHz]	Wavelength [cm]
BDS	**B1**	1561.098	19.20
BDS/Galileo	**B2**/E5b	1207.140	24.83
BDS	B3	1268.520	23.63
QZSS, GPS/Galileo	**L1/E1**	1575.42	19.03
QZSS, GPS	**L2**	1227.60	24.42
QZSS, GPS/**Galileo**	L5/**E5a**	1176.45	25.48

Table 1 shows the different frequencies available from the four satellite systems analyzed, and the frequencies used in this contribution are marked in bold. With long single-baseline RTK we refer to the necessity to model the ionospheric and tropospheric delays, here referred to as the ionosphere-float and Zenith Tropospheric Delay (ZTD) float models. As a consequence of having the ionosphere-float model, the number of overlapping frequencies required between the systems, to allow for strengthening of the model when the ISBs are calibrated, are at least *two*. This since the code ISBs are only estimable on the second frequency and beyond. This will be further elaborated on in the description of the single-baseline RTK functional models. Since the GPS L5 frequency is currently (2014) only available from six satellites, we restrict our analysis to the L1, L2 frequencies. That leaves us with two possible overlapping frequencies for GPS with the other systems in Table 1, namely the L1,L2 frequencies of QZSS. In other words, the calibration of ISBs to strengthen the RTK model is herein only possible between QZSS-GPS. In [11, 15], however, it was shown for the ionosphere-fixed case (short baselines) when combining GPS, BDS, Galileo and QZSS, that *one* overlapping frequency between the systems is sufficient to strengthen the RTK model accordingly.

The ground tracks of BDS, Galileo and QZSS as seen from a station in Perth, Australia are depicted in Figure 1. As the signals on the E5a frequency could not be tracked at this time for the E11 satellite, three out of four available Galileo IOV satellites will be used in this contribution.

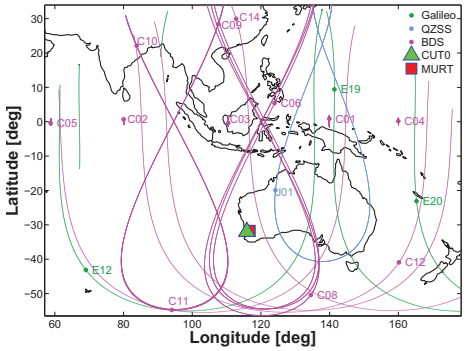

Figure 1: BDS (*magenta*), Galileo (*green*) and QZSS (*cyan*) constellation (February 19, 2014) with satellites location depicted as a *dot* at 15:15 local Perth time for a cut-off angle of 10°. Perth stations CUT0 and MURT are depicted as well

This contribution is organized as follows. First we present the ionosphere-float, ZTD-float single-baseline RTK functional, stochastic and dynamic models used. Two functional models will be given, one referred

to as the "ISBs-float" model where the ISBs are parameterized as unknowns, and one when they are assumed calibrated, the "ISBs-fixed" model. This follows by a description of the GNSS data and the dynamic/stochastic model settings used. A formal analysis of the GPS+BDS+Galileo+QZSS single-baseline RTK performance is then conducted, involving ambiguity dilution of precision (ADOP), bootstrapped success rate, ambiguity convergence times, and the positioning performance. An empirical analysis of the ambiguity/positioning convergence times and positioning performance is then presented based on real data. Emphasis will be on analyzing the combined four-system RTK models, and comparisons will be made to GPS and other possible combinations of the systems. We end this contribution with some conclusions.

SINGLE-BASELINE RTK FUNCTIONAL, STOCHASTIC AND DYNAMIC MODELS

In this Section we will present the ionosphere-float, ZTD-float functional and stochastic models used for the combination of GPS+BDS+Galileo+QZSS. The inter-system biases (ISBs) float and fixed models will be presented, and it will be assumed that all frequencies overlap between the systems for notational convenience. We end the section by describing the redundancy and dynamic model used in the Kalman filter.

ISBs-float, ionosphere-float functional model

In the following observation equations it is assumed that $r = 1,2$ receivers track, at the same instance, the satellites $s_G = 1_G, \ldots, m_G$ and $s_* = 1_*, \ldots, m_*$ on *overlapping* frequencies $j = 1, \ldots, f$, where m_G, m_*, f is the number of satellites and frequencies respectively. The symbol G is for GPS and $*$ for BDS (B), Galileo (E) or QZSS (Q). The time stamps will be omitted in the equations for brevity, and external products are used for satellite orbits. Since between-receiver single-differences (SDs) are performed on the observation equations, the satellite delays common to both receivers are eliminated. The receiver clock is furthermore shared among the systems, and the time-offsets, e.g., GPS-to-Galileo-time-offset (GGTO), are also eliminated by the SDs. The baseline is assumed to be of a length of at most a few hundred kilometers, thus any remaining satellite orbit errors can be assumed negligible.

The system of observation equations is however not of full-rank after the SDs. The number of rank deficiencies is equal to the number of linear combinations of the column vectors of the design matrix that produces the zero vector. These rank deficiencies can be eliminated through S-system theory [16, 17], which implies null-space identification, S-basis constraining and interpretation of the estimable parameters. The number of rank deficiencies and the S-basis choice for the ionosphere-float and ISBs-float model is given by Table 2. The "ISBs-float" model (1) implies that the ISBs are parameterized as unknowns.

Table 2: Single-epoch single-baseline RTK ionosphere-float, ZTD-float and ISBs-float S-basis choice, and # of rank deficiencies for GPS (G) and $*$ (B for BDS, E for Galileo and Q for QZSS), assuming *overlapping* frequencies between systems

Model	S-basis choice	# of rank defects
Iono-float (ISBs-float)	$\Delta x_1, \tau_1, dt_{1,,}$ $d^G_{2,1}, d^G_{2,2}, \iota^{s_G}_1, d^G_{1,j}, \delta^G_{1,j}, z^{1_G}_{2,j}, z^{s_G}_{1,j}$ $d^*_{2,1}, \iota^{s_*}_1, d^*_{1,j}, \delta^*_{1,j}, z^{1_*}_{2,j}, z^{s_*}_{1,j}$	$4+1+$ $+2+m_G+3f+fm_G+$ $+1+m_B+3f+fm_B$ $+1+m_E+3f+fm_E$ $+1+m_Q+3f+fm_Q$

We have in Table 2 the S-basis consisting of the pivot receiver $r = 1$ coordinates (Δx_1), ZTD (τ_1) and clock (dt_1) that solve for $4+1$ rank defects. This follows by 2 rank deficiencies solved by the GPS (G) hardware (HW) code delays on frequencies $j = 1,2$ for $r = 2$ $\left(d^G_{2,1}, d^G_{2,2}\right)$, and $m_G + m_*$ rank defects solved by the ionospheric delays for $r = 1$, all satellites and all systems $\left(\iota^{s_G}_1, \iota^{s_*}_1\right)$. Then there are $3 \cdot 1$ (3 corresponds to 3 additional systems to GPS) rank defects solved by the HW code delays on $j = 1$, $r = 2$ for system $*$ $\left(d^*_{2,1}\right)$, and $2f + 3 \cdot 2f$ rank defects solved by the HW code $\left(d^G_{1,j}, d^*_{1,j}\right)$ and phase delays $\left(\delta^G_{1,j}, \delta^*_{1,j}\right)$, on $j = 1, \ldots, f$, $r = 1$ and for all systems. Further rank defects of size $f + 3 \cdot f$ are solved by fixing the ambiguities on $j = 1, \ldots, f$, $r = 2$ and for the pivot satellites $s_G = 1_G$, $s_* = 1_*$ $\left(z^{1_G}_{2,j}, z^{1_*}_{2,j}\right)$, and a rank deficiency of size $fm_G + fm_*$ that are solved by fixing the ambiguities on $j = 1, \ldots, f$, $r = 1$, for all satellites and systems $\left(z^{s_G}_{1,j}, z^{s_*}_{1,j}\right)$. For more details about the rank defects solved by the S-basis in Table 2, see Appendix A.

The ISBs-float full-rank system of observation equations for the combination of GPS+BDS+Galileo+QZSS on overlapping frequencies $j = 1, \ldots, f$ then read,

$$
\begin{aligned}
p^{s_G}_{12,j} &= -g_2^{s_G T}\Delta x_{12} + m_2^{s_G}\tilde{\tau}_{12} + d\tilde{t}_{12} + \tilde{d}^G_{12,j} + \mu_j \tilde{\iota}^{s_G}_{12} \\
\phi^{s_G}_{12,j} &= -g_2^{s_G T}\Delta x_{12} + m_2^{s_G}\tilde{\tau}_{12} + d\tilde{t}_{12} + \tilde{\delta}^G_{12,j} - \mu_j \tilde{\iota}^{s_G}_{12} + \\
&+ \lambda_j \tilde{z}^{1_G s_G}_{12,j} \\
p^{s_*}_{12,j} &= -g_2^{s_* T}\Delta x_{12} + m_2^{s_*}\tilde{\tau}_{12} + d\tilde{t}_{12} + \tilde{d}^G_{12,j} + \tilde{d}^{G*}_{12,j} + \mu_j \tilde{\iota}^{s_*}_{12} \\
\phi^{s_*}_{12,j} &= -g_2^{s_* T}\Delta x_{12} + m_2^{s_*}\tilde{\tau}_{12} + d\tilde{t}_{12} + \tilde{\delta}^G_{12,j} + \tilde{\delta}^{G*}_{12,j} - \mu_j \tilde{\iota}^{s_*}_{12} + \\
&+ \lambda_j \tilde{z}^{1_* s_*}_{12,j}
\end{aligned}
\tag{1}
$$

The estimable unknown parameters, denoted with a 'tilde', are given in Table 3, and the notations used in (1) are further described in Table 4.

Table 3: Estimable unknown parameters and their interpretation for the ISBs-float model (1)

Notation and interpretation	Estimable parameter	Conditions
$\Delta x_{12} = \Delta x_2 - \Delta x_1$	relative receiver coordinates	$r \geq 2$
$\tilde{\tau}_{12} = \tau_2 - \tau_1$	relative (residual) wet ZTD	$r \geq 2$
$d\tilde{t}_{12} = dt_{12} + \frac{\mu_2}{\mu_2-\mu_1} d^G_{12,1} - \frac{\mu_1}{\mu_2-\mu_1} d^G_{12,2}$	relative receiver clock with GPS HW code delays on $j = 1,2$	$r \geq 2$
$\tilde{d}^G_{12,j} = d^G_{12,j} - \frac{\mu_2-\mu_j}{\mu_2-\mu_1} d^G_{12,1} + \frac{\mu_1-\mu_j}{\mu_2-\mu_1} d^G_{12,2}$	relative GPS receiver HW code delays	$j \geq 3, r \geq 2$
$\tilde{\delta}^G_{12,j} = \delta^G_{12,j} - \frac{\mu_2+\mu_j}{\mu_2-\mu_1} d^G_{12,1} + \frac{\mu_1+\mu_j}{\mu_2-\mu_1} d^G_{12,2} + \lambda_j z^{1_G}_{12,j}$	relative GPS receiver HW phase delays	$j \geq 1, r \geq 2$
$\tilde{d}^{G*}_{12,j} = d^{G*}_{12,j} - \frac{\mu_j}{\mu_1} d^{G*}_{12,1}$	relative code inter-system bias (ISB)	$j \geq 2, r \geq 2$
$\tilde{\delta}^{G*}_{12,j} = \delta^{G*}_{12,j} + \frac{\mu_j}{\mu_1} d^{G*}_{12,1} + \lambda_j z^{1_G 1_*}_{12,j}$	relative phase ISB biased by inter-system double-differenced ambiguities	$j \geq 1, r \geq 2$
$\tilde{\iota}^{s_G}_{12} = \iota^{s_G}_{12} + \frac{1}{\mu_2-\mu_1}\left(d^G_{12,2} - d^G_{12,1}\right)$	relative GPS slant ionospheric delays	$r \geq 2, s \geq 1$
$\tilde{\iota}^{s_*}_{12} = \iota^{s_*}_{12} + \frac{1}{\mu_2-\mu_1}\left(d^G_{12,2} - d^G_{12,1}\right) + \frac{1}{\mu_1} d^{G*}_{12,1}$	relative system $*$ slant ionospheric delays biased by GPS differential code biases (DCBs) and code ISB on $j = 1$	$r \geq 2, s \geq 1$
$z^{1_G s_G}_{12,j} = z^{s_G}_{12,j} - z^{1_G}_{12,j}$	GPS double-differenced integer ambiguities	$j \geq 1, r \geq 2, s \geq 2$
$z^{1_* s_*}_{12,j} = z^{s_*}_{12,j} - z^{1_*}_{12,j}$	system * double-differenced integer ambiguities	$j \geq 1, r \geq 2, s \geq 2$

Table 4: Definition of commonly used symbols

Symbol	Definition	Description
r	$= 1,2$	receivers used
s	$= 1,\ldots,m$	tracked satellites
$G,*$		systems, G for GPS, $*$ equals B BDS, E Galileo and Q QZSS
j	$= 1,\ldots,f$	tracked overlapping frequencies
$(\cdot)_{12}$	$= (\cdot)_2 - (\cdot)_1$	between-receiver SDs
$(\cdot)^{1s}$	$= (\cdot)^s - (\cdot)^1$	between-satellite SDs
$p^j_{12,j}, \phi^j_{12,j}$		SD code and phase observables respectively
g^T_r	$= \frac{(x^s - x_r)^T}{\|x^s - x_r\|}$	line-of-sight unit vector
$(.)^T$		transpose of vector
$\|.\|$		norm
x^s, x_r		vector of satellite and receiver coordinates respectively
λ_j		wavelength for frequency j
m^s_r		mapping function to get a station-wise (wet) ZTD
μ_j	$= f_1^2/f_j^2$	conversion of ionospheric delay from GPS $L1$ to frequency j
$d^{G*}_{12,j}$	$= d^*_{12,j} - d^G_{12,j}$	code inter-system bias (ISB)
$\delta^{G*}_{12,j}$	$= \delta^*_{12,j} - \delta^G_{12,j}$	phase ISB

The Saastamoinen troposphere model has been used to correct the dry part of the troposphere [18] in (1), and we refrain from carrying through SD random observation noise and other systematic effects such as multipath for notational convenience. The shared parameters between GPS and system $*$ in (1) are the receiver coordinates Δx_{12}, relative ZTD $\tilde{\tau}_{12}$, receiver clock $d\tilde{t}_{12}$ and the GPS HW code/phase delays $\tilde{d}^G_{12,j}, \tilde{\delta}^G_{12,j}$. The estimable double-differenced integer ambiguities in Table 3 are differenced with respect to the ambiguities of a system-specific pivot satellite, respectively. Note that the observation equations in (1) has equivalent redundancy to taking a traditional system-specific receiver clock model as the code ISBs are estimable on the second frequency and beyond, whereas the GPS receiver HW code delays are only estimable for $j \geq 3$. Thus the code ISBs play the role of the additional unknowns instead of additional receiver clocks.

One can also make use of a re-parameterization of the code/phase ISBs and GPS receiver HW code/phase delays to get system-specific HW delays for non-overlapping frequencies,

$$\begin{aligned}
&\tilde{d}^*_{12,j_*} = \tilde{d}^{G*}_{12,j} + \tilde{d}^G_{12,j} = \\
&= d^*_{12,j} - \frac{\mu_2-\mu_j}{\mu_2-\mu_1} d^G_{12,1} + \frac{\mu_1-\mu_j}{\mu_2-\mu_1} d^G_{12,2} - \frac{\mu_j}{\mu_1} d^{G*}_{12,1} \\
&\tilde{\delta}^*_{12,j_*} = \tilde{\delta}^{G*}_{12,j} + \tilde{\delta}^G_{12,j} = \\
&= \delta^*_{12,j} - \frac{\mu_2+\mu_j}{\mu_2-\mu_1} d^G_{12,1} + \frac{\mu_1+\mu_j}{\mu_2-\mu_1} d^G_{12,2} + \frac{\mu_j}{\mu_1} d^{G*}_{12,1} + \lambda_j z^{1_*}_{12,j}
\end{aligned} \tag{2}$$

i.e. the delays are now relative to the GPS HW code delays on frequency $j = 1,2$, and the receiver HW phase delays are now solely biased by its own system-specific pivot satellite 1 ambiguity (compare to the phase ISBs in Table 3). More importantly this re-parameterization (2) shows that the full-rank ISBs-float model in (1) is equivalent, in terms of redundancy, to the one where one would choose to parameterize system-specific HW delays.

ISBs-fixed, ionosphere-float functional model

In the previous section it was shown that if we for overlapping frequencies parameterize the ISBs, it does not strengthen the model as compared to a traditional model with system-specific receiver clocks/HW delays. We will refer to the following model (7) as the "ISBs-fixed model", where the ISBs will be assumed completely known (deterministic) and thus subtracted from the code/phase observations.

The code and phase ISBs in the observation equations (1) to be corrected, denoted with a 'tilde', are defined as,

$$\begin{aligned}
\tilde{d}^{G*}_{12,j} &= d^{G*}_{12,j} - \frac{\mu_j}{\mu_1} d^{G*}_{12,1} \\
\tilde{\delta}^{G*}_{12,j} &= \delta^{G*}_{12,j} + \frac{\mu_j}{\mu_1} d^{G*}_{12,1} + \lambda_j z^{1_G 1_*}_{12,j}
\end{aligned} \tag{3}$$

respectively (see Table 3). Now consider the case where we want to determine these ISBs using another data set. The code and phase ISB corrections, denoted with 'overline', can be given as [11],

$$\begin{aligned}\overline{d}^{G*}_{12,j} &= \tilde{d}^{G*}_{12,j}\\ \overline{\delta}^{G*}_{12,j} &= \delta^{G*}_{12,j} + \frac{\mu_j}{\mu_1} d^{G*}_{12,1} + \lambda_j a_{12,j}\end{aligned} \tag{4}$$

respectively, where $a_{12,j} \in \mathbb{Z}$ is an integer ambiguity that in principle is different from $z^{1_G 1_*}_{12,j}$ in the observations that we would like to correct (1). This since the observations used to determine the corrections in (4) are also different. The phase ISBs corrections can thus be re-written as,

$$\overline{\delta}^{G*}_{12,j} = \tilde{\delta}^{G*}_{12,j} - \lambda_j \left(z^{1_G 1_*}_{12,j} - a_{12,j} \right) \tag{5}$$

Consequently when the correction (5) is applied to the phase observations of system * in (1), the ambiguity difference in (5) will be lumped into the ambiguities $\tilde{z}^{1_* s_*}_{12,j}$ (Table 3) as,

$$\tilde{z}^{1_G s_*}_{12,j} = z^{1_* s_*}_{12,j} + \left(z^{1_G 1_*}_{12,j} - a_{12,j} \right) = z^{1_G s_*}_{12,j} - a_{12,j} \tag{6}$$

i.e. the ambiguity of system $*$ (6) is now differenced with respect to the pivot satellite of GPS minus the integer ambiguity $a_{12,j}$. It is thus not problematic that there is an additional ambiguity $a_{12,j}$ since it is only the combined integer ambiguity term $\tilde{z}^{1_G s_*}_{12,j}$ that is estimable.

The full-rank ISBs-fixed system of observation equations on overlapping frequencies $j = 1, \ldots, f$ can be expressed as follows,

$$\begin{aligned}
p^{s_G}_{12,j} &= -g_2^{s_G T} \Delta x_{12} + m_2^{s_G} \tilde{\tau}_{12} + d\tilde{t}_{12} + \tilde{d}^{G}_{12,j} + \mu_j \tilde{\imath}^{s_G}_{12}\\
\phi^{s_G}_{12,j} &= -g_2^{s_G T} \Delta x_{12} + m_2^{s_G} \tilde{\tau}_{12} + d\tilde{t}_{12} + \tilde{\delta}^{G}_{12,j} - \mu_j \tilde{\imath}^{s_G}_{12} +\\
&+ \lambda_j \tilde{z}^{1_G s_G}_{12,j}\\
p^{s_*}_{12,j} - \overline{d}^{G*}_{12,j} &= -g_2^{s_* T} \Delta x_{12} + m_2^{s_*} \tilde{\tau}_{12} + d\tilde{t}_{12} + \tilde{d}^{G}_{12,j} + \mu_j \tilde{\imath}^{s_*}_{12}\\
\phi^{s_*}_{12,j} - \overline{\delta}^{G*}_{12,j} &= -g_2^{s_* T} \Delta x_{12} + m_2^{s_*} \tilde{\tau}_{12} + d\tilde{t}_{12} + \tilde{\delta}^{G}_{12,j} - \mu_j \tilde{\imath}^{s_*}_{12} +\\
&+ \lambda_j \tilde{z}^{1_G s_*}_{12,j}
\end{aligned} \tag{7}$$

where the ambiguity $\tilde{z}^{1_G s_*}_{12,j}$ for system $*$ (6) will also be estimable for $s_* = 1_*$. This gives us f additional unknowns for each system added to GPS as compared to the ISBs-float model. However, since we also have a-priori corrections for the code ($f-1$) and phase ISBs (f) that gives us $2f-1$ corrections, the redundancy of the model (7) increases with $f-1$ for each additional system to GPS as compared to the ISBs-float model (1). In other words at least $f \geq 2$ overlapping frequencies for each additional system is required to strengthen the ionosphere-float model accordingly. This is further clarified by Table 5. Note finally that the other unknown parameters in (7) and their interpretations are given in Table 3, and that the GPS observation equations are still equivalent to the ISBs-float case (1).

Stochastic models

The variance-covariance (VCV) matrix of the code and phase observables in SD form, for a single-system and the ionosphere-float model can be given as,

$$Q^*_{yy} = \text{blkdiag}\left(C^*_p, C^*_\phi\right) \otimes \left(D_n^T D_n \otimes W^{-1}_{m_*}\right) \tag{8}$$

where 'blkdiag' denoted a blockdiagonal matrix, $\otimes$ is the Kronecker product [19], and the a priori variance factors of the code and phase observables are given in the sub-matrices $C^*_p = \text{diag}(\sigma^2_{p,1_*}, \ldots, \sigma^2_{p,f_*})$ and $C^*_\phi = \text{diag}(\sigma^2_{\phi,1_*}, \ldots, \sigma^2_{\phi,f_*})$ respectively. We assume no cross-correlation between code and phase nor between frequencies, otherwise the non-diagonal elements of C^*_p and C^*_ϕ would be populated accordingly with covariances between the observables. We also have D_n^T with -1 for the pivot receiver and a 1 for the second receiver that is the between-receivers SD operator [20], and $W^{-1}_{m_*}$ contains the elevation-dependent weighting function as given by [21]. The combined GPS+BDS+Galileo+QZSS ionosphere-float (1), (7) VCV-matrix reads,

$$Q_{yy} = \text{blkdiag}\left(Q^G_{yy}, Q^B_{yy}, Q^E_{yy}, Q^Q_{yy}\right) \tag{9}$$

Redundancy and solvability condition

The redundancy is computed as the number of observations minus the number of estimable unknowns, which is given in Table 5 for the instantaneous single-baseline RTK ISBs-float (1) and ISBs-fixed (7) models respectively. In the last column a "solvability condition" is given, which is the number of satellites required to solve the models. Note that in this contribution we will have two systems that have the required number of overlapping frequencies $f \geq 2$ that allow for strengthening of the ISBs-fixed model in comparison to the ISBs-float counterpart, namely GPS/QZSS L1,L2 (Table 1). Thus when presenting the ISBs-fixed redundancy/solvability condition in Table 5, we take only these ISBs into account. The single-system model in Table 5 can be found in (1) and (7) for GPS, whereas BDS, Galileo and QZSS only models will have a similar definition of the unknowns. The dynamic model used for the Kalman filter to strengthen the instantaneous RTK models is briefly explained in the following section.

For the single-system in Table 5 we have: 3 receiver coordinates, 1 ZTD, 1 receiver clock, $(f_* - 2)$ receiver HW code delays, f_* receiver HW phase delays, m_* slant ionospheric delays and $f_*(m_* - 1)$ double-differenced integer ambiguities to estimate. More importantly the required number of frequencies and satellites to solve the

Table 5: Single-baseline instantaneous RTK: number of observations, unknowns, redundancy and solvability condition for the (ionosphere-float, ZTD-float) ISBs-float (1) and ISBs-fixed (7) models on overlapping frequencies of L1,L2 GPS/QZSS

Model	# of observations	# of unknowns	Redundancy	Solvability condition
				$f \geq 2$
Single-system (1)	$2f_s m_s$	$3+f_s+m_s+f_s m_s$	$f_s(m_s-1)-m_s-3$	$m_s \geq 5$
4-system ISBs-float (1)	$2fm_G+$ $+2f_B m_B$ $+2f_E m_E$ $+2fm_Q$	$f+m_G+fm_G+$ $+f_B+m_B+f_B m_B$ $+f_E+m_E+f_E m_E$ $+f+m_Q+fm_Q$	$f(m_G-1)-m_G+$ $+f_B(m_B-1)-m_B$ $+f_E(m_E-1)-m_E$ $+f(m_Q-1)-m_Q$	m_G+m_B+ $+m_E+m_Q \geq 8$
4-system ISBs-fixed (7) (QZSS-GPS)	$2fm_G+$ $+2f_B m_B$ $+2f_E m_E$ $+2fm_Q$	$1+f+m_G+fm_G+$ $+f_B+m_B+f_B m_B$ $+f_E+m_E+f_E m_E$ $+m_Q+fm_Q$	$f(m_G-1)-m_G+$ $+f_B(m_B-1)-m_B$ $+f_E(m_E-1)-m_E$ $+fm_Q-m_Q-1$	m_G+m_B+ $+m_E+m_Q \geq 7$

single-system model is two and five respectively. For the 4-system ISBs-float and ISBs-fixed models eight and seven satellites are required respectively. In other words the positioning flexibility is increased in comparison to the single-system, where two satellites for each system would be sufficient to solve the model in the ISBs-float case (minus one satellite for the ISBs-fixed counterpart). Whereas having the same number of satellites using any of the systems separately would not be sufficient to solve the model.

We give in Figure 2 the number of satellites (top) and the redundancies in Table 5 (bottom) for a station in Perth (Muresk), as a function over almost 8 hours of real data. This is given between 13:16:30-21:11:30 local Perth time, February 19, 2014, and for an elevation cut-off angle of 20°. This time period is selected since the satellites from all four systems are visible at the same time instances, see also Figure 1. The higher cut-off angle is depicted as to illustrate an urban canyon like environment or when any existing low-elevation multipath is preferably avoided. The redundancies are depicted as to illustrate the reliability of the dual-frequency GPS (blue), GPS+Galileo+QZSS (green) and four-system (black) RTK models. The ISBs-float models are denoted with dashed lines, whereas the ISBs-fixed models are given by full-lines. Reliability is a measure of the ability of the system to test the observations for modeling errors, and zero redundancy gives infinitely poor reliability as testing is then not possible.

Figure 2 illustrates that GPS-only have zero redundancy 14.2% of all epochs, whereas when Galileo and QZSS is added the redundancy is larger than zero throughout the whole time-period. One can also observe that the GPS+Galileo+QZSS ISBs-float model (dashed green line) is equivalent to GPS (blue line) when one Galileo and one QZSS satellite is visible, respectively. However for the ISBs-fixed counterpart (full green line) the redundancy immediately increases with one ($f-1$, with $f=2$), since the L1,L2 QZSS-GPS code/phase ISBs

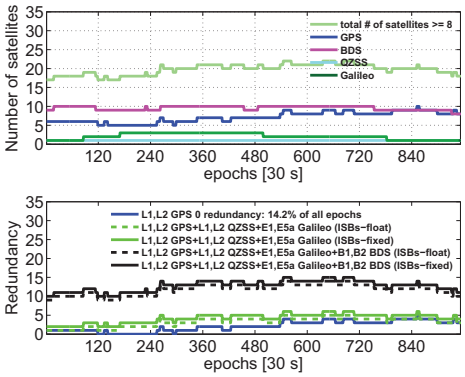

Figure 2: Satellite visibility for GPS, BDS, Galileo and QZSS with 20° cut-off angle in Perth (Muresk), 8 hours in February 19, 2014. At *top* we have the total # of satellites for GPS, BDS, Galileo and QZSS. At *bottom* the redundancies (Table 5) for the instantaneous single-baseline RTK models are given as well. The L1,L2 QZSS-GPS code/phase ISBs are assumed fixed for the ISBs-fixed (7) models

are then fixed. A significant increase in redundancy can also be seen when BDS is added to the three other systems (black lines). This thus indicates the possibility of using higher satellite elevation cut-off angles when combining the systems and still retain sufficient redundancy.

Dynamic model for the Kalman filter

The unknowns in the observation equations for the ionosphere-float models (1) and (7) can be estimated using an extended Kalman filter with a dynamic model. The state vector for which a dynamic model will be used can be expressed in vector form for epoch $i=1,\ldots,k$ as follows,

$$x(i) = \left[\tilde{\tau}_{12}(i), z_{12}^{T}(i)\right]^{T} \tag{10}$$

where we have $\tilde{\tau}_{12}(i)$ the relative (wet) ZTD and the ambiguities in a vector $z_{12}(i) = \left[z_{12}^{GT}(i), z_{12}^{BT}(i), z_{12}^{ET}(i), z_{12}^{QT}(i)\right]^{T}$, with $z_{12}^{*}(i) = \left[z_{12,1_*}^{*T}(i),\ldots,z_{12,f_*}^{*T}(i)\right]^{T}$ and $z_{12,j_*}^{*}(i) = \left[\tilde{z}_{12,j_*}^{1_*2_*}(i),\ldots,\tilde{z}_{12,j_*}^{1_*m_*}(i)\right]^{T}$. For the ISBs-fixed model (7) the ambiguities for QZSS will read $z_{12,j}^{Q}(i) = \left[\tilde{z}_{12,j}^{1_G1_Q}(i),\ldots,\tilde{z}_{12,j}^{1_Gm_Q}(i)\right]^{T}$, i.e. f additional ambiguities (relative to the GPS pivot satellite 1_G) need to be included in the state vector in comparison to the ISBs-float model.

The dynamic model used for the extended Kalman filter follows as,

$$\begin{aligned} x_k &= \Phi_{k|k-1} x_{k-1} + d_k, \\ D(d_k) &= Q_{d_k} \end{aligned} \tag{11}$$

where x_k is the state vector at epoch k connected with the state vector at previous epoch $k-1$, x_{k-1}, by $\Phi_{k|k-1}$ the transition matrix, d_k the process noise with zero mean and VCV-matrix Q_{d_k}, where $D(\cdot)$ is the dispersion. All other parameters (Table 3) are assumed unlinked in time.

The transition matrix for the ISBs-float model is then defined as,

$$\Phi_{k|k-1} = \text{blkdiag}(1, I_n) \tag{12}$$

where 1 corresponds to the ZTD and I_n is the identity matrix of the size $n = f(m_G - 1) + f_B(m_B - 1) + f_E(m_E - 1) + f(m_Q - 1)$ corresponding to the ambiguities. Note that n has an additional size of $+f$ for the ISBs-fixed model (corresponding to the QZSS satellite 1 ambiguities). The process noise VCV-matrix follows as,

$$Q_{d_k} = \text{blkdiag}(\Delta t \cdot q_{\dot{\tau}}, 0_n) \tag{13}$$

where Δt is the time-interval between adjacent epochs, $q_{\dot{\tau}}$ is the spectral density for the relative (wet) ZTD that is modeled as random walk, and 0_n is the zero matrix of dimension n used for the ambiguities since they are treated as time-constant. The dynamic model settings are given in Table 6.

GNSS DATA COLLECTION

The Trimble NetR9 receivers/antennas used to form the baseline analyzed in this contribution is depicted in Figure 1 and Figure 3, with a baseline length of 80 km. The station CUT0 is located in Bentley, Perth and at the Curtin University campus, whereas station MURT is located in Muresk. The number of satellites for a GPS+BDS+Galileo+QZSS system and an elevation cut-off angle of 10° is presented in Figure 3 as well. We see more than double the number of satellites for the combination of the four systems in comparison to GPS as a stand alone system. In this contribution we will focus on the data in February 19, 2014 between 12:34:30-21:40:30 local Perth time, i.e. for a time span of 9 hours and 6 minutes, as all four satellite systems are then continuously tracked over the day for the 10° cut-off angle.

For all of the following analyzes we use a measurement interval of 30 s. The Detection, Identification and Adaptation (DIA) procedure is utilized to detect, identify and adapt for outliers [22], and the LAMBDA method [23] for integer ambiguity resolution. Note that the dual-frequencies of GPS/QZSS L1,L2, Galileo E1,E5a and

(a) CUT0 (*left*) (Bentley) and MURT (*right*) (Muresk) antennas

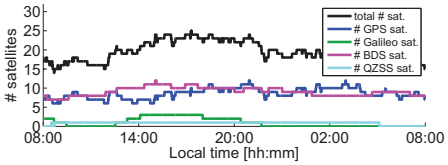

(b) # of satellites for a cut-off angle of 10° in Muresk, and period of analysis 12:34:30-21:40:30 local Perth time

Figure 3: GNSS Trimble NetR9 receivers/antennas for single-baseline RTK in February 19, 2014

BDS B1,B2 will be analyzed throughout this contribution (Table 1), and that the E5a frequency of the E11 satellite could not be tracked for this data set thus three out of four Galileo IOV satellites will be used.

DYNAMIC/STOCHASTIC MODEL SETTINGS

In Table 6 we present the functional models that are investigated and the corresponding dynamic model settings (13) for the Kalman filter solutions. The ambiguities are treated as time-constant and a random walk process noise of 2 mm/$\sqrt{\text{hour}}$ is used for the relative ZTD prediction. This process noise was predicted similarly to Chapter 3.4.3 in [24], as determined from data independent from the data analyzed in this contribution.

Table 6: Dynamic model settings (13). Epoch-by-epoch (ebe) denotes no linkage in time when estimating the parameters

Model	Mode	Dynamic model	Process noise
Iono-float (1),(7)	Single-epoch	All parameters: ebe	-
Iono-float (1),(7)	Kalman filter	Ambiguities time-constant:	0
		Relative ZTD random walk:	2 mm/$\sqrt{\text{hour}}$
		Other parameters: ebe	-

The stochastic model (9) settings are depicted in Table 7. This is based on the exponential elevation weighting function by [21] and zenith-referenced a priori code and phase standard deviations (STDs) respectively for undifferenced observations.

Table 7: Zenith-referenced code and phase STDs (9) for the Trimble NetR9 receivers in Figure 3

System	Frequency	Code $\sigma_{P_{j,*}}$ [cm]	Phase $\sigma_{\Phi_{j,*}}$ [mm]
GPS	L1	30	2
	L2	30	2
BDS	B1	30	2
	B2	30	2
Galileo	E1	30	2
	E5a	30	2
QZSS	L1	30	2
	L2	30	2

FORMAL ANALYSIS OF FOUR-SYSTEM SINGLE-BASELINE RTK MODEL

In this section a formal analysis will be conducted for the four-system ionosphere-float, ZTD-float RTK models. For the following computations we only need the design matrix and VCV-matrix of the observations, i.e. real data is not necessary.

Ambiguity Dilution of Precision

Ambiguity Dilution of Precision (ADOP) is a scalar measure of the model strength for ambiguity resolution and was introduced in [20]. The ADOP is defined as,

$$\text{ADOP} = \sqrt{|Q_{\hat{a}\hat{a}}|^{\frac{1}{n}}} \text{ [cycle]} \tag{14}$$

where $Q_{\hat{a}\hat{a}}$ is the variance-covariance (VCV) matrix of the float ambiguities, $|\cdot|$ is the determinant, and n is the dimension of the ambiguity vector. The ADOP measures the intrinsic precision of the ambiguities, and is also a measure of the volume of the ambiguity confidence ellipsoid [25]. As a rule-of-thumb, an ADOP of 0.12 cycle can be taken as indication of successful ambiguity resolution as it corresponds to an ambiguity success rate (SR) larger than 99.9% [26]. Our earlier studies [8],[27] show that successful instantaneous single-frequency L1+B1 GPS+BDS RTK is feasible for baselines of a few km when the relative atmospheric delays are negligible, whereas dual-frequencies were needed when using any of the systems separately. For a medium baseline length of 17 km, when the uncertainty of the relative ionospheric pseudo-observables can be modeled as a function of the baseline length [28], we found that successful instantaneous dual-frequency L1,L2+B1,B2 GPS+BDS RTK is possible.

To investigate whether successful *instantaneous* dual-frequency ionosphere-float RTK is feasible as well, Figure 4 depicts the single-epoch ADOP time-series in blue for 9 hours of data (see Figure 3). The ADOPs for GPS are given at top, GPS+Galileo+QZSS ISBs-float and ISBs-fixed at the second and third rows respectively, and at the fourth row the four-system ISBs-fixed model is depicted as well. An elevation cut-off angle of 10° is used, and an ADOP-level of 0.12 cycle is indicated by a dashed red line. The number of satellites is depicted at bottom.

The single-epoch ADOP time-series of GPS in Figure 4 is larger than when combining GPS with Galileo, QZSS and/or BDS due to the fewer number of satellites. One can also see for the GPS+Galileo+QZSS ISBs-float model that once two Galileo satellites are tracked, just before 120 epochs have passed, the ADOPs decrease in comparison to GPS. The single QZSS satellite is furthermore only contributing throughout the whole time period when the L1,L2 QZSS-GPS code/phase ISBs are assumed fixed. This is also shown by the redundancies in Table 5 and in Figure 2. More importantly the combination of all four-systems provides for the smallest ADOPs with a mean value of 0.42 cycles, which is, however, larger than the 0.12 cycle level we need to expect successful ambiguity resolution.

Thus we will now investigate the ADOPs using a *Kalman filter* with the dynamic model in Table 6, and the ADOPs are depicted in Figure 5 corresponding to the time-period in Figure 4. The GPS model is given at top and the four-system model at bottom. Note that the ADOP is computed based on the Kalman filtered VCV-matrix of the ambiguities, thus as more time passes the stronger the model becomes (since the float ambiguities become more precise). A zoom-in is therefore given for the first 60 epochs (30 minutes) to illustrate the time to reach the 0.12 cycle level.

The combined GPS+Galileo+QZSS+BDS system in Figure 5 is seen to converge to ADOP levels of 0.12 cycles much quicker than GPS due to larger redundancy of the model. This is a very promising first indication that faster successful ambiguity resolution is possible for the ionosphere-float model when combining the systems.

Positioning

In the following positioning results we will investigate full ambiguity resolution for Kalman filter based dual-frequency GPS+BDS+Galileo+QZSS RTK models. In the previous section it was namely concluded that a Kalman filter is needed for the ionosphere-float model to achieve successful ambiguity resolution.

A formal bootstrapped success rate (SR) criterion will be used to decide when to fix the ambiguities, to allow the float ambiguities to converge. The formal bootstrapped SR is an accurate lower bound to the integer least-squares (ILS) SR [29, 30], and follows as,

$$P[\check{z}_{IB} = z] = \prod_{i=1}^{n} \left[2\Phi\left(\frac{1}{2\sigma_{\check{z}_{i|I}}} \right) - 1 \right] \geq P_0 \tag{15}$$

where $P[\check{z}_{IB} = z]$ denotes the probability of correct integer estimation of the integer bootstrapped estimator $\check{z}_{IB}$,

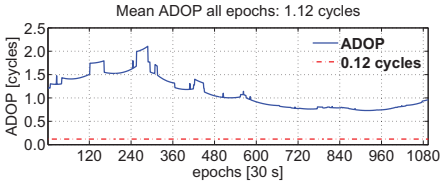

(a) L1,L2 GPS

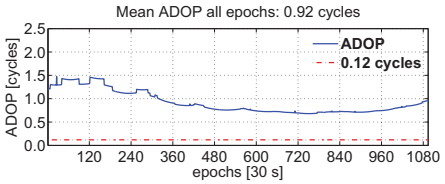

(b) ISBs-float: L1,L2+E1,E5a+L1,L2 GPS+Galileo+QZSS

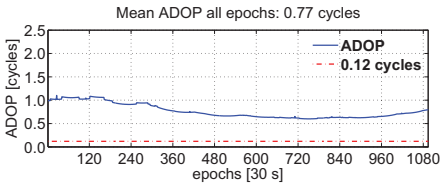

(c) ISBs-fixed: L1,L2+E1,E5a+L1,L2 GPS+Galileo+QZSS

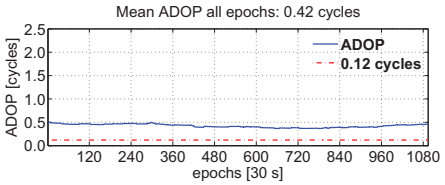

(d) ISBs-fixed: L1,L2+E1,E5a+L1,L2+B1,B2 GPS+Galileo+QZSS+ +BDS

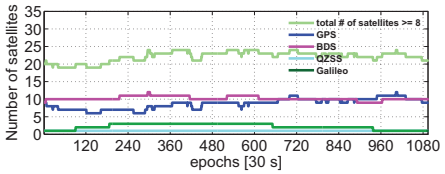

(e) Number of satellites

Figure 4: Ionosphere-float, ZTD-float *single-epoch* ADOP time-series (*blue*) for single-baseline RTK, using 10° cut-off angle. *Light green* represents the total # of satellites. February 19, 2014, and 9 hours of data. The L1,L2 QZSS-GPS code/phase ISBs are assumed fixed for the ISBs-fixed models

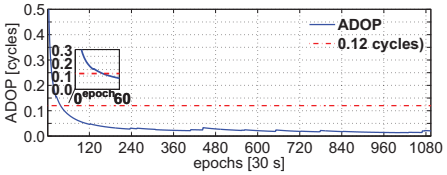

(a) L1,L2 GPS

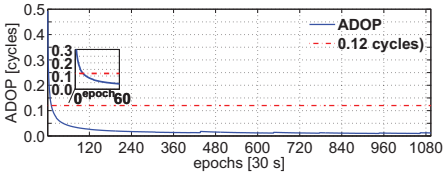

(b) ISBs-fixed: L1,L2+E1,E5a+L1,L2+B1,B2 GPS+Galileo+QZSS+ +BDS

Figure 5: Ionosphere-float, ZTD-float *Kalman filter* ADOP time-series (*blue*) for single-baseline RTK, using 10° cut-off angle. February 19, 2014, and 9 hours of data. The L1,L2 QZSS-GPS code/phase ISBs are assumed fixed

$\Phi(x) = \int_{-\infty}^{x} \frac{1}{\sqrt{2\pi}} exp\left(-\frac{1}{2}v^2\right) dv$ is the cumulative normal distribution, $\sigma_{\hat{z}_{i|I}}$ with $i = 1,\ldots,n, I = 1,\ldots,(i-1)$ is the conditional STDs of the decorrelated ambiguities and P_0 a user-defined bootstrapped success criterion. A value of $P_0 = 99.9\%$ will be used, and if it is not fulfilled we take the float solution instead. This criterion (15) will also decide upon when to include newly risen satellites. The satellites are considered to rise when they exceed the user-defined elevation cut-off angle of e.g. 10°.

In the following we will compute the average ambiguity convergence time, also referred to as time to first fix (TTFF), to fulfill the criterion in (15). The Kalman filter is initialized at the first-epoch, and for each additional epoch included in the filter the bootstrapped SR criterion in (15) is used. Once it reaches 99.9% we obtain the TTFF. Then we re-initialize the filter at the second epoch and the whole procedure is repeated again. The times given in Table 8 are the mean of all these TTFFs over approximately 9 hours in February 19, 2014 for a 10° elevation cut-off angle. The corresponding expected positioning precision in terms of formal STDs in local North (N), East (E), Up (U) of the float and fixed dual-frequency ionosphere-float, ZTD-float solutions are also given in Table 8. The results are given for GPS, GPS+Galileo+QZSS and GPS+Galileo+QZSS+BDS.

Since the ambiguities are treated as time-constant parameters and random walk process noise is used for the relative ZTD in the dynamic model (Table 6), the

Table 8: Formal STDs for ionosphere-float, ZTD-float dual-frequency RTK and a cut-off angle of 10°, ambiguity float/fixed solutions in North, East and Up. The L1,L2 QZSS-GPS code/phase ISBs are assumed fixed (and within brackets the ISBs-float case is given as well). The STDs are mean values of all formal STDs based on re-initializations of the Kalman filter during 9 hours in February 19, 2014 and when the bootstrapped SR in (15) of 99.9% is fulfilled. In the last column the corresponding # of epochs needed is depicted as well.

System/frequency	**Formal STDs float/fixed**			**# epochs**
	N [cm]	E [cm]	U [cm]	[30 s]
L1,L2 GPS	5.9/1.0	14.9/0.9	15.3/2.5	41
L1,L2+E1,E5a+L1,L2	5.8/0.8	11.8/0.7	14.0/2.2	32
GPS+Galileo+QZSS	(5.8/0.9)	(13.2/0.8)	(13.9/2.4)	36
L1,L2+E1,E5a+L1,L2+B1,B2	4.5/0.6	8.0/0.5	10.4/1.7	28
GPS+Galileo+QZSS+BDS	(4.5/0.6)	(8.3/0.5)	(10.4/1.8)	29

ambiguity-float position STDs improve with respect to time. Table 8 illustrates the improvement when going from ambiguity-float to ambiguity-fixed solutions as well as the improvement which a combination of the systems brings. The improvement in ambiguity-float East and Up components are more significant than in the North component. More importantly the combined systems provides for the ambiguity-float precisions in Table 8 earlier (smaller TTFF) than for GPS. Thus when combining the systems we can potentially achieve *faster* ambiguity-float precisions at the dm-level and *faster* availability to ambiguity-fixed positioning precisions at the mm-cm-level. This is particularly true when the L1,L2 QZSS-GPS code/phase ISBs are assumed fixed and/or when BDS is added to the three other systems. We will elaborate more on this in the empirical positioning section. One can finally note in Table 8 that the East component experience larger improvements in comparison to the North and Up components when integer-ambiguity resolution is applied, which is consistent with e.g. [31, 32].

EMPIRICAL ANALYSIS OF FOUR-SYSTEM SINGLE-BASELINE RTK MODEL

In this section real data will be analyzed as to verify the formal claims in the previous sections. The L1,L2 QZSS-GPS code/phase ISBs will safely be taken as zero throughout the analysis for the similar Trimble NetR9 receiver types in Figure 3, see e.g. [15]. The BDS GEO ambiguities are kept as float parameters in the following sections due to site-specific multipath effects in combination with the satellites being stationary [33]. Thus any systematic effects from the GEO satellites cannot be significantly mitigated over time and was shown to negatively affect the ambiguity resolution performance.

Positioning

Table 9 provides the empirical float and correctly fixed ionosphere-float, ZTD-float positioning precision for dual-frequency GPS, GPS+Galileo+QZSS and GPS+Galileo+QZSS+BDS. This is given for a 10° elevation cut-off angle, and the STDs were obtained by comparing the estimated positions to precise benchmark coordinates. These computations are based on the re-initializations of the Kalman filter and the bootstrapped SR criterion (15), similar to the formal STDs in Table 8. The correctly fixed solutions are determined from a reference set of ambiguities. The reference ambiguities were estimated by using a dual-frequency four-system model, with fixed precise benchmark coordinates, making use of a 10° elevation cut-off angle and treating the ambiguities as time-constant over the entire observation time span.

Table 9: Empirical STDs for ionosphere-float, ZTD-float dual-frequency RTK and a cut-off angle of 10°, ambiguity float/correctly fixed solutions in North, East and Up. The L1,L2 QZSS-GPS code/phase ISBs are assumed fixed (and within brackets the ISBs-float case is given as well). The STDs are based on re-initializations of the Kalman filter during 9 hours in February 19, 2014 and when the bootstrapped SR criterion in (15) of 99.9% is fulfilled. In the last column the corresponding # of epochs needed is depicted as well.

System/frequency	**Empirical STDs float/correctly fixed**			**# epochs**
	N [cm]	E [cm]	U [cm]	[30 s]
L1,L2 GPS	7.3/0.9	21.4/0.9	21.6/3.3	41
L1,L2+E1,E5a+L1,L2	8.3/0.7	14.7/0.8	23.5/3.0	32
GPS+Galileo+QZSS	(8.1/0.8)	(17.7/0.8)	(20.7/3.6)	36
L1,L2+E1,E5a+L1,L2+B1,B2	7.2/0.6	11.0/0.6	15.5/2.9	28
GPS+Galileo+QZSS+BDS	(7.6/0.6)	(12.2/0.6)	(15.4/3.2)	29

The empirical STDs in Table 9 are in overall in good agreement with the formal precisions given in Table 8, with somewhat more optimistic formal STDs. Note however that the precision of e.g. the GPS+Galileo+QZSS ISBs-fixed ambiguity-float North and Up components now are slightly larger than for GPS. However this model also has a smaller TTFF of 32 epochs vs 41 epochs for GPS which explain these differences, since the ambiguity-float STDs improve with respect to time. Moreover when combining the systems we can thus reliably fix the ambiguities faster and allow for the precise mm-cm-level positioning at an earlier stage. This will be further elaborated on in the following two sections.

Positioning for higher elevation cut-off angles

When combining the systems higher than customary elevation cut-off angles can be allowed [8], which can be of particular benefit in urban canyon environments or when low elevation-multipath might be present. We depict a snapshot example in Figure 6 for the dual-frequency

ionosphere-float, ZTD-float horizontal (N,E) and vertical (U) RTK positioning and a cut-off angle of 20°, based on real data. The correctly fixed solutions are depicted as green, the wrongly fixed as red, and the float solutions as gray. Under each positioning model we also present the corresponding bootstrapped SR time-series and the total number of satellites as light green. As to illustrate two different convergence time periods the Kalman filter is re-initialized after 300 epochs (150 minutes). The number of Galileo (dark green), QZSS (cyan) and BDS (magenta) satellites is depicted as well.

Figure 6 illustrates that the time until the ambiguities can be fixed for the combined systems is much shorter in comparison to GPS. It is namely sufficient with 53 epochs as TTFF (using the criterion in (15)) at the first initialization for GPS+Galileo+QZSS (ISBs-fixed) to allow for precise ambiguity-fixed positioning availability, whereas for GPS 82 epochs are required. The improvement for this 3-system model is even more significant when all three Galileo satellites are visible, where the TTFF improve to 25 epochs for the second (re-)initialization in comparison to GPS that requires 75 epochs. When BDS is added the TTFFs are further improved, particularly in comparison to the first initialization of the other two models with a TTFF of 17 epochs.

In Figure 7 we give the correctly fixed formal STDs corresponding to the Up-components in Figure 6. Since we use an elevation-weighting strategy in our stochastic model, the formal STDs mostly depend on the satellite geometry and the number of satellites. This illustrates that the performance of ambiguity resolution and positioning do not always go hand-in-hand [8, 20]. For instance when looking into the largest GPS-only Up-component positioning errors in Figure 6 that corresponds to the period of largest formal STDs in Figure 7, we can still correctly fix our ambiguities because of the bootstrapped SRs larger than 99.9%. Fortunately however we have improvements both in formal STDs in Figure 7 and the Up-component positioning errors in Figure 6, particularly between $1-600$ epochs, when combining the systems with GPS. The best improvement can be seen when BDS is added to the systems. Note finally in Figure 6 that there are a few epochs where the solutions are incorrectly fixed (red) for the 4-system model at an early stage of the first initialization, due to a BDS satellite that rises at an elevation angle of 20° in combination with site-specific multipath effects. However as a few number of epochs passes the solutions become correctly fixed (green) as predicted by the bootstrapped SR.

On the ambiguity-float RTK positioning convergence time and the improvement by ambiguity-fixing

The purpose of integer ambiguity resolution is to improve the other parameters by the integer constrains, such as the receiver positions. However once the float ambiguities have converged to deterministic values, the ambiguity-float RTK positioning solutions can also start to take advantage of the very precise phase measurements and integer ambiguity resolution makes less sense. In other words, the faster we are allowed to do integer ambiguity resolution the more will the positions improve.

The ambiguity-float positioning convergence time criterion that we will use follows as,

$$\sqrt{|Q_{\hat{N}\hat{E}\hat{U}}|}^{\frac{1}{3}} \leq \sqrt{|Q_{\check{N}\check{E}\check{U}}|}^{\frac{1}{3}} + 0.01 \quad [\text{m}] \qquad (16)$$

where $Q_{\hat{N}\hat{E}\hat{U}}$ is the formal ambiguity-float position VCV-matrix, 3 is the dimension of the N, E and U positioning vector, and $Q_{\check{N}\check{E}\check{U}}$ is the formal ambiguity-fixed position VCV-matrix. Compare this expression to the ADOP in (14). As the determinant is used, the covariances between the coordinate components are taken into account as well. When the ambiguity-float geometric average on the left hand side of (16) is 1 cm from the ambiguity-fixed geometric average on the right, we can determine the convergence time. Thus we consider here the float and fixed solution of similar quality if they differ less than 1 cm.

We depict the ambiguity-float (gray) and ambiguity-fixed (magenta) geometric averages (16) in Figure 8 corresponding to the positioning results for the 20° cut-off angle in Figure 6. The ambiguity-fixed geometric averages start at the same time-instances as the bootstrapped SR reaches 99.9% in Figure 6, and these times are depicted by vertical dotted blue lines. The ambiguity-float positioning convergence times as determined by (16) are depicted by vertical dashed black lines and at bottom of each RTK model we give the ADOPs as well. Note that the Kalman filter is re-initialized after 300 epochs.

Figure 8 shows that the GPS-only (top) ionosphere-float model in this case has up to 83 minutes of ambiguity-float positioning convergence time (second (re-)initialization). The corresponding time for the GPS+Galileo+QZSS model (middle) is 45.5 minutes, and 32 minutes for the 4-systems (bottom). Moreover the ADOPs are below the 0.12 cycle level once the ambiguity-fixed positioning precisions become available for each model. Most importantly we can conclude from Figure 8 that GPS-only ionosphere-float RTK positioning cannot benefit as significantly from fast reliable integer ambiguity resolution as the corresponding three and 4-system models. This since we have an ambiguity-float geometric average at the level of 5 cm for GPS-only once the bootstrapped SR is 99.9%, whereas the combined 3-

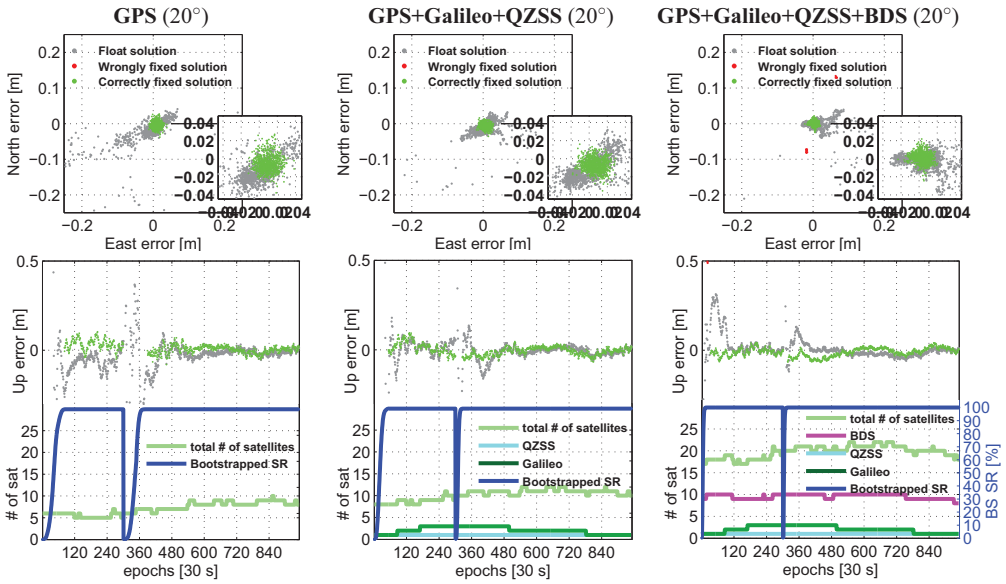

Figure 6: *Top* ionosphere-float, ZTD-float L1,L2 GPS (*left*), ISBs-fixed L1,L2+E1,E5a+L1,L2 GPS+Galileo+QZSS (*middle*) and ISBs-fixed L1,L2+E1,E5a+L1,L2+B1,B2 GPS+Galileo+QZSS+BDS (*right*) RTK for a 20° cut-off angle. At *bottom* the total # of satellites is depicted as *light green* and the bootstrapped SR time-series in *blue*. The Kalman filter is re-initialized after 300 epochs. The # of epochs to reach bootstrapped SR in (15) of 99.9% (2:nd initialization in brackets): 41 (37.5) min for GPS (*left*), 26.5 (12.5) min for GPS+Galileo+QZSS (*middle*), and 8.5 (8) min for GPS+Galileo+QZSS+BDS (*right*)

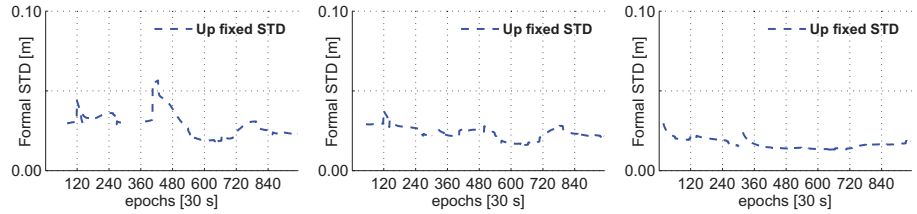

(a) GPS (b) GPS+Galileo+QZSS (c) GPS+Galileo+QZSS+BDS

Figure 7: Dual-frequency ionosphere-float, ZTD-float Up correctly fixed formal STDs corresponding to Figure 6, cut-off angle of 20°

systems have a value close to 10 cm (for the second (re-) initialization), and the 4-system model values even up to 15 cm. Thus we can conclude from Figure 8 that when using an elevation cut-off angle of 20° the combination of the four systems can provide for faster reliable ambiguity-fixed positioning precisions, shorter ambiguity-float positioning convergence times, and give larger precision improvements when going from ambiguity-float to ambiguity-fixed positioning, all in comparison to GPS and the 3-system model.

CONCLUSIONS

In this contribution we studied the combination of dual-frequency L1,L2 GPS, E1,E5a Galileo, L1,L2 QZSS and B1,B2 BDS for long single-baseline RTK. With long baseline we refer to the necessity to model the slant ionospheric delays by the ionosphere-float strategy as well as the residual (wet) Zenith Tropospheric Delay (ZTD). The code/phase inter-system biases (ISBs) were moreover fixed when possible to maximize the redundancy of the models, which also allows for a common pivot satellite between the systems. The analysis was based on real GNSS data collected in Perth, Australia. We can summarize our main findings and conclusions as follows.

Inter-system biases

We illustrated that at least two overlapping frequencies are needed for calibration of ISBs to increase the redundancy for the ionosphere-float model and in comparison to when the ISBs are estimated. This since the code ISBs

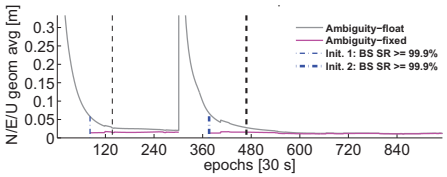

(a) L1,L2 GPS

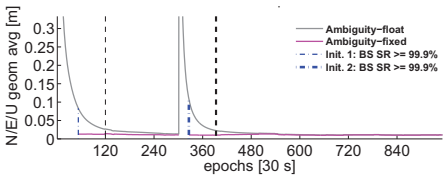

(b) ISBs-fixed: L1,L2+E1,E5a+L1,L2 GPS+Galileo+QZSS

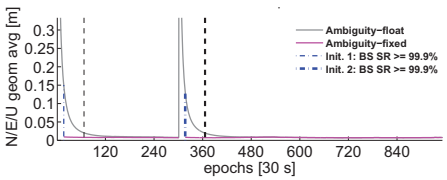

(c) ISBs-fixed: L1,L2+E1,E5a+L1,L2+B1,B2 GPS+Galileo+QZSS+ +BDS

Figure 8: Ambiguity-float positioning convergence time for a 20° cut-off angle, where the dual-frequency ionosphere-float, ZTD-float and ambiguity-float (gray) and ambiguity-fixed (magenta) geometric averages (16) are given, and at bottom the corresponding ADOP time-series. The convergence times are given as (2:nd initialization in brackets): 68.5 (83) min for GPS, 60 (45.5) min for GPS+Galileo+QZSS, and 33.5 (32) min for GPS+Galileo+QZSS+BDS

are only estimable on the second frequency and beyond. The code/phase ISBs of L1,L2 QZSS-GPS were safely neglected throughout this study as similar Trimble NetR9 receiver types were used [15].

Instantaneous RTK and time to first fix

As to investigate whether instantaneous RTK is possible for the ionosphere-float model, a formal ambiguity dilution of precision (ADOP) analysis was conducted. It was predicted that successful instantaneous single-baseline RTK is not possible, and a Kalman filter with a dynamic model is thus needed. The time to first fix (TTFF) was computed for the different combinations of the four systems, as the accumulated time necessary in the Kalman filter to reach an integer bootstrapped success rate of 99.9%. The combination of Galileo and QZSS with GPS provided for smaller TTFFs in comparison to using GPS separately. The improvements were more significant when the code/phase ISBs were fixed and/or when BDS was added to the three systems. The conclusion is therefore that calibration of ISBs is particularly important in environments with obstructed satellite visibility, as each satellite added to GPS can then contribute to the solution as if it was an additional satellite from the same system.

Ambiguity-float vs ambiguity-fixed positioning precisions

The empirical positioning precisions as determined by comparing the estimated positions to precise benchmark coordinates were shown to be in overall good agreement with the formal precisions, with the somewhat more optimistic formal precisions. Most importantly it was shown that the combined systems allow for faster ambiguity-float positioning precisions at the dm-level, shorter TTFFs and thus faster availability of ambiguity-fixed position precisions at the mm-cm level. This was particularly true when all four systems were combined and the code/phase ISBs were fixed. When looking into the positioning results for an elevation cut-off angle of 20°, it could moreover be concluded that the combined systems provide for improved receiver-satellite geometry and thus more precise positioning in comparison to GPS-only RTK.

Position-precision improvement by ambiguity-fixing

The faster we can reliably fix the ambiguities the more will the integer constrains improve the receiver positions. It was found for the elevation cut-off angle of 20° that the 4-system model allows for larger precision improvements when going from ambiguity-float to ambiguity-fixed RTK positioning, and as compared to the GPS and GPS+Galileo+QZSS models.

ACKNOWLEDGEMENTS

This work has been executed in the framework of the Positioning Program Project 1.01 "New carrier phase processing strategies for achieving precise and reliable multi-satellite, multi-frequency GNSS/RNSS positioning in Australia" of the Cooperative Research Centre for Spatial Information (CRC-SI). The second author is the recipient of an Australian Research Council (ARC) Federation Fellowship (project number FF0883188). All this support is gratefully acknowledged.

REFERENCES

[1] Mirgorodskaya, T., "GLONASS government policy, status and modernization plans," in *Proceedings of international global navigation satellite systems (IGNSS) symposium*, (Golden Coast), 16-18 July, 2013.

[2] CSNO, "BeiDou Navigation Satellite System Signal In Space Interface Control Document by China Satellite Navigation Office (CSNO). Open service signal B1I (Version 1.0)," tech. rep., December 2012. 77 pages., 2012.

[3] ESA, "Galileo In-Orbit Validation," in *Fact sheet by European space agency (ESA)*, 2013.

[4] J. Boyd, "Japans Plan for Centimeter-Resolution GPS," in *IEEE Spectrum, news*, 23 April 2014.

[5] C. Shi, Q. Zhao, Z. Hu, and J. Liu, "Precise relative positioning using real tracking data from COMPASS GEO and IGSO satellites," *GPS Solutions*, vol. 17, no. 1, pp. 103–119, 2013. doi:10.1007/s10291-012-0264-x.

[6] O. Montenbruck, A. Hauschild, P. Steigenberger, U. Hugentobler, P. J. G. Teunissen, and S. Nakamura, "Initial assessment of the COMPASS/BeiDou-2 regional navigation satellite system," *GPS Solutions*, vol. 17, no. 2, pp. 211–222, 2013.

[7] R. Odolinski, P. J. G. Teunissen, and D. Odijk, "Quality analysis of a combined COMPASS/BeiDou-2 and GPS RTK positioning model," in *International Global Navigation Satellite Systems Society IGNSS symposium*, (Golden Coast), 16-18 July 2013.

[8] P. J. G. Teunissen, R. Odolinski, and D. Odijk, "Instantaneous BeiDou+GPS RTK positioning with high cut-off elevation angles," *J. Geodesy*, vol. 88, no. 4, pp. 335–350, 2014. doi:10.1007/s00190-013-0686-4.

[9] Y. Yang, J. Li, A. Wang, J. Xu, H. He, H. Guo, J. Shen, and X. Dai, "Preliminary assessment of the navigation and positioning performance of BeiDou regional navigation satellite system," *Science China, Earth Sciences*, vol. 57, no. 1, pp. 144–152, 2014.

[10] N. Nadarajah, P. J. G. Teunissen, J.-M. Sleewaegen, and O. Montenbruck, "The mixed-receiver BeiDou inter-satellite-type bias and its impact on RTK positioning," *GPS Solutions*, 2014. doi:10.1007/s10291-014-0392-6.

[11] D. Odijk and P. J. G. Teunissen, "Characterization of between-receiver GPS-Galileo inter-system biases and their effect on mixed ambiguity resolution," *GPS Solutions*, vol. 17, no. 4, pp. 521–533, 2013.

[12] O. Montenbruck, A. Hauschild, and U. Hessels, "Characterization of GPS/GIOVE sensor stations in the CONGO network," *GPS Solutions*, vol. 15, no. 3, pp. 193–205, 2011.

[13] T. Melgard, J. Tegedor, K. de Jong, D. Lapucha, and G. Lachapelle, "Interchangeable integration of GPS and Galileo by using a common system clock in PPP," in *Proceedings of ION GNSS*, (Nashville, TN), pp. 1198–1206, 16–20 September 2013.

[14] D. Odijk and P. J. G. Teunissen, "Estimation of differential inter-system biases between the overlapping frequencies of GPS, Galileo, BeiDou and QZSS," in *4th International Colloquium Scientific and Fundamental Aspects of the Galileo Programme*, (Prague, Czech Republic), 4–6 December 2013.

[15] R. Odolinski, P. J. G. Teunissen, and D. Odijk, "Combined BDS, Galileo, QZSS and GPS single-frequency RTK," *GPS Solutions*, 2014. doi:10.1007/s10291-014-0376-6.

[16] P. J. G. Teunissen, "Generalized inverses, adjustment, the datum problem and S-transformations," *In: Grafarend EW, Sanso F (eds) Optimization of geodetic networks*, 1985. Springer, Berlin, pp 11-55.

[17] P. J. G. Teunissen, D. Odijk, and B. Zhang, "PPP-RTK: Results of CORS network-based PPP with integer ambiguity resolution," *J Aeronaut, Astronaut and Aviat, Ser A*, vol. 42, no. 4, pp. 223–230, 2010.

[18] J. Saastamoinen, "Contributions to the theory of atmospheric refraction," *Bull Geod*, vol. 105, no. 1, pp. 279–298, 1972.

[19] C. R. Rao, *Linear statistical inference and its applications, 2nd edition*. Wiley, New York, 1973.

[20] P. J. G. Teunissen, "A canonical theory for short GPS baselines. Part I: The baseline precision, Part II: The ambiguity precision and correlation, Part III: The geometry of the ambiguity search space, Part IV: Precision versus reliability," *J. Geodesy*, vol. 71(6):320-336, 71(7):389-401, 71(8):486-501, 71(9):513-525, 1997.

[21] H. J. Euler and C. G. Goad, "On optimal filtering of GPS dual frequency observations without using orbit information," *Bull Geod*, vol. 65, pp. 130–143, 1991.

[22] P. J. G. Teunissen, "An integrity and quality control procedure for use in multi sensor integration," in *Proc of ION GPS*, (CO), pp. 513–522, September 1990. Also in: Vol VII of GPS Red Book Ser: Integr syst, ION Navig, 2012.

[23] P. J. G. Teunissen, "The least squares ambiguity decorrelation adjustment: a method for fast GPS integer estimation," *J. Geodesy*, vol. 70, pp. 65–82, 1995.

[24] Schüler, T., "On ground-based GPS tropospheric delay estimation," *Ph.D. dissertation, Universität der Bundeswehr, Munich, Germany*, 2001. 364 pages.

[25] P. J. G. Teunissen, P. de Jonge, and C. Tiberius, "The volume of the GPS ambiguity search space and its relevance for integer ambiguity resolution," in *"Proc ION GPS*, vol. 9, pp. 889–898, 1996.

[26] D. Odijk and P. Teunissen, "ADOP in closed form for a hierarchy of multi-frequency single-baseline GNSS models," *J. Geodesy*, vol. 82, pp. 473–492, 2008.

[27] R. Odolinski, P. J. G. Teunissen, and D. Odijk, "An analysis of combined COMPASS/BeiDou-2 and GPS single- and multiple-frequency RTK positioning.," in *ION Pacific PNT, Honolulu, HI, USA*, pp. 69–90, 2013.

[28] B. Schaffrin and Y. Bock, "A unified scheme for processing GPS dual-band phase observations," *Bull Geod 62*, pp. 142–160, 1988.

[29] P. J. G. Teunissen, "Success probability of integer GPS ambiguity rounding and bootstrapping.," *J. Geodesy*, vol. 72, pp. 606–612, 1998.

[30] P. J. G. Teunissen, "An optimality property of the integer least-squares estimator.," *J. Geodesy*, vol. 73, pp. 587–593, 1999.

[31] W. Melbourne, "The case for ranging in GPS-based geodetic systems," in *Proceedings of 1st International Symposium on Precise Positioning with the Global Positioning System*, (Rockville, MD, USA), pp. 373–386, 1985.

[32] G. Blewitt, "Carrier phase ambiguity resolution for the global positioning system applied to geodetic baselines up to 2000 km," *J Geophys Res 94(B8)*, pp. 10187–10203, 1989.

[33] G. Wang, K. d. Jong, Q. Zhao, Z. Hu, and J. Guo, "Multipath analysis of code measurements for BeiDou geostationary satellites," *GPS Solutions*, 2014. doi:10.1007/s10291-014-0374-8.

A DESCRIPTION OF THE ISBS-FLOAT RANK DEFICIENCIES

For the derivations in Table 2 we have assumed the baseline length to be of less than a few hundred kilometers, consequently giving line-of-sight unit vectors and mapping functions for the Zenith Tropospheric Delay (ZTD) that are similar between the receivers. This makes rise to 4 rank deficiencies that are solved by fixing the pivot receiver 1 coordinates (x_1) and ZTD (τ_1). This follows by 1 rank defect between the columns of the receiver clocks that is eliminated by fixing the pivot receiver 1 clock (dt_1), and 1 rank defect between the columns of the receiver 2 clock and GPS hardware (HW) code/phase delays that is solved by fixing the GPS HW code delay on the first frequency for receiver 2 $\left(d^G_{2,1}\right)$. Then we have 1 rank defect between the columns of the receiver clock, HW code/phase delays/ISBs and GPS ionospheric delays, which is solved by fixing the GPS HW code delay on the second frequency for receiver 2 $\left(d^G_{2,2}\right)$. The $m_G + m_*$ rank defects between the columns of the slant ionospheric delays are solved by fixing the pivot receiver 1 corresponding delays $\left(\imath^{s_G}_1, \imath^{s_*}_1\right)$.

Then there are $3 \cdot 1$ (3 corresponds to three additional systems to GPS) rank defects between the HW code/phase delays/ISBs and ionosphere of system $*$, which are solved by fixing the HW code delay on the first frequency for the second receiver for that system $\left(d^*_{2,1}\right)$. Following that the rank deficiencies between columns of the HW code/phase delays/ISBs of size $2f + 3 \cdot 2f$ are solved by fixing pivot receiver 1 HW code/phase delays on all frequencies for all systems $\left(d^G_{1,j}, \delta^G_{1,j}, d^*_{1,j}, \delta^*_{1,j}\right)$. Then we have the rank deficiency of size $f + 3 \cdot f$ between the columns of the HW phase delays/ISBs and ambiguities, which are solved by fixing the ambiguities on all frequencies for receiver 2 and the pivot satellite 1 for all systems $\left(z^{1_G}_{2,j}, z^{1_*}_{2,j}\right)$. Finally we have a rank deficiency of size $fm_G + fm_*$ between the columns of the ambiguities that are solved by fixing the ambiguities on all frequencies, for all satellites, the pivot receiver 1 and all systems $\left(z^{s_G}_{1,j}, z^{s_*}_{1,j}\right)$.

9 BDS+GPS RTK POSITIONING FOR SHORT, MEDIUM AND LONG BASELINES

This chapter is covered by the following publication:

Odolinski R, Teunissen PJG, Odijk D (2014e) Combined GPS+BDS for short to long baseline RTK positioning. Measurement Science and Technology (see Appendix C for proof of acceptance)

Noname manuscript No.
(will be inserted by the editor)

Combined GPS+BDS for short to long baseline RTK positioning

Robert Odolinski · Peter J.G. Teunissen · Dennis Odijk

Received: date / Accepted: date

Abstract The BeiDou Navigation Satellite System (BDS) has become fully operational in the Asia-Pacific region, and it is of importance to evaluate what BDS brings when combined with the Global Positioning System (GPS). In this contribution we will look at the short, medium and long single-baseline real-time kinematic (RTK) positioning performance. Short baseline refers to when the distance between the two receivers is of at most a few kilometers so that the relative slant ionospheric and tropospheric delays can be assumed absent, whereas with medium baseline we refer to when the uncertainty of these ionospheric delays can reliably be modeled as a function of the baseline length. With long baseline we refer to the necessity to parameterize the ionospheric delays and (wet) Zenith Tropospheric Delay (ZTD) as completely unknown. The GNSS real data is collected in Perth Australia. It will be shown that combining the two systems allows for the use of higher than customary elevation cut-off angles. This can be of particular benefit in environments with restricted satellite visibility such as in open pit mines or urban canyons.

Keywords Multi-Global Navigation Satellite System (GNSS), real-time kinematic (RTK), LAMBDA, success rate, elevation cut-off angle

R. Odolinski, P.J.G. Teunissen, D. Odijk
GNSS Research Centre, Curtin University, Australia
E-mail: Robert.Odolinski@curtin.edu.au

P.J.G. Teunissen
Mathematical Geodesy and Positioning, Delft University of Technology, The Netherlands

1 Introduction

The next-generation Global Navigation Satellite Systems (GNSSs) consist today (2014) of 32 satellites available for positioning from the American Global Positioning System (GPS), and 14 satellites from the Asia-Pacific regional constellation of the Chinese BeiDou Navigation Satellite System (BDS). This in addition to the 24 Russian GLONASS, four European Galileo, one Japaneze Quasi-Zenith Satellite System (QZSS), and two satellites from the Indian Regional Navigation Satellite System (IRNSS). BDS will by 2020 become global and consist of 5 Geostationary Earth Orbit (GEO), 3 Inclined Geo-Synchronous Orbit (IGSO) and 27 Medium Earth Orbit (MEO) satellites (CSNO, 2013). In this contribution we will focus on single-baseline real-time kinematic (RTK) results when using the current BDS constellation in combination with GPS, of which both are based on the Code Division Multiple Access (CDMA) technique.

In Grelier et al (2007) the BDS signals were described, and in Chen et al (2009); Yang et al (2011) the positional dilution of precision (PDOP) for the combination of GPS and BDS was analysed. Simulation of BDS ambiguity resolution performance can be found in, e.g., Cao et al (2008). Real data results were presented in, e.g., Shi et al (2013) for BDS single point positioning (SPP) and single-baseline RTK based on an initial BDS constellation of 6 satellites. Some BDS positioning results outside of China can be found in, e.g., Montenbruck et al (2013); Odolinski et al (2013); Teunissen et al (2014), and Nadarajah et al (2014).

The models considered for single-baseline RTK in this contribution will be of the short, medium and long baseline types. The short baseline refers to the case when the baseline length is of at most a few km so

that the relative tropospheric and slant ionospheric delays can be assumed negligible, the ionosphere-fixed model. The medium baseline refers to when the uncertainty of the relative slant ionospheric delays can reliably be modeled as a function of the baseline length, the ionosphere-weighted model (Odijk, 2002; Teunissen, 1998b). With long baseline we refer to the necessity to model the slant ionospheric delays by the so called ionosphere-float model, as well as the (wet) Zenith Tropospheric Delay (ZTD).

The GPS and BDS signals are depicted in Table 1. None of the frequencies overlap between GPS and BDS, however if the frequencies would overlap calibration of the inter-system biases (ISBs) would allow for further strengthening of the model (Odijk and Teunissen, 2013; Odolinski et al, 2014a,b). In this contribution the B1, B2 frequencies of BDS will be used, and for GPS L1,L2, since the L5 frequency is currently (2014) only transmitted by six GPS satellites.

Table 1 GPS and BDS signals

Sat. system	Band	Freq. [MHz]	Wavelength [cm]
BDS	B1	1561.098	19.20
	B2	1207.140	24.83
	B3	1268.520	23.63
GPS	L1	1575.42	19.03
	L2	1227.60	24.42
	L5	1176.45	25.48

In Section 2 we present the ionosphere-float, ionosphere-weighted and ionosphere-fixed single-baseline RTK functional models. The corresponding stochastic and dynamic models are given as well. In Section 3 the GNSS data and baselines are described, followed by the stochastic/dynamic model settings. In Section 4 we present empirical single- and dual-frequency instantaneous RTK results for short and medium baselines. This is followed by formal long baseline RTK results in Section 5, which involves ambiguity dilution of precisions (ADOPs), bootstrapped success rates, ambiguity/positioning convergence times, and the positioning performance. In Section 6 the corresponding empirical positioning convergence times and positioning performance are analyzed, based on real data collected in Perth, Australia. We end this contribution with some conclusions in Section 7.

2 Single-baseline RTK functional, stochastic and dynamic models

2.1 Ionosphere-float functional model

We assume that we track from $r = 1, 2$ receivers, at the same instance, the satellites $s_* = 1_*, \ldots, m_*$ on frequencies $j_* = 1_*, \ldots, f_*$, where m_*, f_* is the number of satellites and frequencies respectively. The symbol $*$ equals G for GPS and B for BDS. We omit time stamps in the equations for brevity and for satellite orbits standard broadcast ephemerides are used. We further perform between-receiver single-differences (SDs) and the satellite delays common to both receivers are then eliminated, and we assume that any remaining satellite orbit errors can be neglected as well. The description of the notations used in this Section are given in Table 2.

Table 2 Definition of commonly used symbols

Symbol	Definition	Description
r	$= 1, 2$	receivers used
s_*	$= 1_*, \ldots, m_*$	tracked satellites
$*$	$= G$ or B	systems tracked, with G for GPS and B for BDS
j_*	$= 1_*, \ldots, f_*$	tracked frequencies
$(\cdot)_{12}$	$= (\cdot)_2 - (\cdot)_1$	between-receiver SDs
$(\cdot)^{12}_{1s_*}$	$= (\cdot)^{s_*} - (\cdot)^{1_*}$	between-satellite SDs
$p^{s_*}_{12,j_*}, \phi^{s_*}_{12,j_*}$		SD code and phase observables respectively
$g^{s_*T}_r$	$= \frac{(x^{s_*} - x_r)^T}{\|\|x^{s_*} - x_r\|\|}$	line-of-sight unit vector
$(\cdot)^T$		transpose of vector
$\|\|.\|\|$		norm
x^{s_*}, x_r		vector of satellite and receiver coordinates respectively
λ_{j_*}		wavelength for frequency j_*
$m^{s_*}_r$		mapping function to get a station-wise (wet) ZTD
μ_{j_*}	$= f^2_{1_G}/f^2_{j_*}$	conversion of ionospheric delay from GPS $L1$ to j_*
Δx_r		receiver r coordinate increments
τ_r		ZTD for receiver r
dt^*_r		receiver r clock with respect to GPS time or BeiDou navigation satellite system time (CSNO, 2013)
d^*_{r,j_*}		receiver r hardware (HW) code delays on frequency j_* for system $*$
δ^*_{r,j_*}		receiver r HW phase delays on frequency j_* for system $*$
$\iota^{s_*}_r$		slant ionospheric delays for receiver r and satellite s_*
$z^{s_*}_{r,j_*}$		ambiguity for receiver r on frequency j_* and satellite s_*

The system of observation equations is not of full-rank after the SDs. The number of rank deficiencies is the number of linear combinations of the column vectors of the design matrix that produces the zero vector, and can be eliminated through S-system theory (Teunissen, 1985; Teunissen et al, 2010). This implies null-space identification, S-basis constraining and interpretation of the estimable parameters. The number of rank defects and S-basis choice for the SD ionosphere-float, ionosphere-weighted and ionosphere-fixed model are given in Table 3.

Table 3 Single-epoch single-baseline RTK ionosphere-float, ionosphere-weighted and ionosphere-fixed S-basis choice/# of rank deficiencies for SD GPS+BDS

Model	S-basis choice	# of rank defects
Iono-float	$d^G_{12,1_G}, d^G_{12,2_G}, z^{1_G}_{12,j_G},$	$2 + f_G +$
	$d^B_{12,1_B}, d^B_{12,2_B}, z^{1_B}_{12,j_B}$	$+2 + f_B$
Iono-weighted/fixed	$d^G_{12,1_G}, z^{1_G}_{12,j_G},$	$1 + f_G +$
	$d^B_{12,1_B}, z^{1_B}_{12,j_B}$	$+1 + f_B$

The number of rank deficiencies for the SD ionosphere-weighted model in Table 3 is equivalent as for the ionosphere-fixed one, and the difference in rank deficiencies between the ionosphere-float and ionosphere-weighted/fixed models are further described in the following Section.

The rank deficiency for the ionosphere-float model of size 2 between the columns of the receiver clock and the hardware (HW) code/phase delays, are solved by fixing the HW code delay on $j_* = 1_*$ for each system $\left(d^*_{12,1_*}\right)$. Then we have the rank defects of size 2 between the columns of the clocks, HW code/phase delays and ionosphere, which are solved by fixing the HW code delays on $j_* = 2_*$ for both systems $\left(d^*_{12,2_*}\right)$. Finally we have the rank deficiency of size $f_G + f_B$ between the columns of the HW phase delays and ambiguities, which are solved by fixing the ambiguities on $j_* = 1_*, \ldots, f_*$ and $s_* = 1_*$ for both systems $\left(z^{1_*}_{12,j_*}\right)$.

Once the rank defects in Table 3 have been solved, we have the following full-rank dual-system of observation equations for $* = G$ for GPS and B for BDS. This model (1) is referred to as the "ionosphere-float" model since the slant ionospheric delays are considered completely unknown,

$$\begin{aligned}
p^{s_G}_{12,j_G} &= -g_2^{s_G T}\Delta x_{12} + m_2^{s_G}\tilde{\tau}_{12} + d\tilde{t}^G_{12} + \tilde{d}^G_{12,j_G} + \mu_{j_G}\tilde{\iota}^{s_G}_{12}\\
\phi^{s_G}_{12,j_G} &= -g_2^{s_G T}\Delta x_{12} + m_2^{s_G}\tilde{\tau}_{12} + d\tilde{t}^G_{12} + \tilde{\delta}^G_{12,j_G} - \mu_{j_G}\tilde{\iota}^{s_G}_{12}\\
&\quad + \lambda_{j_G}\tilde{z}^{1s_G}_{12,j_G}\\
p^{s_B}_{12,j_B} &= -g_2^{s_B T}\Delta x_{12} + m_2^{s_B}\tilde{\tau}_{12} + d\tilde{t}^B_{12} + \tilde{d}^B_{12,j_B} + \mu_{j_B}\tilde{\iota}^{s_B}_{12}\\
\phi^{s_B}_{12,j_B} &= -g_2^{s_B T}\Delta x_{12} + m_2^{s_B}\tilde{\tau}_{12} + d\tilde{t}^B_{12} + \tilde{\delta}^B_{12,j_B} - \mu_{j_B}\tilde{\iota}^{s_B}_{12}\\
&\quad + \lambda_{j_B}\tilde{z}^{1s_B}_{12,j_B}
\end{aligned} \tag{1}$$

The Saastamoinen troposphere model has been used to correct the dry part of the troposphere (Saastamoinen, 1972) in (1), and we refrain from carrying through SD random observation noise and other systematic effects such as multipath for notational convenience. The estimable unknowns in (1), denoted with a 'tilde', are given in Table 4. The shared parameters between the two systems are the receiver Δx_{12} coordinates and relative (wet) ZTD $\tilde{\tau}_{12}$. Note that the ambiguities in Table 4 are double-differenced, thus also integers. Remark also that in case the frequencies would overlap between the systems (Table 1), inter-system bias (ISB) calibration is possible that allows for further strengthening of the model and the use of a common pivot satellite when parameterizing the double-differenced ambiguities (Odijk and Teunissen, 2013; Odolinski et al, 2014a,b).

2.2 Ionosphere-weighted functional model

For the ionosphere-weighted model we have ionosphere pseudo-observables available that can provide us with stochastic information of the ionospheric delays between stations, which increases the redundancy and thus strengthens the model (see Table 6). The rank deficiencies for the ionosphere-weighted model given in Table 3 changes as compared to the ionosphere-float model. The difference is that the rank defects in Table 3 of size 2 between the receiver clocks, HW code/phase delays and ionosphere, for both systems, gets eliminated by the additional pseudo-observables.

After the rank deficiencies in Table 3 have been solved, the "ionosphere-weighted" full-rank dual-system of observation equations read,

$$\begin{aligned}
p^{s_G}_{12,j_G} &= -g_2^{s_G T}\Delta x_{12} + m_2^{s_G}\tilde{\tau}_{12} + d\tilde{\tilde{t}}^G_{12} + \tilde{\tilde{d}}^G_{12,j_G} + \mu_{j_G}\tilde{\tilde{\iota}}^{s_G}_{12}\\
\phi^{s_G}_{12,j_G} &= -g_2^{s_G T}\Delta x_{12} + m_2^{s_G}\tilde{\tau}_{12} + d\tilde{\tilde{t}}^G_{12} + \tilde{\tilde{\delta}}^G_{12,j_G} - \mu_{j_G}\tilde{\tilde{\iota}}^{s_G}_{12}\\
&\quad + \lambda_{j_G}\tilde{z}^{1s_G}_{12,j_G}\\
\tilde{\tilde{\iota}}^{s_G}_{12} &= \iota^{s_G}_{12}\\
p^{s_B}_{12,j_B} &= -g_2^{s_B T}\Delta x_{12} + m_2^{s_B}\tilde{\tau}_{12} + d\tilde{\tilde{t}}^B_{12} + \tilde{\tilde{d}}^B_{12,j_B} + \mu_{j_B}\tilde{\tilde{\iota}}^{s_B}_{12}\\
\phi^{s_B}_{12,j_B} &= -g_2^{s_B T}\Delta x_{12} + m_2^{s_B}\tilde{\tau}_{12} + d\tilde{\tilde{t}}^B_{12} + \tilde{\tilde{\delta}}^B_{12,j_B} - \mu_{j_B}\tilde{\tilde{\iota}}^{s_B}_{12}\\
&\quad + \lambda_{j_B}\tilde{z}^{1s_B}_{12,j_B}\\
\tilde{\tilde{\iota}}^{s_B}_{12} &= \iota^{s_B}_{12}
\end{aligned} \tag{2}$$

The estimable unknowns in (2) that are different from the ionosphere-float model (1) are denoted with a double 'tilde', and given in Table 5. The differences in interpretation of the ionosphere-weighted unknowns in comparison to the ionosphere-float counterpart in Table 4 are: the receiver clock and HW phase delays are now only biased by the HW code delay on $j_* = 1_*$; the receiver HW code delays, or Differential Code Biases (DCBs), are now also estimable on $j_* \geq 2$ (instead of $j_* \geq 3$), and the relative slant ionospheric delays are free from HW code delays.

2.3 Ionosphere-fixed functional model

Provided that we have a baseline length of at most a few km, the relative (wet) ZTD τ_{12} and the relative slant ionospheric delays $\iota^{s_*}_{12}$ can be taken as zero to strengthen the model. The number of rank defects and the S-basis choice are then equivalent to the ionosphere-weighted model in Table 3. The full-rank "ionosphere-fixed" model follows as,

$$\begin{aligned}
p^{s_G}_{12,j_G} &= -g_2^{s_G T}\Delta x_{12} + d\tilde{\tilde{t}}^G_{12} + \tilde{\tilde{d}}^G_{12,j_G}\\
\phi^{s_G}_{12,j_G} &= -g_2^{s_G T}\Delta x_{12} + d\tilde{\tilde{t}}^G_{12} + \tilde{\tilde{\delta}}^G_{12,j_G} + \lambda_{j_G}\tilde{z}^{1s_G}_{12,j_G}\\
p^{s_B}_{12,j_B} &= -g_2^{s_B T}\Delta x_{12} + d\tilde{\tilde{t}}^B_{12} + \tilde{\tilde{d}}^B_{12,j_B}\\
\phi^{s_B}_{12,j_B} &= -g_2^{s_B T}\Delta x_{12} + d\tilde{\tilde{t}}^B_{12} + \tilde{\tilde{\delta}}^B_{12,j_B} + \lambda_{j_B}\tilde{z}^{1s_B}_{12,j_B}
\end{aligned} \tag{3}$$

where we have the same interpretation of the unknowns as for the ionosphere-weighted model (2) in Table 5. We

Table 4 Estimable unknown parameters and their interpretation for SD GPS+BDS ionosphere-float, ZTD-float model (1)

Notation and interpretation	Estimable parameter	Conditions
$\Delta x_{12} = \Delta x_2 - \Delta x_1$	relative receiver coordinates	$r \geq 2$
$\tilde{\tau}_{12} = \tau_2 - \tau_1$	relative (residual) wet ZTD	$r \geq 2$
$d\tilde{t}^*_{12} = dt^*_{12} + \frac{\mu_{2_*}}{\mu_{2_*}-\mu_{1_*}} d^*_{12,1_*} - \frac{\mu_{1_*}}{\mu_{2_*}-\mu_{1_*}} d^*_{12,2_*}$	relative receiver clock with HW code delays on $j_* = 1_*, 2_*$	$r \geq 2$
$\tilde{d}^*_{12,j_*} = d^*_{12,j_*} - \frac{\mu_{2_*}-\mu_{j_*}}{\mu_{2_*}-\mu_{1_*}} d^*_{12,1_*} + \frac{\mu_{1_*}-\mu_{j_*}}{\mu_{2_*}-\mu_{1_*}} d^*_{12,2_*}$	relative receiver HW code delays	$j_* \geq 3_*, r \geq 2$
$\tilde{\delta}^*_{12,j_*} = \delta^*_{12,j_*} - \frac{\mu_{2_*}+\mu_{j_*}}{\mu_{2_*}-\mu_{1_*}} d^*_{12,1_*} + \frac{\mu_{1_*}+\mu_{j_*}}{\mu_{2_*}-\mu_{1_*}} d^*_{12,2_*} + \lambda_{j_*} z^{1_*}_{12,j_*}$	relative receiver HW phase delays	$j_* \geq 1_*, r \geq 2$
$\tilde{\iota}^{s_*}_{12} = \iota^{s_*}_{12} + \frac{1}{\mu_{2_*}-\mu_{1_*}} \left(d^*_{12,2_*} - d^*_{12,1_*} \right)$	relative slant ionospheric delays biased by relative receiver Differential Code Biases (DCBs)	$r \geq 2, s_* \geq 1$
$\tilde{z}^{1s_*}_{12,j_*} = z^{s_*}_{12,j_*} - z^{1_*}_{12,j_*}$	double-differenced integer ambiguities	$j_* \geq 1_*, r \geq 2, s_* \geq 2$

Table 5 Estimable unknown parameters and their interpretation for SD GPS+BDS ionosphere-weighted model (2)

Notation and interpretation	Estimable parameter	Conditions
$\Delta x_{12} = \Delta x_2 - \Delta x_1$	relative receiver coordinates	$r \geq 2$
$\tilde{\tau}_{12} = \tau_2 - \tau_1$	relative (residual) wet ZTD	$r \geq 2$
$d\tilde{t}^*_{12} = dt^*_{12} + d^*_{12,1_*}$	relative receiver clock with HW code delays on $j_* = 1_*$	$r \geq 2$
$\tilde{d}^*_{12,j_*} = d^*_{12,j_*} - d^*_{12,1_*}$	relative receiver Differential Code Bias (DCB)	$j_* \geq 2_*, r \geq 2$
$\tilde{\delta}^*_{12,j_*} = \delta^*_{12,j_*} - d^*_{12,1_*} + \lambda_{j_*} z^{1_*}_{12,j_*}$	relative receiver HW phase delays	$j_* \geq 1_*, r \geq 2$
$\tilde{\iota}^{s_*}_{12} = \iota^{s_*}_{12}$	relative slant ionospheric delays	$r \geq 2, s_* \geq 1$
$\tilde{z}^{1s_*}_{12,j_*} = z^{s_*}_{12,j_*} - z^{1_*}_{12,j_*}$	double-differenced integer ambiguities	$j_* \geq 1_*, r \geq 2, s_* \geq 2$

finally remark that the interpretation of the estimable unknown parameters in case the receiver clock is shared among the systems have been shown in Odolinski et al (2014a) for the ionosphere-fixed model, and in Odolinski et al (2014b) for the ionosphere-float model, respectively. The redundancies by doing so are however also shown equivalent to the full-rank RTK models presented in this contribution.

2.4 Stochastic models

The variance-covariance (VCV) matrix for the SD code and phase observables of the single-system ionosphere-float and ionosphere-fixed model is given as,

$$Q^*_{yy} = \text{blkdiag}\left(C^*_p, C^*_\phi\right) \otimes \left(D^T_n D_n \otimes W^{-1}_{m_*}\right) \tag{4}$$

where the code and phase observable a priori variance factors are given in the sub-matrices $C^*_p = \text{diag}(\sigma^2_{p,1_*}, \ldots, \sigma^2_{p,f_*})$ and $C^*_\phi = \text{diag}(\sigma^2_{\phi,1_*}, \ldots, \sigma^2_{\phi,f_*})$ respectively, 'blkdiag' and 'diag' denotes a blockdiagonal and diagional matrix respectively. Here we assume no cross-correlation between code and phase as well as between frequencies, otherwise the non-diagonal elements of C^*_p and C^*_ϕ would be populated accordingly with covariances between the observables. Further $\otimes$ is the Kronecker product (Rao, 1973), D^T_n is the between-receivers SD operator (Teunissen, 1997), and $W^{-1}_{m_*}$ contains the elevation-dependent weighting function as given by Euler and Goad (1991). The combined GPS+BDS ionosphere-float (1) and ionosphere-fixed (3) VCV-matrix reads,

$$Q_{yy} = \text{blkdiag}\left(Q^G_{yy}, Q^B_{yy}\right) \tag{5}$$

The single-system ionosphere-weighted VCV-matrix is given as,

$$\overline{Q}^*_{yy} = \text{blkdiag}\left(Q^*_{yy}, \sigma^2_{\iota^{s_*}_{12}} \otimes W^{-1}_{m_*}\right) \tag{6}$$

where $\sigma^2_{\iota^{s_*}_{12}}$ is the SD variance factor of the slant ionospheric delays that can be modeled as a function of the baseline length (see Section 3). The combined GPS+BDS ionosphere-weighted (2) VCV-matrix then follows as,

$$\overline{Q}_{yy} = \text{blkdiag}\left(\overline{Q}^G_{yy}, \overline{Q}^B_{yy}\right) \tag{7}$$

2.5 Dynamic model for the Kalman filter

The unknowns in the observation equations for the ionosphere-float (1), ionosphere-weighted (2) and ionosphere-fixed (3) models can be estimated using an extended Kalman filter with a dynamic model. The state vector for which we will use a dynamic model can be expressed in vector form for epoch $i = 1, \ldots, k$ as follows,

$$x\left(i\right) = \left[\tilde{\tau}_{12}\left(i\right), z^T_{12}\left(i\right)\right]^T \tag{8}$$

where we have $\tilde{\tau}_{12}\left(i\right)$ the relative (wet) ZTD and the ambiguities in a vector $z_{12}\left(i\right) = \left[z^{G\,T}_{12}\left(i\right), z^{B\,T}_{12}\left(i\right)\right]^T$, with $z^*_{12}\left(i\right) = \left[z^{*\,T}_{12,1_*}\left(i\right), \ldots, z^{*\,T}_{12,f_*}\left(i\right)\right]^T$ and $z^*_{12,j_*}\left(i\right) = \left[\tilde{z}^{12_*}_{12,j_*}\left(i\right), \ldots, \tilde{z}^{1m_*}_{12,j_*}\left(i\right)\right]^T$.

The dynamic model used for the Kalman filter follows as,

$$\begin{aligned} &x_k = \Phi_{k|k-1} x_{k-1} + d_k, \\ &D\left(d_k\right) = Q_{d_k} \end{aligned} \tag{9}$$

where x_k is the state vector at epoch k connected with the state vector x_{k-1} at previous epoch $k-1$ by $\Phi_{k|k-1}$ the transition matrix, d_k the zero-mean process noise with VCV-matrix Q_{d_k}, and $D(\cdot)$ is the dispersion. The transition matrix follows as,

$$\Phi_{k|k-1} = \text{blockdiag}(1, I_n) \tag{10}$$

where 1 corresponds to the ZTD and I_n is the identity matrix of the size $n = f_G(m_G - 1) + f_B(m_B - 1)$ corresponding to the ambiguities. The process noise VCV-matrix follows as,

$$Q_{d_k} = \text{blockdiag}(\Delta t \cdot q_{\dot{\tau}}, 0_n) \tag{11}$$

where Δt is the time-interval between adjacent epochs, $q_{\dot{\tau}}$ is the spectral density for the relative (wet) ZTD that is modeled as random walk, and 0_n is the zero matrix of dimension n used for the ambiguities since they are treated as time-constant. All other parameters in Tables 4 and 5 are assumed unlinked in time.

2.6 The multi-epoch redundancy

The redundancy is computed as the number of observations minus the number of estimable unknowns. In Table 6 we give the number of observations, the number of estimable unknowns and the redundancy for the single-baseline RTK models that we have presented in equations (1)-(3). The last column represents the solvability condition for instantaneous RTK, which is the number of satellites required to solve the models. We give the redundancy based on the temporal constraints in (9), i.e. the ambiguities are considered as time-constant and the relative ZTD is modeled as random walk. Note that setting $k = 1$ in Table 6 gives the single-epoch redundancies, as shown in the 4:th column.

As an example from Table 6, consider the single-system ionosphere-float model number of unknowns $k(2+2f_* + m_*) + 1 + f_*(m_* - 1)$, which consists of $3k$ (relative) receiver coordinates, $1k$ receiver clock, $k(f_* - 2)$ receiver HW code delays estimable on the third and more frequencies, kf_* receiver HW phase delays, km_* slant ionospheric delays, 1 relative ZTD and $f_*(m_* - 1)$ ambiguities. The ambiguities and the relative ZTD do not have any k multiplied with them since they have a dynamic model. The number of observations moreover reads $2kf_*m_*$, which gives us the multi-epoch redundancy as,

$$[f_*(m_* - 1) - m_* - 3] + (k-1)[2f_*(m_* - 1) - m_* - 2] \tag{12}$$

The part on the left hand side within square brackets in (12) is the single-epoch redundancy, whereas the part on the right hand within square brackets and multiplied by $(k-1)$ is the contribution of the $f_*(m_* - 1)$ time-constant ambiguities, 1 relative ZTD, and the single-epoch redundancy for each epoch $k - 1$. Most importantly we see in Table 6 that the ionosphere-fixed model is the strongest and the ionosphere-float is the weakest model, respectively, and that the largest redundancy is obtained when combining GPS and BDS.

We give in Figure 1 and at top the positioning availability for a ZTD-float RTK model for a station in Perth, as a function over one day of real data. This is given in local Perth time, February 19, 2014 and for an elevation cut-off angle of 25°, as to illustrate an environment with obstructed satellite visibility. At bottom we plot the corresponding dual-frequency (single-epoch) ionosphere-weighted (thick line) and ionosphere-float (thin line) redundancy, as to illustrate the reliability of the models. Reliability is a measure of the ability of the system to test the observations for modeling errors, where zero redundancy gives infinitely poor reliability as testing is then not possible. Note in Figure 1 that redundancy is absent when the number of satellites to solve the model (Table 6) is not sufficient.

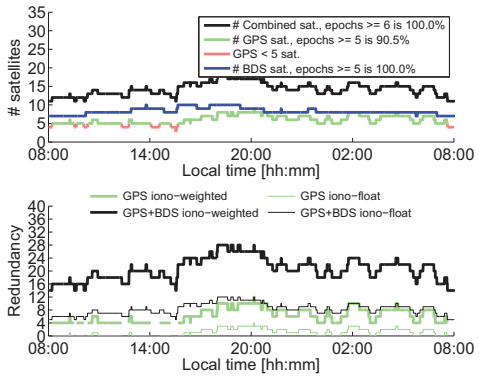

Fig. 1 # of satellites for GPS and GPS+BDS using a cut-off angle of 25° (*top*) in Perth. February 19, 2014. Percentages given of the total # of epochs above or equal to the required # of satellites to solve the models (Table 6). *Light green* and *dark blue* represent GPS and BDS above or equal to five satellites respectively, *light red* are for GPS below five satellites, and *black* is for the combined system above six satellites. At *bottom* the redundancies of the dual-frequency ionosphere-float and ionosphere-weighted instantaneous RTK models are given as well

Note in Figure 1 the significant difference in redundancies between the dual-frequency ionosphere-weighted and ionosphere-float model. Figure 1 also illustrates that GPS+BDS and BDS separately allow for positioning

Table 6 Single-baseline multiple-epoch RTK: # of SD observations, unknowns and redundancy for the ionosphere-float (1), ionosphere-weighted (2) and ionosphere-fixed (3) model and epoch $i = 1, \ldots, k$. Note: the relative ZTD is assumed estimated for the ionosphere-float and ionosphere-weighted model, and a dynamic model is used for the ambiguities (time-constant) and relative ZTD (random walk)

Model (Eq.)	**# of SD observations**	**# of SD unknowns**	**Redundancy** $k=1$	$k>1$	**Solvability condition**
Iono-float:					$f_* \geq 2$
Single-system	$2kf_*m_*$	$k(2+2f_*+m_*)+1+f_*(m_*-1)$	$f_*(m_*-1)-m_*-3$	$+(k-1)(2f_*(m_*-1)-m_*-2)$	$m_* \geq 5$
GPS+BDS (1)	$2kf_Gm_G+$ $+2kf_Bm_B$	$k(1+2f_G+m_G)+1+f_G(m_G-1)$ $+k(2f_B+m_B)+f_B(m_B-1)$	$f_G(m_G-1)-m_G$ $+f_B(m_B-1)-m_B-2$	$+(k-1)(2f_G(m_G-1)-m_G$ $+2f_B(m_B-1)-m_B-1)$	$m_G+m_B \geq 6$
Iono-weighted:					$f_* \geq 1$
Single-system	$2kf_*m_*+km_*$	$k(3+2f_*+m_*)+1+f_*(m_*-1)$	$f_*(m_*-1)-4$	$+(k-1)(2f_*(m_*-1)-3)$	$m_* \geq 5$
GPS+BDS (2)	$2kf_Gm_G+km_G+$ $+2kf_Bm_B+km_B$	$k(3+2f_G+m_G)+1+f_G(m_G-1)$ $+k(2f_B+m_B)+f_B(m_B-1)$	$f_G(m_G-1)$ $+f_B(m_B-1)-4$	$+(k-1)(2f_G(m_G-1)$ $+2f_B(m_B-1)-3)$	$m_G+m_B \geq 6$
Iono-fixed:					$f_* \geq 1$
Single-system	$2kf_*m_*$	$k(3+2f_*)+f_*(m_*-1)$	$f_*(m_*-1)-3$	$+(k-1)(2f_*(m_*-1)-3)$	$m_* \geq 4$
GPS+BDS (3)	$2kf_Gm_G+$ $+2kf_Bm_B$	$k(3+2f_G)+f_G(m_G-1)$ $+k2f_B+f_B(m_B-1)$	$f_G(m_G-1)$ $+f_B(m_B-1)-3$	$+(k-1)(2f_G(m_G-1)$ $+2f_B(m_B-1)-3)$	$m_G+m_B \geq 5$

with ZTD-estimation during the entire day, whereas for GPS this is possible 90.5% of the time. Moreover, we have ionosphere-float redundancy 100% of the time for a combined system, whereas for GPS separately we have it only 57.1% of the time. This thus indicates the possibility of using higher satellite elevation cut-off angles when combining the systems, and still allow for retained redundancy.

3 GNSS data collection and stochastic/dynamic model settings

The Trimble NetR9 receivers/antennas used to form the short, medium and long baselines are depicted in Figure 2. A map over the Asia-Pacific region with the ground tracks of the BDS constellation is further depicted in Figure 3, with the satellites' location denoted with a dot at 15:00 local Perth time, February 19, 2014. The baselines that will be analyzed and the number of satellites for a GPS+BDS system is presented in Figure 3 as well. We see double the number of satellites for a combined GPS+BDS system in comparison to GPS separately.

The GNSS data was collected on April 19-21, 2013 for CUTT (Bentley) to form a 1 km baseline with CUTA (using the ionosphere-fixed model), on May 21, 2013 for KALT (Kalamunda) to form a 17 km baseline with CUTA (ionosphere-weighted model), and on February 19, 2014 for MURT (Muresk) to form a 80 km baseline with CUT0 (ionosphere-float model). The stations CUT0 and CUTA are both continuously operating reference stations located at Curtin University in Bentley. For all of the following analyzes we use a measurement interval of 30 seconds, the Detection, Identification and Adaptation (DIA) procedure to detect, identify and adapt for outliers (Teunissen, 1990), and the LAMBDA method (Teunissen, 1995) for integer ambiguity resolution.

In Table 7 we present the functional models that are investigated and the corresponding dynamic model (11) used in case of the Kalman filter solutions. A random walk process noise of 2 mm/$\sqrt{\text{hour}}$ is used for the relative (residual) wet ZTD, which was predicted similarly to the approach in Chapter 3.4.3 in Schüler (2001), based on data independent from the data analyzed in this contribution.

Table 7 Models processed. Epoch-by-epoch (ebe) denotes no linkage in time when estimating the parameters

Model	**Mode**	**Dynamic model**	**Process noise**
Iono-fixed/weighted	Single-epoch	All parameters: ebe	-
Iono-float	Kalman filter	Ambiguities time-constant:	0
		Relative ZTD random walk:	2 mm/$\sqrt{\text{hour}}$
		Other parameters: ebe	-

The stochastic model settings are depicted in Table 8. This is based on the exponential elevation weighting function by Euler and Goad (1991) and zenith-referenced a priori code and phase standard deviations (STDs) respectively for undifferenced observations. In the last column we depict the between-receiver SD STD of the slant ionospheric delays as well, as used in the stochastic model of the ionosphere-weighted model (6). We follow the rule of thumb by Schaffrin and Bock (1988), where the between-receiver ionospheric STD can be modeled as a function of the baseline length as 0.96 mm/km.

Table 8 Zenith-referenced code and phase STDs for the Trimble NetR9 receivers in Figure 2. Last column represents the a priori SD STD for the relative slant ionospheric delays as used in the ionosphere-weighted model (6)

System	**Frequency**	**Code** $\sigma_{P_{,j*}}$ [cm]	**Phase** $\sigma_{\phi_{,j*}}$ [mm]	**Iono** $\sigma_{\iota^{s*}_{12}}$ [mm/km]
GPS	L1	30	2	0.96
	L2	30	2	0.96
BDS	B1	30	2	0.96
	B2	30	2	0.96

(a) CUTA (*left*), CUT0 (*right*) (b) CUTT, April 19-21, 2013 (c) KALT, May 21, 2013 (d) MURT, February 19, 2014

Fig. 2 GNSS Trimble NetR9 receivers and antennas for GPS+BDS single-baseline RTK

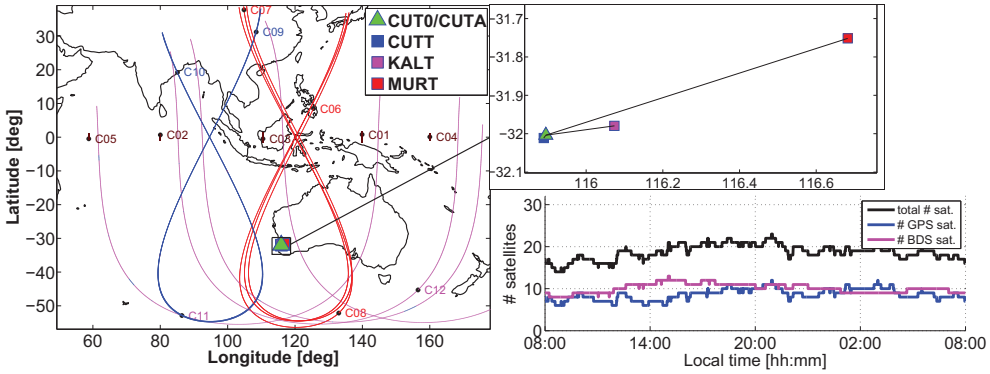

Fig. 3 BDS constellation (February 19, 2014) with satellites location depicted as a *dot* at 15:00 local Perth time (*left*), the three baselines analyzed with reference stations CUT0/CUTA denoted as a *green triangle* (*top right*), and the # of satellites at Muresk station MURT using an elevation cut-off angle of 10° (*bottom right*)

4 Instantaneous single-baseline RTK for short and medium baselines

4.1 Single/dual-frequency ionosphere-fixed RTK

In the following results we will illustrate what is achievable for instantaneous RTK when one is allowed to use the ionosphere-fixed model. We depict in Figure 4 the ionosphere-fixed (3) *single-frequency* L1 GPS (left column), and L1+B1 GPS+BDS (right column) instantaneous RTK positioning results for an elevation cut-off angle of 25° (April 19-21, 2013). The higher elevation cut-off angle is used as to simulate conditions in an urban canyon environment or open pit mine. The correctly fixed solutions are given in green, incorrectly fixed solutions in red and the ambiguity-float solutions in gray color, in local North (N), East (E) and Up (U). The correctly fixed solutions are determined from a reference set of ambiguities. These reference ambiguities were estimated by using a dual-frequency combined system with fixed precise benchmark coordinates, making use of a 10° elevation cut-off angle and treating the ambiguities as time-constant in a Kalman filter over the entire 3 day observation time span. At bottom we give the number of satellites above or equal to 8 as green otherwise as red, as to illustrate the relation between the number of satellites and the wrongly fixed solutions.

In Figure 4 we can see the two-order of magnitude improvement when going from the ambiguity-float and incorrectly fixed solutions at dm-meter level positioning precision, to ambiguity-fixed positioning with mm-cm level precisions. It moreover shows the excellent performance of the L1+B1 GPS+BDS system. The single-frequency combined system has namely an integer least-squares (ILS) success rate (SR) of 100% that allows for *continuous* ambiguity-fixed precise positioning during all three days. When using L1 GPS separately, however, we can only achieve an ILS SR of 33% related to the few number of satellites tracked for this cut-off angle. There are also a few gaps in the GPS positioning time-series when the number of satellites is below

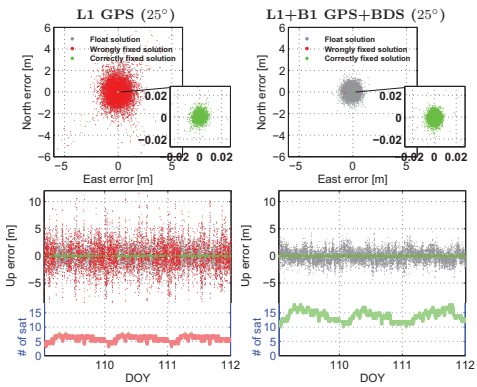

Fig. 4 *Top* ionosphere-fixed (3) *single-frequency* instantaneous RTK using cut-off angle 25°: horizontal (N,E) scatterplots and vertical (U) time-series for L1 GPS (*left column*) with 33% ILS SR and L1+B1 GPS+BDS (*right column*) with 100% ILS SR. At *bottom* corresponding # of satellites above/equal 8 as *green* otherwise as *red*. April 19-21, 2013

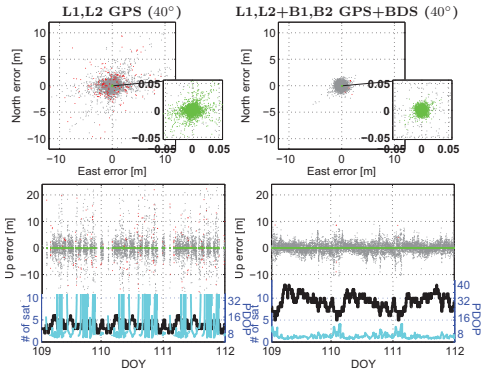

Fig. 5 *Top* ionosphere-fixed (3) *dual-frequency* instantaneous RTK using cut-off angle 40°: horizontal (N,E) scatterplots and vertical (U) time-series for L1,L2 GPS (*left column*) with 95.4% ILS SR and L1,L2+B1,B2 GPS+BDS (*right column*) with 99.9% ILS SR. At *bottom* corresponding # of satellites in *black* and PDOP in *cyan*. April 19-21, 2013

4 and hence we cannot solve the model (see solvability condition in Table 6).

As Figure 4 illustrated, making use of a single-frequency for continuous, successful and instantaneous GPS-only RTK positioning is not feasible. This holds true even when using an elevation cut-off angle of 10° and/or the L2 frequency, see e.g. Teunissen et al (2014). Thus we depict in Figure 5 the corresponding *dual-frequency* L1,L2 GPS and L1,L2+B1,B2 GPS+BDS single-epoch RTK positioning results, but now for an elevation cut-off angle of 40° to simulate a more challenging urban canyon environment. The number of satellites is presented in black together with the positional dilution of precision (PDOP) in cyan, as to illustrate how large excursions in the positioning errors are related to the poor receiver-satellite geometry.

Although we increased the elevation cut-off angle from 25° in Figure 4 to 40° in Figure 5, we can see that adding L2 to single-frequency L1 GPS increases the ILS SR significantly, from 33% to 95.4%. However this does not mean that all the GPS ambiguity-fixed positions are very precise, as the poor receiver-satellite geometry, illustrated by the PDOPs, spoils the positioning performance. This thus shows that the performance of ambiguity resolution and positioning do not always go hand-in-hand, as also demonstrated and explained in (Teunissen, 1997; Teunissen et al, 2014). In addition since the number of satellites decreases to below 4 for many epochs due to the very high cut-off angle of 40°, we also have larger gaps in the GPS positioning time-series in Figure 5 in comparison to Figure 4. More importantly one can see in Figure 5 that when adding B1,B2 BDS to GPS, the poor receiver-satellite geometry and thus positioning performance is significantly improved, the positioning availability is increased to 100%, and the ILS SR reaches a value of 99.9%. Thus the combined GPS+BDS system does not only allow for higher SRs but also significantly better positioning in comparison to GPS, particularly when using higher elevation cut-off angles. In conclusion we have shown that for the ionosphere-fixed model the use of *dual-frequencies* are needed when using GPS separately, whereas when combining GPS and BDS successful instantaneous *single-frequency* RTK is also possible.

4.2 Single/dual-frequency ionosphere-weighted RTK

In the previous section it was illustrated that single-frequency GPS+BDS successful instantaneous RTK is possible, provided that the baseline is so short so that one is allowed to use the ionosphere-fixed model. In the following we will predict by means of the ambiguity dilution of precision (ADOP) whether single-frequency instantaneous RTK is also successfully achievable when one needs to use the ionosphere-weighted model. The ADOP is a formal scalar measure of the model strength for ambiguity resolution, introduced by Teunissen (1997), and is defined as,

$$\text{ADOP} = |Q_{\hat{a}\hat{a}}|^{1/(2n)} \quad \text{[cycles]} \tag{13}$$

The ADOP is computed as the determinant $|\cdot|$ of the VCV-matrix of the ambiguities $Q_{\hat{a}\hat{a}}$ raised to the power

of $1/(2n)$, where n is the dimension of the ambiguity vector, and is expressed in cycles. The ADOP measures the intrinsic precision of the ambiguities, and is also a measure of the volume of the ambiguity confidence ellipsoid (Teunissen et al, 1996).

In Figure 6 we depict for an elevation cut-off angle of 10°, the ionosphere-weighted (2) instantaneous ADOP for *single-frequency* L1 GPS and L1+B1 GPS+BDS (May 21, 2013). The relative ZTD is, however, not parameterized as to strengthen the model. An ADOP-level of 0.12 cycle is indicated by a dashed red line since it corresponds to an ambiguity SR larger than 99.9% (Odijk and Teunissen, 2008). The number of BDS satellites is depicted in magenta and GPS in blue color at bottom.

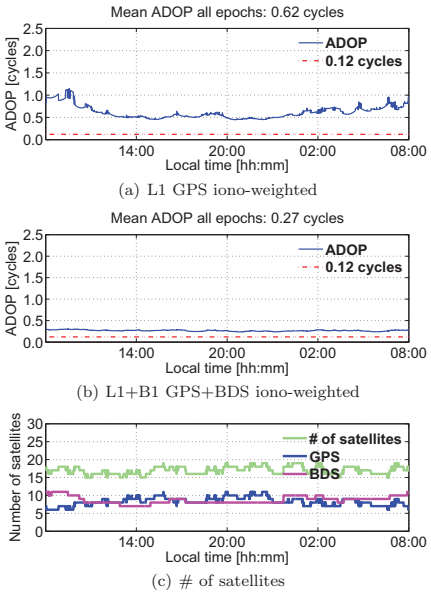

(a) L1 GPS iono-weighted

(b) L1+B1 GPS+BDS iono-weighted

(c) # of satellites

Fig. 6 Ionosphere-weighted (2): *single-frequency* ADOP time-series (*blue*) for single-baseline instantaneous RTK, using 10° cut-off angle. The relative ZTD is not parameterized in the model. May 21, 2013. **a** GPS, **b** GPS+BDS, **c** total # of satellites in *light green*

In Figure 6 one can see larger ADOP time-series for GPS with more variability in comparison to the combined GPS+BDS system, because of the fewer number of satellites. However the daily mean ADOP of 0.27 cycles for single-frequency GPS+BDS is still not sufficient to expect successful instantaneous ambiguity resolution. Thus it is deemed necessary to also use dual-frequencies for the combined system when one has to rely on the ionosphere-weighted model.

In Figure 7 we therefore depict the *dual-frequency* L1,L2 GPS and L1,L2+B1,B2 GPS+BDS instantaneous RTK positioning results for an elevation cut-off angle of 25°, using the ionosphere-weighted (2) model (May 21, 2013). The number of satellites equal or above 5 is depicted in green color, otherwise as red. The dual-frequency L1,L2 GPS model achieves an ILS SR of 91.2%, and the system obtains more wrongly fixed solutions at the same time instances as when there are a few number of tracked satellites (depicted in red color). However, the improvement is significant for the dual-frequency GPS+BDS system, with the larger number of satellites, since we get successful instantaneous dual-frequency RTK over the entire day.

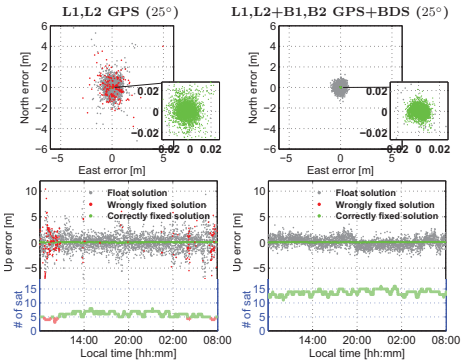

Fig. 7 *Top* ionosphere-weighted (2) *dual-frequency* instantaneous RTK using cut-off angle 25°: horizontal (N,E) scatterplots and vertical (U) time-series for L1,L2 GPS (*left column*) with 91.2% ILS SR and L1,L2+B1,B2 GPS+BDS (*right column*) with 100% ILS SR. At *bottom* corresponding # of satellites above/equal 5 as *green* otherwise as *red*. The relative ZTD is not parameterized in the model. May 21, 2013

We summarize our findings of the number of required frequencies for the ionosphere-fixed and ionosphere-weighted instantaneous RTK models in Table 9. It was concluded that for GPS dual-frequencies are needed for the ionosphere-fixed case, whereas for the corresponding GPS+BDS model single-frequency RTK is also possible (Figure 4). For the ionosphere-weighted case it was further predicted that both models need dual-frequencies (Figure 6), but that only the combined system can then obtain continuous successful ambiguity resolution for the cut-off angle of 25° (Figure 7).

Table 9 Ionosphere-weighted (2) and ionosphere-fixed (3) instantaneous RTK capabilities

Model	System	Min # of req. freq.
Ionosphere-fixed	GPS	L1,L2
	GPS+BDS	L1+B1
Ionosphere-weighted	GPS	L1,L2
(ZTD un-modeled)	GPS+BDS	L1,L2+B1,B2

5 Formal analysis of GPS+BDS long baseline RTK model

5.1 Ambiguity Dilution of Precision

In the previous Section it was concluded that single-frequency GPS+BDS instantaneous RTK is possible when one is allowed to use the ionosphere-fixed model. Whereas when the ionosphere-weighted counterpart is needed dual-frequencies are required.

Because of the promising results in the previous Section, we want to predict whether the dual-frequency ionosphere-float, ZTD-float model (1) also can achieve successful instantaneous ambiguity resolution. The corresponding *instantaneous* ADOP time-series (February 19, 2014) is thus depicted in Figure 8, at the first row for L1,L2 GPS and third row for L1,L2+B1,B2 GPS+BDS, respectively. We use an elevation cut-off angle of 10° to increase the number of satellites, since the ionosphere-float model is much weaker than the ionosphere-weighted model (see Table 6). This is due to the necessity to estimate the slant ionospheric delays without any a priori knowledge about their stochastic behavior. The GPS-only ADOPs are larger and have a higher variability in comparison to when GPS+BDS is combined in Figure 8. The single-epoch ionosphere-float model is however shown too weak to expect successful instantaneous ambiguity resolution for both models, as the ADOPs exceed levels of one cycles for GPS and 0.5 cycles for GPS+BDS.

Nevertheless, by using a *Kalman filter* and treating the ambiguities as time-constant in the dynamic model (Table 7), we can achieve better ADOPs, as also depicted in Figure 8 at the second and fourth rows for GPS and GPS+BDS, respectively. The random walk process noise for the relative ZTD is used as well. Note that the ADOP is computed based on the Kalman filtered VCV-matrix of the ambiguities, thus as more time passes the stronger the model becomes (see Table 6) and the more precise the float ambiguities become. We therefore give a zoom-in for the first 60 epochs (30 minutes) to illustrate the time required to reach an ADOP level of 0.12 cycles.

The combined GPS+BDS system in Figure 8 reaches an ADOP level of 0.12 cycles quicker than GPS due to larger redundancy of the model. This is thus a promising first indication that faster successful ambiguity resolution is possible for the ionosphere-float model when using a combined system and as compared to GPS separately.

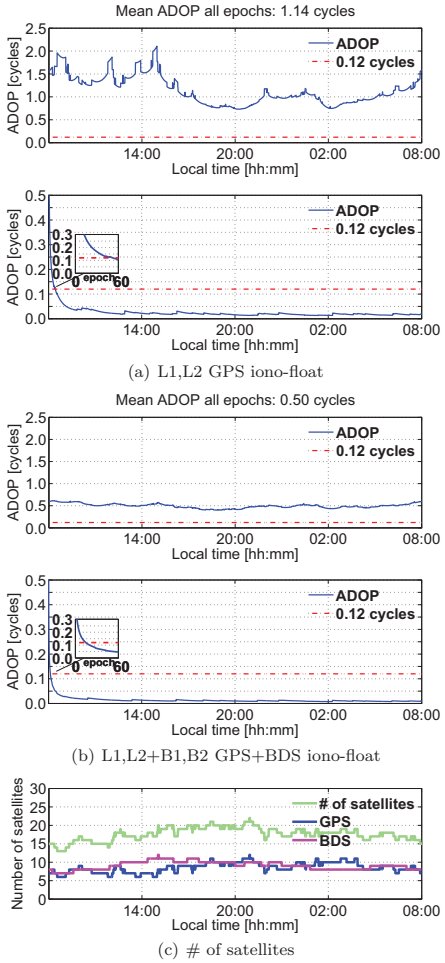

(a) L1,L2 GPS iono-float

(b) L1,L2+B1,B2 GPS+BDS iono-float

(c) # of satellites

Fig. 8 Ionosphere-float, ZTD-float (1): *single-epoch* ADOP time-series at *first* and *third row*, *Kalman filter* based ADOP (*blue*) at *second* and *fourth row*, all for single-baseline RTK and using 10° cut-off angle. February 19, 2014. **a** GPS, **b** GPS+BDS, **c** total # of satellites in *light green*

5.2 Bootstrapped success rate, time to first fix and positioning

In the previous section it was concluded that a Kalman filter with a dynamic model is needed for the ionosphere-float model to achieve successful ambiguity resolution. The formal bootstrapped success rate (SR) is an accurate lower bound to the integer least-squares (ILS) SR (Teunissen, 1998a, 1999). The SR criterion we will use follows as,

$$P\left[\check{z}_{IB}=z\right]=\prod_{i=1}^{n}\left[2\Phi\left(\frac{1}{2\sigma_{\hat{z}_{i|I}}}\right)-1\right]\geq P_0 \qquad (14)$$

where $P\left[\check{z}_{IB}=z\right]$ is the probability of correct integer estimation of the integer bootstrapped estimator $\check{z}_{IB}$, $\Phi\left(x\right)=\int_{-\infty}^{x}\frac{1}{\sqrt{2\pi}}exp\left(-\frac{1}{2}v^2\right)dv$ is the cumulative normal distribution, $\sigma_{\hat{z}_{i|I}}$ with $i=1,\ldots,n, I=1,\ldots,(i-1)$ the conditional STD of the decorrelated ambiguities, and P_0 a user-defined bootstrapped success criterion. In the following we will use $P_0=99.9\%$ as criterion to fix the ambiguities to integers, and if it is not fulfilled we take the float solution instead. The same criterion (14) is adopted before fixing the newly risen satellite's ambiguities to integers, to allow the float ambiguities to converge. The satellite is considered to rise when its elevation exceeds the user-defined elevation cut-off angle (e.g. 10°).

In the following results we will compute the time to first fix (TTFF) to fulfill the criterion in (14) for the dual-frequency ionosphere-float, ZTD-float model. The Kalman filter is initialized at the first-epoch, and for each additional epoch included in the Kalman filter the bootstrapped SR criterion is used. Once it reaches 99.9% we obtain the TTFF. Then we re-initialize the filter at the second epoch and the whole procedure is repeated again. The times given in Table 10 are the mean of all these TTFFs over February 19, 2014 and for a 10° elevation cut-off angle. The corresponding formal STDs in local North (N), East (E), Up (U) of the float and fixed solutions are also given. Since we use a dynamic model for the Kalman filter (Table 7), the ambiguity-float position STDs improve with respect to time.

Table 10 shows the improvement when going from ambiguity-float solutions with dm-level precision, to ambiguity-fixed solutions with mm-cm level precision, as well as the improvement which a combination of the systems brings. There is however no improvement for the ambiguity-float North and Up components in comparison to GPS. This is because the TTFFs in Table 10 are also different between GPS and GPS+BDS, with a value of 42 epochs vs 24 epochs, respectively, as required to obtain a bootstrapped SR of 99.9%. Thus when combining the systems we can potentially achieve faster availability to reliable ambiguity-fixed positioning precisions. Note finally in Table 10 that the East component experience larger improvements in comparison to the North and Up components when integer ambiguity fixing is applied, which is consistent with, e.g., Melbourne (1985) and Blewitt (1989).

Table 10 Formal STDs for ionosphere-float, ZTD-float (1) dual-frequency RTK and a cut-off angle of 10°, ambiguity float/fixed solutions in North, East and Up. The STDs are mean values of all formal STDs based on re-initializations of the Kalman filter during February 19, 2014 and when the bootstrapped SR criterion in (14) of 99.9% is fulfilled. The corresponding # of epochs needed is depicted as well

System/frequency	**Formal STDs float/fixed**			**# epochs**
	N [cm]	E [cm]	U [cm]	[30 s]
L1,L2 GPS	6/1.0	14/0.9	17/2.6	42
L1,L2+B1,B2 GPS+BDS	6/0.7	11/0.6	17/2.1	24

5.3 On the ambiguity-float positioning and the precision improvement by integer ambiguity resolution

The purpose of integer ambiguity resolution is to improve the other parameters, e.g., the receiver positions, by the integer constrains. However once the float ambiguities have converged to deterministic values, the ambiguity-float positions can also start to take advantage of the precise phase measurements. Thus the faster we are allowed to do integer ambiguity resolution the more will the other parameters be improved.

In Figure 9 the ambiguity-float (full lines) and ambiguity-fixed (dashed lines) formal position STDs are given, as a function of time. The procedure is similar to how the STDs in Table 10 were obtained, but instead of the bootstrapped SR criterion (14) to re-initialize the Kalman filter, a fixed window size of 10, 20, 40, 80, 120 epochs (30 s measurement interval), respectively, is used. The initialization of the filter is started at the first epoch and once the window size is reached the filter is re-initialized at the second epoch, and so on. This is done as to obtain information on how the ambiguity-float and ambiguity-fixed STDs vary as a function of the time accumulated in the Kalman filter. The presented STDs in Figure 9 are the mean of all these formal STDs over February 19, 2014. The North component is given as red, East as green, Up as blue color, and an elevation cut-off angle of 10° is used. The thin lines corresponds to the dual-frequency GPS ionosphere-float, ZTD-float model, and thick lines to the corresponding GPS+BDS model.

The ambiguity-float STDs in Figure 9 improve with respect to time. The STDs are also a factor of approximately square root of two more precise for GPS+BDS

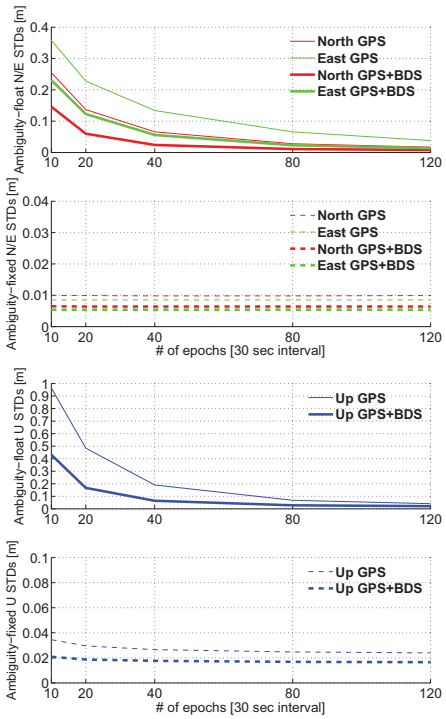

Fig. 9 Ionosphere-float, ZTD-float formal position STDs using a cut-off angle of 10°. The formal STDs are taken as a mean over all formal STDs computed based on re-initializations of the Kalman filter during February 19, 2014. Ambiguity-float STDs are depicted as full lines and ambiguity-fixed STDs as dashed lines

in comparison to GPS-only, since double the number of satellites is then used (Figure 3). It is also illustrated that the faster one is allowed to do successful ambiguity resolution, the more will the precision of the positions improve. For example consider the 20 epoch case where the ambiguity-float STDs (full lines) of the Up-component is approximately 0.5 meter for GPS and slightly below 0.2 meter for GPS+BDS, which improve to approximately 3 cm and 2 cm respectively for the ambiguity-fixed STDs (dashed lines). However when considering the TTFF in Table 10, only the combined GPS+BDS system have bootstrapped SRs of 99.9% after a convergence time of 24 epochs, whereas GPS-only requires 42 epochs. Moreover as time passes on, the less the improvements become. For example after 120 epochs (1 hour) are reached the ambiguity-float STDs are of almost similar magnitude to the ambiguity-fixed ones for both systems. Most importantly we can conclude from Figure 9 in combination with Table 10 that GPS+BDS can provide for shorter ambiguity-float positioning precision convergence times, and faster availability of reliable ambiguity-fixed positioning precisions, in comparison to GPS separately.

6 Empirical analysis of GPS+BDS long baseline RTK model

6.1 Positioning

In this section we compute empirically determined positioning errors by comparing the estimated positions to precise benchmark coordinates. The GEO satellites' ambiguities were not estimated as integers but kept as float parameters to still improve the model strength, due to site-dependent multipath effects in combination with the satellites being stationary (Wang et al, 2014). Systematic effects from the GEO satellites can thus not be mitigated over time and was shown to negatively affect the ambiguity resolution performance.

Table 11 provides the empirical float and correctly fixed ionosphere-float, ZTD-float positioning STDs for dual-frequency GPS-only and GPS+BDS. This is given for February 19, 2014 and a 10° elevation cut-off angle. The STDs were obtained by the re-initializations of the Kalman filter and the bootstrapped SR criterion (14), similar to the formal STDs in Table 10. The correctly fixed solutions are determined from a reference set of ambiguities. The reference ambiguities were estimated by using a dual-frequency combined GPS+BDS system, the ionosphere-float, ZTD-float model, fixed precise benchmark coordinates and an elevation cut-off angle of 10°. A Kalman filter over the entire observation time-span assuming the ambiguities time-constant and using the random walk process noise for the relative ZTD in Table 7 as dynamic model, was used.

Table 11 Empirical STDs for ionosphere-float, ZTD-float (1) dual-frequency RTK and an elevation cut-off angle of 10°, ambiguity float/correctly fixed solutions in North, East and Up. The STDs are based on re-initializations of the Kalman filter during February 19, 2014 and when the bootstrapped SR criterion in (14) of 99.9% is fulfilled. The corresponding # of epochs needed is depicted as well

System/frequency	STDs float/correctly fixed			# epochs
	N [cm]	E [cm]	U [cm]	[30 s]
L1,L2 GPS	7/0.8	18/0.9	20/3.4	42
L1,L2+B1,B2 GPS+BDS	8/0.7	19/0.7	22/3.4	24

The empirical STDs in Table 11 are overall in reasonable agreement with the formal precisions given in Table 10, with somewhat more optimistic formal STDs.

Note that the reason for the lack of improvements in the ambiguity-float positioning STDs when combining the two systems is the shorter TTFF.

6.2 Positioning for higher elevation cut-off angles

Since we found in Section 4 that higher than customary elevation cut-off angles can be used when combining the two systems, we will in the following focus on positioning results using a cut-off angle of 25° for the ionosphere-float model. We first depict in Figure 10 a snapshot of the formal ADOP time-series (blue) at top and the horizontal/vertical dilution of precision (HDOP/VDOP) (gray and black respectively) at bottom, all in support to better understand the empirical RTK positioning results in Figure 11. The L1,L2 GPS ionosphere-float, ZTD-float RTK model is given in the left column, and the corresponding L1,L2+B1,B2 GPS+BDS model is given in the right column. The number of satellites equal or above 5 is depicted in green, otherwise in red color, and is given at bottom. The Kalman filter is re-initialized at 15:30 local time as to illustrate two different convergence time periods, which is also the reason to the very large ADOPs at this time instance. We denote local times between 18:00-02:00 with a black rectangle as the time when GPS is deemed to have a reasonably good receiver-satellite geometry in comparison to other time instances over the day, as shown by the DOPs. The single gap in the GPS-only DOPs just after the re-initialization at 15:30 are due to a few instances when the number of satellites is smaller than four.

Note in Figure 10 the larger variation in the DOPs (particular the GPS VDOPs) as compared to the ADOPs that become more and more precise with respect to the time accumulated in the Kalman filter. This is because the ambiguities are assumed time-constant in the dynamic model, whereas the receiver positions are unlinked in time (Table 7). In Figure 10 we also see some fluctuations at the beginning of the day for the GPS ADOPs, due to the rising/setting and few number of satellites, whereas the combined GPS+BDS model is much less sensitive to these occurrences because of the larger redundancy. The Figure moreover illustrates some large excursions for the GPS VDOPs, particularly after 14:00 local time and before the Kalman filter is re-initialized (at 15:30). This is due to the poor GPS receiver-satellite geometry. The results in Figure 10 thus show, similar to Figure 5, that the performance of ambiguity resolution and positioning are not always united, since the ADOPs are well below the level of 0.12 cycles during this time. However once the number of satellites

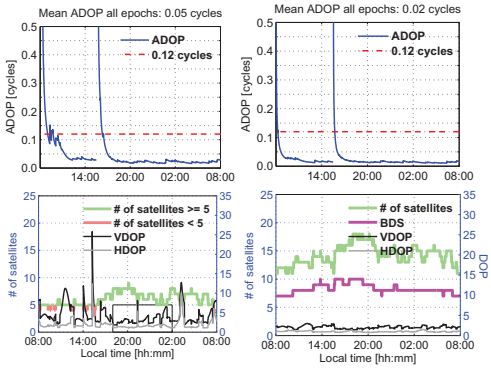

Fig. 10 Ionosphere-float, ZTD-float ADOP time-series (*blue*) at *top*, HDOP (*gray*) and VDOP (*black*) together with the # of satellites at *bottom*, using 25° cut-off angle. L1,L2 GPS is given in the *left column* and L1,L2+B1,B2 GPS+BDS in the *right column*. The Kalman filter is re-initialized at 15:30 local time. February 19, 2014. The time period denoted with a *black rectangle* is when the receiver-satellite geometry is deemed reasonably good for GPS

increases after the second (re-)initialization, the GPS-only DOPs in Figure 10 become overall smaller. More importantly, we see significant improvements when BDS is added to GPS, because of the increase in the number of satellites and improved receiver-satellite geometry. We namely obtain a positioning availability of 100%, smaller DOPs and much faster times to reach ADOPs below 0.12 cycles.

How the formal measures in Figure 10 translates into the corresponding empirical RTK positioning errors are depicted in Figure 11, where L1,L2 GPS is given in the left column and L1,L2+B1,B2 GPS+BDS in the right column. The correctly fixed solutions in green color were determined from the reference set of ambiguities, whereas the float solutions are depicted in gray color. Since ambiguity resolution is only attempted once the bootstrapped SR criterion (14) of 99.9% is fulfilled, we present the corresponding SR time-series in blue at bottom. The empirical RTK positioning results for GPS between 18:00-02:00 local time corresponding to the period of smaller DOPs in Figure 10, are given in Figure 12.

One can particularly see the large excursions of the GPS Up-component positioning errors in Figure 11 after 14:00 and before the Kalman filter is re-initialized at 15:30 local time, corresponding to the period with the largest VDOPs in Figure 10. When looking into Figure 12 we see that the GPS-only RTK positioning results are indeed better in comparison to other time periods of the day, because of the overall larger num-

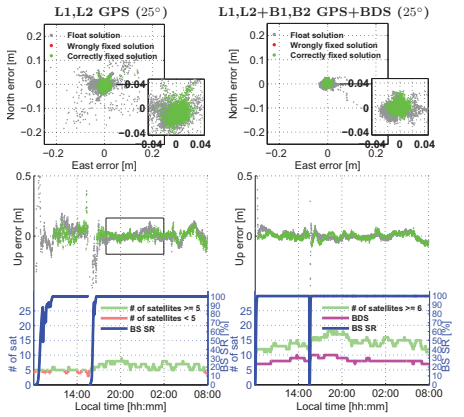

Fig. 11 *Top* ionosphere-float, ZTD-float (1) RTK using cut-off angle 25°: horizontal (N,E) scatterplots and vertical (U) time-series for L1,L2 GPS (*left column*) and L1,L2+B1,B2 GPS+BDS (*right column*). At *bottom* corresponding # of satellites and the bootstrapped (BS) SR in *blue*. The Kalman filter is re-initialized at 15:30 local time. February 19, 2014. The time period depicted in Figure 12 is denoted by a *black rectangle* for GPS. The TTFF to reach the bootstrapped SR criterion in (14) of 99.9% (2:nd initialization in brackets): 160.5 (70.5) min for GPS, and 21 (15) min for GPS+BDS

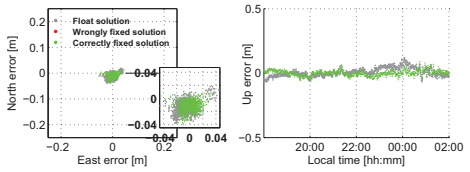

Fig. 12 18:00-02:00 local Perth time of ionosphere-float, ZTD-float (1) RTK using the cut-off angle 25°: horizontal (N,E) scatterplots and vertical (U) time-series for L1,L2 GPS. February 19, 2014

ber of satellites and better receiver-satellite geometry. Note also in Figure 12 that the precision of the fixed solutions resembles the precision of the float solutions because of the long time span that has been accumulated in the Kalman filter for this time period, allowing the ambiguity-float positions to also take advantage of the very precise phase measurements.

When combining GPS and BDS in Figure 11 the empirical positioning precisions are improved (significantly for the Up-component) in comparison to GPS separately, as also predicted by the DOPs in Figure 10. Moreover the ambiguity-float positions obtain a shorter convergence time, and the precise ambiguity-fixed positions become available earlier. We namely need 160.5 and 70.5 minutes as TTFF for GPS to reach a bootstrapped SR of 99.9%, for the first and second initialization respectively. Whereas the GPS+BDS RTK model only need 21 and 15 minutes respectively. The TTFF improvements for the second initializations are because of the overall larger number of tracked satellites as compared to the first initialization. In conclusion we have shown that higher than customary elevation cut-off angles can be used when combining the two systems.

7 Conclusions

In this contribution we studied the combination of single-/dual-frequency GPS with BDS for short (ionosphere-fixed), medium (ionosphere-weighted) and long (ionosphere-float) single-baseline RTK. The analysis was based on real GNSS data collected in Perth, Australia. We demonstrated that higher than customary satellite elevation cut-off angles can be used when combining the systems. This is of particular benefit in urban canyon environments or when low-elevation multipath is preferably avoided.

The analysis was divided into three parts. First we concluded by real data that single-frequency instantaneous RTK positioning is possible when one is allowed to use the ionosphere-fixed model and combine the two systems, whereas for GPS-only or the ionosphere-weighted model dual-frequencies are needed. The second part consisted of a formal analysis of the ionosphere-float model, consisting of instantaneous and Kalman-filter based ambiguity dilution of precisions (ADOPs), integer bootstrapped success rates, and positioning precisions. Their improvements with respect to the increasing number of epochs accumulated in the Kalman filter were illustrated as well. It was predicted that successful instantaneous RTK is not possible when using the ionosphere-float model, and thus a Kalman filter with a dynamic model is needed. The third part was an empirical analysis based on real GPS+BDS data. This analysis consisted of the empirical positioning precisions, as determined by comparing the estimated positions to precise benchmark coordinates.

The time to first fix (TTFF) was computed as the accumulated time necessary in the Kalman filter to reach an integer bootstrapped success rate of 99.9%. It was found that GPS+BDS can provide for significantly shorter TTFFs in comparison to GPS, and thus faster availability to reliable ambiguity-fixed positioning precisions at the mm-cm level. We also demonstrated that the combined system can give shorter convergence times for the ambiguity-float positions to reach a dm-level precision. The empirical positioning precisions were then shown to be in overall reasonable agreement with these

formal precisions, with the somewhat more optimistic formal standard deviations.

When looking into the use of an elevation cut-off angle of 25°, we demonstrated that GPS-only suffer from poor receiver-satellite geometries that can significantly spoil the empirical RTK positioning performance. By adding BDS to GPS, however, the overall positioning availability and performance was significantly improved, because of the increase in the number of satellites and stronger receiver-satellite geometry. It was finally concluded for the cut-off angle of 25° that the combined system also allows for shorter convergence of the ambiguity-float positions and much faster availability of precise ambiguity-fixed positioning.

Acknowledgements This work has been executed in the framework of the Positioning Program Project 1.01 "New carrier phase processing strategies for achieving precise and reliable multi-satellite, multi-frequency GNSS/RNSS positioning in Australia" of the Cooperative Research Centre for Spatial Information (CRC-SI). The second author is the recipient of an Australian Research Council (ARC) Federation Fellowship (project number FF0883188). All this support is gratefully acknowledged.

References

Blewitt G (1989) Carrier phase ambiguity resolution for the global positioning system applied to geodetic baselines up to 2000 km. J Geophys Res 94(B8) pp 10,187–10,203

Cao W, O'Keefe K, Cannon M (2008) Evaluation of COMPASS ambiguity resolution performance using geometric-based techniques with comparison to GPS and Galileo. In: Proc of the 21st Int Technical Meeting of the Satellite Division, Savannah, GA

Chen H, Huang Y, Chiang K, Yang M, Rau R (2009) The performance comparison between GPS and BeiDou-2/COMPASS: A perspective from Asia. Journal of the Chinese institute of engineers 32(5):679–689

CSNO (2013) BeiDou navigation satellite system signal in space interface control document: open service signal, version 2.0, China satellite navigation office. Tech. rep., available on the internet

Euler HJ, Goad CG (1991) On optimal filtering of GPS dual frequency observations without using orbit information. Bull Geod 65:130–143

Grelier T, Ghion A, Dantepal J, Ries L, DeLatour A, Issler JL, Avila-Rodriguez J, Wallner S, Hein G (2007) Compass signal structure and first measurements. In: Proc of ION GNSS-2007, Fort Worth, TX, pp 3015–3024

Melbourne W (1985) The case for ranging in GPS-based geodetic systems. In: Proceedings of 1st International Symposium on Precise Positioning with the Global Positioning System, Rockville, MD, USA, pp 373–386

Montenbruck O, Hauschild A, Steigenberger P, Hugentobler U, Teunissen PJG, Nakamura S (2013) Initial assessment of the COMPASS/BeiDou-2 regional navigation satellite system. GPS Solutions 17(2):211–222

Nadarajah N, Teunissen PJG, Sleewaegen JM, Montenbruck O (2014) The mixed-receiver BeiDou inter-satellite-type bias and its impact on RTK positioning. GPS Solutions doi:10.1007/s10291-014-0392-6

Odijk D (2002) Fast precise GPS positioning in the presence of ionospheric delays. PhD dissertation, Netherlands Geodetic Commission, Publications on Geodesy 264 pages

Odijk D, Teunissen PJG (2008) ADOP in closed form for a hierarchy of multi-frequency single-baseline GNSS models. J Geodesy 82:473–492

Odijk D, Teunissen PJG (2013) Characterization of between-receiver GPS-Galileo inter-system biases and their effect on mixed ambiguity resolution. GPS Solutions 17(4):521–533

Odolinski R, Teunissen PJG, Odijk D (2013) Quality analysis of a combined COMPASS/BeiDou-2 and GPS RTK positioning model. In: International Global Navigation Satellite Systems Society IGNSS symposium, Golden Coast

Odolinski R, Teunissen PJG, Odijk D (2014a) Combined BDS, Galileo, QZSS and GPS single-frequency RTK. GPS Solutions doi:10.1007/s10291-014-0376-6

Odolinski R, Teunissen PJG, Odijk D (2014b) Combined GPS+BDS+Galileo+QZSS for Long Baseline RTK Positioning. In: ION GNSS, Tampa, Florida, USA

Rao CR (1973) Linear statistical inference and its applications, 2nd edition. Wiley, New York

Saastamoinen J (1972) Contributions to the theory of atmospheric refraction. Bull Geod 105(1):279–298

Schaffrin B, Bock Y (1988) A unified scheme for processing GPS dual-band phase observations. Bull Geod 62:142–160

Schüler T (2001) On ground-based GPS tropospheric delay estimation. PhD dissertation, Universität der Bundeswehr, Munich, Germany 364 pages

Shi C, Zhao Q, Hu Z, Liu J (2013) Precise relative positioning using real tracking data from COMPASS GEO and IGSO satellites. GPS Solutions 17(1):103–119, doi:10.1007/s10291-012-0264-x

Teunissen PJG (1985) Generalized inverses, adjustment, the datum problem and S-transformations. In: Grafarend EW, Sanso F (eds) Optimization of geodetic networks Springer, Berlin, pp 11-55

Teunissen PJG (1990) An integrity and quality control procedure for use in multi sensor integration. In: Proc of ION GPS, CO, pp 513–522, also in: Vol VII of GPS Red Book Ser: Integr syst, ION Navig, 2012

Teunissen PJG (1995) The least squares ambiguity decorrelation adjustment: a method for fast GPS integer estimation. J Geodesy 70:65–82

Teunissen PJG (1997) A canonical theory for short GPS baselines. Part I: The baseline precision, Part II: The ambiguity precision and correlation, Part III: The geometry of the ambiguity search space, Part IV: Precision versus reliability. J Geodesy 71(6):320-336, 71(7):389-401, 71(8):486-501, 71(9):513-525

Teunissen PJG (1998a) Success probability of integer GPS ambiguity rounding and bootstrapping. J Geodesy 72:606–612

Teunissen PJG (1998b) The Ionosphere-weighted GPS baseline precision in canonical form. J Geodesy 72:107–117

Teunissen PJG (1999) An optimality property of the integer least-squares estimator. J Geodesy 73:587–593

Teunissen PJG, de Jonge P, Tiberius C (1996) The volume of the GPS ambiguity search space and its relevance for integer ambiguity resolution. In: Proc ION GPS, vol 9, pp 889–898

Teunissen PJG, Odijk D, Zhang B (2010) PPP-RTK: Results of CORS network-based PPP with integer ambiguity resolution. J Aeronaut, Astronaut and Aviat, Ser A 42(4):223–230

Teunissen PJG, Odolinski R, Odijk D (2014) Instantaneous BeiDou+GPS RTK positioning with high cut-off elevation angles. J Geodesy 88(4):335–350, doi:10.1007/s00190-013-0686-4

Wang G, Jong Kd, Zhao Q, Hu Z, Guo J (2014) Multipath analysis of code measurements for BeiDou geostationary satellites. GPS Solutions doi:10.1007/s10291-014-0374-8

Yang Y, Li J, Xu J, Tang J, Guo H, He H (2011) Contribution of the Compass satellite navigation system to global PNT users. Chinese Science Bulletin 56(26):2813–2819

REFERENCES

Astronautica Encyclopedia (2012) Beidou. Encyclopedia Astronautica. Available from: http://www.astronautix.com/craft/beidou.htm, (accessed 27 December 2012)

Axelrad P, Larson K, Jones B (2005) Use of the correct satellite repeat period to characterize and reduce site-specific multipath errors. Proceedings of ION GNSS, Long Beach, CA, 13–16 September 2005

Baarda W (1968) A testing procedure for use in geodetic networks. Netherlands Geodetic Commission, Publ. on Geodesy, New Series, vol. 2, no. 5, 1968

Blewitt G (1989) Carrier phase ambiguity resolution for the global positioning system applied to geodetic baselines up to 2000 km. J Geophysical Research, vol. 94, no.B8, p. 10187–10203

Boyd J (2014) Centimeter-scale GPS coming to Japan. Spectrum IEEE News, May 2014, url: http://ieeexplore.ieee.org/stamp/stamp.jsp?tp=&arnumber=6808446, (accessed 22 June, 2014)

Cao W, O'Keefe K, Cannon M (2008a) Evaluation of COMPASS ambiguity resolution performance using geometric-based techniques with comparison to GPS and Galileo. Proceedings of ION-GNSS-2008, Institute of Navigation, Savannah, GA, 16–19 September, p. 1688–1697

Cao C, Jing G, Luo M (2008b) COMPASS satellite navigation system development. PNT challenges and opportunities symposium. Stanford, California

Chen H, Huang Y, Chiang K, Yang M, Rau R (2009) The performance comparison between GPS and BeiDou-2/COMPASS: a perspective from Asia. J Chinese Institute of Engineers, vol. 32, no. 5, p. 679–689

CSNO (2011) BeiDou Navigation Satellite System Signal In Space Interface Control Document (Test Version) by China Satellite Navigation Office (CSNO). Technical report, December. 9 pages, 2011

CSNO (2012) BeiDou Navigation Satellite System Signal In Space Interface Control Document by China Satellite Navigation Office (CSNO). Open service signal B1I (Version 1.0). Technical report, 77 pages, 2012

CSNO (2013) BeiDou Navigation Satellite System Signal In Space Interface Control Document by China Satellite Navigation Office (CSNO). Open service signal (Version 2.0). Technical report, 82 pages, 2013

de Bakker PF, Tiberius CCJM, van der Marel H, van Bree RJP (2011) Short and zero baseline analysis of GPS L1 C/A, L5Q, GIOVE E1B, and E5aQ signals. GPS Solutions, vol. 16, no. 1, p. 53–64

Deng C, Tang W, Liu J, Shi C (2013) Reliable single-epoch ambiguity resolution for short baselines using combined GPS/BeiDou system. GPS Solutions. doi:10.1007/s10291-013-0337-5

ESA (2013) Galileo In-Orbit Validation. Fact sheet by European space agency (ESA), 2013

Euler HJ & Goad Cg (1991) On optimal filtering of GPS dual frequency observations without using orbit information. Bulletin Geodesique, vol. 65, p. 130–143

Feng Y & Li B (2010) Wide area real time kinematic decimetre positioning with multiple carrier GNSS signals. Science China Earth Sciences, vol. 53, no. 5, p. 731–740

Gibbons G (2013) GNSS News. Inside GNSS, p. 1

Goad C (1998) Short distance GPS models (Chap. 11). In: Teunissen PJG, Kleusberg A (eds) GPS for geodesy, 2nd edn. Springer, Berlin, p. 457–482

Grelier T, Ghion A, Dantepal J, Ries L, DeLatour A, Issler JL, Avila-Rodriguez J, Wallner S, Hein G (2007) Compass signal structure and first measurements. Proceedings of ION-GNSS-2007, Institute of Navigation, Fort Worth, TX, September, p. 3015–3024

Guo H, He H, Li J and Wang A (2011) Estimation and mitigation of the main errors for centimetre-level COMPASS RTK solutions over medium-long baselines. J Navigation, vol. 64, no. S1, p. S113–S126. doi:10.1017/S0373463311000324

Han C, Yang Y, Cai Z (2011) Beidou navigation satellite system and its time scales. Metrologia, vol. 48, no. 4, p. S213–S218. doi:10.1088/0026-1394/48/4/S13

He L, Ge M, Wang J, Wickert J, Schuh H (2013a) Experimental study on the precise orbit determination of the BeiDou navigation satellite system. Sensors vol. 13, no. 3, p. 2911–2928. doi:10.3390/s130302911

He H, Li J, Yang Y, Xu J, Guo H, Wang A (2013b) Performance assessment of single- and dual-frequency BeiDou/GPS single-epoch kinematic positioning. GPS Solutions. doi:10.1007/s10291-013-0339-3

Henkel P, Wen Z, Gunther C (2011) Method for determining code and phase biases of satellite signals. European Patent Application Applicant: Technische Universität Munchen, European patent office, 22 June 2011

Huang Y-S & Tsai M-L (2008) The impact of Compass/Beidou-2 on future GNSS: A perspective from Asia. Proceedings of ION GNSS, p. 2227–2238, Savannah, GA, September 2008

JAXA (2013) Japan Aerospace Exploration Agency (JAXA), navigation service interface specification for QZSS (IS-QZSS), V1.5 Tech. Rep., March 27, 2013

Jiang Y, Yang S, Zhang G, Li G (2011) Coverage performance analysis on combined GEO-IGSO satellite constellation. J Electronics, vol. 28, no. 2, p. 228-234

Klobuchar JA (1987) Ionospheric time-delay algorithm for single-frequency GPS users. IEEE Transactions on Aerospace and Electronic Systems, vol. AES-23, no. 3, p. 325–331

Langley RB (2011) Beidou/Compass declared operational, test ICD released. GPS World, GNSS News, Available from: http://www.gpsworld.com/, published 27 December 2011, accessed 28 December 2011

Li W, Teunissen PJG, Zhang B, Verhagen S (2013a) Precise point positioning using GPS and Compass observations. Sun et al (eds) Lect Notes in Electrical Engineering, Chap. 33, vol. 2, p. 367–378

Li X, Ge M, Zhang H, Nischan T, Wickert J (2013b) The GFZ real-time GNSS precise positioning service system and its adaption for COMPASS. J Advanced Space Research, vol. 51, no. 6, p. 1008–1018

Li J, Yang Y, Xu J, He H, Guo H, Wang A (2013c) Performance analysis of single-epoch dual-frequency RTK by BeiDou navigation satellite system. Sun et al (eds) Lecture notes in Electrical Engineering, Chap. 12, vol. 3, p. 133–143

Melbourne W (1985) The case for ranging in GPS-based geodetic systems. Proceedings of 1st International Symposium on Precise Positioning with the Global Positioning System, Rockville, MD, April 15-19, p. 373–386

Melgard T, Tegedor J, de Jong K, Lapucha D, Lachapelle G (2013) Interchangeable integration of GPS and Galileo by using a common system clock in PPP. Proceedings of ION-GNSS-2013, Institute of Navigation, Nashville, TN, 16–20 September, p. 1198–1206

Mirgorodskaya T (2013) GLONASS government policy, status and modernization plans. Proceedings of the International Global Navigation Satellite System Society (IGNSS) Symposium, Golden Coast, 16–18 July

Misra P & Enge P (2006) Global Positioning System: Signals, Measurements and Performance. Ganga-Jumana Press, Lincoln, MA.

Montenbruck O, Hauschild A, Hessels U (2011) Characterization of GPS/GIOVE sensor stations in the CONGO network. GPS Solutions, vol. 15, no. 3, p. 193–205

Montenbruck O, Hauschild A, Steigenberger P, Hugentobler U, Riley S (2012) A COMPASS for Asia: first experience with the BeiDou-2 regional navigation system. Proceedings of IGS Workshop, July 23–27, Olsztyn, Poland, 2012

Montenbruck O, Hauschild A, Steigenberger P, Hugentobler U, Teunissen PJG, Nakamura S (2013) Initial assessment of the COMPASS/BeiDou-2 regional navigation satellite system. GPS Solutions, vol. 17, no. 2, p. 211–222

Nadarajah N, Teunissen PJG, Raziq N (2013) BeiDou inter-satellite-type bias evaluation and calibration for mixed receiver attitude determination. Sensors, vol. 13, no. 7, p. 9435–9463

Nadarajah N, Teunissen PJG, Sleewaegen J-M, Montenbruck O (2014) The mixed-receiver BeiDou inter-satellite-type bias and its impact on RTK positioning. GPS Solutions. doi:10.1007/s10291-014-0392-6

Odijk D (2002) Fast precise GPS positioning in the presence of ionospheric delays. PhD dissertation, Netherlands Geodetic Commission, Publications on Geodesy, 264 pages

Odijk D, Teunissen PJG (2008) ADOP in closed form for a hierarchy of multi-frequency single-baseline GNSS models. J Geodesy, vol. 82, p. 473–492

Odijk D, Teunissen PJG (2013a) Characterization of between-receiver GPS-Galileo inter-system biases and their effect on mixed ambiguity resolution. GPS Solutions, vol. 17, no. 4, p. 521–533

Odijk D, Teunissen PJG (2013b) Estimation of differential inter-system biases between the overlapping frequencies of GPS, Galileo, BeiDou and QZSS. In:

4th International colloquium scientific and fundamental aspects of the Galileo programme, 4–6 December, Prague, Czech Republic

Odijk D, Teunissen PJG, Zhang B (2012) Single-frequency integer ambiguity resolution enabled precise point positioning. J Surveying Engineering, vol. 138, no. 4, p. 193–202

Odolinski R, Teunissen PJG, Odijk D (2013a) Quality analysis of a combined COMPASS/BeiDou-2 and GPS RTK positioning model. Proceedings of the International Global Navigation Satellite System Society (IGNSS) Symposium Golden Coast, Australia, July 16-18, 2013

Odolinski R, Teunissen PJG, Odijk D (2013b) Combined GPS, BeiDou, Galileo, and QZSS single-epoch, single-frequency RTK performance analysis. Proceedings of the International Association of Geodesy (IAG) symposium in Potsdam, Germany, September 1-6, 2013, accepted

Odolinski R, Teunissen PJG, Odijk D (2013c) An analysis of combined COMPASS/BeiDou-2 and GPS single- and multiple-frequency RTK positioning. Proceedings of the ION Pacific PNT, Honolulu, p. 69–90

Odolinski R, Teunissen PJG, Odijk D (2014a) First combined COMPASS/BeiDou-2 and GPS positioning results in Australia. Part I: single-receiver and relative code-only positioning. J Spatial Science, vol. 59, no. 1, p. 3-24. doi:10.1080/14498596.2013.840865

Odolinski R, Teunissen PJG, Odijk D (2014b) First combined COMPASS/BeiDou-2 and GPS positioning results in Australia. Part II: Single- and multiple-frequency single-baseline RTK positioning. J Spatial Science, vol. 59, no. 1, p. 25-46. doi:10.1080/14498596.2013.866913

Odolinski R, Teunissen PJG, Odijk D (2014c) Combined BDS, Galileo, QZSS and GPS single-frequency RTK. GPS Solutions. doi: 10.1007/s10291-014-0376-6

Odolinski R, Teunissen PJG, Odijk D (2014d) Combined GPS+BDS+Galileo+QZSS for Long Baseline RTK Positioning. Proceedings of ION GNSS, Tampa, Florida, USA, September 8-12, 2014

Odolinski R, Teunissen PJG, Odijk D (2014e) Combined GPS+BDS for short to long baseline RTK positioning. Measurement Science and Technology, accepted

Qu J, Yuan H, Zhang X, Ouyang G (2012) Single-epoch COMPASS carrier-phase ambiguous resolution using three civil frequencies and special constellations. Proceedings of ION GNSS, Nashville TN, September 17–21, 2012

Rao CR (1973) Linear Statistical Inference and its Applications. 2nd ed. Wiley, New York

Saastamoinen J (1972) Contributions to the theory of atmospheric refraction. Bulletin Geodesique, vol. 105, no. 1, p. 279–298

Schaffrin B & Bock Y (1988) A unified scheme for processing GPS dual-band phase observations. Bulletin Geodesique, vol. 62, p. 142–160

Schüler T (2001) On ground-based GPS tropospheric delay estimation. PhD dissertation, Universität der Bundeswehr, Munich, Germany, 2001. 364 pages

Shi C, Zhao Q, Li M, Tang W, Hu Z, Lou Y, Zhang H, Niu X, Liu J (2012) Precise orbit determination of Beidou Satellites with precise positioning. Science

China Earth Sciences, vol. 55, no. 7, p. 1079–1086. doi:10.1007/819s11430-012-4446-8

Shi C, Zhao Q, Hu Z, Liu J (2013) Precise relative positioning using real tracking data from COMPASS GEO and IGSO satellites. GPS Solutions, vol. 17, no. 1, p. 103–119. doi:10.1007/s10291-012-0264-x

Steigenberger P, Hauschild A, Hugentobler U, Montenbruck O (2012) Performance analysis of Compass orbit and clock determination and Compass only PPP. Proceedings of IGS Workshop, July 23–27, Olsztyn, Poland, 2012

Steigenberger P, Hugentobler U, Hauschild A, Montenbruck O (2013) Orbit and clock analysis of COMPASS GEO and IGSO satellites. J Geodesy, vol. 87, no. 6, p. 515–525. doi:10.1007/s00190-013-0625-4

Teunissen PJG (1985) Generalized inverses, adjustment, the datum problem and S-transformations. In: Grafarend EW, Sanso F (eds) Optimization of geodetic networks. Springer, Berlin, p. 11–55

Teunissen PJG (1990) An integrity and quality control procedure for use in multi sensor integration. Proceedings of ION-GPS-1990, Colorado Spring, CO, p. 513–522, also published in: vol. VII of GPS Red Book Series: Integrated systems, ION Navigation, 2012

Teunissen PJG (1995) The least squares ambiguity decorrelation adjustment: a method for fast GPS integer estimation. J Geodesy, vol. 70, p. 65–82

Teunissen PJG (1997) A canonical theory for short GPS baselines. Part I: the baseline precision, Part II: the ambiguity precision and correlation, Part III: the geometry of the ambiguity search space, Part IV: precision versus reliability. J Geodesy, vol. 71, no. 6, p. 320–336, vol. 71, no. 7, p. 389–401, vol. 71, no. 8, p. 486–501, vol. 71, no. 9, p. 513–525

Teunissen PJG (1998a) Success probability of integer GPS ambiguity rounding and bootstrapping. J Geodesy, vol. 72, p. 606–612

Teunissen PJG. (1998b) Minimal detectable biases of GPS data. J Geodesy, vol. 72, p. 236-244

Teunissen PJG (1998c) On the integer normal distribution of the GPS ambiguities. Artifical Satellites, vol. 33, no. 2, p. 49–64

Teunissen PJG (1998d) The Ionosphere-weighted GPS baseline precision in canonical form. J Geodesy, vol. 72, p. 107–117

Teunissen PJG (1999) An optimality property of the integer least-squares estimator. J Geodesy, vol. 73, p. 587–593

Teunissen PJG (2002) The parameter distributions of the integer GPS model. J Geodesy, vol. 76, no. 1, p. 41–48

Teunissen PJG (2003) Adjustment Theory – An Introduction, Series on Mathematical Geodesy and Positioning, Faculty of Aerospace Engineering, Delft University of Technology, the Netherlands

Teunissen PJG (2006) Testing theory - an introduction. Series on Mathematical Geodesy and Positioning, Delft University of Technology, 2006, the Netherlands

Teunissen PJG & Kleusberg A, eds. (1998) GPS for Geodesy: Second Completely Revised and Extended Edition, Springer-Verlag, Berlin

Teunissen PJG & Verhagen S (2009) The GNSS ambiguity ratio-test revisited: a better way of using it. Survey Review, vol. 41, no. 312, p. 138–151

Teunissen PJG, de Jonge P, Tiberius CCJM (1996) The volume of the GPS ambiguity search space and its relevance for integer ambiguity resolution. Proceedings of ION-GPS-1996, vol. 9, p. 889–898

Teunissen PJG, Simons DG, Tiberius CCJM (2008) Probability and Observation Theory. Lecture Notes AE2-E01, Faculty of Aerospace Engineering, Delft University of Technology, 2008, the Netherlands

Teunissen PJG, Odijk D, Zhang B (2010) PPP-RTK: results of CORS network-based PPP with integer ambiguity resolution. J Aeronautics Astronautics Aviation Series A, vol. 42, no. 4, p. 223–230

Teunissen PJG, Odolinski R, Odijk D (2014) Instantaneous BeiDou+GPS RTK positioning with high cut-off elevation angles. J Geodesy, vol. 88, no. 4, p. 335-350. doi:10.1007/s00190-013-0686-4

Verhagen S & Teunissen PJG (2013a) The ratio test for future GNSS ambiguity resolution. GPS Solutions, vol. 17, no. 4, p. 535–548

Verhagen S & Teunissen PJG (2013b) Ambiguity resolution performance with GPS and BeiDou for LEO formation flying. J Advance Space Resesearch http://dx.doi.org/10.1016/j.asr.2013.03.007

Verhagen S, Li B, Teunissen PJG (2013) Ps-LAMBDA: Ambiguity success rate evaluation software for interferometric applications. Computers and Geosciences, vol. 54, p. 361–376

Wang G, Jong K d, Zhao Q, Hu Z, Guo J (2014) Multipath analysis of code measurements for BeiDou geostationary satellites. GPS Solutions. doi:10.1007/s10291-014-0374-8

Yang Y, Li J, Xu J, Tang J, Guo H, He H (2011) Contribution of the Compass satellite navigation system to global PNT users. Chinese Science Bulletin, vol. 56, no. 26, p. 2813–2819

Yang Y, Li J, Wang A, Xu J, He H, Guo H, Shen J, Dai X (2014) Preliminary assessment of the navigation and positioning performance of BeiDou regional navigation satellite system. Science China Earth Sciences, vol. 57, no. 1, p. 144–152

Zhang B, Teunissen PJG, Odijk D (2011) A novel un-differenced PPP-RTK concept. J Navigation, vol. 64, no. S1, p. S180–S191. doi:10.1017/S0373463311000361

Zhang S, Guo J, Li B, Rizos C (2010) An analysis of satellite visibility and relative positioning precision of COMPASS. Proceedings of Symposium for Chinese Professionals in GPS, Shanghai, China, 18–20 August, p. 41–46

APPENDIX A COPYRIGHT PERMISSION STATEMENTS

I warrant that I have obtained, where necessary, permission from the copyright owners to use any third-party copyright material reproduced in this thesis, or to use any of my own published work (e.g. journal articles) in which the copyright is held by another party (e.g. publisher, co-author). These permissions are all attached below

Robert Odolinski

1) **Odolinski R**, Teunissen PJG, Odijk D (2014a) First combined COMPASS/BeiDou-2 and GPS positioning results in Australia. Part I: single-receiver and relative code-only positioning. Journal of Spatial Science, vol. 59, no. 1, p. 3-24. doi:10.1080/14498596.2013.840865,
2) **Odolinski R**, Teunissen PJG, Odijk D (2014b) First combined COMPASS/BeiDou-2 and GPS positioning results in Australia. Part II: Single- and multiple-frequency single-baseline RTK positioning. Journal of Spatial Science, vol. 59, no. 1, p. 25-46. doi:10.1080/14498596.2013.866913:

Journal of Spatial Science, publisher Taylor and Francis,
http://journalauthors.tandf.co.uk/copyright/assignmentAndYourRights.asp
"the right to include an article in a thesis or dissertation that is not to be published commercially, provided that acknowledgment to prior publication in the journal is made explicit"

3) **Odolinski R**, Teunissen PJG, Odijk D (2013a) Quality analysis of a combined COMPASS/BeiDou-2 and GPS RTK positioning model. In Proceedings of the International Global Navigation Satellite System Society (IGNSS) Symposium Golden Coast, Australia, July 16-18, 2013:

Robert Odolinski

From: Krys Henshaw <krys@ignss.org>
Sent: Monday, 16 June 2014 11:39 AM
To: Robert Odolinski
Subject: RE: Request for permission of copyright for paper 68 at IGNSS 2013 for PhD thesis RE: IGNSS 2013 - Proceedings and Plenary Powerpoints

Robert:

Permission granted – that is fine
All the best with your thesis

Krys Henshaw
IGNSS Society Inc
PO Box 413
Tweed Heads NSW 2485
Tel: + 61 7 5599 5007
Fax: + 61 7 55 366 366
www.ignss.org
krys@ignss.org

From: Robert Odolinski [mailto:Robert.Odolinski@curtin.edu.au]
Sent: Monday, 9 June 2014 4:30 PM
To: Krys Henshaw
Subject: Request for permission of copyright for paper 68 at IGNSS 2013 for PhD thesis RE: IGNSS 2013 - Proceedings and Plenary Powerpoints

Dear Krys and IGNSS committee,

Attached is a permission of copyright for inserting a paper into my doctoral thesis at Curtin University. It is my understanding that you/your organisation holds copyrights in the following material:

Odolinski R, Teunissen PJG, Odijk D (2013): Quality Analysis of a Combined COMPASS/BeiDou-2 and GPS RTK Positioning Model. In Proc of *International Global Navigation Satellite System (IGNSS) Society Symposium*, Golden Coast, Australia, July 16-18, 2013. **Paper 68** and in the peer-reviewed section.

I would like to reproduce an extract of this work in a doctoral thesis which I am currently undertaking at Curtin University in Perth, Western Australia. The subject of my research is Multi-GNSS precise positioning. I am carrying out this research in my own right and have no association with any commercial organisation or sponsor. The procedure for the doctoral thesis by publication I am writing is to insert the full paper. Once completed, the thesis will be made available in hard-copy form in the Curtin Library and in digital form on the Internet via the Australasian Digital Thesis Program. The material will be provided strictly for educational purposes and on a non-commercial basis. Further information on the ADT program can be found at http://adt.caul.edu.au

I would be most grateful for your consent to the copying and communication of the work as proposed. If you are willing to grant this consent, please complete and sign the attached approval slip and return it to me at the address shown. Full acknowledgement of the ownership of the copyright and the source of the material will be provided with the material. I would be willing to use a specific form of acknowledgement that you may require and to communicate any conditions relating to its use.

If you are not the copyright owner of the material in question, I would be grateful for any information you can provide as to who is likely to hold the copyright.

If you have a scanner I would be happy if you could sign and return the form to,
robert.odolinski@curtin.edu.au

If you do not own a scanner I can mail you this form together with stamps and envelope to return it to,
Robert Odolinski, 51 Etwell Street, East Victoria Park, 6101 WA, Perth.

I look forward to hearing from you and thank you for consideration of my request,

With best regards Robert Odolinski

4) Teunissen PJG, **Odolinski R**, Odijk D (2014) Instantaneous BeiDou+GPS RTK positioning with high cut-off elevation angles. Journal of Geodesy, vol. 88, no. 4, p. 335-350. doi:10.1007/s00190-013-0686-4:

Format	Print and Electronic
Will you be translating?	No
Print run	20
Author of this Springer article	Yes and you are the sole author of the new work
Order reference number	None
Title of new book	Multi-GNSS Integer Ambiguity Resolution Enabled Precise Positioning
Author of new book	Robert Odolinski
Expected publication date of new book	Nov 2014
Estimated size of new book (pages)	100
Total	0.00 USD

Terms and Conditions

No Amendment Except in Writing
This license may not be amended except in a writing signed by both parties (or, in the case of Springer Science + Business Media, by CCC on Springer Science + Business Media's behalf).

Objection to Contrary Terms
Springer Science + Business Media hereby objects to any terms contained in any purchase order, acknowledgment, check endorsement or other writing prepared by you, which terms are inconsistent with these terms and conditions or CCC's Billing and Payment terms and conditions. These terms and conditions, together with CCC's Billing and Payment terms and conditions (which are incorporated herein), comprise the entire agreement between you and Springer Science + Business Media (and CCC) concerning this licensing transaction. In the event of any conflict between your obligations established by these terms and conditions and those established by CCC's Billing and Payment terms and conditions, these terms and conditions shall control.

Jurisdiction
All disputes that may arise in connection with this present License, or the breach thereof, shall be settled exclusively by the country's law in which the work was originally published.

Other terms and conditions:

v1.3

If you would like to pay for this license now, please remit this license along with your payment made payable to "COPYRIGHT CLEARANCE CENTER" otherwise you will be invoiced within 48 hours of the license date. Payment should be in the form of a check or money order referencing your account number and this invoice number 501325392. Once you receive your invoice for this order, you may pay your invoice by credit card. Please follow instructions provided at that time.

Make Payment To:
Copyright Clearance Center
Dept 001
P.O. Box 843006
Boston, MA 02284-3006

For suggestions or comments regarding this order, contact RightsLink Customer Support:customercare@copyright.com or +1-877-622-5543 (toll free in the US) or +1-978-646-2777.

Gratis licenses (referencing $0 in the Total field) are free. Please retain this printable license for your reference. No payment is required.

5) **Odolinski R**, Teunissen PJG, Odijk D (2013b) Combined GPS, BeiDou, Galileo, and QZSS single-epoch, single-frequency RTK performance analysis. In Proceedings of the International Association of Geodesy (IAG) symposium in Potsdam, Germany, September 1-6, 2013, accepted:

Robert Odolinski

From: Essenpreis, Alice, Springer DE <Alice.Essenpreis@springer.com> on behalf of Permissions Heidelberg, Springer DE <Permissions.Heidelberg@springer.com>
Sent: Monday, 16 June 2014 10:16 PM
To: Robert Odolinski
Subject: WG: Request for permission of copyright for paper, who to contact? IAGS: Your manuscript entitled Combined GPS, BeiDou, Galileo, and QZSS single-epoch, single-frequency RTK Performance Analysis
Attachments: IAG.pdf

Hello,

Thank you for your e-mail.

Springer is pleased to announce our partnership with Copyright Clearance Center to meet your licensing needs.

With Copyright Clearance Center's Rightslink® service it's faster and easier than ever before to secure permission from Springer journal titles to be republished in a secure intranet site, restricted internet site, CD-ROM/DVD, journal (print/online), book (hardcopy or electronic), coursepack, e-reserve, doctoral thesis, research project, magazine, newsletter, directory, newspaper, brochure/pamphlet, presentation, or photocopies/handouts.

Simply visit: http://www.link.springer.com and locate your desired content: http://link.springer.com/article/10.1007/s10291-014-0376-6

Go to the article's abstract and click on "Reprints and Permissions" (in the section "Other Actions"):

1. Select the way you would like to reuse the content
2. Create an account if you haven't already
3. Accept the terms and conditions and you're done!

For questions about using the Rightslink service, please contact Customer Support via phone 877/622-5543 (toll free) or 978/777-9929, or email customercare@copyright.com

Kind regards,

Springer
Permissions.Heidelberg@springer.com

-------- Message original --------
Sujet: Request for permission of copyright for paper, who to contact? IAGS: Your manuscript entitled Combined GPS, BeiDou, Galileo, and QZSS single-epoch, single-frequency RTK Performance Analysis
Date : Mon, 9 Jun 2014 06:46:32 +0000
De : Robert Odolinski <Robert.Odolinski@curtin.edu.au>
Pour : Pascal Willis <willis@ipgp.fr>

Dear Dr Pascal Willis,

As I am aware of there is still quite some time before the IAG proceedings from 2013 will be available online. This means that any permissions to use this paper in my Doctoral thesis with due date in August cannot be made online by using Springer Rightslink.

I therefore wonder if you know who I can submit the attached Copyright request form to sign for permission to put the paper into my thesis?

With best regards Robert Odolinski

6) **Odolinski R**, Teunissen PJG, Odijk D (2014c) Combined BDS, Galileo, QZSS and GPS single-frequency RTK. GPS Solutions. doi: 10.1007/s10291-014-0376-6:

SPRINGER LICENSE
TERMS AND CONDITIONS

Jun 11, 2014

This is a License Agreement between Robert Odolinski ("You") and Springer ("Springer") provided by Copyright Clearance Center ("CCC"). The license consists of your order details, the terms and conditions provided by Springer, and the payment terms and conditions.

All payments must be made in full to CCC. For payment instructions, please see information listed at the bottom of this form.

License Number	3405841496612
License date	Jun 11, 2014
Licensed content publisher	Springer
Licensed content publication	GPS Solutions
Licensed content title	Combined BDS, Galileo, QZSS and GPS single-frequency RTK
Licensed content author	Robert Odolinski
Licensed content date	Jan 1, 2014
Type of Use	Book/Textbook
Requestor type	Publisher
Publisher	Not listed below
Portion	Full text
Format	Print and Electronic
Will you be translating?	No

Print run	20
Author of this Springer article	Yes and you are the sole author of the new work
Order reference number	None
Title of new book	Multi-GNSS Integer Ambiguity Resolution Enabled Precise Positioning
Author of new book	Robert Odolinski
Expected publication date of new book	Nov 2014
Estimated size of new book (pages)	100
Total	0.00 USD

Terms and Conditions

Springer Science + Business Media hereby objects to any terms contained in any purchase order, acknowledgment, check endorsement or other writing prepared by you, which terms are inconsistent with these terms and conditions or CCC's Billing and Payment terms and conditions. These terms and conditions, together with CCC's Billing and Payment terms and conditions (which are incorporated herein), comprise the entire agreement between you and Springer Science + Business Media (and CCC) concerning this licensing transaction. In the event of any conflict between your obligations established by these terms and conditions and those established by CCC's Billing and Payment terms and conditions, these terms and conditions shall control.

Jurisdiction
All disputes that may arise in connection with this present License, or the breach thereof, shall be settled exclusively by the country's law in which the work was originally published.

Other terms and conditions:

v1.3

If you would like to pay for this license now, please remit this license along with your payment made payable to "COPYRIGHT CLEARANCE CENTER" otherwise you will be invoiced within 48 hours of the license date. Payment should be in the form of a check or money order referencing your account number and this invoice number 501325380. Once you receive your invoice for this order, you may pay your invoice by credit card. Please follow instructions provided at that time.

Make Payment To:
Copyright Clearance Center
Dept 001
P.O. Box 843006
Boston, MA 02284-3006

For suggestions or comments regarding this order, contact RightsLink Customer Support:customercare@copyright.com or +1-877-622-5543 (toll free in the US) or +1-978-646-2777.

Gratis licenses (referencing $0 in the Total field) are free. Please retain this printable license for your reference. No payment is required.

7) **Odolinski R**, Teunissen PJG, Odijk D (2014d) Combined GPS+BDS+Galileo+QZSS for Long Baseline RTK Positioning. In Proceedings of the Institute of Navigation (ION) GNSS, Tampa, Florida, USA, September 8-12, 2014:

THE INSTITUTE OF NAVIGATION

COPYRIGHT RELEASE FORM

ION PROCEEDINGS

Signing of "Statement A" or "Statement B" is required except that employees of governments other than the U.S. Government may submit equivalent statements. It is essential that The Institute of Navigation (ION) and its agents or assignees have the right of publication and reproduction.

Proceedings to Appear in: **ION GNSS+ 2014**

Session Number & Title: _____

Paper Title *(exactly as it appears on the paper)*: _____

_____

Author(s) & Affiliation(s) *(in the exact order they appear on the paper)*: _____

_____

Primary Author Address: _____

_____

Phone/Fax/E-Mail: _____

STATEMENT A:
The undersigned "Copyright Owner," desiring to publish a paper (the "Paper") in ION Proceedings and/or through other publications of The Institute of Navigation ("ION"), hereby grants to ION the following rights in exchange for good and valuable consideration:

1.) the exclusive, royalty-free right of first publication of the above Paper throughout the world as part of the proceedings named above and;
2.) a non-exclusive, perpetual, royalty-free, worldwide license to reprint and/or provide in electronic format the above Paper, either in excerpt, in summary, or in completed form, for free or in exchange for a fee.

Copyright Owner reserves all rights not specifically granted to ION herein and has the right after the Paper has been published, to reprint the Work in any publication, provided that the terms of such republication do not conflict with this license. Copyright Owner agrees to include the proper credit to ION for prior publication of the Paper in any reprint of the Paper in a publication, including date (month and year) and location (city and state) of the meeting at which the paper was presented.

Copyright Owner warrants that the Paper is original with him/her, that its publication will not infringe the rights of others, that the Paper is factually accurate and contains no defamatory or otherwise unlawful material, and that Copyright Owner has full power to make this agreement. Copyright Owner further warrants that the Paper has not been published elsewhere in whole or in part (except as set out in a rider attached thereto if applicable) and that no agreement to publish the Paper or any part or version thereof is outstanding. Should the Paper contain any material which requires permission for inclusion in the Paper, Copyright Owner agrees to obtain such permission in writing and provide a copy of such permission to ION.

1. _____ _____
PRIMARY AUTHOR'S SIGNATURE EMPLOYER FOR WHOM WORK WAS PERFORMED

_____ _____
AUTHORIZED SIGNATURE DATE FORM SIGNED

STATEMENT B:
This will certify that all authors of the above Paper are employees of the U.S. Government and that the authors created the Paper as part of their employment and that the Paper is therefore not subject to U.S. Copyright protection.

2. _____ _____
PRIMARY AUTHOR'S SIGNATURE EMPLOYER FOR WHOM WORK WAS PERFORMED

_____ _____
AUTHORIZED SIGNATURE DATE FORM SIGNED

Crown Copyright Certification (where applicable)

This will certify that all authors of the Work are employees of the British or applicable Commonwealth Government and prepared the Work in connection with their official duties. As such, the Work is subject to Crown Copyright and is not assigned to the ION as set forth above. The Undersigned acknowledges, however, that the ION has the right to publish, distribute and reprint the Work in all forms and media.

3._____ _____
AUTHORIZED SIGNATURE DATE FORM SIGNED

(Authors who are British or applicable Commonwealth Government employees should also sign line (1) above to indicate their acceptance of all terms other than the copyright transfer.)

8) **Odolinski R**, Teunissen PJG, Odijk D (2014e) Combined GPS+BDS for short to long baseline RTK positioning. Measurement Science and Technology, accepted:

Measurement Science and Technology

Form Completion

Follow the instructions below to submit the form. You can either click the "Save as Draft" button to save your work and return to it later, or click the "Submit" button to submit the form to the journal. If you have any questions or concerns, please email copyright@iop.org quoting your article reference number.

IMPORTANT INFORMATION – YOU WILL BE AGREEING TO TRANSFER YOUR COPYRIGHT IN THE ARTICLE

The wording below sets out the terms and conditions under which the authors and/or owners will transfer or license the copyright in their article. Please read it carefully and then tick the appropriate box to confirm the basis upon which you are submitting your article.

- If you wish your article to be published on a **subscription publication** basis, the Subscription Copyright Assignment outlined in **Part 1** of this agreement will apply.
- If you wish your article to be published on a **Gold Open Access** basis, for which an Article Publication Charge applies, the Open Access Copyright Assignment outlined in **Part 2** of this agreement will apply.
- If you do not own the copyright in your article because, for example, it was prepared as part of your duties as an employee, this agreement must be submitted by the owner of the copyright. If this is the case, the owner, or an authorised signatory of the owner, must enter their name in the "name of copyright owner(s)" section and the Submitting Author should also enter their name where indicated.
- If there are several Named Authors, one author (the Submitting Author) should submit the form on behalf of their co-authors in a representative capacity.

Assignment of copyright and publication agreement

IOP Publishing Limited ("IOP") agrees to publish:

Manuscript Title: Combined GPS+BDS for short to long baseline RTK positioning (the "Article") written by

Names of all authors: Odolinski, Robert; Teunissen, P; Odijk, Dennis ("the Named Authors") in the following journal Measurement Science and Technology ("the Journal")

Name of copyright owner(s) (if not the Named Author(s) – see Important Information above):

Curtin University **("the Institution")**

IOP Ref: MST-101654

Part 1 - Subscription Copyright Assignment

Assignment of copyright

1.1 In consideration for acceptance and publication of the Article, the Named Authors of the Article and/or the Institution hereby assign, where necessary by present assignment of future copyright, to IOP with full title guarantee the entire copyright in all original material published as part of the Article (which expression includes but is not limited to the text, abstract, tables, figures and graphs, related corrigenda or "comments" and multimedia content but excludes any other item referred to as supplementary material) throughout the world for the full term of copyright (including any extensions or renewals thereof) for all media and formats, whether known or unknown. Such assignment shall be effective only if the Article (or any resubmission of the Article) is accepted for publication. For the avoidance of doubt, copyright does not subsist in any fundamental data underlying the Article and nothing in this agreement is intended to limit access to or use of such data.

1.2 If the Article, or any part of it, is protected by Crown Copyright, in consideration for acceptance and publication of the Article, the relevant Named Authors and the relevant originating department or agency hereby grant IOP a royalty-free worldwide freely-transferrable licence for the full term of copyright (including any extensions or renewals thereof) for all media and formats, whether known or unknown, to do in relation to the Article all acts restricted by copyright worldwide including, but not limited to, the right of action under section 101A of the Copyright Designs and Patents Act 1988. Such licence shall be effective only if the Article is accepted for publication and shall be exclusive to IOP for a period of twelve calendar months following the date of online publication of the Article. Thereafter, the licence shall be non-exclusive.

1.3 In consideration for acceptance and publication of the Article, the Named Authors and/or the Institution hereby grant IOP a royalty-free non-exclusive worldwide freely transferrable licence for the full term of copyright (including any extensions or renewals thereof) to do in relation to any supplementary material not deemed to be part of the Article and/or any video abstract all acts restricted by copyright worldwide. This shall include, but not be limited to, making the material available under any licence that IOP deems appropriate for purposes including, but not limited to, the maximisation of visibility and the long term preservation of the content.

1.4 Each of the Named Authors consents to the publication and processing by IOP of their email addresses.

Representations and warranties

2.1 The Institution and/or the Submitting Author on behalf of the Named Authors (as appropriate) represent and warrant that:

2.1.1 the Article is the original work of the Named Authors;

2.1.2 the Article has not been published previously in any form, other than as part of the Named Authors' research theses or dissertations (which fact has been notified to IOP in writing) or as a preprint, for example on the arXiv.org service;

2.1.3 each of the Named Authors has made a material contribution to the conception and/or writing of the Article, has received the final version of the Article, has agreed to its submission on the terms contained herein and takes responsibility for it and submission has been approved as necessary by the authorities at the establishment where the research was carried out;

2.1.4 the Submitting Author completes and returns this agreement as authorised agent for and on behalf of all the Named Authors and has the full power to enter into this agreement and to make the grants and assignments it contains;

2.1.5 the Article has not been and shall not be submitted to another publisher prior to withdrawal or rejection by IOP;

2.1.6 the Article does not infringe any third party rights, it contains nothing libellous or unlawful, all factual statements are to the best of the Named Authors' knowledge true or based on valid research conducted according to accepted norms and all required permissions have been obtained in writing;

2.1.7 the Article expressly acknowledges any third party funding and/or potential conflicts of interest; and

2.1.8 any supplementary material or video abstract is the original work of the Named Authors, or is the property of the Institution, or permission has been obtained from its owner(s) for its publication by IOP and permission has been obtained for the inclusion of any third party content (including music).

2.2 The Named Authors and/or the Institution (as appropriate) indemnify and will keep indemnified IOP against all costs and expenses suffered or incurred by IOP as a result of and/or arising out of any breach of the representations and/or warranties in this section 2.

The Named Authors' rights

3.1 IOP grants the Named Authors the rights specified in paragraphs 3.2 and 3.3. All such rights must be exercised solely for non-commercial purposes. Where possible, any use should display citation information and IOP's copyright notice, and, for electronic use, best efforts must be made to include a link to the online abstract in the Journal.

Exercise of the rights in paragraph 3.2 may use the version of the Article published in the Journal ("Final Published Version").

Exercise of the rights referred to in paragraph 3.3 must not use the Final Published Version and extend only to the Named Authors' own format (which may include amendments made following peer review but not any editing, typesetting or other changes made by IOP) (the "Accepted Manuscript") and must be accompanied by the following statement of provenance:

'This is an author-created, un-copyedited version of an article accepted for publication in Measurement Science and Technology. IOP Publishing Ltd is not responsible for any errors or omissions in this version of the manuscript or any version derived from it. The Version of Record is available online at [insert DOI].'

3.2 The rights are:

3.2.1 To make copies of the Article (all or part) for teaching purposes;

3.2.2 To include the Article (all or part) in a research thesis or dissertation;

3.2.3 To make oral presentation of the Article (all or part) and to include a summary and/or highlights of it in papers distributed at such presentations or in conference proceedings; and

3.2.4 To use figures and text from the Article falling within the quota outlined in the STM Permissions Guidelines (http://www.stm-assoc.org/permissions-guidelines/) at the relevant time in force.

For the avoidance of doubt, the Named Authors retain all proprietary rights in the Article other than copyright.

3.3 Additional rights of the Named Authors are to:

3.3.1 Use the Accepted Manuscript (all or part) without modification in personal compilations of the Named Authors' own works (provided not created by a third party publisher); and

3.3.2 Include the Accepted Manuscript (all or part) on the Named Authors' own personal website(s), institutional website(s) and third party websites in accordance with the Author Rights set out at the following url legal.ioppublishing.org/author-rights on the date of submission of this agreement.

Miscellaneous

4. To the extent that there are moral rights in the Article, all the Named Authors expressly reserve and assert their moral rights to be identified as the authors of the Article.

5. The Named Authors and/or the Institution shall execute such further documents, and take such actions and do such things, as may be requested by IOP at IOP's reasonable expense to give full effect to the terms of this agreement.

6. For the avoidance of doubt, the grants and assignment envisaged herein shall become effective only upon acceptance of the Article for publication. In the event that the Article is withdrawn prior to acceptance, or is rejected, this agreement shall have no effect and no party shall be bound by it.

7. This agreement shall be governed by English Law and subject to the non-exclusive jurisdiction of the English courts.

Confirmation

8. By typing the Submitting Author's name into the box at Part 3 below and clicking "Submit", the Named Authors agree to these terms. Authorised signatories of any third party copyright owner(s) agree, on behalf of such owner(s), to these terms by typing the owner's name into the "Institution" box at the top of the page.

Part 2 - Open Access Copyright Assignment

Assignment of copyright

1.1 In consideration for acceptance and publication of the Article, the Named Authors of the Article and/or the Institution hereby assign, where necessary by present assignment of future copyright, to IOP with full title guarantee the entire copyright in all original material published as part of the Article (which expression includes but is not limited to the text, abstract, tables, figures and graphs, related corrigenda or "comments" and multimedia content but excludes any other item referred to as supplementary material) throughout the world for the full term of copyright (including any extensions or renewals thereof) for all media and formats, whether known or unknown. Such assignment shall be effective only if the Article (or any resubmission of the Article) is accepted for publication. For the avoidance of doubt, copyright does not subsist in any fundamental data underlying the Article and nothing in this agreement is intended to limit access to or use of such data.

1.2 If the Article, or any part of it, is protected by Crown Copyright, in consideration for acceptance and publication of the Article, the relevant Named Authors and/or the relevant originating department or agency hereby grant IOP a royalty-free worldwide licence for the full term of copyright (including any extensions or renewals thereof) for all media and formats, whether known or unknown, to do in relation to the Article all acts restricted by copyright worldwide.

1.3 In consideration for acceptance and publication of the Article, the Named Authors and/or the Institution hereby grant IOP a royalty-free non-exclusive worldwide freely transferrable licence for the full term of copyright (including any extensions or renewals thereof) to do in relation to any supplementary material not deemed to be part of the Article and/or any video abstract all acts restricted by copyright worldwide. This shall include, but not be limited to, making the material available under any licence that IOP deems appropriate for purposes including, but not limited to, the maximisation of visibility and the long term preservation of the content.

1.4 Each of the Named Authors consents to the publication and processing by IOP of their email addresses.

1.5 Each of the Named Authors and, where relevant, the Institution consents to the publication of the Article under the Creative Commons Attribution 3.0 Unported licence (https://creativecommons.org/licenses/by/3.0/) or any successor to that licence.

Representations and warranties

2.1 The Institution and/or the Submitting Author, on behalf of the Named Authors (as appropriate) represent and warrant that:

2.1.1 the Article is the original work of the Named Authors;

2.1.2 the Article has not been published previously in any form, other than as part of the Named Authors' research theses or dissertations (which fact has been notified to IOP in writing) or as a pre-print, for example on the arXiv.org service;

2.1.3 each of the Named Authors has made a material contribution to the conception and/or writing of the Article, has received the final version of the Article, has agreed to its submission on the terms contained herein and takes responsibility for it and submission has been approved as necessary by the authorities at the establishment where the research was carried out;

2.1.4 the Submitting Author completes and returns this agreement as authorised agent for and on behalf of all the Named Authors and has the full power to enter into this agreement and to make the grants and assignments it contains;

2.1.5 the Article has not been and shall not be submitted to another publisher prior to withdrawal or rejection by IOP;

2.1.6 the Article does not infringe any third party rights, it contains nothing libellous or unlawful, all factual statements are to the best of the Named Authors' knowledge true or based on valid research conducted according to accepted norms and all required permissions have been obtained in writing;

2.1.7 the Article explicitly acknowledges any third party funding and/or potential conflicts of interest; and

2.1.8 any supplementary material or video abstract is the original work of the Named Authors, or is the property of the Institution, or permission has been obtained from its owner(s) for its publication by IOP and permission has been obtained for the inclusion of any third party content (including music).

2.2 The Named Authors and/or the Institution indemnify and will keep indemnified IOP against all costs and expenses suffered or incurred by IOP as a result of and/or arising out of any breach of the representations and/or warranties in this section 2.

The Named Authors' rights

3.1 The Named Authors and all third parties will have the rights to use the Article as described in the licence applied to the Article pursuant to paragraph 1.5, above, which shall include the right to copy, distribute and display the published version of the Article and create derivative works, subject to appropriate attribution.

3.2 Where the Article is used in accordance with paragraph 3.1 above, the following attribution shall be included:
Article title
Named Author(s)
DOI
Journal citation

Miscellaneous

4. To the extent that there are moral rights in the Article, all the Named Authors expressly reserve and assert their moral rights to be identified as the authors of the Article.

5. The Named Authors and/or the Institution shall execute such further documents, and take such actions and do such things, as may be requested by IOP at IOP's reasonable expense to give full effect to the terms of this agreement.

6. For the avoidance of doubt, the grants and assignment envisaged herein shall become effective only upon acceptance of the Article for publication. In the event that the Article is withdrawn prior to acceptance, or is rejected, this agreement shall have no effect and no party shall be bound by it.

7. This agreement shall be governed by English Law and subject to the non-exclusive jurisdiction of the English courts.

Confirmation

8. By typing the Submitting Author's name into the box at Part 3 below and clicking "Submit", the Named Authors agree to all these terms. Authorised signatories of any third party copyright owner(s) agree, on behalf of such owner(s), to these terms by typing the owner's name into the "Institution" box at the top of the page.

Part 3 – Confirmation and Execution

req Please tick the box below to confirm the basis upon which you are submitting the Article.

- (•) Subscription Copyright Assignment – Part 1 Applies
- ( ) Open Access Copyright Assignment – Part 2 Applies
- ( ) US Government (where **all** the Named Authors are employees of the US Government **and** the Article was prepared as part of their duties and consequently the Article is not eligible for copyright)
- ( ) Other (none of the above apply). Please state brief reason below. IOP may contact you for more details.

req Type your name here:

Robert Odolinski (the "Submitting Author")

req Date:

10-Oct-2014

By clicking "Submit" and typing your name above, you shall be assumed to have read and understood all of the terms and conditions of the relevant part of this agreement and you will be agreeing to all of the terms and conditions and assignment (as the case may be) detailed above.

LAST UPDATED June 2014

Save as Draft Submit

APPENDIX B STATEMENT OF CONTRIBUTIONS BY OTHERS

This thesis presents 7 first author publications and 1 additional article that were published in journals and conference proceedings. In this Appendix, author and co-author contributions for these papers are stated and signed.

To Whom It May Concern,

I, Robert Odolinski, wrote the manuscripts, derived the functional models, and extended an existing GNSS software to process/analyse the multi-GNSS data. Prof Peter JG Teunissen and Dr Dennis Odijk provided their comments as to improve the manuscripts for submission, and conducted some software development as well. All the above holds for the following publications,

1) First combined COMPASS/BeiDou-2 and GPS positioning results in Australia. Part I: single-receiver and relative code-only positioning. Journal of Spatial Science, vol. 59, no. 1, p. 3-24. doi:10.1080/14498596.2013.840865 (Odolinski et al., 2014a)
2) Part II: Single- and multiple-frequency single-baseline RTK positioning. Journal of Spatial Science, vol. 59, no. 1, p. 25-46. doi:10.1080/14498596.2013.866913 (Odolinski et al., 2014b)
3) Quality analysis of a combined COMPASS/BeiDou-2 and GPS RTK positioning model. Proceedings of the International Global Navigation Satellite System Society (IGNSS) Symposium, Golden Coast, Australia, July 16-18, 2013 (Odolinski et al., 2013a)
4) Combined GPS, BeiDou, Galileo, and QZSS single-epoch, single-frequency RTK performance analysis. In Proceedings of the International Association of Geodesy (IAG) symposium in Potsdam, Germany, September 1-6, 2013, accepted (Odolinski et al., 2013b)
5) Combined BDS, Galileo, QZSS and GPS single-frequency RTK. GPS Solutions. doi: 10.1007/s10291-014-0376-6 (Odolinski et al., 2014c)
6) Combined GPS+BDS+Galileo+QZSS for Long Baseline RTK Positioning. Proceedings of the Institute of Navigation (ION) GNSS, Tampa, Florida, USA, September 8-12 (Odolinski et al., 2014d)

7) Combined GPS+BDS for short to long baseline RTK positioning. Measurement Science and Technology, accepted (Odolinski et al., 2014e)

And, I, Robert Odolinski, contributed to all numerical results as well as on commenting on the following publication. The first author was Prof Peter JG Teunissen that wrote the manuscript, and Dr Dennis Odijk provided his comments to the manuscript before submission as well:

8) Instantaneous BeiDou+GPS RTK positioning with high cut-off elevation angles (Teunissen et al., 2014)

Robert Odolinski _____

I, as a Co-Author, endorse that this level of contributions by the candidate indicated above is appropriate.

Peter JG Teunissen _____

Dennis Odijk _____

APPENDIX C PROOF OF PEER-REVIEWED AND ACCEPTED PUBLICATIONS

Provided below is the proof that the conference publications:

1) Quality analysis of a combined COMPASS/BeiDou-2 and GPS RTK positioning model. In Proceedings of the *International Global Navigation Satellite System Society (IGNSS) Symposium,* Golden Coast, Australia, July 16-18, 2013
2) Combined GPS, BeiDou, Galileo, and QZSS single-epoch, single-frequency RTK performance analysis. In Proceedings of the *International Association of Geodesy (IAG) symposium* in Potsdam, Germany, September 1-6 2013

were published in peer-reviewed conference proceedings and accepted respectively. Following that proof is provided that the following journal paper has been accepted:

3) Combined GPS+BDS for short to long baseline RTK positioning. Measurement Science and Technology (Odolinski et al., 2014e)

Robert Odolinski

From: Krys Henshaw <krys@ignss.org>
Sent: Friday, 21 June 2013 10:35 AM
To: Robert Odolinski
Subject: IGNSS 2013 - Peer Review Results
Attachments: Paper 68 Comment Sheet (1).doc; Paper 68 Comment Sheet (2).doc

Results of Review of your Paper for IGNSS2013 Proceedings

Attention: Robert Odolinski

Thank you for submitting a paper for Peer Review for the IGNSS2011 Symposium Proceedings which will be published on the IGNSS Website shortly after the symposium. The symposium will be held at Outrigger, Surfers Paradise, Australia from 16-18 July, 2013.

The review process for your paper has now been completed and each paper was submitted to a minimum of 2 reviewers.

1. Your **Paper No 68** has been accepted for the Peer Review Section of the Proceedings.
2. Your paper must be presented as either an Oral or Poster Presentation at IGNSS2013 to qualify to be included in the Peer Review Section of the Proceedings
3. Reviewers were requested to complete a Reviewers Comment Sheet and the Comment Sheet from both Reviewers is attached.
4. Some Reviewers have provided suggested changes for your paper in the attached Comment Sheets.
5. Some Reviewers have provided suggested changes via comment or track changes on the paper you submitted. If this is the case, the paper with suggested changes is attached.
6. It is strongly recommended that you consider the changes (if any) that have been suggested and implement these into your paper before resubmitting it. Changes are recommendations only and are not compulsory.
7. The Full Paper is required as a **PDF document** for inclusion in the Proceedings and should follow the format of the Full Paper Template exactly.
8. The Full Paper should be emailed to krys@ignss.org by **no later than 30th June, 2013.**
9. Your paper should be named as **Paper 68.pdf**

Please check your paper thoroughly once it has been converted to pdf to ensure that text and graphs are correct before returning it.

Papers will not be included in the Proceedings if they are not returned by **30th June, 2013.**

Kind Regards
Krys Henshaw
IGNSS Society, PO Box 413, TWEED HEADS NSW 2485 AUSTRALIA
PH: + 61 7 5599 5007 Fax: +617 55 366 366 Email: krys@ignss.org Web: www.ignss.org
Ref: 7594

Robert Odolinski

To: Pascal Willis
Subject: RE: IAGS: Your manuscript entitled Combined GPS, BeiDou, Galileo, and QZSS single-epoch, single-frequency RTK Performance Analysis

-----Original Message-----
From: em.iags.3e8.378614.e6a31076@editorialmanager.com
[mailto:em.iags.3e8.378614.e6a31076@editorialmanager.com] On Behalf Of Pascal Willis
Sent: Monday, 2 December 2013 9:15 PM
To: Robert Odolinski
Subject: IAGS: Your manuscript entitled Combined GPS, BeiDou, Galileo, and QZSS single-epoch, single-frequency RTK Performance Analysis

CC: willis@ipgp.fr, pawel.wielgosz@uwm.edu.pl

*** PLEASE ACKNOWLEDGE RECEIPT TO willis@ipgp.fr *** DO NOT USE REPLY

PW/IAGS 13.1908

Ref.: Ms. No. IAGS-D-13-00051
Combined GPS, BeiDou, Galileo, and QZSS single-epoch, single-frequency RTK Performance Analysis International Association of Geodesy Symposia

Dear Mr Odolinski,

Reviewers have now commented on your paper. You will see that they are advising that you revise your manuscript.

I then invite you to prepare and submit a revision.

For your information, a major revision means that your future revised manuscript will be sent back with the rebuttal letter to at least one of the reviewers.

The reviewers' comments can be found at the end of this email or can be accessed by following the provided link.

This is your login information:

When revising your work, please submit a list of changes or a rebuttal against each point which is being raised when you submit the revised manuscript.

Your revision is due by 01-01-2014.

To submit a revision, go to http://iags.edmgr.com/ and log in as an Author. You will see a menu item called 'Submissions Needing Revision'. You will find your submission record there.

Yours sincerely

Pascal Willis, Ph.D.-habil.
Editor-in-Chief
International Association of Geodesy Symposia

Robert Odolinski

From: em.iags.3e8.37fa89.863d4d0a@editorialmanager.com on behalf of Pascal Willis <willis@ipgp.fr>
Sent: Monday, 23 December 2013 2:07 PM
To: Robert Odolinski
Subject: IAGS: Your manuscript entitled Combined GPS, BeiDou, Galileo, and QZSS single-epoch, single-frequency RTK Performance Analysis

CC: willis@ipgp.fr, pawel.wielgosz@uwm.edu.pl

PW/IAGS 13.2159

Ref.: Ms. No. IAGS-D-13-00051R1
Combined GPS, BeiDou, Galileo, and QZSS single-epoch, single-frequency RTK Performance Analysis International Association of Geodesy Symposia

Dear Mr Odolinski,

I am pleased to inform you that your work has now been accepted for publication in International Association of Geodesy Symposia.

Thank you for submitting your work to this journal.

With kind regards

Pascal Willis, Ph.D.-habil.
Editor-in-Chief
International Association of Geodesy Symposia

Measurement Science and Technology

Preview

From: mst@iop.org

To: robert.odolinski@curtin.edu.au, p.teunissen@curtin.edu.au, d.odijk@curtin.edu.au

CC:

Subject: Our final decision on your revised article: MST-101654.R1

Body: Dear Mr Odolinski,

Re: "Combined GPS+BDS for short to long baseline RTK positioning" by Odolinski, Robert; Teunissen, Peter JG; Odijk, Dennis
Article reference: MST-101654.R1

We are happy to tell you that we have accepted your revised article for publication in Measurement Science and Technology as a Paper. Any further comments from the referees can be found below and/or attached to this message.

We will contact you soon, when proofs of your article are ready for final approval. Please ensure you return your article proofs by the date given, or your article may be published without your corrections.

All articles published by IOP Publishing are available online to readers at http://iopscience.org/. For more information, please contact our Customer Services department at custserv@iop.org.

Thank you for your interest in Measurement Science and Technology. We look forward to publishing your article.

Yours sincerely

Ian Forbes PhD

Publishing Team
Ian Forbes - Publisher
Joan Patrick and Graham Stinton - Publishing Editors
Adam Gough - Publishing Administrator
Alan Evans - Production Editor
mst@iop.org

IOP Publishing
Temple Circus, Temple Way, Bristol
BS1 6HG, UK

www.iopscience.org/mst

REFEREE REPORT(S): n/a

Letter reference: DRWA01

Date Sent: 24-Nov-2014

Close Window